The influence of welding parameters and parent plate metallurgical characteristics on solidification of austenitic stainless steel weld metals.

A Thesis Submitted for the Degree
of Doctor of Philosophy

by

M.M.Hosseinioun

Department of Materials Technology
Brunel University

September 1986

CONTENTS

Brunel University
Department of Materials Technology
Uxbridge, Middlesex UB8 3PH

M.M.Hosseinioun

The influence of welding parameters and parent plate metallurgical characteristics on solidification of austenitic stainless steel weld metals.

Ph.D.Degree
1986

ABSTRACT

The present work reports the effect of heat input, cooling rate, parent plate deformation and restraining conditions on the formation and morphology of delta ferrite in welds on AISI 316L and 321 steels.

The experiments were carried out on commercially produced plates in the following conditions:

(i) as received condition

(ii) further deformed by cold rolling.

(iii) further deformed by hot rolling.

The effect of heat input and cooling rates were examined using bead-on-plate Submerged Arc welds on the same parent plate material. The parent plate condition was assessed using bead-on-plate metal Inert Gas (MIG) and Subm rged Arc butt welds. The results suggest that :

1. The weld metal solidification proceeds epitaxially from the existing unmelted base metal. The weld exhibited surface marking i.e. deformation bands or close packed plane, in the austenite matrix, but not passing through delta ferrite phase.
2. The solidification substructure, the ferrite content, and morphology are influenced by the (i) thermal stress induced during welding, (ii) parent plate chemical composition, (iii) the parent plate microstructural and deformation characteristics i.e. strain energy.
3. Rapidly cooled welds have lower ferrite content than welds produced with slower cooling rates. The randomly distributed elongated ferrite with some lath type ferrite morphology was predominantly attributed with the welds produced with high cooling rates.
4. The ferrite is the first solidified phase to form and austenite is formed from the liquid rather than by solid phase transformation of primary ferrite to austenite.
5. The ferrite formation is a diffusion controlled phase transformation, the degree of its dendrites development depends upon the welding parameters i.e. heat input, cooling rates.
6. Two types of ferrite morphology were observed; (a) alongated type dendrites identified as vermicular by previous investigators and (b) the cellular type morphology which has not been classified in previous investigations.

ACKNOWLEDGEMENTS

I am greatly indebted to my supervisors Dr T.S. Eyre and Mr D.E. Talbot for their continuing encouragement and guidance.

The author would like to thank Professor M.J. Bevis and Dr I.O. Saunders for reading the manuscript and, for their valuable comments.

I would like to thank Dr T.G. Gooch of The Welding Institute for his helpful comments and discussion of the thesis.

Thanks are due to the departments teaching and technical staff, the staff of the E.T.C. and my colleagues for their assistance and friendship during the course of the research work.

TO MY DAUGHTERS WHO WERE TOO YOUNG TO

UNDERSTAND DADDY'S ABSENCE.

1. Introduction

The construction of many structural components involves welding fabrication on which there is a great need for reliability. Weld metals in common with other metals are strengthened by combining phase transformation with the deliberate introduction and interaction of alloying elements. The weld microstructure is generally determined by the cooling rate and the chemistry. The cooling rate is controlled by process parameters; whilst plate, wire, and flux specifications affect chemistry, other inter-related variables such as parent plate microstructural and mechanical characteristics, compositional variation, interpass temperature, bead shape, dilution with parent plate, bevel angle, thermal stresses, and to some extent slag characteristics also play an important role in the weld metal microstructural variation.[7,8,9,12,23]

In the case of austenitic stainless steel welds further restrictions follow from balancing the alloy composition to produce a certain amount of delta ferrite which is essential to reduce or completely eliminate the risk of solidification cracking.[48,52-57] To achieve these requirements and obtain a weld with desirable metallurgical characteristics,(i.e. microstructural and mechanical properties)the material and design engineers must meet a number of structural and mechanical requirements. Traditionally, the selected composition for a specific application reflects a compromise and is frequently pronounced as a function of chromium and nickel equivalent and thus the ferrite content of weld metal.

Extensive investigations have been carried out to obtain a better understanding of the austenitic stainless steel weld metal solidification behaviour.[86-106] Of the techniques discussed previously the use of

the improved spatial resolution of the chemical analysis technique by STEM provides essential information for a better understanding of the solidification process and the nature of solid phase transformation.

Previous studies based on Fe-Cr-Ni ternary equilibrium phase diagram showed that, solidification occurs by either a peritectic or eutectic type reaction [39,41,86-91]. The observed microstructure, the ferrite content, and its morphology depends not only on the composition i.e. Cr and Ni equivalent, but also on the solidification behaviour, and possibly on the amount of applied strain induced by thermal cycle during welding. Recent investigations [41,83,90] show the variation in cooling rate as well as chemical composition influences the solidification mode, and consequently the microstructure and mechanical properties.

Published reports based on Fe-Cr-Ni pseudo binary section for a constant iron indicate that the weld solidifies as either primary ferrite or austenite [39-41,86-92]; the solid phase transformation of primary ferrite to austenite occurring either by diffusion controlled transformation [87-91] or diffusion less massive transformation [86,103,104]. The final segregation profiles are produced by a combination of micro-segregation during solidification and partitioning of alloying elements during the solid state reaction.

This controversy over the nature of the solidification, solid phase transformation of primary ferrite to austenite, the ferrite content, and its morphology in austenitic stainless steel welds is still unresolved. Comparison of previous work revealed conflicting results and in many cases similar experimental procedures and results have been used to support a variety of interpretations.

1.1 Aim and scope of the present study

The objective of the present work is to study the solidification behaviour

of selected austenitic stainless steel weld metals in order to classify the complexity of their microstructure, particularly in respect of the ferrite content and morphology. In the present work, effort has been devoted to the study of the effect of welding parameters, i.e. heat input, cooling rates, and different parent plates metallurgical characteristics, i.e. microstructural and mechanical properties.

Extensive metallographic observations have been carried out and emphasis is placed on studying those variables affecting the nucleation and growth of ferrite dendrites during the solidification of austenitic stainless steel welds.

In this investigation Transmission Electron Microscopy (T.E.M.), Scanning Electron Microscopy (S.E.M.) Light Metallography, and Scanning Transmission Electron Microscopy (S.T.E.M.) were used. Detailed STEM analysis was carried out in selected thin foil welds in order to study the microstructure of different welds and the partitioning of both Cr and Ni in ferrite, austenite and their interphases.

1.2 Thesis Format

The metallurgical characteristics i.e. microstructural and echanical properties of austenitic stainless steels are explained in Chapter Two in terms of variables which influence the weld metal microstructure. These include the solidification behaviour, the effect of alloying elements and cooling rates on ferrite content and morphology. In Chapter Three the material and their preparation, welding procedure and details of experimental techniques are explained. The results in Chapter Four are divided into the following subsections:

(i) Submerged Arc (SA) Bead-on-plate welds with duplex structure

produced on AISI type 316L stainless steel plates.

(ii) Metal Inert Gas (MIG) Bead-on-plate welds with duplex structure produced on AISI types 316L and 321 stainless steel plates of different metallurgical characteristics.

(iii) Metal Inert Gas (MIG) Bead-on-plate welds with austenitic type structure produced on AISI types 316L, 321 and 304 stainless steel plates.

(iv) Submerged Arc (SA) Butt welds with duplex structure produced on AISI types 316L and 321 stainless steel plates of different micro-structural and mechanical characteristics.

The results of the present work are discussed in Chapter Five, and the subsections are written in parallel fashion with the previous Chapter. Conclusions and outlines of areas for further work are presented in Chapter Six and Seven respectively.

2. Literature Survey

2.1 General Characteristics of Stainless Steel

Previous investigations concerning the addition of alloying elements to iron led to the realisation that the addition of above 12% Cr* could improve its corrosion resistance.[1-4] Further additions of Ni (1 - 40%) produced stainless steel with good mechanical properties, durability and versatility.

The term "stainless steel" embraces a large number of corrosion resistant ferrous alloys.[1-7] They generally contain a minimum of 11% Cr as well as other alloying elements such as Ni, Mo, Ti and Nb. Cr improves the corrosion resistance by the formation of its oxide Cr_2O_3 on the surface of the steel. If this film is damaged either by abrasion or by cutting the steel, a new film will form to protect the new surface of the steel. The presence of alloying elements alters the constitution, thus forming different phases which influence the microstructure. The proportion of each phase present influences the microstructure, mechanical properties and behaviour in service.

There are several basic types of stainless steels and they are classified according to their microstructure.[6-9]

(i) Austenitic containing 18-25% Cr, 8-20% Ni, and other alloying elements such as Mo, Nb, Ti etc, carbon content should be as low as possible in the range 0.01 to 0.04% to maximise corrosion resistance.

(ii) Ferritic containing 15-35% Cr, maximum carbon level of 0.1% and the occasional additions of Mo, Nb or Ti

(iii) Martensitic containing 12-17% Cr, 0-4% Ni, 0.1-1.0% Cr and occasional additions of Mo, V, Nb, Ti, Al and Cu.

*composition listed in wt% throughout this manuscript

iv. precipitation hardening containing 10-30% Cr with varying amount of Ni and Mo. Precipitation hardening phases are formed by additions of Cu, Al, Ti and Nb.

Details of nominal composition of common grades of stainless steels are given in Table 2.1.

2.2 Austenitic Stainless Steels: The austenitic stainless steels are classified as a group because of their similarity in chemical properties and welding procedures.[1-10] They contain both Ni and Cr and other alloying elements such as (i) Mo (type AISI 316) to further enhance the corrosion resistance, (ii) S or Se (type AISI 303 S and 303 Se) for improving machinability, and (iii) Ti and Nb (type AISI 321 and 347) to overcome intergranular corrosion and weld decay. The addition of Ti and Nb produces the "stabilised" range of stainless steels; they react with carbon preferentially and thus hinder chromium carbide formation.

Nickel is an austenite stablizer, the addition of nickel to Fe - Cr alloys containing 18% Cr enlarges the austenite field and gradually eliminates the ferrite and ferrite plus carbide fields. It is known that increasing Ni concentration enlarges the austenite field as illustrated in Fig.2.1.

Recently, extra low carbon level ("L" grade) stainless steel has been produced by using vacuum treatments in the VAD/VOD process, or by argon/oxygen blowing in the AOD steel making process.[8,9] The low carbon modification is desirable to avoid sensitization and grain boundary chromium carbide precipitation. However, despite

the low carbon content (less than 0.03%), there is still a risk of harmful carbide formation under certain conditions.

One recent advance in stainless steels has been the development of steels containing up to 0.25% N.[10-13] The nitrogen content is dependent on the amount of Mo and Cr present, both of which can enhance the nitrogen solubility. Nitrogen acts as a solid solution strengthening agent, providing high austenite stability and partially replacing nickel as an austenite stabilizing element. It increases the yield strength and improves the pitting resistance. However, possible disadvantages are the effect on the cryogenic properties and also on the weldability of these steels, e.g. eruption can occur in the weld which results in excessive weld splatter, concavity, and porosity.[10-13] Steels formulated to produce austenite stability are useful where dimensional stability, non-magnetic behaviour and high strength are desirable.[6-16] The austenitic stainless steels have moderately high strength, high stiffness, good fabrication characteristics and they are available in a variety of product forms. As far as welding is concerned, the physical properties of these steels i.e. high coefficient of thermal expansion (CTE) and low thermal conductivity (high electrical resistivity) are matters to consider, as they could influence the solidification behaviour and consequently the micro-structure of weld metal.[7-9] Due to their relatively stable FCC lattice structure these steels maintain their properties both at elevated and cryogenic temperatures.[10-19] They are not susceptible to brittleness by cleavage which is a characteristic of the ferritic steels and they are immune from brittle fracture. The non-magnetic properties, good ductility and cleavage immunity, especially at very low temperature (i.e. -269^{o}C) make them desirable

as a constructional material for low temperature applications.[14-22] For instance, they are used as main structural supports of super conducting magnetic systems for fusion reactors and for the production of storage and transportation vessels for various liquified gases namely, e.g. petroleum gas - 51°C, liquid natural gas - 162°C, liquid nitrogen - 196°C and liquid helium - 269°C (see Fig.2.2).[16]

Another feature associated with these steels is their excellent corrosion and heat resistance properties due to the formation of the protective oxide film.[7-9] The choice of a suitable steel for a specific application depends on the severity of the aggressive chemical environment and hence the need for higher austenite stability. For example to handle aggressive organic acids such as citric and ascorbic acid (vitamin C), the addition of alloying elements e.g. from AISI type 304 to AISI type 316 and/or from AISI type 317 to AISI type 310 gives excellent corrosion resistance and mechanical properties at elevated and low temperatures.[1-4,7-10] However, the principle disadvantages are the high cost and some problems arising from micro-structural stability and control. Whilst general mechanical properties have been compiled in various reference books,[1,2,6-8,14-20] care should be taken when using this information because there may be significant changes in the properties due to the presence of interst-itial elements, i.e. carbon and nitrogen. A further important variable is the mechanical deformation history of the steel because the mechanical properties are not substantially changed by standard heat treatments used for low alloy steels. In addition to nominal microstructural changes thermo-mechanical treatments can provide a variety of interfaces which represent regions of mismatch between

phases i.e. chemically and structurally similar phases such as austenite/austenite - structurally dissimilar phases austenite/ferrite and chemically dissimilar phases austenite/carbides or non-metallic particles. These interfaces, like other defects, act as sites for impurities or secondary components. The practical significance of these effects is indicated by the magnitude of the cohesive forces at the interface, and thus the stresses required to separate them. Any interface within a crystalline solid can be modified by the influence of thermo-mechanical treatment parameters e.g. temperature, interface orientation, local segregation etc.

A summary of the mechanical properties of the common grades specified by BS 1449 Part 2[20] is given in Table 2.2.

In this investigation austenitic stainless steels AISI 316L and 321 were employed.

2.3 Welding Characteristics of Austenitic Stainless Steels

One of the objectives in the fabrication of engineering materials and welded assemblies is to exploit their particular mechanical characteristics and to correlate them with desirable microstructures.[7-12, 21-31] Variation in microstructure can be associated not only with anticipated changes in properties, but also with deficiencies in performance i.e. cracking and reduced corrosion resistance, etc.[14-17, 25-29]

Every distinct application of stainless steel e.g. cryogenic service, high temperature service, etc, placing special demands upon the qualities and properties of the materials and on welds in particular.[24-28] For example, the chemical industry is especially dependent on the availability of stainless steels, filler metals, and functionally stable methods of welding, permitting a high degree of reproducibility

and consequently welds of high quality. Investigations in the field of welding technology have been intensified to meet the increasing demands for quality and productivity.[21-31] The problem occurring with welding is the fact that the welding electrode, and thus welement itself are not finished engineering products, this is in contrast with materials fabricated by a combination forming/working techniques where the finished component is in a condition where mechanical properties can be guaranteed. During arc welding, however, the electrode is ideally used to produce continuous, stable and homogeneous products, but during operation the welder can unintentionally alter the chemical composition, and thus the mechanical properties of the finished product i.e. the weld. To overcome this, welding conditions and the properties of filler metals have been improved and adjusted to ever stricter requirements imposed by the quality of the weld metal. This is accomplished by developing new methods as well as by modifying the older techniques, resulting in technological growth in this field.[31-37]

In fusion welding, the weld is subject to a complex thermal cycle induced by the heat source, the weld metal properties being influenced by the high rate of heating, cooling and the associated stresses, such that phase changes may not go to completion with the realization that the welding energy is a major factor altering the cooling rate.[29,31,34] A heat input rate formula has been used to express the intensity of the welding heat source, which governs heating and cooling rates as well as weld pool size for the particular welding technique. Various equations have been used to evaluate the weld metal cooling rate in terms of welding process variables.[7,8,9] The most useful one appears to be that involving the equations developed by Rosenthal[38] in terms of material and process variables as follows :

$$\left(\frac{dT}{dt}\right) = 2K\frac{(T - To)^2}{Ep} \qquad (2.1)$$

where: $\frac{dT}{dt}$ is the three dimensional cooling rate at temperature T

K is the thermal conductivity

To is the pre-heat temperature

Ep is the energy input to the plate

One problem associated with the application of this formula is the variation in parent plate temperature during welding. This effects the temperature differential between solidifying weld metal and adjacent parent plate. To solve this problem it is usual to assume that the temperature is increased uniformly in parent plate from the origin along the length of the weld. The variation in heat input and parent plate temperature could influence cooling rate, and consequently the solidification behaviour of weld metal.[28,29,31,34-38] It could change the holding time in the liquid/solid region and/or the length of time from initiation to completion of solidification. For instance, the variation in cooling rate in the liquidus stage could influence the high temperature phase transformation and the amount of non-metallic inclusions which are able to agglomerate and float out of the melt. The variation of cooling rate through the solidification range will control the solid phase transformation, segregation of alloying elements and finally, at low temperature it could affect subsequent precipitation and ageing processes.[8,29,34]

Regarding the effect of cooling rate on the microstructural variation of austenitic stainless steel welds contradicting results were reported in terms of ferrite content and morpholdgy.[39-46] The general

view was that ferrite is the first solidification product and it subsequently transformed to austenite through solid phase transformation. Depending on the cooling rate the amount of retained ferrite at room temperature would reflect the proportion of ferrite existing at elevated temperature. Therefore, it was concluded that, increasing cooling rate could increase the ferrite retained at room temperature.[8,40,44,45] Some authors were concentrating on a specific temperature range i.e. above 1250°C, and relating the ferrite content to the cooling rate at that range of temperature.[7,8]

Extrapolating this view further, it was suggested that the high energy processes (i.e. spray transfer, and submerged arc welding) require the wire of higher ferritic tendency than moderate energy processes.[21]

In submerged arc welding both filler wire and flux influence the weld metal composition and final micro-structure.[23,25,28,29,34] There are rules which should be observed in the welding procedure for matching the required chemical composition of weld metal with that of the parent plate.[34-36,46,47] The transfer of alloying elements across the arc is largely controlled by certain oxygen bearing constituents in the flux e.g. SiO_2, CaO, and CaF_2 these affect the welding behaviour, slag removal and oxidation of Cr, Si, Ti etc.[23,32,33] The effect of welding flux constituents and the loss of alloying elements can be attributed to the influence of the welding parameters such as voltage, rate of welding, etc. Losses of Ni and Mo are low and there is usually no need to compensate for them. The burn-out of chromium, should it occur, is more serious and the chromium content can be adjusted by the selection of an appropriate flux. Care must also be exercised in producing a weld metal with a very low carbon content by choosing a special electrode wire of low carbon content and preventing carbon

pick-up from the flux. Any compositional variation in the weld metal changes the inherent properties such as corrosion resistance, ferrite content, second phase particles and mechanical properties. [23,33,34]

In sub arc welding, alloying elements can be introduced in the weld metal either through the electrode wire or by recovery from oxides added to the flux. For high alloy steel (e.g. austenitic stainless steel) the facility to introduce alloying elements from the flux is limited and it is usual to select an electrode wire of the composition required in order to match the weld metal, parent plate composition and to maintain their properties through the service life.

Consideration of cost and availability favour the use of electrodes of standard composition, but thesecan cause difficulties in producing good welds in high alloy steels.

2.4 Delta Ferrite in Austenitic Stainless Steel Weld Metal

Historically, solidification cracking is the main problem associated with the welding and casting of austenitic stainless steels and extensive investigations have been carried out to solve this problem. [48-56] From experimental investigations it has been shown that the risk of cracking can be reduced or eliminated by the introduction of a small proportion of residual delta ferrite (≈ 5%) into the nominally austenitic structure. [48,55] This was established empirically with no theoritical appreciation of the effect at the time. It was however appreciated that the most convenient means of controlling the microstructure was to control the chemical composition. This was achieved by altering the balance of ferrite and austenite forming elements whilst reducing those impurities which could enhance cracking. [48-70] Based on the early works concerning the compositional variation, many authors concentrated on the influence of the electrode coating and/or the effect of various filler metal compositions. [7,8,18,26-29,36,65-70]

The conventional practice for arc welding these steels has been developed based on the principle of producing a duplex structure in which both austenite and ferrite are present. An important part of a successful welding operation is in controlling the composition and thus the micro-structure through the proper selection of consumables and welding procedures. However, for some applications the presence of ferrite is not always desirable so that it may be necessary to limit or even eliminate it, thus giving a fully austenitic structure, e.g. to meet magnetic permeability requirements which may be imposed for special applications such as submarine defence equipment, or electrical equipment for nuclear and other energy applications. Completely austenitic structures lead to the problem already discussed i.e. microfissuring and cracking.[10,12,13,30,48]

The presence of delta ferrite can significantly alter the physical and mechanical properties of the weld metal,[32,39,46] and depending on the nature of the application and its temperature range it may be beneficial or deleterious. Although retained ferrite is needed to reduce the incidence of hot cracking and microfissuring it can[1-3,10-13] present some problems for high temperature applications by transforming to the brittle sigma (δ) phase, which impairs certain mechanical properties.[7,8] A further problem is that the sigma phase can provide a path for selective corrosive attack of weldments. In general, retained delta ferrite increases the strength but lowers the fracture toughness of the weld metal especially in cryogenic applications.[14-20]

In view of the foregoing discussion,[21-31,37,48,49,58-60] the objectives in welding austenitic stainless steels can be summarised as follows :

(a) preservation of the corrosion resistance of the weldment,

(b) avoidance of harmful effects from sigma phase formation,

(c) prevention of cracking or micro-fissuring in, or near the joint, the latter effect (case C) being the most troublesome feature.

2.5 The Effect of Alloying Elements on Delta Ferrite Content

Extensive research has been carried out relating weld micro-structure, and in particular the ferrite content with variations in composition. [7,8,42-60] In this context, Schaeffler [53] published a diagram which provides a means for predicting the retained ferrite content of weld metal as a function of composition, in which the effect of austenite stabilizing elements (i.e. Ni, C and Mn) were combined with the effect of ferrite stabilizing elements (i.e. Cr, Si, Mo and Nb). The original work applied to weld metal in the as-welded condition and was based on the normal cooling rate of the weld metal. The welds were deposited from coated manual electrodes with a nitrogen content of about 0.06%. Nitrogen was not included in the computation because it was not considered to vary significantly and was not commonly reported in the chemical analysis. In steel making, however, nitrogen is known to vary directly with the Cr content, and to transfer efficiently across the welding arc so that the nitrogen levels of the core wire and weld metal are expected to be equal, unless intentionally altered through the coating or by holding a long arc in welding.

From the geometry of the Schaeffler diagram [53] it is possible to predict the ferrite content of weld metal of known composition (Fig.2.3(a)) In this way Saferian [7] derived the following equation for the ferrite content of weld metal of nominally austenitic steels exhibiting duplex structure :

$$\% \text{ Ferrite} = 3\,(\text{Cr eq} - 0.93\,\text{Ni eq} - 6.7) \qquad (2.2)$$

Later Delong modified the Schaeffler diagram to include the strong austenitising effect of nitrogen in the computation and, adjusted the location and slope of some of the ferrite lines for several of the alloys in the central portion of the diagram. [45,48,50,54] This diagram thus relates ferrite content in volume percent (Vol. %) to chromium and nickel equivalents (Fig.2.3 (b))Furthermore, due to the linearity of the isoferrite lines he obtained the following expression for ferrite content in the range 0-20%

$$\text{Ferrite \%} = -30.65 + (\text{Cr} + \text{Mo} + 1.5\,\text{Si} + 0.5\,\text{Nb}) - 2.5\,(\text{Ni} + 30\,\text{C} + 30\,\text{N} + 0.5\,\text{Mn}) \quad (2.3)$$

The original Schaeffler diagram was determined to an accuracy of $\pm$ 4 Vol % by quantitative metallographic techniques. [53] Delong claimed a better accuracy of $\pm$ 2 Vol % for his diagram which was determined magnetically. [54] For the more highly alloyed materials the Delong diagram predicts higher ferrite contents than the Schaeffler diagram.

Hull modified the Delong diagram to include the inversion behaviour of Mn from an austenite to a ferrite stabiliser for weld metals with high Mn content. [42,80] Using this information Johnson[7] obtained the following expression for ferrite content

$$\text{Ferrite \%} = 13.77 + 2.88\,\text{Cr eq} - 3.125\,\text{Ni eq} \quad (2.4)$$

It is important to appreciate that predictions using Schaeffler type diagrams do not yield absolute values of ferrite content but only the ferrite-forming tendency as indicated by the quantity of delta ferrite retained at room temperature in welds produced under a standardised reference condition. [42-67] The diagram does not necessarily apply to welds produced under other conditions for which different weighting factors must be given to the alloying elements. It has been shown experimentally that the weighting factors for the alloying elements depends on the alloy composition, welding parameters, and cooling rate. [39,40,44,65-70]

All these effects are of course expected because a weld is essentially produced under non-equilibrium conditions. At equilibrium, none of the compositions considered would contain significant amounts of delta ferrite.

Recently it has been established that the amount of retained ferrite and its morphology depend not only upon the composition but also on the history of the solidification behaviour, [39-69] and possibly on the amount of applied strain induced by the welding thermal cycle. Furthermore, it has been reported that the quantity of weld metal deposited influences the shrinkage, it can also influence the content and morphology of delta ferrite.

To summarise, the experimental work concerning the quantity and morphology of delta ferrite in weld metal has concentrated mainly on the effects of chemical composition. Little if any attention has been given to the influence of other factors. These include

(a) The influence of parent plate characteristics, e.g. internal (residual) stresses.

(b) The overall cooling rate of weld metal from the liquidus temperature to room temperature.

(c) Welding parameters, e.g. heat input.

All these variables are expected to have significant effects on the structure and hence the properties of the weld. They form the principle objectives of the present investigation.

2.6 Measurement of Delta Ferrite

The Schaeffler type diagrams [53,54,65,67] already discussed yield predictions for the expected ferrite content of welds, but direct methods of measurement [46,51,67-71] are also required.

Because ferrite is ferromagnetic this led to the development of N.D.T. gauges for ferrite determination based on the measurement of the magnitude of magnetic attraction, which is directly [72-74] proportional to the amount of ferrite present. Different ferrite meters such as the Magne gauge, the Severn gauge, the Ferritscope, etc, have been employed for ferrite measurement. [73-77] Standard samples are used for calibration of these measuring instruments, but due to different calibration methods and differences associated with every type of meter, accurate ferrite readings have been difficult to obtain. In addition, because of the effects of structural variation, e.g. particle shape, size, orientation and possibly texture, some limitations are experienced in the accuracy and consistency of the results obtained. To solve these problems some investigators suggested [54,73-77] that for better consistency in ferrite measurement it is necessary to determine the ferrite content under conditions of total magnetic saturation, [73,76] claiming that under these conditions an accuracy of $\pm$ 2% can be obtained. [54] This depends only on the amount of ferrite and its ferromagnetic characteristics. [75] With this technique the main problem is the production of magnetic saturation, since field strengths in excess of 10 Koe are required. [78]

Attempts have been made to standardise the calibration and use of [50,54,74,79] these magnetic instruments and in this context, a test programme consisting of an extensive comparison of all the common instruments was carried out using samples with a wide range of ferrite content. The results confirmed the conclusion of previous work in 1968 for the American Welding Society, [64] i.e. that there is no consistent accurate method of determining ferrite content.

The National Bureau of Standard (U.S.A.) developed a set of standard tests based on the magnetic response of randomly distributed ferrite in a representative selected area of a sample.[45,64] By agreement the ferrite content was expressed in terms of a new parameter the ferrite number, F.N. in place of the value for the actual ferrite content. The ferrite number is referred to as a scale calibrated from the magnetic response of test blocks coated with various thickness of non-magnetic material. The ferrite content determined by this method is arbitrary and is not necessarily the true ferrite content.

For a given specimen the ferrite number particularly if it is 10 or less, gives a good indication of the ferrite content.[8,9,45] Subsequently, the following expression was suggested to relate the ferrite number and ferrite content of weld metal[81]

$$\text{Ferrite number} = 1.70\% \text{ delta ferrite content.} \qquad (2.5)$$

Other slow and time consuming techniques for ferrite measurement are available.[84,85] Of these, X-ray spectroscopy. Integrated Mossbauer spectra, Eddy current, and chemical extraction techniques are useful.[83,84] In the latter extraction of ferrite from duplex matrix can be carried out by electrolitic separation or by potentiostatic dissolution. Every one of these techniques has shown some self-consistency and their main advantages are that they are mainly independent of the shape size and orientation of the ferrite phase particles. However, so far no comparative study with the various techniques available has been reported.

Quantitative metallography is one of the most common optical techniques used for determining ferrite content. The most common systems in this context are area measurement, point analysis and linear intercept analysis.

It is usual in quantitative microscopical methods to assume that the volumetric proportions are equal to the proportions viewed on a two dimensional plane.

When using optical techniques extensive counting is necessary to compensate for the wide intrinsic variation in ferrite content within a given structure. A further limitation to the accuracy is the subjective nature of the evaluation because of difficulties in obtaining acceptable contrast levels between the ferrite and other phases. To improve the precision it is necessary to increase the number of readings in random sampling.[81,82]

Furthermore, with the help of modern electronic systems such as video or computer based image analysis the accuracy over large numbers of fields of view is improved. However, the basic problems remain, i.e. specimen preparation, the degree of metallographic etching or the strength of chemical reagent and the presence of other phases with structures which can be confused with ferrite.[75] Despite all of these difficulties encountered in quantitative metallography, the use of two dimensional studies at high magnification can yield values with acceptable accuracy ($\pm$ 4%) for ferrite measurements on welded structures.

2.7 Morphology of Delta Ferrite

The micro-structural classification and morphology of austenitic stainless steel weld metal and castings have been extensively studied.[83,87-106]

It is generally believed that the solidification behaviour, the mechanism of ferrite formation and its transformation to austenite are governed by the balance between austenite and ferrite forming elements, as described by the appropriate expression for the ratio of chromium equivalent to nickel equivalent on the Schaeffler type

diagram. In this approach the chemical composition is used to show the relationship between different micro-structural features, i.e. different compositions have been considered and a solidification sequence has been suggested for each composition.

This view is over-simplified and it has been established that in addition to composition, the cooling rate also has a significant effect on the micro-structural variation of austenitic stainless steel weld metal. [38,41,54,65,86,88,91]

Lack of information on the cooling rate at different stages of solidification along with a wide range of other variables,especially the welding characteristics, has produced a situation in which the variation in delta ferrite content and the terminology for different ferrite morphologies are not well explained. In this context the ferrite morphology has not hitherto received sufficient attention. Terms such as "typical micro-structure" and "general micro-structure" are often used in literature, but they are inadequate because they do not distinguish ferrite morphology.

Recently the position has improved and ferrite morphologies are now being defined by different investigators, e.g. four distinct types of delta ferrite morphologies in AISI type 308 weld were identified by David et al [87] as follows: [87,88-103]

(a) Vermicular morphology: where, the ferrite can appear as an aligned skeletal network (as illustrated in Figure 2.4 (a)).

(b) Lathy morphology: with long columns of an interlaced ferrite network oriented along the growth direction in an austenite matrix; the ferrite is located within the cellular dendrites Figure 2.4 (b).

(c) Acicular morphology: with the random arrangment of needle-like ferrite distributed in an austenite matrix with no directionality or conformation to the solidification sub-structure;(Figure 2.4 (c)) and finally,

(d) Globular morphology: with randomly distributed globules in a matrix of austenite (Figure 2.4(d))

David et al concluded that the first solidified phase is ferrite which after partial solidification is enveloped by austenite until solidification proceeds to completion, this solidification sequence is characteristic of a peritectic reaction rather than the eutectic solidification. They suggest that upon cooling, a large fraction of the primary ferrite is consumed by austenite in a diffusion controlled solid state transformation.

Suutala et al described different types of weld metal microstructure [100-102] based on the composition and solidification mode.

(i) Welds with $\frac{Creqv}{Nieqv}$ ratio < 1.48 solidify primarily as austenite, the ferrite, if any, is formed from the remaining melt between austenite cells or dendrites as eutectic.

(ii) Welds with ratio of 1.48 - 1.9 solidify primarily as ferrite, the austenite is also formed from the melt, the retained ferrite has a vermicular morphology with any lathy ferrite present located mainly on the cell axis.

(iii) Welds with ratios of 1.96 - 2.3 will solidify as single phase ferrite, the austenite nucleates only in the solid state preferentially at a ferrite grain boundaries resulting in a lathy morphology.

Fig 2.5 shows the solidification mode and subsequent transformation of austenitic stainless steels in terms of $\frac{Cr}{Ni}$ eqv.ratio.

Similar micro-structural classification in terms of $\frac{Cr_{eqv}}{Ni_{eqv}}$ ratio and carbon equivalent was carried out by Hammer and Sevensson. (106) They estimated and predicted the mode of soldification with the following expression :

$$C\ eqv = C + 0.65\ N \qquad (2.6)$$

$$Ø = -0.75\ Cr\ eq + 0.257 + Ni_{eqv} \qquad (2.7)$$

where at $C_{eqv} < 0.04$ the primary phase is ferrite followed by the austenite as a secondary phase

at $0.04 < C_{eqv} < 0.066$ Both phases are formed simultaneously

at $C_{eqv} > 0.66$ The primary phase is austenite

Referring to the $\frac{Cr}{Ni}$ equivalent ratio the following solidification modes were defined.

Ø <o	$\ell \rightarrow \ell + \delta \rightarrow \ell + \delta + \gamma \rightarrow \gamma + \delta$	primary ferrite solidification
Ø =o	$\ell \rightarrow \ell + \gamma \rightarrow \gamma \rightarrow \gamma + \delta$	ferrite and austenite will be precipitated simultaneously
Ø >o	$\ell \rightarrow \ell + \gamma \rightarrow \gamma$	primary austenite solidification

They showed that the change between ferrite and austenite freezing occurs at $\frac{Cr}{Ni}$ equivalent conditions just below or equal to 1.35.

More recently Leone et al (90) predicted the solidification modes, transition from one freezing mode to another, and the resulting micro-structure as follows:

$\frac{Cr_{eqv}}{Ni_{eqv}} > 3$	ferritic structure
$\frac{Cr_{eqv}}{Ni_{eqv}} \geq 1.8$	Duplex structure in which austenite forms in the solid
$1.8 > \frac{Cr_{eqv}}{Ni_{eqv}} > 1.2$	Duplex structure in which austenite forms in the liquid

1.2	$\frac{Cr_{eqv}}{Ni_{eqv}}$	Austenite structure with eutectic ferrite, if any

Their results were defined by basing on Schaeffler equivalent type diagram as shown in Figure 2.6. It was also recognised that the ferrite content and location in the room temperature micro-structure is influenced by the cooling rate and nitrogen content; the faster cooling rate or higher nitrogen content favoured formation of primary austenite.

In one of the earlier papers, Hull[82] suggested a similar interpretation to Suutala[100] by referring to the primary austenite solidification with the variation in the amount of eutectic phase formation. Fredrikson[17,39,40] also referred to the presence of eutectic phase. However, the micro-structure of austenitic stainless steel weld produced in non-equilibrium condition is in contrast with the observed micro-structure in eutectic alloys.

2.8 Solidification of Metals

2.8.1 Solidification Microstructure

Engineering materials are normally multicomponent alloys forming several phases during or after solidification. Some have wide melting ranges and thus solidify over a range of temperature which can give rise to micro-segregation within the alloys. Solidification involves aspects of crystal growth on both macroscopic and microscopic scales and studies of both of these facilitates the understanding and description of the as-cast microstructure of the solidified product.[106-114]

In the as-cast structure of most alloys there are three distinct regions i.e. the chill, columnar, and central equiaxed zones which are functions of the casting process parameters, alloy composition etc.

In the solidification of stainless steel ingots, however, the as-cast structure does not show the typical three zones and as a result of the solidification mode they contain only large columnar grains extending from the edge to the centre of an ingot.[108] It is common practice to control the grain structure of cast stainless steel by adding known grain refiners such as titanium, zirconium and/or by inoculating the melt with various metallic powders e.g. ferrochromium or by increasing the nitrogen content. However, the production of a fine grain structure in these alloys has not been consistently successful and contradictory results have been obtained.[106-114]

The solidification of weld metals generally differs from that of ingots. In welds the base metal acts as the "mould" but with different characteristics from those of conventional moulds.

In welds the dominant mechanism comprises a coherent growth of columnar grains on the partly molten grains of the base material. As a result of the fast cooling rate this growth is accompanied by a steep temperature gradient so that the chill zone, a possible source of nuclei in ingot casting, is replaced by an epitaxial growth of initially solidified crystals on the substrate. The subsequent growth and its substructure development are dependent on the degree of under-cooling. The original grains are therefore compelled to grow further with suitably oriented grains surviving and growing to the centre of the weld.

The way in which the subsequent growth occurs is determined by various parameters such as the temperature gradient in the melt, the composition of the melt and even turbulence brought about by the steep temperature gradient in the vicinity of the arc.

It is more difficult to obtain a grain refined structure in weld metal than in cast ingots, grain refinement requires the suppression of columnar growth, either by the addition of nucleants or the fragmentation of nuclei, ensuring both the production of nuclei and their survival in the melt as stable solid particles. However, despite all of these difficulties some degree of success has been achieved in this field. This has been accomplished by the addition of nucleants or by disturbing the weld pool ahead of the arc. The latter expedient can increase the nucleation frequency of new grains and here suppress columnar growth. It would appear that, while grain refinement can sometimes be achieved, its origin and operative mechanism are not fully understood because of the complexity of the solidification mode and welding variables.

2.8.2 Microscopic Equilibrium Solidification

The normal solidification of the liquid phase occurs by a process of nucleation and growth.[107-114] For pure metals, growth of the solid phase involves only the extraction of heat sensible and latent from the melt. For alloys solidification involves both the dissipation of this heat liberated during freezing, and the diffusion of alloying elements. This leads to the redistribution of the solute elements along the solid liquid interface, changing the growth morphology, and solute segregation.

Despite the redistribution of the solute elements, the study of solidification theory can be simplified by assuming that equilibrium prevails at the solid liquid interface during growth of solidified phase, i.e. the equilibrium concentration for the solid and liquid phases are present over narrow regions in contact with one another at the interface.[107,113]

The type of solute segregation which accompanies solidification depends upon various parameters, i.e. nominal composition, the equilibrium distribution co-efficient, the temperature gradient in the liquid and the growth rate at the solid liquid interface.

In solidification theory it is usual to discuss different limiting cases for the behaviour of liquid while compositional equilibrium is maintained at the solid liquid interface. In this context, Davies[107] schematically summarized four different types of compositional profiles (segregation curves) in the solid for normal freezing as shown in Fig. 2.7, in which the equilibrium distribution co-efficient* K<1. These are: (i) equilibrium freezing; (ii) complete solute mixing in the liquid; (iii) solute mixing in the liquid by diffusion only, (iv) partial solute mixing in the liquid.

To apply these concepts to the solidification of weld metal account must be taken of the conditions which exist in the weld pool. In welding, equilibrium is generally not established and therefore case one, the curve (a) in Fig.2.7 can be eliminated. As a result of turbulance and convection in the weld pool it can be assumed that initially the redistribution of the solute is very effecient. However, as the heat source moves away and solidification is completed it is likely that the convectional mixing of the solute gives way to a diffusion process. Thus the solidification of welds is probably a compromise between cases considered in Fig.2.7.

2.8.3 Solidification Modes of Austenitic Stainless Steels

Extensive investigations have been carried out to study the complex solidification behaviour of austenitic stainless steel welds and casting. The Fe - Cr - Ni ternary system provides the basis for

---

* $K = \frac{C_S}{C_L}$ where C_S and C_L are the equilibrium percentages of a given element in the solid and liquid respectively at a particular temperature.

understanding the constitution of stainless steel alloys. Solid phase transformation involving the allotropic forms of iron and transition between ferrite stabilising elements which gives rise to complex region in the tenary systems.[115,116,117] Fig.2.8 is a schematic representation of these relations involved for such a tenary system and may be interpreted as follows:

In the Fe-Cr system all alloys solidify as BCC solid solution δ phase. It shows a simple liquidus which passes through a minimum at ∿ 1510°C and about 1 8% Cr. The system has a γ loop region and beyond 13% Cr austenite does not form. The Cr-Ni system shows extensive solid solubility of Cr in Ni and vice versa with a eutectic reaction in this system. The eutectic horizontal at 1345°C extends from 41 to 53% Ni. The Fe-Ni system contains a peritectic reaction. Ni dissolves in FCC iron and the FCC phase therefore accounts for most of the reactions occurring below the solidus. The reaction between liquid and δ to give γ has been investigated quantitatively as follows:[117]

$$L\ (5.5\%\ Ni) + \delta\ (4.3\%\ Ni) \underset{\longleftarrow}{\overset{1513}{\longrightarrow}} \gamma\ (4.7\%\ Ni) \qquad (2.8)$$

the line pxe in Fig.2.8 starts from p as a peritectic line,and finishes at e as eutectic line in the liquidus surface. The liquidus and solidus surface of the simple Fe-Cr-Ni system are illustrated in Figs.2.9 (a) and (b) respectively, showing the transition between different phases.

The average compositions for several commercial alloys are often close to the trough joining the pertectic in the Fe-Ni binary to the eutectic in the Cr-Ni binary. This suggests further transition from peritectic to eutectic equilibrium, as composition changes from the Fe-Ni to Cr-Ni edge. Various reports were published considering the changes in the location of the phase boundary concerning the transition from peritectic reaction to a eutectic. In this context Schurmann and Brauchmann[117] showed that, this transition occurs at 75.8% Fe, 9.6% Ni and 14.6% Cr.

Furthermore, referring to Fe-Cr-Ni ternary system, phase equilibrium in the iron-rich region over a range of temperatures can be represented by pseudo-binary section for a constant iron content. It is important to note that pseudo-binary sections through ternaries are only providing a rough guide and they are only qualitative. However, they are used to illustrate the solidification modes of stainless steels as a function of composition. Figure 2.10 (a-c) shows a pseudo-binary section of different iron content. [90,94,100-104]

The two phase liquid + delta ferrite and liquid + austenite regions are separated by a three phase eutectic triangular region. A three phase equilibrium exists between austenite + ferrite + liquid phase within the triangular eutectic region. The primary solid phase is ferrite or austenite depending on whether the nominal composition has a high or low Cr equivalent, i.e. a high or low proportion of ferrite formers. In alloys solidifying to primary austenite, the divorced phase at the subgrain and grain boundaries is delta ferrite. In alloys solidifying to primary delta ferrite the divorced phase is austenite. The micro-structure of alloys solidified in the compositional range in the vicinity of the eutectic triangle are more complex. However, it is generally believed that alloys of nominal composition on the Ni rich side of the eutectic trough will be austenite. Alloys with nominal composition on the Cr rich side of the eutectic trough usually solidify as primary ferrite. Furthermore, recent investigations[90] indicate that high cooling rates promote primary austenite solidification in some weld metals composition which would ordinarily solidify as primary ferrite - this behaviour is still not well understood.

In addition to Cr and Ni, other alloying elements in particular C

and N have a marked effect on the solidification behaviour of austenitic stainless steel.[10] In this context a schematic section of a constitutional diagram for Fe - Cr - Ni alloy containing 18% Cr and less than 0.03% C are illustrated in Figure 2.11. These diagrams are not true equilibrium, but they are very useful for qualitative illustrations of solidification modes as a function of composition. Figure 2.11shows that the alloy containing up to 11% Ni solidifies as delta ferrite, or at least very high proportions of this phase. Beyond this percentage a peritectic reaction occurs and solidification takes place to delta ferrite and austenite. For high Ni content alloys the first solidification phase would be austenite.

2.8.4 Solidification of Austenitic Stainless Steel

The weld metal micro-structure depends on both the solidification mode and the consequent solid phase transformation of ferrite to austenite.[39-41,87-107] Calculations based upon diffusion co-efficients indicate that diffusion controlled transformation can occur in stainless steel welds during cooling associated with conventional arc welding processes.[87-92] [41,99,103] Recently studies performed by some workers led to the hypothesis that primary ferrite can transform to austenite by a solid state transformation whereby the ferrite dendrites are partially consumed by the growth of austenite.[41,44,93-95] [41,44,93] It has been assumed that the solid state transformation occurs only for alloys that undergo primary ferrite solidification.[41,44,88-90,104] The nature of this solid phase reaction is still controversial. Reports have been published citing either diffusion controlled transformation or a diffusionless massive transformation. However, it appears that the transformation is influenced by variations in composition, cooling rate and possibly the solidification behaviour.[87-97]

Recently Lippold and Savage[41,44] applied the solution of Smith, Tiller

and Rutter [118] for mixing in the liquid by diffusion only to the solidification of stainless steel welds and the formation of different ferrite morphologies. For primary ferrite solidification a composition profile similar to that shown in Figure 2.12(a) is predicted. For primary austenite solidification the profile predicted is illustrated in Figure 2.12(b), they used both electron probe micro-analysis (EPMA) and STEM to support their solidification model. They suggested that the skeletal ferrite morphology is the result of Cr-enriched and Ni depleted dendrite cores formed during the initial transient stage of solidification, and that the transformation of the ferrite to austenite is a solid phase transformation of a massive reaction. Furthermore, they suggested that the bulk of a dendrite with composition of Co is stable at room temperature, and that the ferrite - austenite boundary moves until it reaches a point where the compositional driving force is insufficient for further boundary motion. They used an argument based on the following equation:

$$\bar{X} = 4\,Dt^{\frac{1}{2}} \qquad (2.9)$$

where : $\bar{X}$ = the average of diffusion distance

D = the average of diffusion co-efficient in the temperature interval

t = the corresponding time within the same interval

They presented data for Cr and Ni diffusion in austenite to suggest that the diffusion distances are too great for a diffusion - controlled transformation during the short period of time available in weld metal solidification.

More recently Brooks et al [95] reviewed the origin of the ferrite and its morphologies. They determined the Cr/Ni profiles across both

the primary and secondary arms of the skeletal ferrite. Their results showed the presence of different profiles across the primary and secondary arms and the absence of any final Cr transient region in the austenitic matrix. They predicted that a considerable amount of diffusion occurs in the solid phase. They also predicted that from available diffusion co-efficients that the diffusion distance is some 10 - 50 times greater than that predicted by Lippold and Savage.[41]

Brooks et al[95,97] concluded that skeletal ferrite is the result of a diffusion controlled solid state reaction occuring during cooling in which the Cr diffuses to the ferrite and Ni diffuses to the austenite. The final segregation profiles are produced by a combination of micro-segregation and partitioning during the solid state reaction.

Published data based on the solidification behaviour indicated by the pseudo binary phase diagram such as that shown in Fig.2.10 showed the following solidification mode for austenitic stainless steels.

(i)Solidification completely to primary ferrite. (ii)Solidification as primary ferrite followed by a three phase reaction between liquid, ferrite and austenite.(iii)Solidification as delta ferrite until partitioning of austenite stabilising elements to the remaining liquid causes this liquid to solidify as austenite.(iv) Solidification completely to primary austenite. (v) Solidification as austenite with the formation of a divorced eutectic ferrite at the dendrite interstices during the terminal transient stage of solidification.

Generally the transition $\delta+L \rightarrow \gamma$ is called peritectic reaction, as long as the delta phase is in direct contact with the liquid, when the delta ferrite is completely surrounded by austenite phase and the reaction rate is governed by solid state diffusion of the alloying elements through austenite, this process is denoted peritectic transformation.[92]

2.8.5 Growth and Substructure in Weld Metal

In ingot casting and weld pool solidification it is usual to consider the condition of normal growth by continuous random addition of atoms with rapid growth rates. In normal growth, the macroscopic form of the interface is determined by conditions adjacent to the interface and the interface may change from planer through cellular to dendritic forms as the growth conditions change.[107-110]

The summarized factors which influence the solidification conditions for particular growth modes are illustrated in Figure 2.13. The ordinate corresponds to the concentration of the solute experiencing redistribution during solidification.[109] In general the solidification mode becomes more dendritic and less desirable, as the solute content rises. The abscissa is the function of $GR^{-\frac{1}{2}}$ which reflects the phenomenon of constitutional supercooling, i.e. low values of $GR^{-\frac{1}{2}}$ indicates a susceptibility to extensive constitutional supercooling, which favours the dendritic mode of solidification. On the other hand, steep temperature gradients in the liquid and slow growth rates which yield high values of $GR^{-\frac{1}{2}}$ favour cellular growth.[109-113]

Following Tiller,[118] extensive investigations have been carried out to quantify the boundary solidification conditions for particular growth modes and the nature of substructure in ingot casting as well as weld metals.[119] In this context, Calvo et al first applied the concepts of constitutional supercooling to explain weld structure morphologies they observed, i.e. cellular, cellular - dendritic and free dendritic growth modes and found that the higher the alloy content of the weld pool or the flatter the thermal gradients, the greater was the tendency for cellular -

dendritic and ultimately free dendritic type structure. These results were later confirmed by Savage and his co-workers, who extended the work to include substructures observed in normal weld beads produced for a range of welding conditions. They found that it is possible to generate a range of growth substructures in melt runs in a given material simply by changing the welding conditions, e.g. increasing the weld current at fixed welding speed can cause the melt run substructure to change from a cellular to cellular - dendritic growth mode.

3. Materials and Test Procedures

3.1 Selection of Materials:

The material and welding procedures were procured to produce various welds with the objective of studying the weld metal micro-structural features independently, or in conjunction with their parent plate characteristics. The parent plate conditions were varied systematically as described in the next Section, 3.2. The welding technique, electrode wire and flux or shielding atmosphere chosen to suit the particular welding techniques are described in Section 3.4.

3.2 Parent Plate Preparation

Experimental parent plates were prepared from commercially supplied forged billets,* (750 x 90 x 90mm) of AISI 316L and AISI 321 austenitic stainless steel, whose chemical analysis is given in Table 3.1.

The preliminary plates from billets were further worked and heat treated to produce a range of plates 12mm thick, with identical chemical composition but differing micro-structural characteristics.

In parent plate preparation the rolling temperature and the rate of cooling following rolling were varied. In addition two further conditions were examined, i.e. the billet material in the as received condition and the solution treated at 1150°C. The rolling schedules adopted were constrained by

(a) the maximum thickness acceptable by the laboratory rolling mill, i.e. 25mm

*Kindly supplied by the British Steel Corporation.

(b) the need to conserve the limited quantity of material available, especially the AISI 321.

For these reasons, the total reduction given to the AISI 321 and AISI 316L materials were 33% and 50% respectively. These reductions were applied by a multipass schedule.

The rolling temperatures used were 20°C(i.e. cold rolling) and 400°C, 950°Cand 1150°C (i.e. hot rolling). One or the other of two cooling rates were applied following rolling, (i) water quenching, (ii) furnace cooling. The materials prepared in this way are described in detail in Table 3.2.

3.3 The Test Plate (Jig Preparation) for Restraining the Parent Plates.

The jig for restraining the parent plates prior to the welding operation was made from a mild steel plate 540 x 360 x 25 mm, because stainless steel was not available. To overcome difficulties due to differences in thermal conductivity and thermal expansion between mild steel and the experimental stainless steel plates the jig was constructed as follows:

A recess, 300 x 220 x 10mm, was milled in the middle of the top surface (longitudinal horizontal section) of the restraining plate. This recess was then filled with an austenitic stainless steel overlay applied by MIG welding. The strain induced by welding was relieved by thermal treatment and the top surface of the composit plate was machined flat. To prevent rapid cooling of the experimental welds a slot of 250 x 25 x 25mm was machined longitudinally (vertical section) in the middle of the top surface of the restraining plate. Several angle sections were welded to the ends and underside of the restraining plate to increase its rigidity and to prevent elastic deformation.

For each experiment the parent plates making up specimens for butt welding were machined square to provide a good fit and to prevent burning through during welding. The plate surface and weld area were properly cleaned to remove any contamination. Before a welding operation was commenced, both ends of the plates were tack welded. The joints were restrained by fillet welding to the prepared jig to prevent the root from opening ahead of the arc and inhibited any possible movement . Austenite stainless steel run-on and run-off pieces having the same thickness and machined square edges were tack welded on to the start and the end of the weldment so that welding started and finished on the stainless steel plates. After welding, the weldments were removed by milling away the fillet welds, and the jig surface was remachined in preparation for the next test. All plates were similarly positioned so that the heat sink effects were similar and the welding conditions were maintained constant as far as possible for each set of welding operations.

3.4 Welding Techniques and Conditions

Welding procedure : A series of welds were deposited by submerged arc (SA) and Metal Inert Gas (MIG) welding processes. Nominal electrode wires and flux compositions are listed in Table 3.3. Welds of two kinds were prepared, i.e. (i) Butt welds and (ii) Bead-on-plate welds.

3.4.1 Butt Welds :

single run butt welds were produced using only the SA welding processes. In these experiments, nominally identical welding parameters were employed for the parent plates, all of which were restrained during welding. Details of parent plates and welding conditions are given in Table 3.4 and 3.5.

3.4.2 Bead-on-Plate Welds : Various bead-on-plate welds were prepared using both the SA and MIG welding processes.

3.4.2.1 SA Welds on AISI 316L : The SA welds were produced by using parent plates in the as received condition, but with different welding heat inputs ; they were varied by altering the current and voltage (implying a varying wire feeding rate), for constant welding travel speed and electrode wire extension (Table 3.6). The welds were prepared for the conditions (1) unrestrained, (2) restrained, (3) rapidly cooled (4) ultra rapid cooled and (5) miscellaneous, as detailed below:

(1) Unstrained Welds : These welds were prepared on parent plates which were simply located by clamping or tack welding them to the base plate of jig.

(2) Restrained Welds : When required the weldments were restrained using a special jig. The parent plates were restrained flat by fillet welding them to the jig prior to the experimental welding operation. The design and use of the restraining jig was discussed in detail in Section 3.3. After welding the welded plates were removed from the jig by milling, and the jig surface was remachined and prepared for further experimental work.

(3) Rapidly Cooled Welds : The rapidly cooled welds were prepared by using special heat abstracting paste based on Bentonite mixed with copper powder and water in a copper jig. This was carried out in order to reduce distortion and increase cooling rate of the weld metal.

(4) Ultra Rapidly Cooled Welds : In the study of delta ferrite formation in austenitic stainless steel, it is common practice

to use the interrupted solidification technique (i.e. rapid quenching of droplets from the liquids - solidus region). For an experimental innovation in the present work complete welds rather than droplets were prepared using the highest possible cooling rate from the liquidus region as follows :

(a) Weld No. 15 RN This weld was prepared in restraining condition while a whole parent plate of as received AISI 316L together with the flux were immersed in the liquid nitrogen at least for 10 minutes before and after welding.

(b) Weld No. 18 FN This weld was prepared in the same manner as for weld No. 15 RN except that, the flux and the weld area were protected from direct contact with the liquid nitrogen.

(5) Miscellaneous Conditions

(a) Weld No. 16 R : This weld was prepared on a cold rolled parent plate in restrained condition. This was carried out in order to examine the effect of unrelieved stress in the deformed parent plate on the micro-structural variation of weld metal.

(b) Weld No. 250RH : This weld was prepared in a situation where the as received condition parent plate and flux were both preheated for 1 hour at 300^{o}C before welding. This was carried out in order to examine the effect of preheating on the micro-structural variation of weld metal. The parent plate was in restrained condition.

3.4.2.2 MIG Welds produced on different types austenitic stainless steels

Various Bead-on-plate welds were prepared using MIG welding. The welds were prepared with the following conditions.

(i) Nominally identical welding conditions but parent plates with different characteristics

Several Bead-on-plate welds were prepared using nominally identical welding conditions but using parent plates with different characteristics. Details of the parent plates and welding conditions are given in Table 3.7.

(ii) Fully austenitic stainless steel welds using parent plates with different characteristics and similar welding parameters.

Parent plates of AISI type 304, 316L and 321 steel with different mechanical and microstructural characteristics were used. MIG welds were prepared with the addition of nitrogen gas to the argon atmosphere of the shielding gas to encourage austenite formation. Details of the parent plate and welding conditions are given in Table 3.8.

3.5 Mechanical Testing

The weldments and their parent plates were evaluated using tensile, charpy-vee-notch impact (CVN), and micro hardness tests.

3.5.1 Charpy Impact Test.

CVN testing was carried out in accordance with British Standards B.S.131 Part 2 1959 and B.S.709 - 1964. After preliminary trimming and cutting eight charpy blanks (10 x 10 x 55mm) were machined from each parent plate and six from the associated butt welds for testing at room temperature (293k) and 77k. The blanks were then notched (2mm depth at 45^{o} angle) with the notch located at the centre of the transverse cross-section of the weld metal, perpendicular to the plate surface as illustrated in Fig.3.1. Every specimen was checked with the Avery charpy caliper B.S.131, and tested in accordance with British Standard B.S.131, Part 2. In the present work the charpy-v-notch impact test results are

given in terms of energy absorbed (Joules) and lateral expansion (mm) as shown in Fig.3.2 in accordance with B.S. 131 Part 2 and ASTM A370[120] respectively. The lateral expansion requirement is based on the American Society of Mechanical Engineers (ASME) pressure vessel code adopted from the charpy-v-specimens. For stainless steel tested at cryogenic service temperatures 27J and 0.38mm (0.015 in) lateral expansion are often the minimum acceptance standards for charpy-v-notch impact energy and lateral expansion respectively. This requirement has been correlated with the data obtained from the ferritic steels and has the advantage of automatically compensating for different levels of material strength and weld or specimens thickness. This code was chosen because it offers a good possibility for estimating fracture mechanics values without the need for expensive and complex experiments.

3.5.2 Tensile Testing

Tensile tests of parent plates and weld metals were carried out at room temperature (293k) and 77k in accordance with British Standards B.S.709 - 1964 and B.S.4165 - 1971. The parent plate tensile test specimens were oriented in the longitudinal direction. For welds the specimens were oriented along the length of the welds, so that the entire sample was from an all-welded metal joint. An Instron 1185-100kN. capacity machine was used. The lowest crosshead speed ($0.5\frac{mm}{min}$ or $8.3 \times 10^{-4} \frac{cm}{sec}$) was chosen to minimise the localised heating of the specimen during testing at 77k. The test was performed by direct immersion in liquid nitrogen in specially made equipment similar to the cryostat described by Read, Reed and Schramm.[121] Specimens of every plate were tested at 77k in duplicate..

3.5.3 Micro-hardness Testing

A hardness evaluation was carried out using a Vickers micro-hardness tester on transverse cross-sections of the welds and parent plates.

The specimens were lightly etched and a 200g, load was used for the measurement. Hardness values were determined as the mean of a minimum of five different indentations in each case.

3.6 Metallography

A variety of metallographic techniques was used to characterise and quantify the micro-structure of the welds and their parent plates. In this context it was important to distinguish between solidification occuring either by primary ferrite or primary austenite formation in weld metals, i.e. if the ferritie was located at the dendrite core or cell boundaries.

3.6.1 Optical Microscopy

Samples of metallography were prepared by conventional metallography techniques, i.e. grinding with silicon carbide paper followed by polishing with diamond pastes. In all cases mirco-structural studies were carried out on the transverse cross sectional area, unless specifically indicated otherwise. Three dimensional views of specimen preparation are schematically shown in Fig.3.3.
Various etching reagents were used as listed in Table 3.9. However, on the basis of reproducibility, contrast and ease of use, for light microscopy and SEM examination, samples were in most cases etched electrolytically with a 10% aqueous solution of ethanedioic acid (oxalic acid $C_2O_2(OH)_2$) unless otherwise indicated. This etching reagent preferentially attacks the ferrite/austenite inter-phase boundaries, whilst increasing etching time it reveals austenite grain boundaries as well as ferrite phases.

Furthermore, by increasing the etching period it can also reveal strain-induced martensite. However, if the specimen contains ferrite this procedure leads to considerable surface relief and pitting, which make metallographic examination difficult.

Quantitative metallography for grain size measurements was

carried out using a mean linear intercept measurement technique with test pattern of either circular or straight parallel lines. The circular pattern consisted of three concentric, and equi-spaced circles having a total circumference of 500 mm , the linear pattern comprised five parallel straight lines 500 mm length. These patterns were applied to five successive randomly selected fields and five readings were made for every field.

Quantitative information on the proportion of delta ferrite in the weld metal was produced using Quantitative Television Microscopy (Q.T.M.) process, the ferritescope and the point counting procedure.

For ferrite measurements the most reliable etchant was found to be Murakamis etchant which clearly resolved the delta ferrite without darkening the adjacent austenite or revealing other structural characteristics of the weld metal. The transverse cross sectional area of each weld was examined, photomicrographs were taken at 1000X magnification of ten randomly selected fields. A field of 368 points spaced lattice was superimposed on a photomicrograph of 75 x 114 mm, and the measurement of delta ferrite content made by counting the number of lattice points in each field that coincides with an area of ferrite whilst carbides and inclusions were excluded. At the selected magnification each particle of ferrite to be counted coincides more or less with a single lattice point.

The measurements were analysed using standard statistical procedures, i.e. mean values ($\bar{X}$) and variances (σ^2) and the results of the analysis are given in Section 4.

3.6.2 Scanning Transmission Electron Microscope (S.T.E.M.) Analysis

Transmission electron microscopy T.E.M.) studies were conducted on some of the welds and parent plates with both the JEOL 100 C and the EM 6 electron microscopes.

The solidification sequence of austenitic stainless steel weld metal has been studied using STEM analysis. It was conducted on the JEOL 100 C unit equipped with a computer controlled dispersive X-ray spectrometer with a link system 860 analyser. The RTS, FLS programme was used for composition analysis from the integrated intensities derived from the intensities of the characteristics peaks of every element considered. Typical counting times were 100 seconds. The STEM advantages for microprobe work over electron probe microanalysis (EPMA) and scanning electron microscopy (SEM) are due to a combination of a fine spot (beam) size, higher acceleration voltage (100 kv) and the use of thin foil specimen ($< 0.1 \mu m$), these offer the possibility of elemental resolution of < 10 nm.

The primary concern for this study is the nature of the concentration profile measured in the region analysed. For simplicity in this analysis, the weld metal specimens were treated as Fe - Cr - Ni ternary systems, excluding other elements e.g. Mn, Si, etc. The sum of the Mn and Si content is < 2 wt%, and since they were expected to partition to some extent within ferrite and austenite the values for Cr and Ni obtained are probably 2% higher than true values. Similar assumptions also apply to Mo.

Assuming the steels are ternary alloys, the measured intensities

were converted to compositions using the relation :

$$C_{Cr} = I_{Cr} K_{Cr} / I_{Cr} K_{Cr} + I_{Ni} K_{Ni} + I_{Fe} K_{Fe} \qquad (3.1)$$

where :

C_{Cr} = concentration of the element

I_{Cr} = net peak intensity of Cr

K = calculated correction factor (the values of K were determined analytically by RTS, FLS programme so that the analysis does not require the use of standard

I_{Fe} , I_{Ni} = net peak integrals of these elements in the specimen

K_{Ni},K_{Fe} = correction factors for Ni and Fe in the specimen

Two similar equations can be written for Ni and Fe. It is further assumed that $C_{Fe} + C_{Ni} + C_{cr} = 1$.

The foil programme used does not consider absorption in the chemical analysis, since foil thickness corrections are not made. However, since Fe, Cr and Ni have similar mass absorption coefficients their intensity ratios are not largely affected.

3.6.2.1 TEM Specimen Preparation

The orientation of samples used for TEM and STEM thin foil specimens was transverse cross section. The specimens were ground to a thickness of 0.2 mm using rotary wheels, usually both sides of the specimens being equally ground to a 600 mesh finish. A jet (Struer's Tenupol") and window technique was used as a thinning process. Either a solution of 1000 ml Glacial acetic

acid, 42 ml perchloric acid (72% strength) and 8 ml distilled water or a solution of 10% perchloric acid (72% strength) in dry methanol was used (Table 3.9). After polishing, the specimens were washed by a direct jet of distilled water followed by a similar washing in methyl alcohol (methanol) then dried between absorbent tissue.

3.6.3. Scanning Electron Microscope (SEM)

SEM studies were conducted on some of the weld metals and parent plate on a Cambridge instrument "S 250 microscope" fitted with a computer controlled energy dispersive micro-probe system. Fractographic studies were carried out using 25 kv accelerating voltage and 35^{o} tilt angle. Several broken charpy specimens minimum and maximum impact energy and some of the tensile test specimens selected from every parent plate and the associated weld metals. Microanalysis were made to study the chemistry of inclusions, i.e. second phase particles.

4. Experimental Observations and Results

4.1 Characterisation of Parent Plates

4.1.1 Microstructural Considerations

4.1.1.1 General Features

The microstructural features of the parent plates were influenced by (a) the severity of etching reagent, and (b) the initial thermomechanical treatment associated with every plate.

(a) The Effect of Etching Reagent

The following etching methods were employed to prepare the microstructure of different parent plates.

(i) Electrolytic etching with oxalic acid: specimens were etched electrolytically in a 10% aqueous solution of oxalic acid using a potential of 6 V. In the course of the experimental work it was noticed that the resistance of materials to the etching reagent varied according to the steel specification and the thermomechanical treatments employed, i.e. the cold rolled plates had the least and hot rolled solution treated had the highest resistance to the etching reagent. For the same etching conditions, the form r was heavily etched whilst the latter exhibited a microstructure suitable in contrast for optical microscopy.

Furthermore, it was noted that the microstructure revealed by this etching reagent was time-dependent, i.e. the degree of contrast and the nature of the microstructural features revealed were changed by increasing the etching time.

The parent plates of AISI 316L and 321 in the as received condition were etched electrolytically with standard etching

procedures, and an etching time of about 20 seconds. . .
They exhibited microstructures consisting of equiaxed/twinned austenite grains with contrast suitable for optical microscopy as illustrated in Fig. 4.1.

Microstructural studies on the AISI 321 revealed the presence of fine cubic particles with the appearance and colour of typical titanium carbonitride illustrated in Fig.4.2. The general matrix analysis and the composition of these particles were analysed by EDAX analysis as shown in Fig.4.3 and 4.4. Carbon and nitrogen were not however identified.

(ii) Chemical Etching with Mixed Acid

Etching the parent plate in a as-received condition with this etching reagent revealed microstructures consisting of equiaxed twinned austenite grains. Increasing the etching period revealed a cored structure superimposed on the original equiaxed austenite structure as illustrated in Fig.4.5.

(b) The Effect of Thermomechanical Treatments

(i) Cold Rolled Plates

Etching the cold rolled plates with 10% oxalic acid revealed heavily deformed austenite grains with copious lines of slip as expected. Increasing the etching period revealed a typical deformed structure with the randomly distributed blocky structure as illustrated in Figures 4.6 and 4.7.
Etching with the mixed acid for a longer period revealed a typical deformed structure in conjunction with the cored structure and strain patterns.
The microstructure of AISI 321 plate was similar to the corresponding material for AISI 316 plate but with the presence of some titanium carbonitride particles.

(ii) Hot Rolled Plates

Etching the hot rolled plates with the standard etching procedure in 10% oxalic acid revealed a uniform recrystallised structure with some areas of grain growth as illustrated in Fig.4.8.

At high magnification dispersed precipitated particles were revealed distributed both randomly within the austenite grains and selectively along slip lines and the grain boundaries as illustrated in Fig.4.9.

In addition to the fine precipitated particles, other second phase particles were also observed in different specimens. Typical particles viewed in the SEM are illustrated in Fig.4.10. EDAX spectra for matrix and selected particles are given in Figs.4.11 and 4.12.

These spectra show that the particles varied in composition and the elements identified included Cr,Ni,Si, S, and Mn.

Unfortunately carbon and oxygen could not be identified using the equipment available, but the spectra were consistent with the view that the particles were oxides and silicates. The microstructure of AISI 321 plates were similar to the corresponding materials produced for AISI 316L plates with the exception that cubic particles of titanium carbonitride were present.

Longer time etching with mixed acids revealed a cored structure superimposed on the original equiaxed austenite structure as illustrated in Fig.4.13. Furthermore, microstructural studies revealed that the degree of coring varied from plate to plate. In this context, the AISI 316L exhibited more cored structure than the AISI 321.

The influence of the thermomechanical treatments employed on degree of coring was as follows. The specimens prepared from the hot-rolled, furnace-cooled AISI 316L plates exhibited the most severe cored structure as illustrated in Fig.4.14. Whilst specimens prepared from hot-rolled plates with solution treatment after hot-rolling exhibited the least coring. Further microstructural studies of long-time solution-treated specimens of AISI 316L, i.e. 4 hours at 1150^{o}C showed

that, despite the long period of solution treatment the cored structure has not been completely removed.

Microstructural studies of hot rolled plates at 950°C revealed recrystallised austenite grains together with some second phase particles and a cored structure as illustrated in Figure 4.15-4.17.

On comparing different steel plates, it is noticed that the amount of martensite formed in cold rolled plates AISI 316L and 321 were0.25% and 1% respectively.

4.1.1.2 Austenite Grain Size Measurement

The austenite grain size of all of the parent plates were measured quantitatively. Only whole grains were included in the counts and twins were ignored. The results are given in Table 4.1.

As expected, the austenite grain size was determined by the degree of recrystallization that had occured which in turn depended on the thermal and mechanical treatments given to the materials. Generally the hot rolled plates at 1150°C had the coarser and more variable grain sizes.

4.1.1.3 Scanning Transmission Electron Microscopy (STEM)

The prepared thin foils quite often exhibited irregular edges. A typical electron micrograph is illustrated in Figure 4.18. This was taken to indicate some residual inhomogenity inherited from the as-cast metal structure which had persisted through hot-rolling.

In all of the materials examined the microstructure consisted of elongated grains. Carbide particles were visible at the grain boundaries of the hot-rolled plates.

All plates exhibited high dislocation densities at high magnification.

Dislocations were generally distributed within the austenite grain as cellular networks and piled up at the grain boundaries. Their degree of cellular network depends on the employed thermo-mechanical treatment. Typical micrographs of different specimens are illustrated in Figs. 4.19 and 4.20.

The cold rolled plates exhibited a high density of dislocations and elongated bands which appeared as an internal defect. At lower magnification they formed parallel lines, apparently orientation dependent as illustrated in Fig.4.21. Further detail could be resolved at higher magnification within these bands. Fig.4.22 illustrated typical micrographs of these bands which could be deformation twin bands. Their thickness varied in different regions and no precipitated particles were observed on these bands.

Electron diffraction patterns taken from foils representing heavily deformed plates exhibited streaky spots as in the example given in Fig.4.23 indicating microstrain reflecting internal stress.

4.1.2 Mechanical Properties

(a) Charpy tests : A minimum of eight impact test specimens from every plate were tested at room temperature and in cryogenic conditions with liquid nitrogen i.e. at - 196^{o}C. The results are given in Figs.4.24 and 4.25. The highest impact energies were obtained with the specimens prepared from plates hot rolled at 1150^{o}C (plates Z and H), whilst much lower impact energies as expected obtained with the plates rolled cold or at 400^{o}C. Rolling at 400^{o}C slightly improved the ductility of AISI 316 steel. The plates in the as-received condition yielded high impact energy values but with a wide scatter of the results. Lateral expansion values of

different parent plates impact test specimens tested at cryogenic conditions (77 k) are given in Table 4.2.

(b) Tensile Tests

A minimum of four specimens from each plate were tested at room temperature and in cryogenic conditions with liquid nitrogen. The results are given in Table 4.3.

The room temperature results revealed that reducing plate rolling temperature increases the yield strength, i.e. the cold-rolled plate has the highest strength at the expense of ductility. However, rolling at 400^{o}C produced a combination of very high strength and reasonably good ductility.

The results for cryogenic conditions revealed that, in this condition both strength and ductility are increased. The cold-rolled plate had the highest strength but the plate rolled at 400^{o}C had almost as high strength as the cold-rolled plates but with higher ductility.

The stress/strain curves of most of the specimens tested in cryogenic conditions (-196^{o}C) showed that the yield was followed by a high rate of work hardening.

A significant observation made during testing at cryogenic temperature was the appearance of serrations in the stress/strain curves for samples from the hot-rolled plates H and Z(AISI 321 and 316L,respectively), indicating discontinuous work-hardening associated with the thermo-mechanical treatment in these plates.

(c) Fractography

Fracture surfaces from both charpy and tensile tests selected to represent material with high and low strength and ductilities were examined. All of the fracture surfaces exhibited dimples indicative

of ductile fracture with some microcracks.

Further work was carried out to study the cause of microcracks in broken charpy impact test specimens. SEM analysis results on fracture surface of hot-rolled plates at 950^{o}C revealed the presence of second phase particles within the cracks. The general matrix analysis and the composition of these particles were analysed by EDAX analysis as illustrated in Fig.4.26 (a to d). EDAX spectra obtained for these particles revealed that they were mainly consisted of Ti and/or Al,Si.Carbon and nitrogen were not however identified.

Microstructural studies were performed on some gently polished and etched fracture surfaces of tensile test specimens. The results showed that; (i) The microcrack (decohesion) were mainly initiated by the fracture of second phase particles, and by their separation from the matrix along the common interface as illustrated in Fig.4.27 (a to c). (ii) Some microcracks were also nucleated at the grain bounderies as illustrated in some of the micrographs at Fig.4.27. Microstructural studies of fractured specimens showed that, after the onset of necking the cracks developed into cavities which coalesced and leading to final separation as illustrated in Fig.4.28.

(d) Hardness Tests

Microhardness test survey was carried out for each sample from every parent plate. Fig.4.29 shows the average value of five different readings obtained from each sample.

The hardness values varied from plate to plate in accordance with their employed thermomechanical treatment (i.e. degree of recrystallization, precipitation and strain hardening). The cold-rolled plates had the highest hardness and plates rolled with the highest rolling temperature

had the lowest hardness value. Referring to the plates in the as-received condition, they yield a high and wide scatter hardness value.

4.2 Characterisation of Welds

4.2.1 Microstructural Consideration

The nominal composition of some of the welds selected to study their microstructures in this investigation are shown in Table 4.4.

Transverse sections from welds produced by S.A and MIG welding techniques were polished and electrolytically etched in an aqueous solution of 10% oxalic acid for metallographic examination. Other sections were etched in concentrated mixed acids for macroscopic observation.

For quantitative assessment of the proportion of delta ferrite the sections were etched with Murakamis' reagent.

The etching characteristics were sensitive to (i) the specification and condition of the materials. (ii) the period of etching and the strength of the etching reagent. These variables were adjusted to reveal the desirable microstructural features.

Welds produced on AISI 316L were more resistant to etching than those produced on AISI 321. Welds produced on cold-rolled plates and welds with fully autenitic structures were heavily attacked by the etching reagent and their microstructure was exposed more quickly than other welds.

The effect of varying the etching period were as follows:

1. A six seconds exposure to electrochemical etching revealed the detailed microstructure of weld metals, but had little effect on the heat-affected zone or on the parent plate.
2. More prolonged etching increased the contrast and depth of

attack - this revealed the H.A.Z. and parent plate microstructure.

3. Further prolonged etching was needed to reveal the dendritic solidification pattern together with H.A.Z. structure for viewing at lower magnification.

In addition to optical microscopy, the microstructural studies were carried out by scanning electron microscopy. The advantage of the SEM over the optical microscope are :

1. The SEM discriminates between delta ferrite which appears white and other minority phases present.
2. The SEM reveals whether or not the delta ferrite phase stands proud of the surface in the etched microsection.
3. The SEM reveals any internal fissures or interphaseseparation between delta ferrite and the austenite matrix.

In the following sections detailed descriptions of microstructural observation of different welds are given for the four main categories of welds as follows:

(i) SA bead-on-plate welds of duplex structure.

(ii) MIG bead-on-plate welds of duplex structure.

(iii) MIG bead-on-plate welds of austenitic structure.

(iv) SA butt welds of duplex structure.

4.2.1.1 S.A. Bead-on-Plate Welds of Duplex Structure

Several welds were prepared to assess the influence of three main variables:

1. The effect of restraining the parent plate
2. The effect of heat input
3. The effect of cooling rate

1. Unstrained Air-Cooled Welds with Different Heat Inputs

These welds were identified as F1, F4, F7 and F 12 in decreasing order of heat input.

For high heat input welds, large wide growth units of columnar dendrites growing from the fusion boundaries separated by a central region i.e. axial or raft structure. For low heat input the growth units changed direction towards the top surface of the weld with no central line structure. These structures are illustrated in Fig.4.30 (a and b). A further difference was evident in solidification growth mode of the welds near the fusion boundaries and where for high and low heat inputs there was a greater tendency towards columnar dendrites and cellular dendrites structure respectively.

The welds exhibited the ripple bands which were becoming less pronounced towards the weld centre. The close inspection of the rippling proved in this region that the austenite matrix was preferentially etched away leaving a continuous network of proud delta ferrite phase as illustrated in Fig.4.31. Furthermore, the absence of discrete bands of solute enrichment which give rise and characteristic of light or dark lines formed on etched surface of welds were noticeable in this investigation. Micro-structural studies at higher magnification revealed differences between the microstructure of welds produced using different heat inputs. For high heat input welds the individual ferrite dendrites were elongated with wide well developed secondary and tertiary arms. Individual dendrites were separated by a narrow band of austenite as in Fig.4.32. For lower heat inputs the ferrite morphology was of the form similar to vermicular ferrite as defined by David et al. [87] The ferrite dendrites were less well developed than those in high

heat input welds and were separated by wide bands of the austenite matrix containing isolated dispersed ferrite as in Fig.4.33.
Fig.4.34 shows micrographs of three mutually perpendicular sections through the high heat input weld. This set of micrographs gives a three dimensional impression of the ferrite morphology and illustrates the growth of the dendrites in the transverse cross section, i.e. in the opposite direction to the direction of heat extraction through the parent plate.
For high heat input welds the ferrite content varies in different regions along the length of the weld bead and in the transverse cross sectional area. For instance, the ferrite content increases slightly along the length of the weld towards the end, and in transverse cross section the upper part of the weld (nugget) has higher ferrite content than the lower part. This could possibly be due to the variation in cooling rate and dilution with parent plate.
Occasional second phase particles (i.e. oxides) and internal microfissure were observed, but they were not determined quantitatively.

The proportion of delta ferrite determined by quantitative metallography (QTM), 10 line optical microscopy technique and/or by the ferritescope are given in Table 4.5.

The ferrite content represents the mean of 20 reading by QTM, 10 different region by optical microscopy and/or 5 point counting by the ferritescope. Fig.4.35 illustrates a typical micrograph of selected area for QTM reading. Value for ferrite content measured by QTM are generally higher than the correasponding values measured by the ferritescope. Comparison of the SEM and the optical microscopy microstructural observation revealed that, in the former second phase particles and internal microfissure were simply distinguished, while in the latter it is difficult to distinguish them from the ferrite phase.

Typical second phase particles embodied in ferrite phase and some internal microfissures are illustrated in Fig.4.36.

Comparison of different weld ferrite content revealed that the ferrite content increased with increasing heat input (decreasing cooling rate), that is 7.5% and 5% ferrite for the highest and the lowest heat input respectively.

2. Restrained Air-cooled Welds with Different Heat Inputs

These welds were identified as R_8, R_9, R_{10} and R_{11} in decreasing order of heat input. The columnar growth units for restrained welds were generally smaller and not so strongly oriented as for the corresponding unrestrained welds.

For high heat inputs the columnar dendrites growth directions were toward the centre and top surfaces of the welds. The columnar growth on either side did not extend to the central plane but was separated by a central region of randomly oriented equiaxed dendrites around the weld axes as illustrated in Fig.4.37(a).

The solidification growth mode of the welds near the fusion boundaries towards the centre of weld was cellular to cellular dendritic type structure. One point of differences between restrained and unrestrained welds was the appearance of an undulating pattern in the structure near the fusion boundaries in some of the restrained welds especially for high heat inputs as illustrated in Fig.4.37(b).

Microstructural studies at higher magnification revealed that for high heat input welds the ferrite dendrites were well developed but occasionally with some ferrite side-plate morphology. In the central region with the axial structure some less well developed ferrite dendrites were present. Despite slight mis-orientation they maintained their general directionality within the weld axis.

The general appearance of the microstructure of these welds was consistent with multiple fracture of the columnar units of dendrites leaving isolated fragments of ferrite in the inter-dendritic region as illustrated in Fig.4.38.

For low heat inputs, the general growth directions were towards the top surface of the welds with no zone of axial structure but with a large quantity of cellular type pattern structure present.

By reducing the heat input the solidification growth mode changed to more irregular cellular pattern in which the orientation of the dendrites was less directional with a ferrite structure similar to the vermicular morphology. Another microstructural feature associated with these welds was the presence of isolated ferrite in the austenitic matrix. Towards the central region of the weld the microstructure changed to discontinuous columnar growth units with better developed dendritic arms.

Oxide particles were visible similar to those observed in the unrestrained welds; and the microfissuring was more pronounced. No quantitative measurement of these features were made.

The weld structures also exhibited ripple bands with the same characteristics as those observed in the unrestrained welds.

The proportion of delta ferrite determined by quantitative metallography and by the ferritscope are given in Table 4.5 showing a slight increase in ferrite content with increasing heat input, i.e. 7% and 6% ferrite for the highest and the lowest heat input respectively.

3. Rapidly Cooled Welds with Different Heat Inputs

These welds were identified as C_3, C_5, C_8 and C_{13} in decreasing order of heat input. For high heat inputs growth directions of the columnar dendrite were towards the centre and top surfaces of the welds. The columnar growth from the fusion boundaries on either side did not extend to the central plane, but were separated by a central region (i.e. an axial structure, or a raft structure). The microstructure of central region consisted of directionaly oriented dendrite type ferrite along the weld axes as illustrated in Figure 4.39.

Near the fusion boundaries the welds contained elongated dispersed ferrite forming a general pattern of cellular dendritic type solidification growth mode. Comparing the microstructure of different regions it appears that in these welds the dendrite growth units become longer and wider as they grow inwards as illustrated in Figure 4.40.

The general microstructural appearance was that the dendrites arms were not well developed and were separated by wide bands of austenite matrix with isolated dispersed ferrite. The ferrite dendrites exhibited a misoriented vermicular type morphology mostly with open arms (branches) with some lath type structure. In some of the dendrites the spines were not straight but undulating. Towards the central region the ferrite dendrites were better developed, slightly misoriented and separated by wide areas of austenite. Figure 4.41 and 4.42 illustrate typical microstructures of region near the fusion boundaries and from upper part of the weld in transverse cross sectional area respectively.

For low heat inputs the growth units changed direction towards the top surface of the weld. Microstructural studies of the fusion boundaries revealed the presence of elongated type ferrite with no symetrical side branch structure as illustrated in Fig.4.43. The ferrite dendrites became coarser and wider with some side plate (lath) morphology as they grew inwards as illustrated in Fig.4.44.

A significant observation associated with welds produced with higher cooling rates was the lack of development of dendrite arms and the presence of wider austenitic bands separating the ferrite dendrites with some isolated ferrite in the inter-dendrite region.

Oxide particles with internal fissures were observed occasionally. Microfissures were present mainly at the austenite/ferrite boundaries but also, within the inter-dendrite region of the austenite matrix.

The proportions of delta ferrite determined by quantitative metallography and by the ferritescope are given in Table 4.5. The ferrite content of various welds produced with different heat input varied between 5.5% and 7%.

4. Ultra Rapidly Cooled Welds

The welds 15RN and 18FN of group four were produced with the highest possible cooling rates. As described earlier, the former was produced while both the parent plate and flux were in contact with the liquid nitrogen. The latter was produced while only the parent plate was in contact with liquid nitrogen; that is the flux and weld metal were protected from any contamination and possible direct contact with liquid nitrogen.

(a) Weld Metal 15RN

Microstructural studies of this weld revealed the presence of four distinct regions.

(i) A thin region of cellular dendritic type pattern structure adjacent to the fusion boundaries consisting of elongated ferrite without a clear side arm (branch) morphology.

(ii) An intermediate region exhibiting columnar dendritic pattern. Microstructural studies revealed better developed but disoriented dendrites of ferrite with some side branching giving a cellular structure. As the dendrites grew inwards the side arms became more clearly defined.

(iii)A central region with a cellular - dendritic pattern structure. At higher magnification segregated impurities were revealed within the dendritic structure. There was no distinct ferrite morphology in this region as evident in Fig.4.45. Optical and SEM examination in this region failed to detect the ferrite usually expected in weld.

(iv)The central region of the weld cap where the ferrite was predominantly of a blocky type pattern with a ferrite of cellular morphology within the blocks.

Because of uncertainty in the distribution and inconsistency in the morphology of the ferrite in this weld quantitative microscopy was inappropriate but the proportion of ferrite determined by the ferritescope was found to be about 2%.

(b) Weld Metal 18FN

Examination at low magnification revealed that the solidification growth directions were towards the top surfaces of the weld. Near the fusion boundaries a cellular type structure with elongated ferrite was observed. The dendrite arms became more clearly defined as they grew inwards as illustrated in Fig.4.46.

In the fusion boundaries region many elongated ferrite dendrites were present some with lath type structure but with no symetrical cellular side branch development as illustrated in Fig.4.47.

In the central region instead of well developed dendritic type structure there was a vermicular ferrite well separated by austenite matrix which contained some isolated ferrite as illustrated in Fig.4.48. The ferrite content as determined by the ferritescope was in the range of 2.5 - 4%.

5. Miscelleneous Welds

(a) Weld Metal 16R : This weld was produced in cold rolled plate in the restrained condition.

At low magnification a cellular pattern solidification growth mode was observed with the general direction towards the top surface of the weld.

Near the fusion boundaries, elongated ferrite dendrites with different orientations were present, some with no symetrical side branch arms as illustrated in Fig.4.49.

Further into the weld the microstructure changed to disoriented ferrite similar to vermicular type morphology with open arms. These dendrites were poorly developed and the austenite matrix contained some randomly distributed isolated ferrite as illustrated in Fig.4.50.

Towards the centrel region the ferrite dendrites became more elongated and wider as they grew inward but,there were also some discontinuous

columnar units of dendrites, leaving isolated fragments of ferrite in inter-dendritic regions as illustrated in Figure 4.51. Near the top surface and central region there were many units of the cellular (blocky) pattern structure with randomly oriented ferrite networks. The proportion of delta ferrite determined by quantitative metallography and ferritescope was in the range of 5 to 7%.

(b) Weld Metal 250RH: This weld was produced with both parent plate and flux preheated for one hour at 300^{o}C.
Low magnification revealed a cellular pattern solidification growth with the general direction towards the top surface of the weld. Higher magnification revealed elongated ferrite near the fusion boundary.Away from the fusion boundaries the dendrite arms developed in preference to the spine leading to a general microstructure of the vermicular ferrite type with well-developed arms.

Typical micrographs illustrating the ferrite morphology in the fusion boundary region and the middle of the weld are given in Figure 4.57(a)and(b) respectively.

The proportion of delta ferrite determined by quantitative metallography and ferritescope was found to be about 6.5.

4.2.1.2 MIG Bead-on-Plate Welds of Duplex Structure

Duplicated welds were prepared on AISI 316L and 321 using similar welding conditions, but with parent plates of different characteristics as follows:

(i) As-received condition, solution-treated plates,

(ii) Cold-rolled plates,

(iii) Hot-rolled plates

The objective of these tests was to assess the effect of different parent plate characterisation on the weld metal microstructure i.e. ferrite morphology and content. Nominally identical welding parameters, i.e. similar heat input and standard procedure of pure Argon shielding atmosphere were used.

4.2.1.2.1. Weld Metal Produced on AISI 316L Parent Plate

(i) As-received condition, Solution-treated Plates:

These welds were identified N1 and M1. Low magnification microstructural studies revealed the presence of mostly elongated ferrite in the fusion boundary region together with some ripple bands.

SEM studies revealed relief in the ripple band region. In this region the austenitic matrix surface was preferentially etched leaving a continuous network of the delta ferrite phase.

The growth unit direction was from the fusion boundaries towards the top surface of weld with no central line structure. Towards the central region elongated and blocky pattern ferrite were both present. The ferrite formed a pattern surrounded by austenite exhibiting a cellular dendritic type structure as illustrated in Fig.4.53.

At higher magnification both disoriented short and elongated ferrite was observed, exhibiting a vermicular morphology, some with lath type structure appearance. Further inwards from the fusion boundaries the microstructure changed to more developed formed vermicular ferrite as inward growth proceeded.

(ii) Cold-Rolled Plates

These welds were identified T1 and T2 : they exhibited a cellular -

dendritic type structure grown from the fusion boundaries towards the top surface of weld with no central line structure. Away from the fusion boundaries the ferrite formed a cellular structure of more equiaxed block-like pattern as inward growth proceeded.

High magnification microstructural studies revealed the presence of complex ferrite morphologies. Further inward from the fusion boundaries the ferrite dendrites appear to be more developed but with a combination of vermicular and lath type morphologies as illustrated in Figure 4.54. Towards the centre, blocky type patterns structure with cellular ferrite network, within the block, were observed. These blocks were embedded in the austenite matrix which formed grooves around them as illustrated in Figure 4.55.

Internal fissures, and oxide particles were observed associated mainly with the surrounded austenitic matrix rather than the ferrite phase.

(iii) Hot-Rolled Plates

These welds were identified Z_1 , X_1 , Y_1 and S_1 . Near the fusion boundaries the solidification substructure was of the cellular dendritic type. In regions away from the fusion boundaries toward the centre, the solidification substructure changed to a cellular pattern morphology.

Higher magnification microstructural studies revealed some differences between the microstructure of these various welds. The details were as follows:

Weld Z_1 Directionally oriented ferrite was observed in the fusion boundaries and fine cellular structural patterns were observed away from the fusion boundaries as illustrated in Figure 4.56 and 4.57

respectively. The ferrite in the fusion boundaries maintained its directional orientation and on the whole the general directional solidification orientation was towards the top surface of weld metal.

Higher magnification revealed both short and disoriented ferrite dendrites mainly with vermicular morphology, but with not very well developed arms (branches) as illustrated in Fig.4.58. No relief was developed in the etched microsections, i.e. the ferrite did not appear as a relief phase.

Welds X and Y : Low magnification revealed a cellular solidification substructure. High magnification revealed vermicular ferrite and lath type ferrite morphology as illustrated in Fig.4.59. Internal fissures and oxides were visible similar to the other welds.

Weld S : Low magnification revealed dispersed elongated ferrite (vermicular) with no side branch (arms) and some ferrite with cellular pattern form near the fusion boundaries. Towards the centre, the solidification substructure changed to a cellular dendritic type morphology. High magnification revealed a mostly blocky type pattern structure with lath type ferrite and irregular cellular ferrite network, but not with the ordinary developed dendrites of vermicular ferrite. Usually the individual cells were surrounded by the austenite matrix forming a groove around the cell, but the ferrite network and austenite were not in relief within each cell. Internal fissures and oxide particles were observed as in other welds.

4.2.1.2.2 Weld Metals Produced on AISI 321 Parent Plate.

(i) As-received, Solution Treated Plates.

These welds were identified B_1 and B_2 . Low magnification revealed

randomly distributed ferrite with no clear directionality in the fusion boundaries. For regions away from the fusion boundaries more equiaxed block-like pattern structures were observed as inward growth developed.

In these welds, the ferrite morphologies consisted mostly of a cellular network with some lath type structure within the blocks but there was no vermicular-type ferrite. The block-like patterns were generally surrounded by austenite matrix forming a groove around them.

(ii) Cold-Rolled Plates

These welds were identified K_1 , K_2 and K_3 : Low magnification revealed a cellular type substructure with no elongated growth of dendrites as illustrated in Fig.4.60. Microstructural studies revealed disoriented ferrite forming a cellular structure initiated at the fusion boundaries and developed throughout the whole cross-sectional area of the welds. Figs.4.61 (a,b) illustrate typical micrographs for the cellular growth mode of solidification sub-structure in the fusion boundary region at different magnifications.

The general microstructural feature was of a block-like pattern with complex ferrite morphology within the blocks, i.e. cellular and lath type with no elongated dendritic type ferrite as illustrated in Fig.4.62. Further microstructural studies were carried out in all three mutually perpendicular sections through the weld. Fig.4.63 shows the ferrite morphology in a three dimensional montage assembly and shows the cellular nature of the ferrite network in this weld.

(iii) Hot-Rolled Plates

These welds were identified 3F, 3G, and 3E

Low magnification revealed randomly distributed ferrite with the blocky type pattern in the fusion boundary region. Regions away from the fusion boundaries show an equiaxed block-like pattern structure as inward growth develops. There was a cellular type ferrite network within the blocks with no vermicular type ferrite as illustrated in Figures 4.64 and 4.65.

The proportions of delta ferrite for welds produced by MIG welding are given in Table 4.6. Despite the similarity in welding parameters and welding conditions, the welds produced in cold-rolled plates had higher ferrite contents than the rest of the welds.

4.2.1.3. MIG Bead-onPlate Welds of Austenitic Structure Induced by Nitrogen

Duplicated welds were prepared on austenitic stainless steel AISI 304L, 316L and 321 plates in the as-received condition. The welding parameters used were identical with those described in Section 4.2.1.2 but nitrogen was added using a shielding gas mixture of 95% Ar+5% N2 The addition of nitrogen as a strong austenitic stabiliser was expected to alter the compositional balance, and consequently modify the solidification mode to a primary solidified austenite with no subsequent solid phase changes.

Examination of these welds revealed some differences between their microstructure as follows:

(i) AISI 304L Welds:

Low magnification revealed that the solidification substructure growth units grew from the fusion boundaries with orientation towards the top surface of the weld.

The general microstructural feature was a dendritic type pattern within the coarse austenite grains as illustrated in Fig.4.66.

Examination at higher magnification revealed austenite grain boundaries and many spots like microstructural features inside the austenite grains. Generally both the austenitic grains and the arrays of spots within the grains maintained their directionality as growth units developed Fig.4.67. The peculiar substructures inside the austenite grains evident in Fig.4.66 could possibly be as a result of coring and/or directionally-oriented etch pits in the weld. However, further work is needed to study them in greater detail.

No ferrite could be detected in this weld using the ferritescope.

Second phase particles and some internal fissures were observed in this weld but they were not assessed quantitatively.

(ii) AISI 321 Welds

Examination of the fusion boundary region at low magnification revealed narrow bands of elongated microstructural features with varying orientation. At higher magnification, a dendritic type structure was revealed with a similar appearance to the delta ferrite observed in duplex weld metal. Under SEM examination no relief was observed in the etched microsection, but there were grooves on the dendrites as illustrated in Figs.4.68 and 4.69. This is a contrast with the structure of ordinary weld metal with a duplex structure in which ferrite was observed standing as a proud phase in the austenite matrix.

Examination of other regions away from the fusion boundaries revealed the same microstructural feature but with a different morphology. The feature was distributed more uniformly in the cellular and isolated forms

with no relief as in the micrograph illustrated in Figure 4.70.
No clear austenite grain boundary was detected in this weld.

Near the top surface in the central region there were many units of the cellular (blocky) pattern structure forming a groove within the austenitic matrix. The ferrite content varied between 0.5% to 1% in different regions as determined by the ferritescope.

Second phase particles and some internal fissuring were observed in these welds,but these features were not assessed quantitatively.

A significant microstructural observation of these welds with 0.2% nitrogen content was the presence of a narrow band of columnar structure at the fusion boundary and a cellular type structure in the rest of the transverse cross-sectional area. The latter could be partly associated with the grain refinement tendency of Ti and N in this weld.

(iii) AISI 316L Welds

Examination of the fusion boundary at low magnification revealed a narrow band of elongated dendritic type structure. The width of this band of dendrite structure was greater than in the corresponding welds for AISI 321. Examination of regions of the weld towards the centre revealed the structural features illustrated in Figure 4.71 with no distinct austenite grain boundaries and no grooves.

Near the top surface in the central region there were many units of the cellular (block-like) pattern structure in the austenite matrix.

The ferrite content was 1% as determined using the ferritescope.

Second phase particles and internal fissure were observed in this weld. This particular weld exhibited more internal fissuring than any of the other austenitic welds produced with applied nitrogen.

4.3 Submerged Arc Butt Welds of Duplex Structure

Single run square groove joints butt welds were produced. In these austenitic stainless steel AISI 316L and 321 plates of different characteristics were used in the restrained condition. The results were as follows.

Examination of fusion boundary region at low magnification revealed a cellular dendritic type of solidification sub-structure. Examination of other regions away from the fusion boundaries revealed a uniformly distributed cellular-type structure.

High magnification examination revealed that the general micro-structural features and ferrite morphology were almost similar to those described in corresponding bead-on-plate welds. Welds produced in AISI 321 plates consisted mainly of a block type pattern structure with irregular cellular ferrite networks within the blocks. The AISI 316L welds exhibited a more elongated cellular structure. A significant microstructural observation was the presence of a completely cellular type austenitic structure in the central region of some of the high heat input single run 316L welds as illustrated in Fig.4.72.

High heat input welds in deformed plates exhibited many surface marking, i.e. deformation bands or close packed plane in the welds as illustrated in Figs.4.73-4.75 which gives micrographs of the following welds T13 and F_2 from AISI 321, and U_2 from AISI 316L.

The surface marking did not pass through the delta ferrite phase, but there was a continuity between these marks in either side of

the ferrite sometimes with a change in orientation, so that in most cases the numbers of lines were equal.

Second phase particles, i.e. oxides, surface fissure and voids were observed in these welds but the austenite/ferrite inter-phase separation was the most common feature observed in the single-run high heat input welds. Typical micrographs of different welds are illustrated in Figs.4.76 and 4.77. In the defective regions the ferrite dendrites were continuous whilst the cavities and separation were associated with the austenite phase which appeared to be hot-short in solidification.

The results of delta ferrite content measurements of these various welds are given in Table 4.7.

4.4 Microstructural Studies of the Heat Affected Zone (HAZ)

Examination of the HAZ region of different welds revealed that the microstructural features in this region varied from plate to plate. This variation was dependent upon the welding heat input, the parent plate specification and its thermomechanical treatment. The main microstructural features observed in the HAZ region of various welds were :

(i) variation in austenite grain size,

(ii) variation in fusion line,

(iii) variation in internal fissuring and segregations,

(iv) variation in ferrite content.

(i) Welds produced with different heat inputs revealed that the austenite grain size in the HAZ region slightly increased with increasing heat input.

Comparison of the HAz region of different welds produced by MIG welding revealed that the heavily deformed plates exhibited many re-crystallized austenite grains whilst there were virtually no changes of the austenitic grains in the HAZ region of the other plates.

(ii) The weld was generally bonded at the fusion line by a true HAZ of the base metal. However, in sub-arc butt welds produced with high heat inputs, there were some regions in which the weld was bonded to the HAZ with a narrow band of partially melted zone as illustrated in Fig.4.78.

High heat input butt welds produced in deformed plates in the restrained conditions revealed the continuity of austenitic grains and surface marking from the HAZ across the fusion line into the weld as illustrated in Fig.4.79. It is apparent that the grains in the fusion zone grow directly from the unmelted base metal and surface markings, i.e. close packed plane are perpetuated into the fusion zone. This suggests that the weld metal grains grow epitaxially by wetting the partially melted grains in the base metal.

(iii) The degree of fissuring varied from plate to plate but no logical pattern was established.

The segregation (coring) in the parent plate described earlier persisted through the thermal cycle produced in the HAZ by the welding processes.

(iv) Only cold rolled plates revealed a considerable amount of ferrite in the HAZ as illustrated in Fig.4.80, whilst the ferrite

phase was not observed in the parent plate prior to welding. It appears that the presence of ferrite is associated not only with the decomposition of austenite above the AC4 temperature, but also with the nature of the cold rolled plates, e.g. residual strain, finer grain size and higher dislocation density etc, which provide favourable conditions for ferrite formation and/or ferrite retention at room temperature. However, further work is necessary to study the microstructural features of HAZ regions in more detail.

4.5 The Weld Metal Scanning Transmission Electron Microscopy (STEM) Results

Thin foil specimens obtained from the transverse cross sectional area of some of the welds were examined by STEM. This analysis was carried out to clarify some of the microstructural features and to supplement the information derived from optical and scanning electron microscopy. In this context the inclusion chemistry and the solid state partitioning of Cr and Ni in δ ferrite and γ were considered. In accomplishing this, the microstructure of these welds were also characterised.

The solute distribution of chromium and nickel were studied by determining the concentration profiles and more accurately by point count measurements at various locations. The distribution coefficient, Ke,Ie and the segregation ratio, Is for selected elements, were also measured, where :

$$Ke = \frac{C_D}{C_o} = \frac{\text{Wt \% of X in ferrite at the dendrite core}}{\text{nominal composition wt\%}} \qquad (4.1)$$

$$Ie = \frac{C_{ID}}{C_o} = \frac{\text{wt\% of X at the interdendritic spaces}}{\text{nominal composition wt\%}} \qquad (4.2)$$

$$I_s = \frac{C_{ID}}{C_D} = \frac{\text{wt\% of X at the interdendritic spaces}}{\text{wt\% of X at the core of dendrites}} \qquad (4.3)$$

where : C_D = is the concentration measured in primary dendrite core

C_{ID} = is the concentration in the last solidified region (at interdendritic region)

C_o = nominal composition

the detailed observation made was as follows :

(i) Weld Metal 250RH Bead-on-Plate - 316L Preheated Parent Plate

STEM studies of thin foil specimens revealed dislocations in both austenite and ferrite. The dislocations formed cellular networks and they accumulated mainly at the austenite/ferrite phase boundaries as illustrated in Fig.4.81. STEM spot analyses were carried out at intervals along a line completely traversing ferrite regions starting and finishing in the adjacent austenite. The results yielded the concentration profiles for chromium and nickel given in Fig.4.82 (a to d). The maximum of the chromium and the minimum of the nickel concentrations were located not at the core of the ferrite but towards the adjacent austenite near the interphase boundaries. In some cases, there were a large relatively uniform concentration of chromium and nickel across the ferrite in the cell core and the absence of a chromium final transient as proposed by Lippold et al.[41] Typical concentration profiles for chromium and nickel are given in Fig.4.82(d) and the values found for the chromium and nickel at ferrite/austenite interphase boundary were different for selected regions. The interphase region with high chromium and low nickel concentration also had the lowest iron concentration, i.e. 67%. Moreover, the concentration

profiles in the austenite interphase region on either side of a ferrite region were different and usually the nickel concentration varied inversely with the chromium content.

Replicate determination of concentration profiles across several selected ferrite regions all yielded similar results in principal. Table 4.8 gives the distribution coefficients and segregation ratio, obtained respectively.

(ii) Weld Metal 18FN, Bead-on-Plate 316L S.A.W.

STEM studies of thin foil specimens of this weld metal revealed the presence of adendritic and isolated grain boundary ferrite structure as illustrated in Fig.4.83. Their presence is consistent with the ferrite observed by optical microscopy. Dislocations were distributed in both ferrite and austenite phases. Comparison of ferrite and austenite grains revealed that the former exhibited less dislocations and were more strain free than the austenite grains. Dislocation tangles were generally accumulated at the austenite/ferrite interphase boundaries. In some regions the austenite grains exhibited micro-strain possibly due to the rapid cooling rate experienced by this weld metal (i.e. thermal strain transformation strain and solidification shrinkage). Typical STEM micrographs are illustrated in Fig.4.84.

The results associated with different regions consistently revealed that the Ni and Cr concentrations are a minimum and a maximum at the core of ferrite respectively.

The nickel concentration increases continually towards the interphase boundary and within the austenite grains in both sides of the ferrite. It reaches a maximum within the austenite region as illustrated in Fig.4.85(a to d). The chromium concentration is inverse to that of

nickel in that it is a minimum in the austenite and increases continually towards the interphase with the maximum at the core of delta ferrite phase.

The significant observation was the presence of the maximum chromium concentration in the core of ferrite rather than at the interphase boundaries of austenite and delta ferrite as observed in weld 250RH. Furthermore, the chromium and nickel concentrations were more symetrically distributed around the ferrite towards the austenite grains on both sides of the ferrite. The core of ferrite dendrite has the highest chromium, (i.e. 27%), the lowest nickel, (i.e. 5%) and iron concentrations (i.e. 68%). The concentration gradient of chromium and nickel in the austenitic grains were more uniform than in weld metal No.250RH. The spot analysis of chromium and nickel concentration in the austenite phase were 20% and 10% respectively which is close to the nominal composition obtained for this weld (i.e. 17.8% Cr and 11.7% Ni).

Table 4.8 gives the distribution and segregation ratio obtained from thin foils specimens.

(iii) Single Run Butt Weld. SAW, 316L and 321 Plates

Thin foil specimens from welds K and U were examined by STEM. Dislocations were distributed in both the austenite and ferrite phases and were mainly piled up at the austenite/ferrite interphase boundaries. In some regions the ferrite appeared to contain less dislocations and to be less highly strained than the austenite phase. Typical micrographs of these welds are illustrated in Fig.4.86 and 4.87 respectively. Generally the austenite/austenite grain boundaries were free from dislocations and any precipitated particles as illustrated in Fig.4.88, but in a few cases fine precipitates were observed at the austenite grain bounderies. Attempts were made to identify

these precipitates but the electron diffraction patterns were too complex to be interpreted as they did not correspond to simple carbides. At this stage it was not possible to identify them, but they appeared to be genuine and not the result of surface contamination. Further work would be necessary to identify them.

Second phase particles were observed occasionally within both the austenite and ferrite phases as illustrated the typical micrographs given in Figs.4.89 and 4.90.

Furthermore, selected particles were analysed by EDAX. The results are given in Fig.4.91, which shows that the particles varied both in composition and in the elements identified.

STEM analysis results revealed that chromium accumulated at the austenite/ferrite interphase boundaries. The concentration profiles of nickel and chromium in the austenite grains on both sides of the ferrite phase at the interphase boundaries (δ/γ) . were different.

Fig.4.92 gives surveys of spot analyses yielding the concentration profiles of nickel and chromium in different regions. Table 4.8 gives the distribution coefficients and segregation ratio obtained. Thin foils obtained from these welds exhibited edge cracks as illustrated in Fig.4.93. It is difficult to decide whether these cracks are an artifact introduced during thin foil preparation or an effect reflecting some feature of the bulk material, e.g. grain boundary weakness or stress relaxation.

4.6 Mechanical Properties of Different Welds

(a) Charpy test data : A minimum of six impact test specimens from each weld metals were tested at room temperature and at cryogenic temperature using liquid nitrogen (77 K) and the results are

given in Fig. 4.94 and 4.95

The highest impact energy value was associated with the weld prepared with hot-rolled furnace-cooled conditions plates and the weld prepared with cold-rolled parent plates shows the most scattered results. Lateral expansion values obtained from different weld metal impact test specimens tested at cryogenic condition (77 K) are given in Table 4.9.

(b) Tensile Testing

Duplicate tensile test specimens from selected welds were tested in cryogenic conditions. The results are given in Table 4.10.

(c) Fractography

Fractured surfaces of test pieces from both the charpy and tensile tests were selected to represent materials with high and low strength and ductilities and examined. All of the fracture surfaces exhibited equiaxed dimples indicative of ductile fracture with some micro cracks as illustrated in Fig.4.96. Microstructural studies were performed on some gently polished and etched fracture surfaces. The results revealed the presence of interphase boundary separation (delta ferrite/austenite boundaries) and/or void initiation in the austenite matrix (Fig. 4.97). In many cases the austenite matrix was broken apart, but the delta ferrite was unbroken in the same regions (Fig.4.98). In some cases the crack was propagated in the austenite and arrested by the delta ferrite phase.

Moreover, as the separation of the austenite phase was considered to be due to hot tearing as well as to void coalesence during

the fracture sequence, further work was carried out to study the microstructure of these welds in the as-welded condition, i.e. prior to mechanical testing. The results of microstructural studies of these specimens confirmed that some voids and inter-phase boundary separation were already present in the welds before testing. Possibly the void coalesence can be associated with the cavities formed by hot tearing induced during solidification of the weld metal. In some cases the cavities were observed in the region of surface marking (close packed plane) in the austenitic matrix.

Further experimental work was carried out to study the presence of surface marking in austenite grains. A single run butt weld with a low heat input was produced in the unrestrained condition. Microstructural studies of this weld revealed that no surface marking was present in the austenitic matrix. Tensile tests were performed in this weld. Microstructural examination of the deformed tensile test specimens showed very complex microstructures. However, deformation bands were observed passing through both austenite and delta ferrite phases. It therefore appears that the presence of deformation bands could be associated with the early stages of solidification, possibly as a result of induced stresses, i.e. solidification shrinkage or thermal stresses. However, further work is necessary to study this phenomenon in more detail.

(d) Hardness Tests

The results of microhardness testing for various bead-on-plate welds are as follows:

(i) Submerged Arc Welds:

Table 4.11 shows the hardness values of various welds. The results revealed that the hardness was increased by reducing the heat input

and/or by increasing the cooling rate. On the basis of microstructure the high heat input welds with well developed dendritic type structure were softer than those of lower heat input with regions of interdendritic austenite, dispersed and/or isolated ferrite.

(ii) Mig Welds :

Table 4.12 shows the hardness values of various welds. Despite using similar welding conditions the hardness value changes in different welds. Generally welds with cellular and lath (side plate) type ferrite morphology had the highest and the lowest hardness values respectively.

Comparison of different ferrite morphologies revealed that the hardness value decreases in order from the sequence cellular, varmicular and lath type ferrite.

5. DISCUSSION

5.1 Introduction

The literature survey presented in Section Two was concerned with the metallurgical characteristics of austenitic stainless steel and its weld metal it placed particular emphasis on ferrite content and its morphology. A desirable weld metal microstructure contains a small amount of ferrite; the content and morphology are dependent on the electrode/base metal composition, welding parameters, and weld metal cooling rate. The weld metal mechanical properties can be improved by (i) adjusting the alloying composition or $\frac{\text{Cr eqv.}}{\text{Ni eqv.}}$ ratio, (ii) reduction of impurities, (iii) controlling welding parameters, (iv) protecting the weld pool from atmospheric contamination.

A great deal of work has been carried out to study the solidification of weld metals by considering either the solidification sequence or focusing on grain refinement mechanisms. However, the details of the solidification mode, the mechanisms of grain refinement, ferrite formation and ferrite morphology remain controversial issues, due to the variation in the parent plates, electrode wire, fluxes, welding techniques and parameters such as heat input, cooling rates used previously.

In the present work the approach adopted was to study these variables individually. The parent plates were prepared from billets of AISI types 316L and 321. The plates were further worked, heat treated to produce a range of plates 12mm thick. These plates have identical chemical composition, but differing microstructural characteristics. Details of parent plate preparation are given in Section 3.2. The microstructure of both parent plates of different characteristics and their weld metals were studied and particular

attention was given to the effect of titanium as a grain refiner in AISI type 321 welds. Unlike previous studies which were solely based on the variation in weld metal composition the approach adopted in the present work was to consider variables such as (i) welding parameters and (ii) the parent plate of different microstructural and mechanical behaviours.

Four main categories of welds were prepared as follows:

1. Submerged Arc Bead-on-plate welds of duplex structure by using parent plates in the as-received condition but with different welding parameters and conditions, (plates of identical chemical composition).
2. Metal - Inert - Gas (MIG) Bead-on-plate welds of duplex structure by using nominally identical welding conditions but with parent plates of different characteristics (plates of identical chemical composition).
3. Metal - Inert Gas (MIG) Bead-on-plate welds of austenitic structure by using nominally identical welding parameters, but with the addition of nitrogen gas to the argon atmosphere of the shielding gas to encourage austenite formation.
4. Submerged Arc (S.A) Butt welds of duplex structure by using nominally identical welding parameters with parent plates of different characteristics, (plates of identical chemical compositions).

Details of the welding procedure and conditions are given in Section 3.4.

In the present work, the effect of alloying elements, welding parameters, i.e. heat input, cooling rates and parent plates metallurgical characteristics were considered.

In addition, an attempt has been made to study the effect of nucleation and growth phenomena in the solidification behaviour of weld metal.

The experimental work was approached in the present investigation by considering each variable individually and this has provided necessary guidelines for the examination of microstructure, and solidification behaviour of welds. This could form the basis for further attempts to study the ferrite dendrite development and the grain refinement of austenitic stainless steels which have not been considered by previous investigators. Furthermore, it could help to elucidate the entire question of ferrite formation, morphology, content and location in the final grain size which is important in assessing the beneficial role of ferrite in preventing hot cracking in austenitic stainless steel welds.

The results presented here show that the outcome of the final microstructure; the ferrite content, its morphology and thus the mechanical properties are determined by (i) the nature of the solidification which is a diffusion controlled process, (ii) the cooling rate, (iii) the presence of certain alloying elements, ie. Ti which enhanced the weld metal grain refinement , (iv) metallurgical characteristics of the parent plate which influenced the nature of solidification mechanism by the epitaxiality of growth and/or providing a suitable number of nuclei for the start of solidification. The results from the work described in this thesis provide a basis to aid the selection of parent plate, as well as designing welding parameters which will permit a greater control of the microstructure of austenitic stainless steel welds in terms of ferrite content, its morphology and thus their mechanical properties. The following

discussion relates the results of the present work to the previously published results of other workers.

5.2 Microstructural Variation in Austenitic Stainless Steel Welds

An attempt has been made to relate the microstructural features of the welds with the information given in published work with specific references to:

(i) weld metal microstructure classified by S.David[87] and Suttana.[100,102]

(ii) weld metal ferrite content and its morphology.

(iii) weld metal Cr and Ni equivalent based on schaeffler type constitutional diagram[53,54,65,67] (Figs.2.3 (a and b).

(iv) weld metal classification based on the Hammer and Sevensson[106] relations represented by equations 2.6 and 2.7.

(v) weld metal solidification characteristics as modified by previous investigators.[41,88,90,91,93,96,97,103,109]

5.2.1 AISI 316 Bead-on-plate S.A. Welds

Several welds were prepared by using different welding conditions as described in Section 3.4. Details of microstructural studies of various welds and their representative micrographs were given in Section 4.2.1.1. The objective of this part of the research was to illustrate the effect of various parameters such as (i) cooling rate, (ii) heat input, and (iii) restraining condition of parent plates on the solidification behaviour and room temperature microstructure of welds.

(a) the weld metal ferrite content The ferrite measurements were carried out by using (i) ferritescope, (ii) quantitative metallography and (iii) calculation from the chemistry of welds by considering the geometry of the schaeffler-Delong diagram

(Figs.2.3 (a,b)). The results of the ferrite content are shown in Table 4.5. Comparison of different welds showed that the ferrite content measured by quantitative optical metallography was slightly higher than that measured by the ferritescope. This is probably due to the presence of other microstructural features taken into account in conjunctionwith the ferrite as explained in Section 4.2.1.1. It appears that other measuring devices, such as the ferritescope are not sensitive to such a microstructural feature, i.e. internal fissure whilst the results obtained by quantitative metallography are influenced by them; and therefore recorded less ferrite content than that given by quantitative metallography.

Another factor that influences the ferrite measurement by QTM is the extremelysensitive adjustment of this equipment known as "threshold setting" which determines the point at which the machine discriminates light from dark and makes it possible to measure the amount of second phase present in the weld metal. The representative micrographs in Fig.4.35 demonstrate the error in ferrite measurement that can result from adjustment by "threshold setting" for revealing the ferrite phase.

Table 4.5 shows the ferrite content of different bead-on-plate welds. It shows that, weld F1 with the high heat input and weld F12 with low heat input have 7.5% and 5% ferrite content respectively. Welds produced by using similar welding parameters but different cooling rates in group v of Table 3.8 had different ferrite content, i.e. weld 18FN had a lower ferrite content and, weld 250RH had a higher ferrite content in this group.

The results presented above show that the ferrite content is a function of heat input and cooling rates. In order to investigate more fully the effect of cooling rates a simplified Rosenthal equation[38] as given in Section 2.3 was used. Comparison of different welds showed that weld F1 (with the highest heat input) has a lower cooling rate, weld F12 (with the lower heat input) had a higher cooling rate and weld 18FN, which was prepared with similar heat input as weld F12 but under different conditions, had the highest cooling rate. Weld 250RH which was produced on a preheated parent plate and flux, shows a lower cooling rate and a higher ferrite content than corresponding welds of a similar heat input.

Comparison of various welds revealed that there is a tendency for the ferrite content to increase as the heat input is raised, i.e. reducing cooling rate, or as the parent plate ambient temperature is increased. These results are in agreement with the findings of previous work.[54,86,88] In addition to the variation in ferrite content between various welds, some differences were observed in the ferrite content of the individual welds both in transverse cross section and along the length of the weld. Variation in ferrite content and its morphology were noticed in different regions in the transverse cross section area of the welds. The ferrite content measurement of some welds by ferritescope showed the presence of a higher ferrite content in the upper part nugget area of the weld than the lower part. This may be associated with the (i) heterogenity of the weld microstructure which was inherited from the solidification mechanism; (ii) variations in growth rate with reference to the cooling rate; (iii) compositional variation due to the dilution with parent plate, and (iv) effect of chemical reactions which affect the presence of

certain alloying elements, i.e. Cr Ni in the weld pool. However, further work is required to identify which of these parameters is responsible for the reported variations in ferrite content within welds.

The slight increase in ferrite content along the length of the weld could be associated with the heat build-up resulting from the heating of the parent plate during welding. As welding progresses the temperature of the plate increases from the origin to the final temperature. The cooling rate is controlled by the temperature differential between the solidifying weld and the adjacent parent plate at the beginning and the end of the weld bead, this suggests that the weld metal microstructure is influenced by the length of the weld bead. Another possible reason for the variation in ferrite content in high welding energy input welds could be due to the self-resistance heating of the electrode core. In these cases a deeper arc crucible with a greater rate of flow of metal across the arc occurs towards the end of the weld than at the beginning of the weld. Alteration of the weld pool chemistry is likely with the possible reduction in the amount of nitrogen and the consequent increase in the ferrite content.

Furthermore, predicting the ferrite content by considering equations 2.2, 2.3 and 2.4 showed inconsistency in the amount of ferrite in each weld, using these expresions, and contributed to the variations in weighting factors used in the establishment of these expressions as well as the variation in alloy composition, welding conditions and cooling rate for the different welds.

(b) Microstructural Variation in Low Heat Input Welds

Microstructural studies showed that the solidification substructure

and the consequent dendrite morphology changed from the fusion boundary towards the centre and the top surface of the weld. The ferrite morphology was that of a skeleton of dendrites with austenite formed as an envelope around the dendrites. The ferrite dendrites become better developed as the growth proceeds towards the centre of the weld.

The main microstructural features associated with low heat input welds was the presence of wide bands of austenite matrix separated by ferrite dendrites, some isolated dispersed ferrite within the austenite. A substantial proportion of the austenite/ferrite interphase was linear.

(c) Microstructural Variation in High Heat Input Welds

Welds produced with high heat input had a higher ferrite content. They showed more elongated ferrite dendrites with wide, well developed secondary and tertiary arms. The individual ferrite streams were separated by a narrow band of austenite, and the austenite/ferrite interface had a more rounded shape. The solidification substructure was comprised of raft or axial type structure in transverse cross section, the fusion boundary region has a cellular dendritic to columner dendritic type growth, as shown in Fig.4.32 (b), whilst the central region promoted a transition to a more dendritic growth mode with the absence of any refined structure. The cellular type structure in the fusion boundary region could be associated with steep thermal gradients and a comparatively low solidification rate with a low level of constitutional super cooling. Moving away from the fusion boundary towards the central region there were more dendritic type structures because of the shallower thermal gradient in that region. These results are in agreement with the findings of

Savage et al.[109]

(d) Microstructural Variation in Rapidly Cooled Welds

In the fusion boundary region these welds showed elongated dispersed ferrite forming in a general pattern of cellular dendritic type structure. As the growth proceeds, the dendrites widen and elongate. They are separated by wide bands of austenite matrix together with some isolated dispersed ferrite within the austenite. The ferritic dendrites consisted of open branches with some tendency to a lath type structure. These welds showed more elongated type ferrite with no symmetrical side branch structure and some lath type ferrite morphology.

The presence of lath ferrite structure in weld metal was suggested[88] to be associated with the primary ferrite solidification, and/or high $\frac{Cr}{Ni}$ ratio. More investigation concerning the transition from skeletal ferrite to the lath ferrite morphology revealed that, the formation of lath ferrite is related to the degree of primary ferrite solidification and the cooling rate, as well as the transformation temperature.[88] That is, if the transformation,occured at sufficiently high temperatures with moderate cooling rates the ferrite to austenite interface could recede in a planar fashion, producing the skeletal ferrite morphology. If the transformation proceeds at lower temperatures, (higher $\frac{Cr}{Ni}$ ratios) or faster cooling rates, the ferrite to austenite interface breaks down and grows by an edge-wise growth of existing austenite consuming the ferrite. The present results showed that the lath ferrite morphology was associated with weld metal, produced at high cooling rate.

(e) Microstructural Variation in Ultra Cooled Welds

Welds in group five in Table 3.6 were produced under specific conditions. Weld 18FN had a slightly higher nitrogen content of 0.05% compared with

the rest of the welds with duplex structure recorded in Table 4.4. However, the nitrogen content of 0.05 was far less than that of weld L10 which exhibited the austenitic type structure. The nitrogen content of these welds were within the range of basic compositions[7,65] as specified for the type AISI 316L weld. As a result of the high cooling rate these welds showed lower ferrite content than the remainder of the welds. The general solidification growth is towards the centre and top surface of the weld with the solidification substructure appearing in a cellular type pattern structure as shown in Fig.4.46.

The presence of elongated ferrite with no side branch structure adjacent to the fusion boundary could be associated with the high cooling rate and probably corresponds to the eutectic type structure as classified by Fridrikson et al,[40] Schurmann et al. The latter showed that the Fe-Ni peritectic changes to a eutectic at 75.8% Fe, 9.6% Ni and 14.6% Cr. As growth proceeds inwards more dendritic type structure is formed, some with lath type structure which has no symmetry in respect of the ferrite dendrite core.

5.3 The Effect of Parent Plate Characteristics and Restraining Conditions

In the previous section the influence of various welding process parameters; cooling rate, thermal gradient, and solidification rate on the weld metal microstructure were discussed. Here, the influence of other variables regarding the parent plate such as : (i) thermo-mechanical treatment, (ii) restraining conditions and (iii) chemical composition on the weld metal microstructural features are discussed:

(a) Microstructural studies of different welds produced on a parent plate in the as-received condition after solution treatment showed

that, they generally consisted of dendritic ferrite of vermicular morphology. The dendritic ferrite became more developed as inward growth proceeded.

(b) Welds produced on a parent plate with different metallurgical characteristics (as explained in Table 3.7) showed various ferrite morphologies in different welds as well as the different regions within the transverse cross-section area of each individual weld.

High magnification microstructural studies at the fusion boundary region of welds produced on deformed plates showed the presence of differently oriented ferrite dendrite with no symmetrical side branch arms or in some welds a cellular type ferrite morphology. Mircostructural studies showed that, further into the weld, there was disoriented ferrite similar to the vermicular type morphology with open arms and some randomly distributed isolated ferrite within the austenite matrix. Usually the weld metal microstructure in the central region and towards the top consisted of block type patterns with a cellular ferrite network within the block. The blocks were embedded in the austenite matrix with grooves formed around them. The presence of grooves in austenitic regions suggests the formation of primary ferrite solidification mode and the formation of austenite from chromium depleted liquid which is more sensitive to the etching reagent and attacked more quickly than ferritic structure.

The cellular ferrite morphology observed in these welds was not identified in the classification of ferrite morphology given by David et al[87,88] or Suutala et al[89,91] shown in Figs. 2.4 and 2.5 respectively.

Comparison of different weld ferrite content showed that the welds

produced on heavily cold rolled plates had higher ferrite content than the other welds as shown in Table 4.5. Considering the similarity in the welding condition, i.e. heat input, cooling rate, and parent plate composition revealed that, the increase in ferrite content is attributed to the variation in metallurgical characteristics of cold rolled plate such as smaller grain size, (Table 4.1) higher strain energy, and high dislocation density in cold rolled parent plate. It is apparent that, the associated characteristics of the cold rolled plates has increased the ferrite content by allowing the growth of more nuclei of the first solidified phase (i.e. primary ferrite) during the early stages of solidification.

Different types of hot cracks were observed in austenitic stainless steels and many explanations have been proposed to describe the cause of hot cracking.[8,80,123] All these cracks, however, form while a small amount of liquid is still present, which allows the grains to separate under the thermal shrinkage stresses resulting from cooling. This liquid is often present below the bulk solidus resulting from the segregation of minor alloying elements or impurities.[123] The comparison of different welds show the presence of large quantities of internal fissures, (micro cracks) and ferrite/austenite interphase boundary decohesion were pronounced in welds produced in restrained parent plates and at high cooling rates, as explained in Section 4.3. The interphase boundary separation along the ferrite/austenite with low interfacial energy could be due to high straining and cooling rates under these welding conditions.

Comparison of the microstructure of different welds produced on AISI type 316L and AISI type 321 plates showed that, the ferrite morphology of welds produced on 316L plates was that of skeleton of dendrites with austenite formed as an envelope around the dendrites. Welds produced on AISI type 321 plates showed that the ferrite was in a form of cellular network (block type pattern) surrounded by austenite which was forming

a groove around ferrite. The ferrite appears as a core of dendrite and stands as a relief phase embedded in the austenite matrix. The presence of grooves in surrounded austenite recorded in this investigation are due to the compositional variation during solidification. The STEM analysis showed that the compositional profiles exhibited a shape consistent with that expected from solidification with $K_{Ni} < 1$ and $K_{Cr} > 1$ as recorded in Table 4.8. This suggests that the solidification involves the formation of primary ferrite and the formation of austenite from the chromium depleted liquid which is less resistant to etching reagent and is dissolved quickly by it.

Depending on the thermal gradients and solidification rate the ferrite dendrite development varied in different regions of transverse cross-sections, i.e. fusion boundary and central regions. The ferrite dendrite became more well developed as the growth procedes towards the centre of the weld. However, the ferrite morphology remains vermicular despite its dendritic development for AISI type 316L and cellular structure for AISI 321. The absence of vermicular ferrite morphology was noticeable in welds produced on AISI type 321 plates. This type of ferrite morphology was not identified by David et al[87] or Suutala et al[100,102] classification of ferrite morphology. Considering the similarity in welding conditions for these welds,the presence of cellular type ferrite morphology in welds produced on AISI type 321 is attributed to their solidification behaviour in the presence of certain alloying elements, i.e. Ti and C inherited from the parent plates and acting as a grain refiner agent.

5.4 Bead-on-Plate Welds with Austenitic Type Structures

These welds were produced on different type austenitic stainless steel (discussed in Section 3.4.2.2) with the addition of nitrogen to the Argon atmosphere of the shielding gas. The microstructural studies of

these welds showed the presence of an austenitic type structure where a columnar mode of solidification was dominant. The transition from ferritic freezing to "austenitic freezing" observed in the welds was in agreement with the transition predicted by the chromium and nickel composition equivalent diagrams to be considered in the next Section.

The addition of nitrogen changes the solidification sequence from having the primary ferrite to having the primary austenite as the leading phase. Therefore, its influence on the freezing mode is consistant with the nature of nitrogen as an austenite stabilizing element and is in agreement with the work of Fredriksson[40] and Delong.[54]

Despite the use of similar welding conditions, small amounts of ferrite in the range 0.5-1% and 1% were detected by the ferritescope in samples provided from welds AISI 321 and AISI 316L respectively; whilst welds prepared from AISI 304 did not show any ferrite. The variation in ferrite contents is attributed to the large scale segregation associated with the solute rejection at the advancing solidification front. The addition of nitrogen enhanced the formation of primary austenite at the core of the cellular dendrites enriched in nickel and depleted in chromium. As a result the last liquid to solidify is enriched in chromium and promotes the formation of a divorced eutectic mixture of austenite and delta ferrite located at interdendritic regions.[44,90,96] Furthermore, it has been stated[86] that, at low ferrite levels, the ferrite is usually distributed along triple points, or corners of the cell boundaries. As the amount of eutectic ferrite increases, the number of cell boundaries which contain

ferrite increases and it sometimes becomes difficult to distinguish it from skeletal ferrite; this ferrite is sufficiently enriched in ferrite stabilizing elements to remain ferritic upon cooling without solid phase transformation to austenite.

An attempt was made to investigate different microstructural features of the welds by using scanning electron microscopy. Scanning electron microscopy revealed complex microstructures, such as dendritic type patterns similar in appearance to delta ferrite within the austenite matrix, but with no relief, as illustrated in Figs.4.6 6. and 4.6 9.

From the above discussion, it is clear that there is scope for further work to investigate the origin of the reported microstructural features, the effect of parent plate as well as a study of the amount of nitrogen required for the production of desirable microstructure in austenitic stainless steel welds.

5.5 Summary

The presence of cellular type solidification substructure in the fusion boundary regions associated with a steep temperature gradient, and elongated ferritic dendrites in the central region of welds associated with shallow thermal gradients and high degree of constitutional super cooling, are in agreement with the previous works[109] which have related to microstructural variations in weld metal.

The solidification substructure of different welds were shown to depend on their heat input; for low heat input welds the growth unit changed direction towards the top surface of weld with no central line or axial type structure. For high heat input welds in general, a raft or axial type structure was observed. However, depending on the welding condition for rapidly cooled welds a raft structure was

shown to consist of columnar dendrites developed parallel to the welding direction, whilst for restrained welds it consisted of a more equiaxed rather than columnar dendrite. The microstructural variation in different welds showed that, increasing the heat input/ or lowering the cooling rate at a fixed welding speed provided a greater growth of dendrites by flattening the thermal gradient in the weld pool. This resulted in an increase in the constitutional super-cooling ahead of the advancing interface as explained by Savage et al. [109]

The absence of refined grains in the central region is in agreement with the work of Garland[110] who showed that the level of constitutional super-cooling in the melt is not the sole criterion determining the onset of a completely equiaxed solidified structure. Furthermore, for high heat input welds neither significant nuclei generation (i.e. free surface dendrite remelting) would take place nor enough nuclei would grow to a sufficient size to generate an equiaxed zone as expected in casting. Bearing in mind that other grain refinement mechanisms such as chill zone and surface nucleation and growth were absent in the weld pool solidification.

The microstructural studies in this investigation have indicated that most welds exhibited either cellular, cellular-dendritic or a mixture of both substructures.

An attempt has been made to measure the dendrite arm spacing, but because of the complexity in different weld microstructures there were some inconsistencies in results and, therefore, they were not reported in this thesis. However, in general dendrites spacing decreased with increasing cooling rates as shown in Figs.4.3 2, 4.4 7 and 4.5 1. The result of the present work showed that the

increase in ferrite content as well as development of ferritic dendrite arms are an indication of local solidification, thus determining the time available for a diffusion controlled transformation i.e. high cooling rates allow less time for lateral diffusion of the rejected solute.

5.6 Microstructural Classification of Different Welds in terms of Compositional Variation

(a) Chromium and Nickel Content

Traditionally weld metal microstructures were classified according to their compositional variation and basically in respect to Cr eqv., Ni eqv, and their ratio.

In the present work a revised Delong[54] constitutional diagram was considered, and the ferrite forming tendencies of the alloys are reflected in their net chromium and nickel equivalent calculated as follows:

$$\text{Cr eqv} = \%\text{Cr} + \%\text{ Mo} + 1.5\%\text{ Si} + 0.5\%\text{ Nb} \qquad (5.2)$$

$$\text{Ni eqv} = \%\text{ Ni} + 30\%\text{ C} + 30\%\text{ N} + 0.5\%\text{ Mn} \qquad (5.3)$$

The results of Cr eqv, Ni eqv and $\frac{Cr}{Ni}$ ratio are shown in Table 5.1.

The composition of various welds revealed that despite the variation in welding conditions and consequent changes in ferrite dendrite development (i.e. morphology) the Cr eqv and Ni eqv were not changed substantially as a result of the dilution with the parent plate. This could be attributed to the use of the welding parameters within the range recommended by the electrode wire and flux manufacturer. However, the change in the weld metal microstructure could demonstrate the important effect of cooling rate on the ferrite dendrite development during the solidification stage as illustrated in Figs.4.32 , 4.33 and 4.43.

Comparison of $\frac{Cr}{Ni}$ eqv for different welds showed that the lowest value of 1.2 was associated with the weld L10 which exhibited the austenitic type structure and the highest value of 1.61 was associated with the weld K321 with the duplex structure. Furthermore, the Cr and Ni equivalent values calculated by the following expression[92] are given in Table 5.2.

$$Cr\ eq = Cr + 1.37\ Mo + 1.5\ Si + 2\ Nb + 3\ Ti \qquad (5.4)$$

$$Ni\ eq = Ni + 0.31\ Mn + 22\ C + 14.2\ N + 1\ Cu \qquad (5.5)$$

Table 5.2 showed that the Cr and Ni equivalent ratio values were within the range of 1.42-1.74 which exhibited a primary ferrite solidification mode for all the welds including weld L10 which has austenitic type structure.[92] Comparison of results of Table 5.1 and 5.2 showed the variation in Cr and Ni equivalent values for each weld. This is attributed to the variation in weighting factors used in establishing these expression for welds produced under certain standardised conditions unlike those used in the present investigation.

Microstructural Classification based on Schaeffler Type Diagrams

The compositions of different welds were expressed in terms of Cr and Ni equivalent and plotted on the Schaeffler type diagram to demonstrate the systematic relationship between the location of welds; the amount of ferrite, and the type of microstructure. Studies of Schaeffler - Delong diagrams (Fig.2.3) showed that weld L10 was located in the austenitic region and the others were within the austenite plus ferrite region. The room temperature microstructure observed in this investigation was consistant with the type of structure predicted by the Schaeffler diagram in terms of their positions on the diagram.

Consideration of the Schaeffler - Leone diagram (Fig.2.5) showed that welds K, Z, 14R, 11R and K321 were located in the region of $\delta + \gamma$ with the formation of γ phase from the liquid. The welds 8R and 18FN were located in the border line between austenite and $\delta + \gamma$ region with the formation of γ from the liquid. The weld L10 was placed in the austenitic region. Microstructural studies recorded in this investigation showed consistency with those predicted by Schaeffler - Leone- Kerr diagrams[90] in terms of position of the alloys on the diagram. Referring to the Leone-Kerr classification of weld metal microstructure in respect to $\frac{Cr}{Ni}$ eqv given in Section 2.7, the present work shows that the $\frac{Cr}{Ni}$ eqv varied between $1.2 < \frac{Cr}{Ni} < 1.8$ Comparison of the present work results with the Leone-Kerr classification of weld metal microstructure showed that, the first solidified phase is ferrite and austenite forms from the liquid. Microstructural studies showed that the ferrite was surrounded by austenite forming a groove around them, the formation of grooves is attributed to the effect of etching reagent on the surrounding austenite which formed from the chromium depleted liquid as a second phase and therefore sensitive to the etching reagent.

Using Hammer and Sevensson's expression[106] (equations 2.6 and 2.7) showed that for weld L10 the $\phi > 0$ and the solidification sequence is as follows:

$$L \rightarrow L + \gamma \rightarrow \gamma$$

this indicates the formation of austenite as a primary phase, in the remainder of the welds where $\phi < 0$ the solidification sequence is as follows:

$$L \rightarrow L + \delta \rightarrow L + \gamma + \delta \rightarrow \gamma + \delta$$

this confirms the formation of ferrite as a primary phase and the

austenite from the liquid. Microstructural studies recorded in this investigation showed consistency with those predicted by Hammer and Sevensson's expression.

Comparison of the present work results with the Suutala et al[100,102] classification of weld metal microstructure in terms of $\frac{Cr}{Ni}$ eqv explained in Section 2.7 shows that, bead-on-plate weld K321 with the $\frac{Cr}{Ni}$ eqv ratio of 1.61 classified as primary ferrite solidified phase on which the austenite was forming from the melt. According to their classifications, the ferrite in this weld should have a vermicular morphology with any lath ferrite present being located mainly on the cell axis. Microstructural studies for this weld showed the primary ferrite solidification but the presence of cellular type ferrite morphology was not identified by the Suutala et-al[100,102] ferrite morphology classification. The $\frac{Cr}{Ni}$ eqv for welds 8R, 14R, 18FN and 11R produced in different welding conditions were <1.48. According to their classification these welds were solidified as primary austenite with ferrite forming from the melt between austenite or dendrites as eutectic. Microstructural studies of these welds showed that this view is not consistant with the finding of the present work.

The results of the present work concerning the ferrite morphology and solidification mode are not in general agreement with the finding of the Suttala's[100-102] work; microstructural studies show the presence of ferrite surrounded by austenite forming a groove around it. This is attributed to the primary ferrite solidification and the formation of austenite from the Cr depleted liquid. Whilst this type of microstructure has been classified as primary austenite solidification according to their $\frac{Cr}{Ni}$ eqv in Suttala[100,102] classification.

The differences in solidification behaviour and ferrite morphologies in the present work with the generalised classification of weld metal microstructure stated by Suutala et al[100-102], were associated with the alteration of the variables such as (i) weld metal composition, (ii) parent plate metallurgical characteristics, (iii) welding conditions, (iv) cooling rate, involved in the present investigation. The present work result show the important role of these variables on the ferrite morphology and the solidification mode of weld metal and emphasised on the necessity for classification of weld metal microstructure in terms of given variables rather than only $\frac{Cr}{Ni}$ eqv as stated by Suutala et al.[100,102]

(b) Carbon and Nitrogen Content

The presence of carbon and nitrogen as austenite stabilizing elements, alter the primary solidified phase and hence the solidification sequence of welds. The combined total C + N was represented as C equivalent as given in equation 2.6 and expressed by Hammer and Sevensson[106] The results of Ceqv for different welds are given in Table 5.3. Based on the Hammer and Sevensson[106] classification the bead-on-plate welds K321 and 14R were solidified as primary ferrite followed by secondary austenite. Weld L10 with 0.2% N was solidified as primary austenite with no solid state phase transformation. Butt weld K321 showed a simultaneous solidification of ferrite and austenite and both were classified as a primary phase. All of the remaining welds, i.e. 8R, 18FN and 11R were solidified as primary austenite with an inter-dendritic ferrite.

Despite the high Nitrogen content of weld L10, microstructural studies showed the presence of a columnar structure which originated directly from the melt without any equiaxed or refined grains. The

occurance of solidified columnar austenite grains observed in this weld indicates that the beneficial role of nitrogen as a grain refiner is nullified in weld L10. This is probably associated with the high cooling rate involved in welding.

The transition from primary ferrite to primary austenite with increased C eqv is in agreement with the freezing mode predicted by Hammer and Sevensson's [106] function. Moreover, the present work shows that an increasing cooling rate as well as increasing Ceqv shifts the bulk composition gradually towards the austenite phase field in a solidified weld. This is in agreement with the finding of Leone [90] in which he suggested that, with increased Ceqv the growth temperature of a phase (s) decreased. This is consistent with a shift in bulk composition towards the austenite phase fields which is accompanied by a decrease in the freezing temperature of the alloys.

The results of the present work indicate that by decreasing the cooling rate of the solidified weld, the holding time in the liquidus/solidus region is increased and, this consequently alters the solidification rate. For instance, by reducing the cooling rate then the length of time from initiation to completion of solidification increased. However, despite a relatively short resident time in the solidification stage, a more well developed dendritic type structure was formed. Furthermore, for the growth of ferrite in such a short residence time the following expression was proposed by Hammer and Sevensson [106]

$$Fs \propto t^{n} \qquad (5.6)$$

where Fs is the fraction of ferrite

t = is the residence time

n = is 0.5 -1.0

Now considering welds prepared with fast cooling rate (i.e. 18FN, F12), then the amount of t would decrease and, therefore there is a shorter period of time for ferrite to grow and branch out. The contrary applies for welds with prepared slow cooling rate (i.e.F1) where the residence time would increase and there is more time available for ferrite dendrite development. The ferrite increase in content and its dendritic development for different welds observed in this investigation are in good agreement with the expression of Hammer and Sevensson[106] referred to above. Furthermore, the presence of well developed ferrite dendrite in the central region of high heat input welds could be explained in terms of reduction[40] in cooling rate and their consequent flatter thermal gradient and corresponding longer residence time. On the other hand the presence of elongated, less well developed ferrite dendrites in the fusion boundary region, especially in the higher cooling rate welds, could be explained in terms of their steep temperature gradient and shorter residence time in that region. The presence of elongated ferrite suggests the solidification of individual dendrites as a primary phase. This could be due to the sudden increase in cooling rate which under cools the liquid into the $L \rightarrow \gamma + \delta$ region where both phases formed simultaneously. This type of structure was referred to as a eutectic by Fredrikson.[40] However, the scale of diffusion required is large and the pattern is much less regular than normally observed in eutectic alloys.

Considering the hypothesis stated by previous investigators

concerning the possible solid phase transformation of primary ferrite to austenite, one should notice that any increase in the cooling rate reduces the time for any possible solid state transformation of ferrite to austenite. Therefore, a greater volume fraction of untransformed ferrite would be expected to be retained to room temperature. The findings of the present investigation were in contradiction to such a hypothesis.

The formation of primary ferrite and occurance of a peritectic reaction in austenitic stainless steels have been studied by some investigators.[39,40,88] In this context, Fredrikson[40] showed that at the start of the peritectic reaction austenite is formed at the interface between δ and L and completely surrounds the ferrite. During subsequent reaction austenite will grow into the liquid as well as into the ferrite. They consider Scheil's segregation equation and calculated the concentration of alloying elements distributed in austenite for an alloy with 9.5% Ni and 13% Cr. Fredrikson et al[40] found a reasonable agreement between calculated results and those obtained by experimental work. Referring to the present work the quantitative STEM analysis results for welds 18FN and 250 RH showed that, the Ni concentration at ferritic dendrites and ferrite/austenite interface (Figs.4.82 and 4.85) were close to the figures found for a peritectic type reaction identified by equation 2.8. However, the present results showed the development of ferritic dendrites and a consequent increase in the ferrite content with reducing cooling rate, this is in contrast with the consideration of diffusion controlled peritectic type reaction on which the δ Fe is expected to be consumed by γ and the retained ferrite should be decreased by reducing the cooling rate.

5.7 Solidification and Solute Concentration Trends

Contradictory reports have been published concerning the solidification behaviour of austenitic stainless steel. This has been partly because of the complexity of ternary Fe-Cr-Ni systems and the presence of other alloying elements which have provided a complicated situation with quaternary or quinterary systems. In such a condition, many difficulties were observed in determining the detailed analysis of the phase relationship within the solidus-liquidus gap and consequently the solidification concentration profiles of the alloying elements. With welds the particular problem is associated with the high cooling rate during which phase changes may not go to completion as it has been proposed. However, it has been generally accepted that the variation in concentration of alloying elements within austenite and ferrite is due to the segregation during solidification and partition of alloying elements as a result of solid phase transformation upon cooling.

Various data were produced with the aid of STEM studies and consideration of appropriate constant iron pseudo binary sections of the Fe-Cr-Ni system. In the present work, the quantitative STEM analysis results show changes in composition across the ferrite and austenite interface and in some cases the presence of large relatively uniform concentration of chromium and nickel across the ferrite in the cell core with no final transient for chromium as proposed by Lippold.[44] STEM data showed that the chromium concentration changes only within $\simeq$ 0.5μm of the phase boundaries. This could be attributed to more diffusion leveling of Cr than Ni at the final stages of the transformation. However, it appears that the high Ni concentration in the oell boundaries results from secondary austenite solidification

due to Ni enrichment and Cr depletion of the liquid during primary ferrite solidification.

The STEM analysis shows that in the regions of ferrite analysed and shown in Figs.4.82 and 4.85, the measured Fe concentration was variable. This is inconsistent with partition of only Cr and Ni within the ferrite and γ proposed by other workers which resulted the solid state transformation of ferrite to austenite.

5.8 Microstructural Consideration in Terms of Fe-Ni-Cr Ternary System

Under equilibrium conditions the structure of austenitic stainless steel should be completely austenitic. However, non equilibrium conditions present during welding lead to the formation of some delta ferrite. It is common to demonstrate the solidification mode of stainless steels by a section of the Fe-Cr-Ni system. In this context a section of a ternary diagram containing 18% Cr and the pseudo binary section of Fe-Cr-Ni system are shown in Figs.2.11 and 2.10 respectively. According to these diagrams it has been generally accepted that a large fraction of primary ferrite is formed during early solidification stages and this ferrite transformed back to austenite upon cooling.

By considering the pseudo-binary section of the Fe-Cr-Ni ternary system Fredrikson[40] and David[88] suggested that on cooling through the ferrite and austenite two phase field, partitioning of Cr and Ni between ferrite and austenite occurs by solid state phase transformation.

More recent work[83] concerning the effect of cooling rate by splat quenching on the microstructure of AISI type 308 stainless steel weld metal indicated that the splat surface was 100% austenite and towards

the centre of the splat there were regions containing about 5-10% delta ferrite in the inter cellular area similar to those observed in ordinary welds.

The study of the solidification mode for this weld showed that the weld composition is placed well within the primary ferrite region (δ + L) of the pseudo-binary section of constant iron. Furthermore, the ternary Fe-Cr-Ni liquidus diagram and the solidus diagram for the equilibrium condition as shown in Figs.2.9(a) and 2.9(b) respectively indicated that primary ferrite solidification and further solid phase transformation of primary ferrite to austenite will occur during the subsequent cooling, this view is in contradiction with the results of experimental work by David and Vitek[83] and indicates the importance of the cooling rate, non equilibrium condition involved in welding.

Consideration of Fe-Cr-Ni Ternary System for Different Welds

Depending on the weld metal composition, a section of Fe-Cr-Ni alloy containing 18% Cr (as shown in Fig.2.11) and the nearest pseudo-binary section of Fe-Cr-Ni system in respect of their iron content (as shown in Fig.2.10) are used to outline the solidification behaviour of different welds. Table 4.4 shows the chemical analysis of different welds. It showed that the variations in iron and chromium content for various welds are between 65-69% and 17.5-19% respectively. Depending on the weld metal composition the section of Fe-Cr-Ni alloy containing 18% Cr shows that the primary solidified phase depends upon the Ni concentration. The bead-on-plate welds L10 and K321 contained less than 11% Ni, and should solidify as primary ferrite. However, microstructural studies of weld L10 showed

that, this weld with 0.2% N exhibited an austenitic type structure and the bead-on-plate weld K321 exhibited a duplex structure.

According to the Schaeffler type diagrams,(Fig.2.6) explained previously in Section 5.6, in weld K321 the ferrite forms as a primary solidified phase and austenite forms from the liquid. Considering Fig.2.11 the remainder of the welds with 11% or more nickel content are within the triangle and a peritectic type reaction is expected to occur. Therefore, weld pool solidification should take place as ferrite plus austenite with the reaction $L+\delta \rightarrow \gamma$ The microstructural studies carried out as part of the present work showed that the increasing cooling rate experienced upon weld pool solidification had restricted the growth of primary ferrite dendrites and thus reduced the ferrite content of these welds. As a result of high cooling rates and non equilibrium conditions during which phase changes are not going to completion; halting of the expected diffusion controlled peritectic reaction could occur, leaving dispersed elongated ferrite dendrites in contact with nickel enriched liquid and consequent solidification of weld pool as austenite.

Considering a pseudo-binary section of Fe-Cr-Ni system as shown in Fig.2.10, the systematic investigation of different welds showed that their chemical composition did not correspond to the appropriate constant iron pseudo-binary section and the chromium and nickel were separately associated with different corners of the eutectic triangle. This difference could be associated with the non equilibrium condition which results from high cooling rates applying in welds, and the presence of a small percentage of other

alloying elements which were not taken into account in the original pseudo-binary section of Fe-Cr-Ni system for austenitic stainless steels.

The present work results are in agreement with the work of David and Vitek[83] and indicate the importance of the cooling rate, non equilibrium condition involved in welding and limitation in using pseudo-binary section of constant iron for establishing a solidification mode of weld metals which encounter sufficiently high cooling rates.

It is interesting to note that in previously published work these discrepancies were over-looked when using the pseudo-binary section of the appropriate Fe content. Attempt has been made to consider the original pseudo-binary section of the ternary Fe-Cr-Ni system by applying a correction factor in respect of other alloying elements. In this context instead of nominal composition a new normalised equivalent was replaced by ignoring other alloying elements. Therefore, the replaced value for Cr, Ni and Fe would be as follows

$$Cr_o = \frac{Cr \times 100}{Cr + Ni + Fe}$$

$$Ni_o = \frac{Ni \times 100}{Cr + Ni + Fe}$$

$$Fe_o = \frac{Fe \times 100}{Cr + Ni + Fe}$$

By substituting these new values for Cr, Ni and Fe a closer correlation between composition with pseudo-binary section of appropriate Fe content was expected to be observed. Table 5.4 showed the new normalised equivalents for the alloying elements. The use of the

obtained data given in Table 5.4 and with the aid of the appropriate pseudo-binary section given in Fig.2.10 shows that the welds were basically close to the eutectic triangle. However, the partition with Cr and Ni was observed and they did not correspond to these diagrams as originally modelled for solidification of 18/8 austenitic stainless steel.

Furthermore, another important observation was made by comparison of different pseudo-binary sections of constant iron used by various authors. In this context, the systematic investigation of solidification mode for each weld studied in this investigation has been carried out by considering a representative vertical section of the Fe-Cr-Ni equilibrium phase diagrams used by Leone[90] et al and Lippold et al[86] The results showed that there is inconsistency in the solidification behaviour of these welds in terms of diagrams. For example, the S.A.Butt weld K321 with 18.3% Cr and 11% Ni showed the alloy position in diagram illustrated in Fig.2.10 (a,b,c) are as follows.

For pseudo-binary section with 70% Fe (Fig.2.10(b)) the alloy position is in the region of L + δ ; for pseudo-binary section of 70% Fe (Fig.2.10(a)) the alloy position is within the eutectic triangle, and for pseudo-binary section of 68% Fe (Fig.2.10(c)) the alloy position does not correspond with this diagram. There is a partition between chromium and nickel on this diagram. It is interesting to note the differences in the position of alloy and the solidification mode in terms of the 70% and 68% Fe content, whilst in some of the previous works a generalised illustration of pseudo-binary section of constant iron has been used inappropriately for a wide range of alloy composition and iron content. It appears that there is a

need for evaluation of proper pseudo-binary section of constant iron in respect of the weld metal composition and cooling rate. Therefore, further work is necessary to simulate elevated temperature equilibrium microstructures in order to determine the shape of the Fe-Cr-Ni ternary system or more phase diagram, and the possible solid state transformation of ferrite to austenite in welds.

5.9 Tensile Ductility/notch Toughness Correlation

The mechanical properties were evaluated for parent plates produced using different thermomechanical treatments. The objective was to specify various parent plates metallurgical characteristics in conjunction with their microstructural variation. In addition, the mechanical properties for selected weld metal were evaluated for comparison with their associated parent plates. The tests were carried out on parent plates prior to welding and the Butt welds produced on these plates. Details of parent plate preparation and welding condition, are given in Table 3.2 and 3.5 respectively. The mechanical testing specifications are given in Section 3.5. The welds were prepared using constant electrode wire and flux composition with consistant joint preparation and welding parameters.

Tensile and impact test specimens from parent plate and welds were tested at 295 k and 77 k, and results are discussed as follows:

The results of the present investigation show that the charpy-v-notch toughness of different parent plates decreased by reducing their plate rolling temperature. The impact energy of specimens from all the plates except the AISI 316L cold rolled exceeded the 27 joule requirement often used in codes and standards.[16,20] The highest impact energies were obtained for specimens prepared from plates hot rolled at 1150^{o}C; whilst lower values were associated with the cold rolled plates. Rolling at 400^{o}C improves the ductility of AISI 316L steels.

These results showed that, reducing parent plate rolling temperature increases the yield strength at the expense of ductility. Tensile test results showed that the greatest elongation was obtained from the hot rolled parent plates and/or solution treated plates whilst low values were obtained from the cold rolled plates. The results of the impact and tensile tests carried out at cryogenic temperatures showed high strength and ductility for the parent plates in this condition. This could possibly be because of the work hardening and strain induced martensite transformation in the parent plates. Because of the similarity in chemical composition, the variation in tensile strength appears to be due to the specific thermomechanical treatment applied in this investigation. Comparison of test results detailed in Section 4.6 for different plates showed that charpy-v-notch impact values and lateral expansion correlated ductility behaviour observed in tensile test specimens. Those specimens exhibiting low elongation during tensile tests had also low impact energy and lateral expansion.

It is known that the yield strength of a metal depends on its grain size, the presence of alloying elements for solid solution hardening, and any precipitation that has occured. The variation in grain size and parent plate yield strength (σ_y) are given in Table 4.1 and Table 4.3 shows the dependence of σ_y on the grain diameter, d, in reasonable agreement with the Hall-petch equation.

Furthermore, experience on low alloy steel has indicated that tensile strength depends on the carbon equivalent as well as cooling rate. The fast cooling rate tends to keep alloying elements in solution, and forms solid solution hardening, whereas a slow cooling rate will favour precipitation hardening. Considering the different thermomechanical treatments employed in this investigation, it appears

that all the above variables could have some participation in the recorded variation in strength.

The tensile test specimens did not show any marked yield point. Generally the ratio of yield to tensile strength was low (i.e. about 0.4) but with cold rolled plates some improvement was observed (i.e. a ratio of about 0.9) as a result of work hardening. This makes the cold rolled plates more attractive from the designers point of view.

Comparison of results of impact energy for various welds when tested at 77 k show that the welds produced on cold rolled plates had lower and more scattered impact energy values than the remainder of the welds. However, such a difference in values was not observed for specimens tested at 295 k. With the exception of welds produced on cold rolled plates, the welds tested at 295 k and 77 k had lower impact energies than those corresponding to their parent plates. The increase in strength of different welds could be due to the solid solution strengthening, work hardening, and formation of plastic strain induced martensite. The transformation of austenite to martensite in these metastable steels is reported by many authors.[14,16,18] The degree of transformation could be increased by lowering the temperature or by the application of stress. It has been suggested that the temperature at which martensite transformation starts (MS) is a function of chemical composition and the addition of alloying elements lowers the MS temperature of austenite.In this context different expressions for evaluation of MS temperature have been given by various authors.[18,19,122] Larbalestier and King's[122] expression gives MS temperatures of 30 k, 112 k for AISI 316L and 321 respectively.

Parent Plates of AISI types 304, 316L and 321 were plotted on the Schaeffler type diagram and checked by ferritescope for ferrite measurement. No ferrite was detected in parent plates in the as-received conditions.

In order to investigate the possibility of strain induced martensite in these metastable steels, magnetic measurements were made on the tensile test specimens prior to testing and on the fracture surface of specimens tested at 295 k and 77 k. Comparison of initial and final martensite measurements for specimens tested at room temperature showed that, (i) cold rolled plate had an insignificant amount of martensite prior to tensile testing, i.e. less than 0.25% for AISI 316L with 50% reduction and less than 1% for AISI 321 with 30% reduction at room temperature. The rest of the plates did not reveal any martensite content..

(ii) the martensite content in the fracture surface of tensile test specimens varied from sample to sample, depending upon the type of steel, i.e. chemical composition and initial metallurgical characteristics, e.g. the degree of thermomechanical treatment employed. For tensile test specimens from AISI 316L rolled at high temperatures and/or in solution treated condition the martensite content was less than 2%; whilst for plates rolled at lower temperatures a high martensite content was measured, i.e. 7% martensite for cold rolled plates. Tensile tests from AISI 321 specimens had generally higher martensite content, but they exhibited similar trends as AISI 316L. For example, specimens obtained from plate rolled at high temperature and/or solution treated showed about 7% martensite content, those from cold rolled plates showed about 18% martensite content in their fracture surface.

The results of the present investigation showed that sensitivity and the stability of austenitic stainless steel decomposition by cold working is largely dependent on the initial metallurgical characteristics rather than solely their chemical composition. The results of magnetic measurements made on the fracture surfaces of weldments were compared with their initial ferrite content;the result showed that the specimens were strongly ferromagnetic. They contained more than 30% martensite, the maximum amount distinguishable by available equipment.

The high amount of weld metal martensite content could be associated with microstructural features, i.e. initial ferrite content and deformation behaviour.

Microstructural studies of the different welds in this investigation showed that the changes in mechanical properties depended on the following:

(i) the alteration in weld bead dimension due to the amount of penetration and dilution with parent plate.

(ii)different macrostructural solidification substructure.

(iii) the variation in ferrite morphology and content.

Furthermore, the results of thin foil studies showed the presence of second phase particles and variations in dislocation density in austenite, ferrite and their interphase boundary . However, it is necessary to quantify these variables in more detail.

The reduction in strength could be related to the presence of residual elements, i.e. phosphorous, sulphur and silicon, as they were not considered in terms of a variation of transformation

characteristics, but also by precipitation processes. These residual elements tend to nucleate embrittling phase at the interphase ferrite/austenite boundaries.[9,12,14,15,18] It appears that because of the many variables and complex conditions involved it is not possible to simply relate the weld metal strength to any one variable. This applies particularly to ferrite content. Nevertheless, previous reports[9,12,14,15,18] showed that the presence of continuous or highly directional delta ferrite phase has been deleterious to toughness.

Comparisons of weld metals and their parent plates when tested at room temperature showed that the weld metal strength and elongation were less than the corresponding base metal. However, the low temperature testing results showed that welds had higher strengths and ductility than those obtained at room temperature. This could be because of the deformation mechanism of the welds, i.e. stress induced martensite. The reduction in weld metal mechanical properties could be due to the weld metal solidification behaviour and their microstructural features, i.e. the presence of ferrite, second phase particles, precipitated particles, internal fissures and variations in alloying content. For example, it is known that,[10,12] the presence of C, N and O decrease the toughness of weld metal, as the second phase particles form sites for the initiation of microvoids, and that the ductile fracture resistance decreases as the number of microvoids increases.

A comparison of the chemical analysis of these materials as given in Table 4.4 show that their minor alloying elements are close together and therefore it appears that these alloying elements have

had only a small effect on the notch bar impact properties of these materials. Furthermore, because of the similarity in welding conditions, the degradation of mechanical properties could be associated with a combination of thermal and transformation strains induced during parent plate preparation or the mechanically restraining condition used during the welding operations.

Although the welds produced in the present study were not required to meet any particular specifications, it is felt that comparison with the relevant specification is of interest. The impact energy values obtained were generally well in excess of the specification BS.639. However, weld metal produced in the cold rolled parent plate does not meet the specification of the electrode manufacturer Orlikon OP71Cr Carbowire 18/12/3RLC (AISI 316L). The typical weld metal charpy-v-notch energy at low temperature was expected to be about 35 joules.

Fractography of tensile test and charpy impact fracture surfaces showed that the fracture mode was dimpled rupture with some micro-cracks. The fracture appearance was predominantly by microvoid coal-escence in both tensile and impact test specimens tested at 295 k and 77 k. For improving the toughness of these materials in the ductile range, the presence of second phase particles should be reduced. This could be done either by improving the cleanliness of the material via deoxidation practice, or avoiding the precipitation of undesirable particles, i.e. carbides. However, it is necessary to improve the toughness of the material matrix itself in order to resist void growth. The latter could be achieved by controlling the metallurgical factors such as microstructural features, i.e. grain size, the presence of alloying elements in solid solution, dislocation density and segreg-ation of impurities of limited solubility.

The presence of microcracks in parent plates were associated with the fracture of second phase particles and/or their separation from matrix interface within the austenite or at grain boundaries. The matrix particle interface separation could be due to the low values of interfacial energy between them, which caused low strain failure there. Furthermore, previous works[12,14] identified these particles as carbides possible $M_{23}C_6$. The presence of such complex carbides, i.e. (FeCr) C_6 or $M_{23}(CN)_6$ were considered to be the cause of the further reduction in toughness of these materials.

In weld metals the presence of microcracks were mainly associated with austenite/ferrite interface boundaries which were inherited from the solidification stage possibly as a result of hot tearing.

6. CONCLUSIONS

The microstructural variation of austenitic stainless steels AISI type 316L and 321 welds produced by various welding conditions were described in this thesis. This provided an explanation for solidification behaviour as well as consequent room temperature microstructural features of these welds and indicated experiments which could lead to a more complete understanding of weld metal microstructural variations, these are :

(i) The welds exhibited epitaxial nucleation as shown by (a) the continuity of grain boundaries and (b) twinned structure across the fusion line. Once epitaxially nucleated, the grains in the fusion zone of welds experience competitive growth during solidification.

(ii) For the welds investigated the freezing mode and resultant microstructure corresponds with the Schaeffler type diagrams. However, the systematic investigation of welds under investigation showed that resultant microstructure and their chemical composition did not correspond to the appropriate pseudo-binary section of the Fe-Cr-Ni system at a fixed Fe content.

(iii) Ferrite forms as a primary solidified phase, and austenite forms from the liquid. The domination of ferrite freezing was characterised by segregation of nickel to the liquid and chromium to primary ferrite phase.

The primary ferrite dendrites became more well developed as the growth proceeded towards the centre of the weld. Despite ferrite dendrite development, the ferrite morphology remained vermicular for AISI 316L and cellular (block type structure) for AISI type 321.

(iv) The ferrite content and morphologies were susceptible to alteration

in (a) cooling rates, (b) minor changes in composition and (c) parent plate metallurgical characteristics. Welds produced by slower cooling rates and/or higher heat input showed an increase in ferrite content; whilst rapidly cooled welds and/or those with lower heat input showed lower ferrite content. Microstructural studies of rapidly cooled welds showed the presence of dispersed, elongated ferrite within an austenitic matrix with some lath type ferrite morphology.

(v) Welds produced on restrained parent plates generally showed the presence of a cellular type pattern of solidification substructure. Despite the similarity in welding conditions the welds produced on heavily cold rolled plates had higher ferrite content than the other welds.

(vi) Microstructural studies of austenitic type structures showed the presence of a columner mode of solidification. The formation of an austenitic type structure was favoured by increase in weld metal nitrogen content or faster cooling rates. Despite using similar welding parameters, welds produced on AISI 304L parent plates showed completely austenitic type structure, whilst welds produced on AISI 316L and 321 parent plates contained little ferrite. This revealed the important role of minor alloying elements on solidification behaviour, indicating the need for rationalising the welding parameters for particular parent plates and the amount of nitrogen present for selected austenitic stainless steel composition to obtain an austenitic type structure.

(vii) Microstructural studies showed that the interphase boundary separation resulting from the interaction of γ grain boundaries and ferrite were the main cause of microcracking which leads to final separation.

This investigation has enhanced the understanding of the solidification behaviour of normally austenitic stainless steel alloys and has established some basis for further work for solidification mode and elimination of microcrack in this class of alloys.

7. Suggestions for Further Work

(i) In order to clarify the ambiguity of weld metal solidification behaviour for welds with composition close to the eutectic trough it is necessary to study the factors which lead to mixed solidification mode; in this context, techniques such as STEM could be explored to determine more accurately the effect and the distribution of primary alloying elements, as well as the minor alloying elements on welds produced with different cooling rates.

(ii) Study of the effect of specific alloying additions on the equilibrium shape of the Fe-Cr-Ni ternary system with techniques such as Gleeble[41] when equipped with a quenching fixture in order to simulate the elevated temperature equilibrium microstructure suitable for micro-analysis and establishing the equilibrium shape of the Fe-Cr-Ni ternary systems for different welds.

(iii) Solidification rate and the time available for diffusion controlled transformation are playing a major role in solidified weld metal microstructure. However, detailed study of the factors which influence the growth rate of primary dendrites and the rate of ferrite consumption by austenite, if any, would be particularly fruitful.

(iv) Increasing cooling rates, thermal and deformation stresses increase the number of microcracks (austenite/ferrite interphase boundary separation) in austenitic stainless steel weld metal. In order to understand the microcrack initiation and the consequent effect on weld metal mechanical properties, further work is necessary to study the solidification mode and the wetting characteristics of different phase boundaries.

(v) Further work is necessary to study the effect of overall thermal stress induced during welding as well as volume changes associated with thermal strain and phase transformation on the solidification substructure and ferrite morphology of different welds.

(vi) Further work is necessary to study the effect of minor alloying elements, e.g. Ti acting as grain refining agent as well as restraining the parent plates on the solidification substructure and ferrite morphology of different welds.

REFERENCES

1. J.Moneypenny; "Stainless Iron and Steel", Vol.1. 1951 London Chapman and Hall.

2. J.Moneypenny; "Stainless Iron and Steel", Vol.2. 1951 London Chapman and Hall.

3. Thielsch Helmut; Weld.Jnl.Suppl. 39(12) 1950, 557_s- 621_s.

4. Thielsch Helmut; Welding Processes and Procedures employed in joining. Welding Research Council Bulletin No.14. Sept 1952.

5. Hume Rothery; The Structure of Alloys of Iron. Pergamon Press 1966.

6. J.G.Parr and A.Hanson; An Introduction of Stainless Steel, ASM,1966.

7. D.Saferian; The Metallurgy of Welding; Chapman and Hall, London. Translated by E.F.Bishop 1962.

8. R.J.Castro and decadent; Welding Metallurgy of Stainless Steel and Heat Resisting Steels. Cambridge University Press, 1974.

9. J.F.Lancaster; The Metallurgy of Welding, Brazing and Soldering. G.Allen and Unwin Ltd, London.

10. Y.Arata, F.Mutsuda; Trans.J Weld.Res.Institute 3(1) 1974. 79-88.

11. R.H. Espy ; Weld.Jnl. 61(5) 1982. 149_s- 156_s.

12. Properties of Austenitic Stainless Steels and their Weld Metals (Influence of slight chemistry variation) ASTM Proc.Conf.Atlanta-Ga., 14 Nov 1977.

13. C.V.Shirwaikar and G.P. Reddy; Weld.Jnl. 54(1), 1975, 12_s- 15_s.

14. P.Marshall; Austenitic Stainless Steels: Microstructure and Mechanical Properties. Elsevier Applied Science Publishers, London 1985.

15. D.Elliott and S.M.Tupholme; Engineering Design Guides (No.43), An Introduction to Steel Selection: Part 2, Stainless Steels. Oxford University Press.

16. D.A.Wigley; Material for Low Temperature. Materials Engineering Design Guides. Vol.26. Oxford University Press 1978.

17. Mechanical and Physical Properties of the Austenitic Chromium-Nickel Stainless Steels at subzero temperatures. International Nickel Ltd.

18. E.R.Szumachowski and H.F.Reid; Weld.Jnl. 57(11) 1978, 325-333.

19. G.P.Sanderson and D.T. Llewellyn; Jnl.Iron Steel Inst. 1969. 1129-1140.

20. British Standards Institute, B.S.1449 Part 2.

21. Trends in Welding Research in the U.S.A. Proc.Conf.sponsored by the Joining Division of American Society for Metals. New Orleans Louisiana 16-18 Nov 1981. Edited by S.A.David.

22. Stainless 84; Goteborg. The Institute of Metals, 1985.

23. D.Schalten and P.Mueller; British Weld.Jnl 14(5) 1967, 221-232.

24. T.Boniszewski; Correct Choice of Stainless Steel Electrodes for High Temperatures. Paper 6 of Conf. Trends in steels and consumables for welding. Welding Inst. Nov 1978.

25. T.Boniszewski; Metals and Materials. Dec 1978/Jan 79. 41-47.

26. R.A.Walker and T.G. Gooch; Metals and Materials, Jan 1986. 18-24.

27. Le Grand ; Welding Austenitic Stainless Steels; Manufacturing Engineers Manual 1971.

28. S.Bukovinsky and L.H. Keys; Australian Welding Jnl. March/April 1978, 10-14.

29. J.Honeycombe, T.G.Gooch and J.A. Barlow; Int.Conf. on new developments in stainless steel technology. ASM Metals/Materials Technology Series 17-20 Sept 1984.

30. A.W.Marshall and J.C.M. Farrar; Int.Conf. Welding Inst. Nov 1983, London. 24_{-1} - 24_{-13} .

31. R.A.Daemen; British Weld.Jnl. 14(10), 1967, 550-558.

32. N.N.Potapov; Scientific and Technical Welding Production, No.7, 1980, 1-4.

33. British Standards Institute, B.S.5465, 1977.

34. I.M.Campbell, R.L.Apps and E.Smith; Metal Construction British Weld Jnl. 6(1), 1974, 1-6.

35. I.Herman Thier; Schweiben and Schneiden. Translation Vol.34. No.1. 1982.

36. British Standards Institute, B.S. 2962.

37. British Standards Institute, B.S. 2901 Part 2: 1970.

38. D.Rosenthal; Weld Jnl. 20(5) 1941, 220_s - 234_s.

39. G.M.Goodwin, N.C.Cole; Weld Jnl.51(9), 1972, 425_s - 429_s .

40. H.Fredrikson; Met.Trans. 3(11), 1972, 2989-2997.

41. J.C.Lippold; Weld Jnl. 1979 58(12), 362_s - 374_s .

42. F.C.Hull; U.S. Patent 3, 201, 233, 1965, "Crack Resistance Stainless Steel Alloys".

43. L.Pryce and K.W.Andrews; Jnl. Iron Steel Inst. 195(8), 1960 415-417.

44. J.C.Lippold and W.F.Savage; "Modelling of Casting and Welding Processes". Proc.Conf. AIME Aug 1980, edited by H.D.Brody and D.Apelian.

45. W.T.Delong; Weld.Jnl. 52(2), 1973, 69_s - 73_s .

46. C.Long and W.Delong; Weld.Jnl. 52(7) 1973, 281_s - 297_s .

47. M.Watanabe; Trans.J .Weld.Soc. 3(2), 1972, 34-44.

48. P.P.Puzak and W.S.Pellini; Weld Jnl. 35(1) 1956, 9_s - 17_s.

49. R.Scherer, G.Riedrich and G.Hosh; Archiv fur das Eisen - huttenwesen 13(7), 1939, 53-57. Brutcher Translation No.891.

50. W.T.Delong, G.A.Ostrom; Weld Jnl. 35(11), 1956, 521_s - 528_s .

51. W.T.Delong; Metals Progress 77(2) 1960, 98-100.

52. W.S.Pellini; The Foundary, 80(11), 1952, 125-133, 192-194,196-199.

53. A.L.Schaeffler; Metals Progress 65(5) 1949, 680-680b.

54. W.T.Delong; Weld Jnl. 53(7), 1974, 273_s - 286_s .

55. R.D.Thomas; Weld Jnl. 34(12), 1955, 583_s - 595_s.

56. T.G.Gooch and J. Honeycombe; Metal Const: and British Weld Jnl. 4(12) 1972, 456-460.

57. T.G.Gooch and J.Honeycombe; Weld Jnl. 59(8), 1980, 233_s - 241_s.

58. A.W.Brewer and R.L. Moment; Weld Jnl. 55(6), 1976, 159-164.

59. A.Whipple and D.J. Kotecki; Weld Process Study for 316L Stainless Steel weld metal for liquid service, in materials studies for Magnetic Fusion energy Applications at low temperatures IV. N.B.S.I.R. 81-1645. - NBS Boulder, Colorado (1981) 303-321.

60. H.Astrom, Arata; Metal Science, 10, 1976, 225-234.

61. Schneider H; Foundry Trade Jnl. 108(5), 1960, 562-653.

62. American Welding Society : Standard Procedures for Calibrating Magnetic Instruments to measure the ferrite content of austenitic stainless steel weld metal. Published by the American Welding Society A4, 2-74.

63. M.J.Cieslack, W.F.Savage; Weld Jnl. 61(1), 1982, 1_s - 8_s .

64. R.B.Gunta, G.A.Rutz; Welding Research Council Bulletin. No.132 Aug 1968.

65. Y.Arata, F.Matsuda; Trans.of J .Weld Res.Inst. 5(2) 1976, 35-51.

66. P.N. Bidjulja, S.A.Iodkovskii, and N.N. Sashchinkhin; Russian Castings and Production. (English translation). 1961(6), 237-240.

67. E.A.Schoefer; Weld Jnl. 53(1) 1974, 10_s - 12_s .

68. G.Molinder; Metals Progress, 116(6) 1979, 56-59.

69. N.T.Williams; British Weld Jnl. 3(9), 1965, 435-441.

70. N.M. Novozhilov and A.V. Surkov; Welding Production 78(6), 1978 12-13.

71. S.T.Mayerhofer and H.Kohl; British Iron and Steel Industry translation No.5304, March 1967.

72. B.Strauss, and E.Maurer; Die hochlegieret en chrom-nickel Stachle als nichtrostende stahle. Krupp Monotsh, 1(8), 1920, 129-146.

73. T.V. Simpkinson; Metals Progress 55(2), 1949, 164-167.

74. T.V. Simpkinson; Iron Age 170(12), 1952, 166-169.

75. H.A.Meiyer; British Weld Jnl. 13(1) 1966, 12-17.

76. H.S.Avery and H.J. Chapin; Weld Jnl. 33(9), 1954, 459-468.

77. R.M.Bozorth; Ferromagnetism, Published by D.Van Nostrand Co.Inc, New York, 1951.

78. H.Dietrich; Schweissen Und Schneiden, 18(11), 1966, 552-557.

79. E.Stalmasek; Int.Inst. of Welding. Commission No.2 "Arc Welding" Summary of work 1963 - 1973.

80. F.C.Hull, Weld Jnl. 46(9), 1967, 399-409.

81. P. Merinov, G.Entin, B.Beketor and A.Runov; N.D.T. International 11(2), 1978, 9-14.

82. F.C.Hull; Weld Jnl. 52(5), 1973, 193-203.

83. J.M.Vitak, S.A.David; Met.Trans 14A(9), 1983, 1833.

84. N.K.Jaggi, K.R.P.N. Rao; N.D.T. Int., 11(6), 1978, 281-286.

85. T.P.S. Gill, R.K.Dajal; Weld Jnl. 58(12), 1979, 375_s - 378_s .

86. J.C.Lippold,W.F.Savage; Weld Jnl. 59(2) 1980, 48_s - 58_s .

87. S.A.David; Weld Jnl. 60(4), 1981, 63_s - 71_s .

88. S.A.David; G.M.Goodwin and D.N.Braski; Weld Jnl. 58(11), 1979, 330_s - 336_s.

89. N.Suutala, T.Takalo and T.Moisio; Technical note: Weld Jnl. 61(5) 1981, 92-93.

90. G.L.Leone; Solidification Modes and Grain Structure of Normally Austenitic Stainless Steels. Ph.D.Thesis. Waterloo-Ontario. University of Waterloo 1980.

91. V.Kujanpaa and N.Suutala; Weld Res.Int. 9(2), 1979, 55-96.

92. A guide to the Solidification of Steels. Jernkontoret-Stockholm 1977.

93. Y.Arata, F.Mutsuda and Nakatak; Trans.J. Weld.Res.Inst. 5(1), 1976, 47-52.

94. M.J.Cieslak and W.F.Savage; Weld Jnl. 59(5) 1980, 136_s - 146_s.

95. J.A.Brooks; Met.Trans. 14A (7), 1983, 1271-1281.

96. J.A.Brooks; Weld Jnl. 54(6), 1975, 189_s - 195_s .

97. J.A.Brooks; F.J.Lambert Jr; Weld Jnl.Vol 57(5), 1978, 139_s - 143_s.

98. S.Derosa, M.H.Jacobs and D.G.Jones; Int.Conf. on Solidification and Casting, Sheffield, July 1977, Part 2. 22.

99. W.E.Brower and M.C.Fleming; Solidification of Iron Base Alloys at large degree of under cooling. United States Army Materials Research Centre, Waterdown, Massachusettes, C.R. 69-14 110. 1969.

100. N.Suutala, T.Takalo and T.Moisio; Met.Trans. 10A(4) 1979, 512-514.

101. N.Suutala, T.Takalo and T.Moisio; Met.Trans. 10A(8) 1979, 1183-1190.

102. N.Suutala, T.Takalo and T.Moisio; Met.Trans. 11A(5), 1980, 717-725.

103. C.E.Lyman, P.E. Manning, D.J.Duquette and E.Hall; Scanning Electron Microscopy, 78(1) 1978, 213-220.

104. C.E.Lyman; Weld Jnl. 58(7), 1979, 189-194.

105. T.B. Massalski; Materials Science and Engineering, 25, 1976, 119-125.

106. O.Hammar and U.Svensson; Influence of steel composition on segregation and microstructure during solidification of austenitic stainless steels. Solidification and Casting of metals. 401-410. London, The Metal Society, 1979.

107. G.J.Davies; Solidification and Casting App.sc.Pub.Ltd 1973.

108. M.G.Flemings; Solidification Processing. McGraw Hill, 1974.

109. F.W.Savage; 1980 Houdremont Lecture, Solidification, Segregation and Weld Imperfections; Weld in the World 18(5/6) 1980, 89-114.

110. J.Davies and J.G. Garland; Int.Met.Reviews 20 (196) 1975, 83-105.

111. F.Matsuda, T.Hashimoto and T.Senda; Trans.National Res.Inst.Metals 11(1) 1969, 43-58.

112. W.F.Savage, C.D.Lundin and A.H.Aronson; Weld Jnl. 44(4) 1965, 175_s - 181_s .

113. W.Kurz, D.J.Fisher; Fundamental of Solidification. Trans. Tech. Pub. 1984. Switzerland.

114. H.T.Hall andW.J.Jackson; Grain refinement in cast austenitic steels. Prof.Conf. on the Solidification of Metals. The Iron and Steel Inst.London.Publication 110, 1968, 313.

115. American Society for Metals, Metal Handbook, 8th Ed. Vol.8. 424. Metal Park Ohio.

116. J.W.Pugh and J.D.Nisbet; Trans. AIME 188(2) 1950.

117. Phase equilibria in Fe-Ternary Alloys. Critical evaluation of constitution of Cr-Fe-Ni system. Int.Metals. Reviews. Review 248, No.1, 1980, 21.

118. V.G.Smith, W.A.Tiller and Rutter; Can.Jnl.Phys.33, 1955, 733.

119. F.A.C. Calvo, K.P.Bentley, R.G.Baker; Acta.Met.8, 1960, 898.

120. ASTMA 370-77. Standard Methods and definitions for mechanical testing of steel products. "American Society for Testing and Materials" Philadelphia, Pensylvania.

121. R.P.Reed, Schramm; "A cryostat for tensile tests in the temperature range 300 to 4K" in advances in cryogenic engineering, Vol.7 Plenum Press, New York, 1962, 448-454.

122. D.C.Larbalestier, and H.W.King; Proc. 4th Int.Cryogenic Eng.Conf. IPC, Surrey, 338. (1974).

123. J.G.Borland and R.N.Younger; British Weld Jnl. 7. 1960, 22-59.

Table 2.1 Chemical composition of standard austenitic stainless steels

British Standard designation	Common designation	Composition† (%) C	Si	Mn	P	S	Cr	Mo	Ni	Others
(1) 301S21	301	0.15		0.50–2.00		0.030	16.0–18.0		6.0–8.0	
(2) 302S17	302	0.08		0.50–2.00		0.030	17.0–19.0		8.0–11.0	
(3) 303S21	303	0.12		1.00–2.00		0.15–0.30	17.0–19.0	-	8.0–11.0	
(4) 303S41	303Se			1.00–2.00		0.060	17.0–19.0	-	8.0–11.0	Se 0.15 0.30
(5) 304S15	304	0.06					17.5–19.0		8.0–11.0	
(6) 304S16	304DO						17.5–19.0	-	9.0–11.0	
(7) 304S12	304L	0.03					17.5–19.0		9.0–12.0	
(8) 305S19	305	0.10					17.0–19.0	-	11.0–13.0	
(9) 309S24	309	0.15			0.045		22.0–25.0	-	12.0–16.0	
(10) 310S24	310				(1)–(19)		23.0–26.0		19.0–22.0	
(11) 315S16	315	0.07					16.5–18.5	1.25–1.75	9.0–11.0	
(12) 316S16	316						16.5–18.5	2.25–3.00	10.0–13.0	
(13) 316S12	316L	0.03					16.5–18.5	2.25–3.00	11.0–14.0	
(14) 317S16	317	0.06					17.5–19.5	3.0–4.00	12.0–15.0	
(15) 317S12	317L	0.03					17.5–19.5	3.0–4.00	14.0–17.0	
(16) 320S17	320	0.08	0.20–1.00	0.50–2.00			16.5–18.5	2.25–3.00	11.0–14.0	Ti 4 × C–0.60
(17) 321S12	321			(5)–(26)			17.0–19.0	–	9.0–12.0	Ti 5 × C–0.70
(18) 347S17	347					0.030	17.0–19.0	–	9.0–12.0	Nb 10 × C–1.00
(19) 304S49	Creep-resisting grade 304					(5) (26)	17.5–19.0	–	8.0–11.0	Nb 0.65
(20) 316S49	Creep-resisting grade 316	0.04–0.09					16.0–18.0	2.00–2.75	10.0–13.0	Nb 0.65 B 0.001–0.006
(21) 321S49	Creep-resisting grade 321	(19)–(22)			0.040		17.0–19.0	–	9.0–12.0	Nb 0.65
(22) 347S49	Creep-resisting grade 347						17.0–19.0	–	9.0–12.0	Nb 10 × C–1.00
(23) 304S62	Hiproof 304L	0.03					17.5–19.0	–	9.0–12.0	
(24) 304S65	Hiproof 304	0.06			0.045		17.5–19.0	–	8.0–11.0	N 0.15–0.25
(25) 316S63	Hiproof 316L	0.03					16.5–18.5	2.25–3.00	11.0–14.0	(23)–(26)
(26) 316S66	Hiproof 316	0.07					16.5–18.5	2.25–3.00	10.0–13.0	

† Maximum unless range is specified.

TABLE 2.2

Mechanical properties of common stainless steels as given by BS 1449, Part 2 (minimum values)

Steel	Tensile strength (N/mm²)	0.2 % proof stress (N/mm²)	Elongation on 50 mm gauge length (%) 0.5–1.6 mm thick	1.6–3.0 mm thick	over 3.0 mm thick	Hardness (max.) sheet and strip (HV)	Hardness (max.) plate (HB)
Austenitics							
301S21	540	215	30	35	40	220	–
302S17	510	210	30	35	40	190	–
304S15	510	210	30	35	40	190	192
304S16	510	210	30	35	40	190	–
304S12	490	195	30	35	40	190	192
305S19	460	170	30	35	40	185	–
309S24	540	215	30	35	40	–	207
310S24	540	215	30	35	40	205	207
316S16	540	210	30	35	40	195	197
316S12	490	200	30	35	40	195	197
317S16	540	210	25	30	35	–	205
317S12	490	195	25	30	35	195	197
320S17	540	210	30	35	40	205	207
321S12	510	210	30	35	40	200	202
347S17	510	210	30	35	40	202	200
Ferritics							
403S17	420	245	17	20	22	175	192
405S17	420	245	17	20	22	175	192
409S17	420	230	17	20	22	180	179
430S15	430	245	17	20	22	175	192
434S19	430	245	17	20	22	185	–
Martensitics							
410S21 softened	–	–	–	–	–	–	183
hardened	550–700	340	–	–	20	185	–

Notes.

1. Mechanical properties are for steels in the softened condition, with the exception of 410S21 which is hardened and tempered.
2. The properties are not always applicable both to plate and to sheet/strip. For grades 301S21, 302S17, and 305S19 there are no properties for plate quoted in BS 1449, Part 2.
3. Mechanical properties for sheet and strip are not mandatory but are for information purposes. It is customary to order steel to hardness and bend test requirements, rather than to tensile properties. Bend test requirements are mandatory.

TABLE 3.1 Chemical Composition of Parent Plates wt%

Mark	C	Si	Mn	P	S	Co	Cr	Ni	Cu	Mo	Nb	Ti	V	W	Fe	N	O
AISI 321	0.040	0.58	1.25	0.031	0.023	0.15	17.8	10.3	0.38	0.64	0.05	0.38	0.06	0.15	Bal	0.018	0.0044
AISI 316L	0.014	0.52	1.57	0.034	0.005	0.15	16.8	11.3	0.20	2.47	0.03	L0.01	0.07	0.13	Bal	0.051	0.0048

TABLE 3.2 Parent Plate Preparation

Preparation	Cooling	Identity
(i) AISI 321 (33% reduction)		
1 - As-received billet i.e. not rolled	-	A,B
2 - Hot rolled , 1150°C	Furnace cooled	F, G
3 - Hot rolled , 1150°C	Water quenched	H
4 - Hot rolled , 950°C	Water quenched	D
5 - Hot rolled , 950°C	Furnace Cooled	E
6 - Hot rolled , 400°C	-	I, J
7 - Cold rolled, 20°C	-	K, L
(ii) AISI 316L (50% reduction)		
1 - As-received billet i.e. not rolled	-	M, N
2 - Hot rolled , 1150°C	Furnace cooled	X, U
3 - Hot rolled , 1150°C	Water quenched	Y, V
4 - Hot rolled , 1150°C (solution treated at 1150°C for 45 minutes after hot rolling).	Water quenched	Z
5 - Hot rolled 950°C	Furnace cooled	P
6 - Hot rolled 950°C	Water quenched	S
7 - Hot rolled 400°C	-	Q, W
8 - Cold rolled + 20°C	-	T

TABLE 3.3 Nominal Electrode Wire and Flux Compositions
(i) electrode wire composition (wt%) for SAW
(4mm wire diameter)

Alloying elements:

C	0.03X
Mm	1.5 - 2
Si	0.6 X
S	0.025 X
P	0.025 X
Cr	16-19
Ni	12.5-14
Mo	2.2 - 2.7
X	denotes max.

(ii) Flux Composition % (Oerlikon OP71 Cr) for SAW.

35 Ca + Mg , 25 CaF2 , 25 SiO_2 and 15 Al_2O_3

Note: contains 2% ferrochrome to compensate for arc losses.

(Basicity = 1.8)

(iii) Electrode wire composition for MIG welding

EAS 2TG D/N 8556 - AWS ER308L 1.2mm wire diameter

C 0.03

Cr 19

Ni 9.5

TABLE 3.4

Details of single run square groove butt joint submerged arc welds

Remarks	Parent plate conditions
Plate 316L	
M, N	As received condition
X, U	Hot rolled furnace cooled
Y, V	Hot rolled water quenched
Z	Hot rolled - solution treated - water quenched
T	Cold rolled
Plate 321	
B	As received condition
F, G	Hot rolled furnace cooled
H	Hot rolled water quenched
K, L	Cold rolled

TABLE 3.5

	Welding Conditions
Welding mode	Butt weld submerged arc welding - parent plates of different characteristics
Welding current	650^{A}
Welding voltage	23^{V}
Travel speed	$400\ \frac{mm}{min}$
Arc length	20mm
Welding position	Flat

TABLE 3.6

Details of submerged arc bead-on-plate welds

The electrode wire stick out is 20mm and travel speed is 400 $\frac{mm}{min}$ on 25mm thick parent plates:

	Specimens	Current	Voltage
I	F1	750	40
	C3	750	40
	R8	750	40
II	C5	650	30
	F4	650	30
	R9	650	30
III	C6	440	23
	F7	440	23
	R10	440	23
IV	F12	380	22
	C13	380	22
	R11	380	22
V	15 RN	380	22
	18 FN	380	22
	16 R	380	22
	250 RH	380	22

KEY: R = Restrained parent plate

F = Unrestrained parent plate

C = Copper bead rapidly cooled

TABLE 3.7 Bead-on-plate MIG welding

Nominally identical welding conditions - parent plates of different characteristics.

All welds were prepared at a speed of 0.6cm s^{-1} in Argon shield gas -10mm thick plate.

Parent plate conditions. 321 S/S	Remarks	Current I/A	Voltage E/V
As received condition	B	155	22
Hot rolled -1150°C Furnace colled	F, G	155	22
Cold rolled	L, K	155	22
Hot rolled 950°C Furnace colled	E	155	22
Parent plate 316L S/S			
As received condition	M, N	155	22
Hot rolled 1150°C - solution treated water quenched	Z		
Hot rolled 1150°C Furnace colled	,X, Y	155	22
Hot rolled 950°C water quenched	S	155	22
Cold rolled	T	155	22

TABLE 3.8 Bead-on-plate MIG Welding.

Fully austenitic stainless steel welds

All welds were prepared at a speed of 0.6 cm s^{-1} - 10mm thick plates.

Weld Remarks	Current	Voltage	Shielding gas
AISI 304	155	22	95 Ar + 5% N
AISI 316L	155	22	95 Ar + 5% N
AISI 321	, 155	22	95 Ar + 5% N

TABLE 3.9 Chemical reagents for microstructural studies

(i) Etching procedure to reveal the microstructure

1 - oxalic acid: 10% oxalic acid by weight in distilled water used electrolytically at 6 volts for 10 seconds or more.

2 - mixed acid: 1/3 HCL 1/3 HNO3 and 1/3 acetic acid. Since this etchant decomposes rapidly, samples had to be etched within several minutes after mixing.

3 - Murakamis :

$K_3Fe(CN)_6$ potassium ferricyamide	10 gms
KOH potassium hydroxide	10 gms
H_2O distilled	100^{ml}

etch must be freshly made, bring to boil, immerse the specimen for 8min.

(ii) Thin Foil Preparation

Struers tenupel polishing apparatus:

1. Solution of 10% perchloric acid (72% strength) in dry methanol at $-10^{o}C$ with a potential of 55 volts D.C.
2. 1000^{cc} Glacial acetic acid , 42^{cc} perchloric acid (72%) 8^{ml} distilled water with a potential of 75 volts.

TABLE 4.1 Quantitative metallography of parent plates austenite grain size using mean linear intercept and 95% confidence limits, values given in microns

Remarks	Austenite grain size
AISI 316L S/S	
M	41.8 ± 2.6
S	30 ± 4.2
T	22.9 ± 4
X	95.4 ± 4.8
Y	71 ± 3.5
Z	93.8 ± 3.5
AISI 321 S/S	
B	22.9 ± 5.3
3E	13.8 ± 1.7
3F	16.6 ± 1.5
3G	19.7 ± 1.12
K	10.8 ± 1.4

TABLE 4.2 The lateral expansion measurement from charpy-v-notch for different parent plate specimens - tested at 77 k

AISI 316L	ΔL (mm)
M	1.15
Q	1. 6
X	1. 3
Y	1.36
Z	1.85
P	1.29
S	0.95
W	0.35
T	0. 2
AISI 321	
B	1.25
H	1.53
F	1.72
D	0.98
E	0.75
I	0.45
J	0.47
K	0. 5

TABLE 4.3

Tensile strength of different austenitic stainless steels parent plate tested at room temperature and cryogenic conditions.

Remarks	YS (Mpa)		UTS(Mpa)		Elongation %	
AISI 316L	295K	77K	295K	77K	295K	77K
M	305	611	611	1296	77	63
P	407	586	688	1401	61	53
S	708	611	662	1406	62	62
T	853	1048	1075	1450	15	45
X	215	458	570	1299	63	68
Y	316	474	595	1313	77	64
Z	287	417	582	1330	76	66
Q	713	876	805	1477	22	50
W	662	917	831	1478	30	51
AISI 321						
B	264	450	604	1354	70	55
D	397	357	660	1427	60	46
E	331	323	627	1426	63	50
F	275	334	596	1382	70	53
H	305	356	611	1401	68	54
K	838	950	896	1546	17	40
I	662	713	713	1518	29	49
J	688	739	738	1523	32	47

TABLE 4.4 Chemical Composition of Weld Metals wt%

Mark	C	Si	Mn	P	S	Co	Cr	Ni	Cu	Mo	Nb	Ti	V	W	Fe	N	O
Butt weld K(321)	0.028	0.52	1.33	0.035	0.018	0.23	18.3	11.2	0.30	1.13	0.03	0.18	0.05	0.10	Bal	0.02	0.06
Butt weld Z(316L)	0.010	0.46	1.48	0.032	0.008	0.23	17.5	11.7	0.17	2.27	0.02	<0.01	0.06	0.08	-	0.037	0.055
Bead-on-plate 8R (316)	0.055	0.4	1.30	0.03	0.007	0.3	18.5	11.3	0.18	2.4	0.02	<0.01	0.07	0.07	-	0.042	-
Bead-on-plate 14(R)	0.026	0.51	1.57	0.038	0.006	0.35	17.5	11.7	0.16	2.32	0.025	<0.01	0.017	0.072	-	0.034	-
Bead-on-plate 18(FN)	0.032	0.37	1.52	0.039	0.0075	0.28	17.8	11.7	0.15	2.37	0.029	<0.01	0.06	0.085	-	0.050	-
Bead-on-plate 11(R)	0.046	0.47	1.43	0.035	0.0083	0.27	17.1	11.7	0.19	2.24	0.02	<0.01	0.075	0.085	-	0.034	-
Bead-on-plate L(10)	0.031	0.51	1.2	0.02	0.01	0.1	17.85	9.8	0.3	0.34	0.02	0.2	0.04	0.14	-	0.20	-
Bead-on-plate K(321)	0.048	-	-	-	-	-	19.1	10.3	-	-	-	-	-	-	-	0.04	-

Short dash (-) denotes not determined.

TABLE 4.5

Delta ferrite content of differend Bead-on-Plate Submerged Arc welds produced under different welding conditions.

Remarks	Ferrite content
F_1	7.5
F_4	7
F_7	5.5
F_{12}	5
R_8	7
R_9	7
R_{10}	7
R_{11}	6
C_3	7
C_5	6.5
C_6	6.5
C_{13}	5.5

TABLE 4.6

δ Fe content of different Bead-on-Plate MIG welds produced under similar welding conditions but different parent plate characteristics.

Remarks	δFe
AISI 321S/S	
B_1	6.5
3E	7
3F	7
3G	6.5
K_1	9.5
AISI 316L	
M_1	5.5
S_1	7
T	8
X	7.5
Y	6.5
Z	6

TABLE 4.7

Delta ferrite content of different Butt welds produced by Submerged Arc welding.

Remarks	δ Fe/top surface	δ Fe/Transverse cross section
AISI 321 S/S		
B	6	5.5
F	6.5	5
K	9	7.5
AISI 316L S/S		
M	6.5	5
T	7.5	4
U	5	4
X	6.5	4
Y	6.5	4.5
Z	6.5	5

TABLE 4.8

Segregation measured in different welds.

Remarks	Ke_{Cr}	Ke_{Ni}	Is_{Cr}	Is_{Ni}
Bead-on-plate weld 250 RH				
A1	1.51	0.4	0.79	2.1
A2	1.35	0.57	0.83	1.4
A3	1.56	0.34	0.71	2.47
A4	1.35	0.57	0.82	1.42
Bead-on-plate weld 18FN				
A1	1.47	0.45	0.73	2.0
A2	1.5	0.44	0.72	2.1
A3	1.45	0.47	0.74	1.85
A4	1.44	0.51	0.74	1.67
Butt weld K321				
A1	1.16	0.75	0.92	1.12
A2	1.1	0.78	0.99	1.11
A3	1.13	0.89	0.94	1.1

TABLE 4.9

The lateral expansion measurement for charpy-v-notch impact test specimens for different butt weld metal tested at cryogenic conditions (77 K)

AISI 316L.	ΔL (mm)
M	0.8
X	0.6
Z	0.65
T	0.3
AISI 321	
B	0.7
H	0.9
F	1.1
K	0.6

TABLE 4.10

Tensile strength of selected AISI 316L and 321 Butt welds tested at cryogenic conditions (77).

Remarks	Ys(Mpa)	UTS(Mpa)	Elongation %
AISI 316L			
Ni	524	1263	60
N_2	540	1258	57
Mi	586	1284	60
M_2	561	1223	56
Ti	560	1284	60
T_2	579	1280	60
U_1	433	1477	58
U_2	490	1402	57
AISI 321			
B_1	458	1304	55
B_2	454	1303	49
F_1	357	1376	46
F_2	389	1402	43
G_1	459	1325	46
G_2	398	1339	49
H_1	453	1284	40
H_2	382	1309	48
K_1	448	1325	50
K_2	431	1390	52

TABLE 4.11 The microhardness measurement results (VPN) of different AISI 316L bead-on-plate submerged arc weld metals

Remarks	Hardness values (VPN)
F1	171
F4	197
F7	230
F12	235
C3	218
C5	234
C6	207
R8	224
R9	167
R10	173
R11	211
250RH	206
15 RN	281
18 FN	283

TABLE 4.12

The micro-hardness measurement results (VPN) for different AISI 316L and 321 Bead-on-Plate MIG welds

AISI 321	Hardness values
B_1	260
3E	274
3F	200
G	179
K_1	244

AISI 316L	
3N	280
3S	284
Ti	224
X	204
Y	216
Z	325

Table 5.1 Chromium, Nickel equivalent and their ratio for different welds, using equations (5.2) and (5.3).[54]

Remarks	Cr eqv.	Ni eqv.	$\frac{Cr}{Ni}$ eqv. ratio
Butt Weld K(321)	20.2	13.1	1.54
Butt Weld Z(316L)	20.5	13.86	1.47
Bead-on-plate 8R(316L)	21.6	14.85	1.45
Bead-on-plate 14R(316L)	20.7	14.2	1.45
Bead-on-plate 18FN(316L)	20.77	14.86	1.39
Bead-on-plate 11R(316L)	20.77	14.8	1.4
Bead-on-plate L10(321)	19.82	16.48	1.2
Bead-on-plate K321	20.99	12.99	1.61

Table 5.2 Chromium, Nickel equivalent and their ratio for different welds, using equations (5.4) and (5.5).[92]

Remarks	Cr eqv.	Ni eqv.	$\frac{Cr}{Ni}$ eqv. ratio
Butt Weld K(321)	20.58	12.6	1.63
Butt Weld Z (316L)	22.13	13.1	1.69
Bead-on-plate 8R(316L)	22.45	13.69	1.64
Bead-on-plate 14R(316L)	21.52	13.4	1.6
Bead-on-plate 18FN(316L)	21.69	14.2	1.53
Bead-on-plate 11R(316L)	20.9	13.8	1.51
Bead-on-plate L10(316L)	19.72	13.89	1.42
Bead-on-plate K321	22.1	12.63	1.74

TABLE 5.3 Carbon Equivalent for Different Welds

Remarks	Carbon Equivalent
Butt weld K 321	0.037
Butt weld Z 316	0.04
Bead-on-plate 8R	0.075
Bead-on-plate 14R	0.046
Bead-on-plate 18FN	0.062
Bead-on-plate 11R	0.066
Bead-on-plate L10	0.15
Bead-on-plate K321	0.05

Table 5.4 The chemical analysis and rationalised values of alloying elements for different welds.

	Chemical analysis values					Rationalised values		
	Cr	Ni	Cr+Ni	Total alloying elements	Fe	Cr_o	Ni_o	Fe_o
Butt weld K(321)	18.3	11	29.3	33.33	66.67	19	11.46	69.47
Butt weld Z(316L)	17.5	11.7	29.2	34.12	65.87	18.4	12.3	69.2
Bead-on-plate 8R(316L)	18.5	11.3	29.8	34.7	65.3	19.45	11.9	68.66
Bead-on-plate 14R(316L)	17.25	11.7	29.2	34.34	65.66	18.45	11.33	68.5
Bead-on-plate 18FN(316L)	17.8	11.7	29.5	33.5	65.5	18.7	11.32	68.9
Bead-on-plate 11R(316L)	17.8	11.7	28.8	33.7	66.3	18.7	12.3	68.9
Bead-on-plate L10(321)	17.85	9.8	27.65	30.76	69.24	18.5	10.2	71.8
Bead-on-plate K(321)	19.1	10.3	29.4	-	-	-	-	-

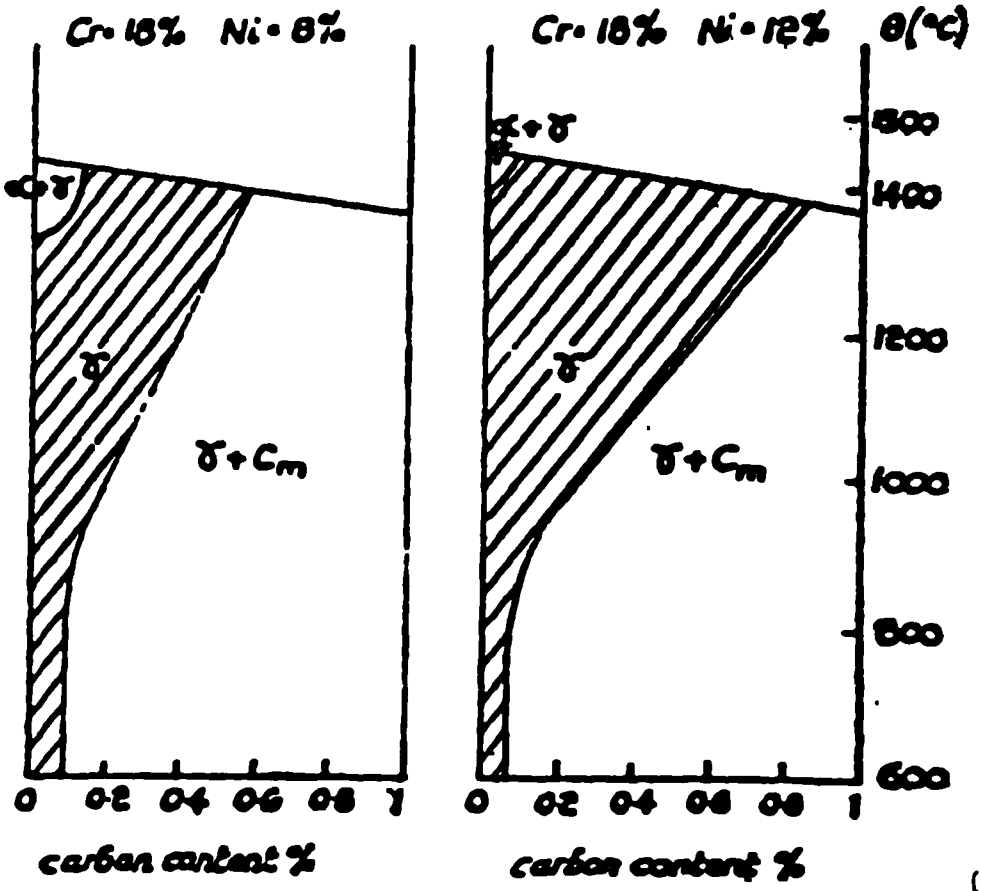

Fig 2.1 *The influence of nickel on the gamma phase field in steel with 18% Cr* [7]

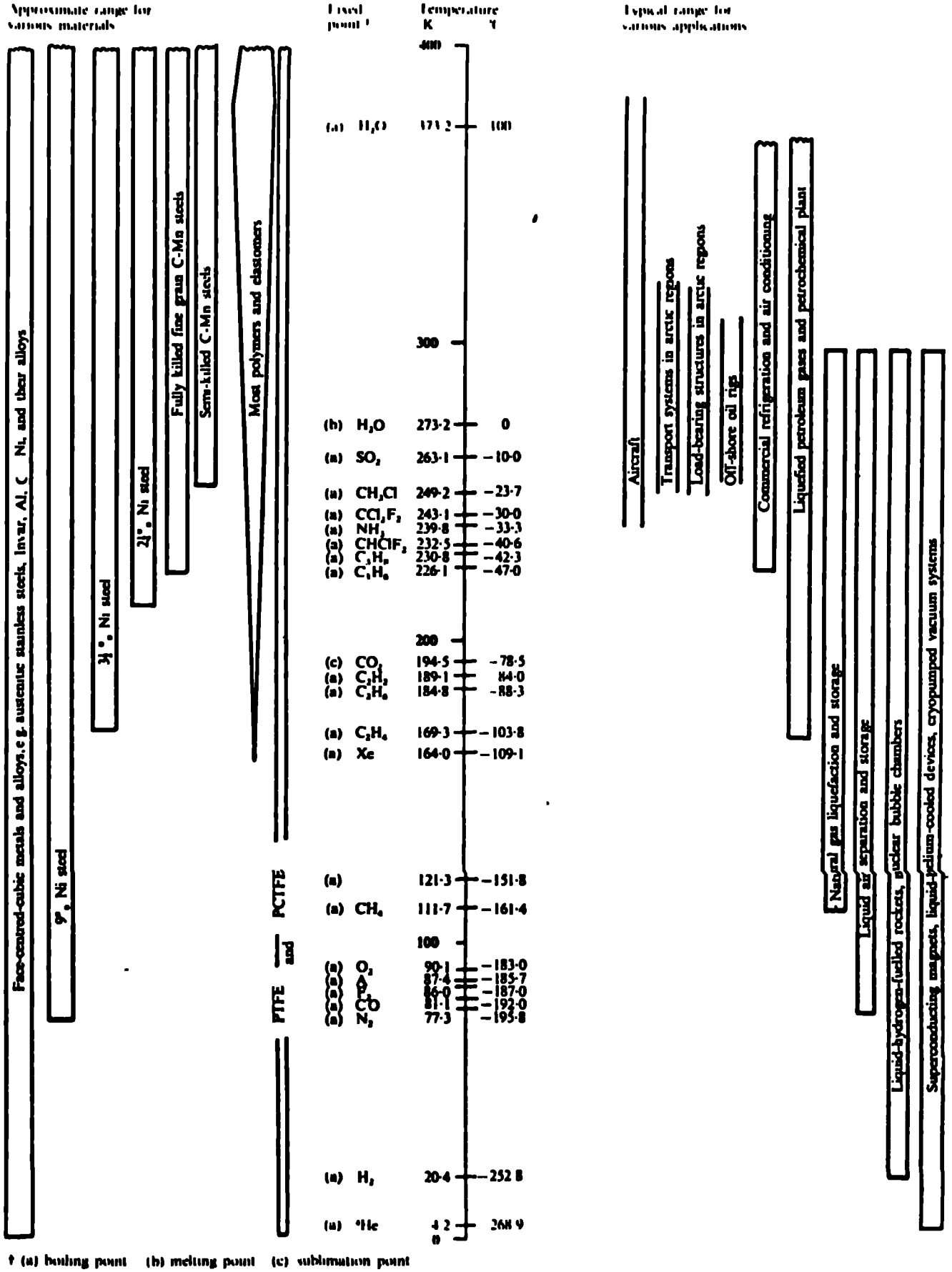

16)

g.2.2 **Some significant temperatures and typical operating temperature ranges for various structures and constructional materials**

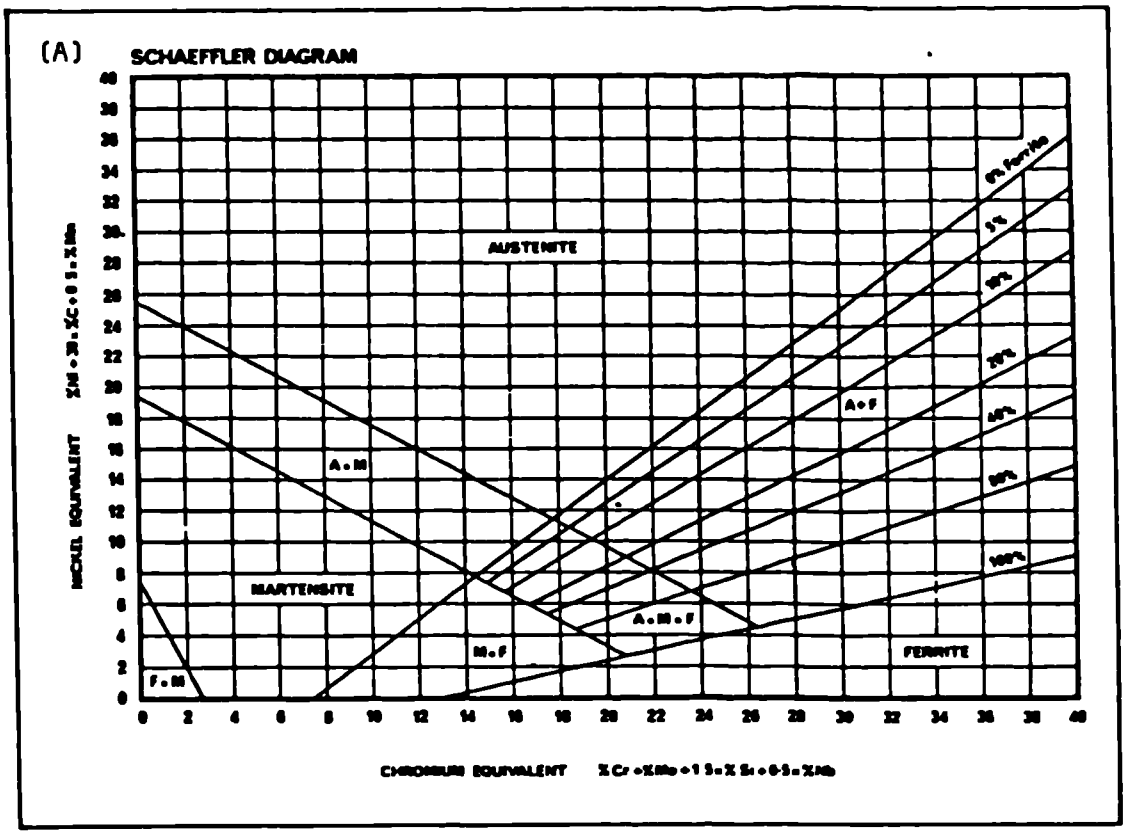

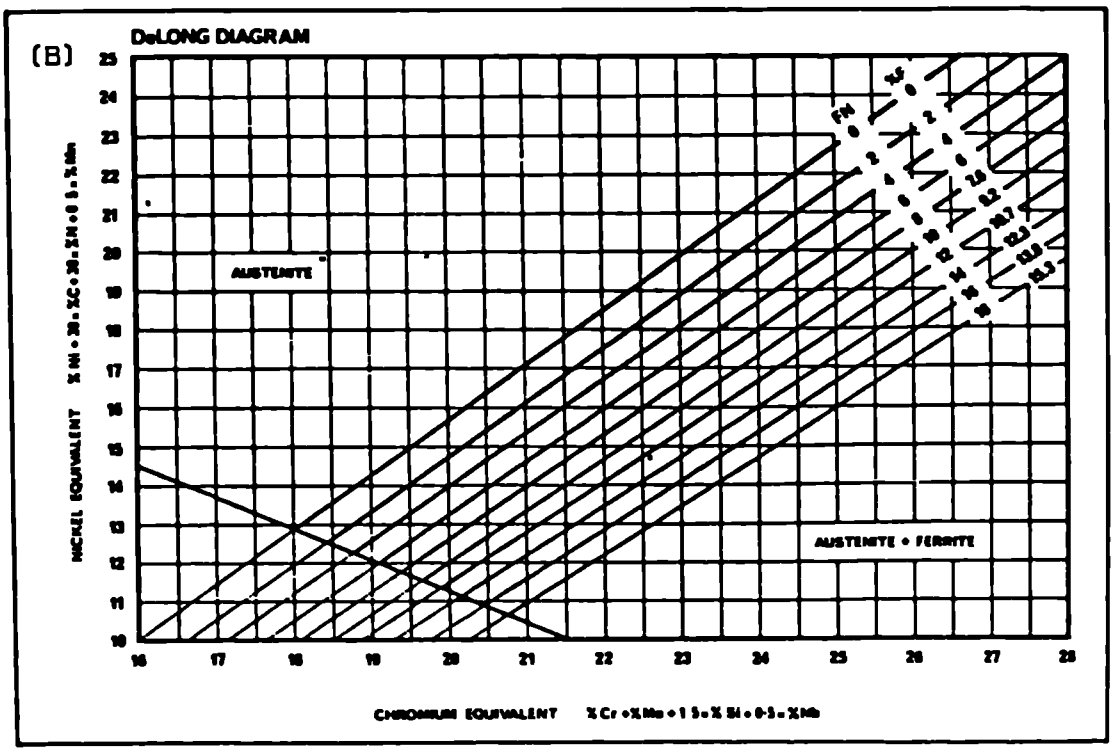

Fig.2.3 Constitution Diagram for Stainless Steel Weld Metal. (26)

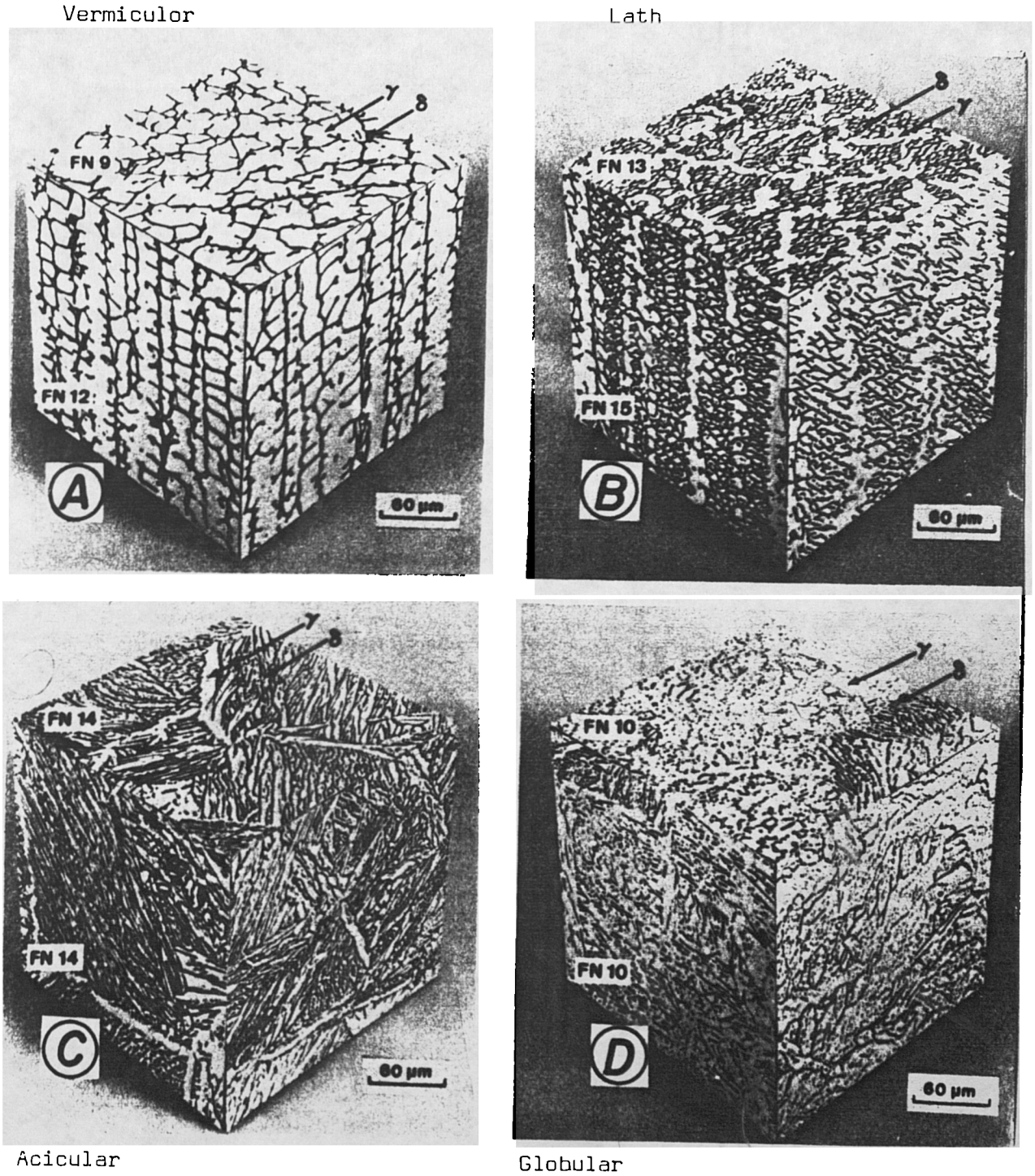

Fig.2.4 Classification of different ferrite morphology after David et al[87]

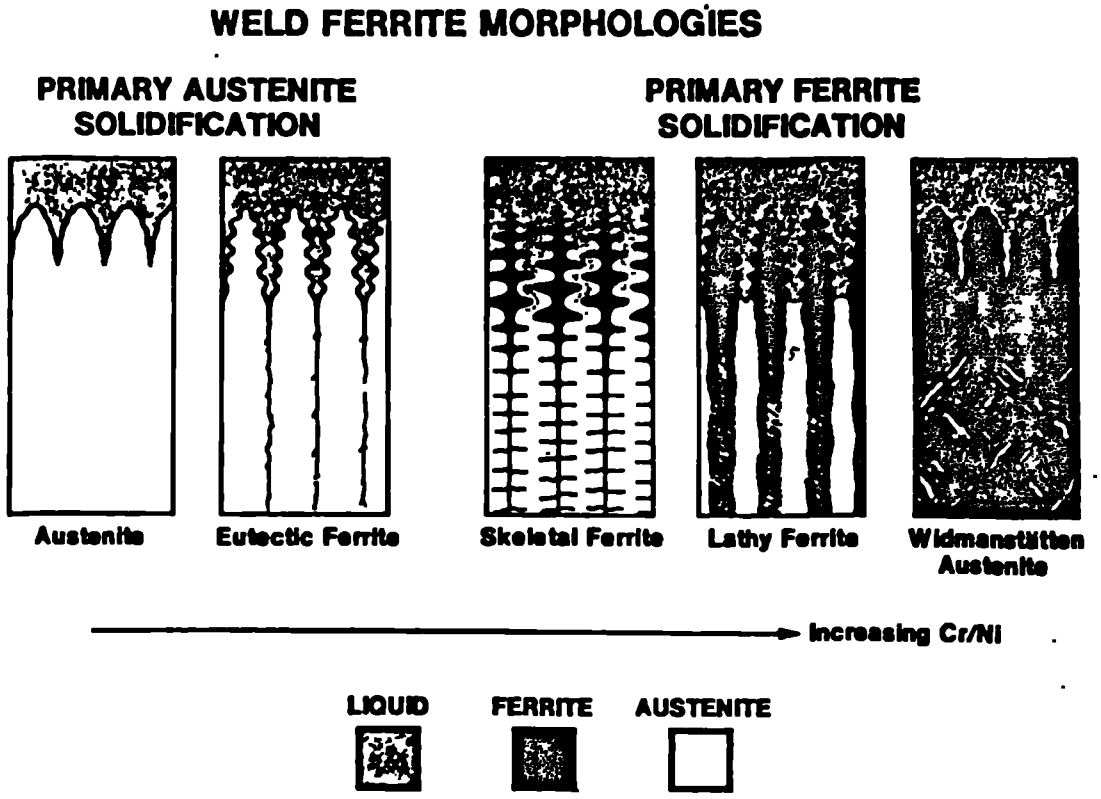

Fig.2.5 Schematic of the solidification and transformation behavior resulting in a range of weld ferrite morphologies (91)

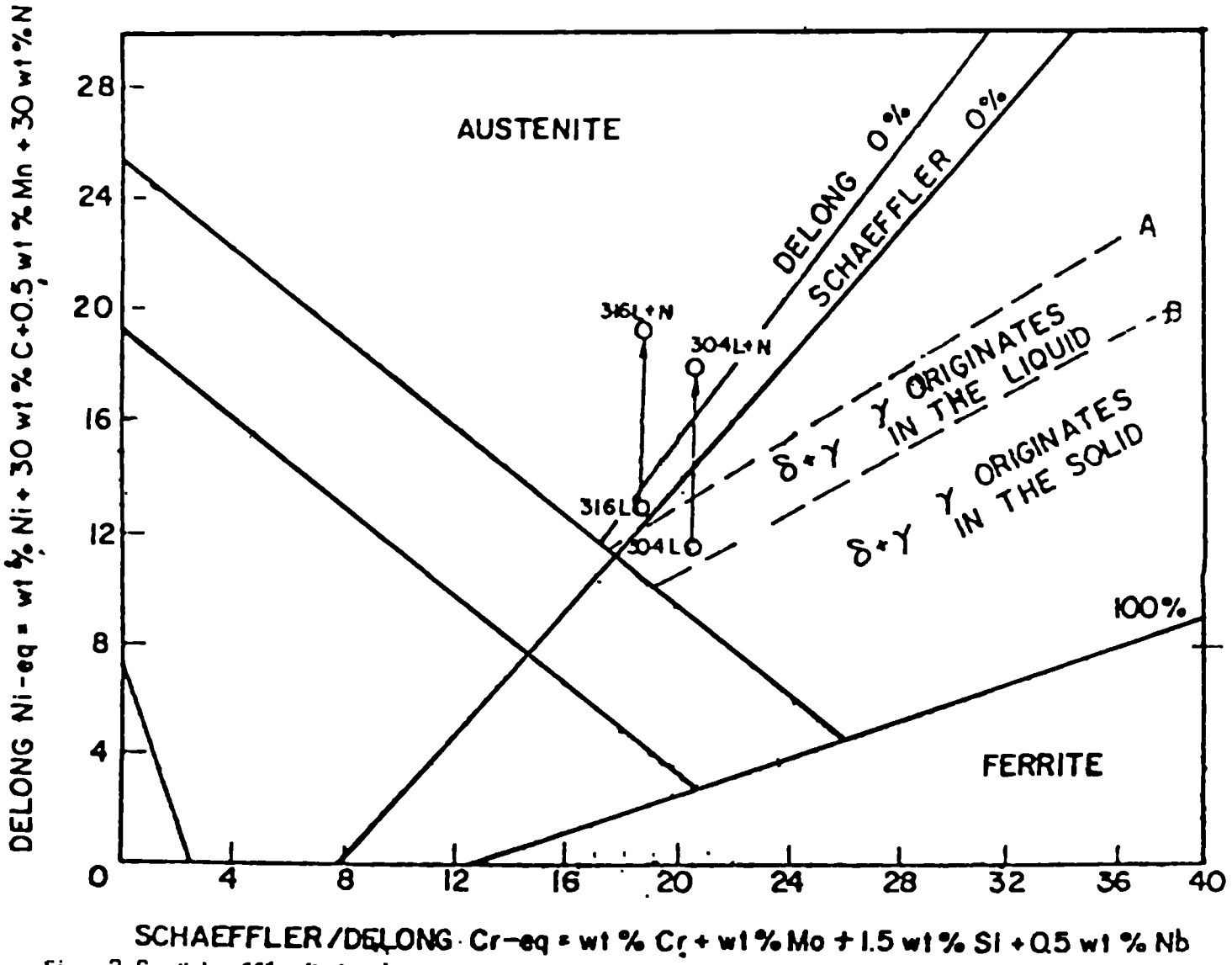

Fig. 2.6 Schaeffler/Delong diagram illustrating the position of boundary lines A and B separating the δ + γ region with respect to the origin of ferrite and austenite (90)

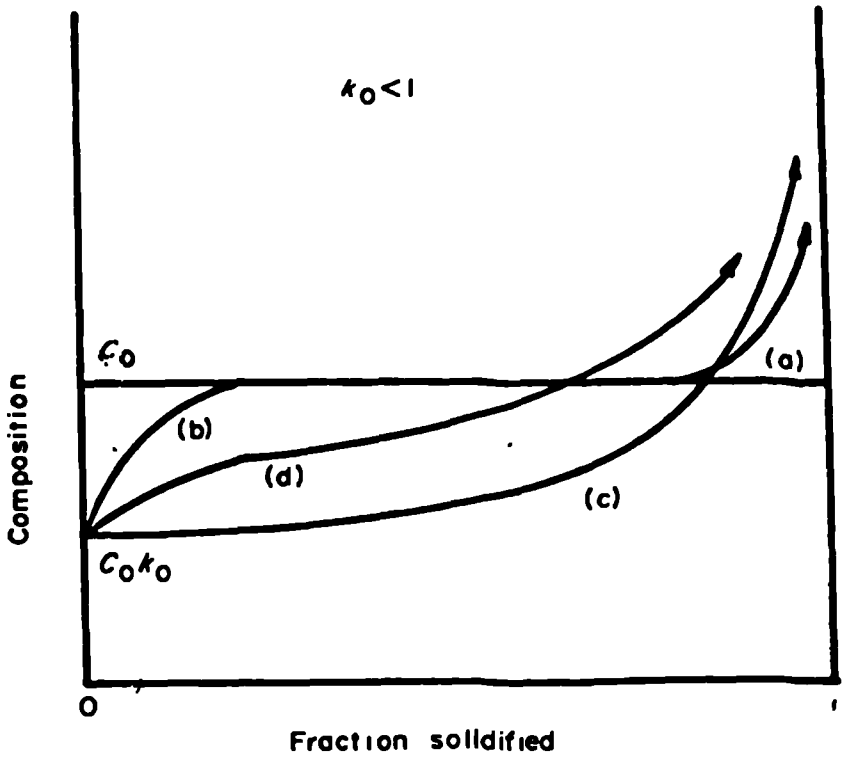

Fig. 2.7 Solute distributions in a solid bar frozen from liquid of initial concentration C_0, for: (a) equilibrium freezing; (b) solute mixing in the liquid by diffusion only; (c) complete solute mixing in the liquid; (d) partial solute mixing in the liquid. [107]

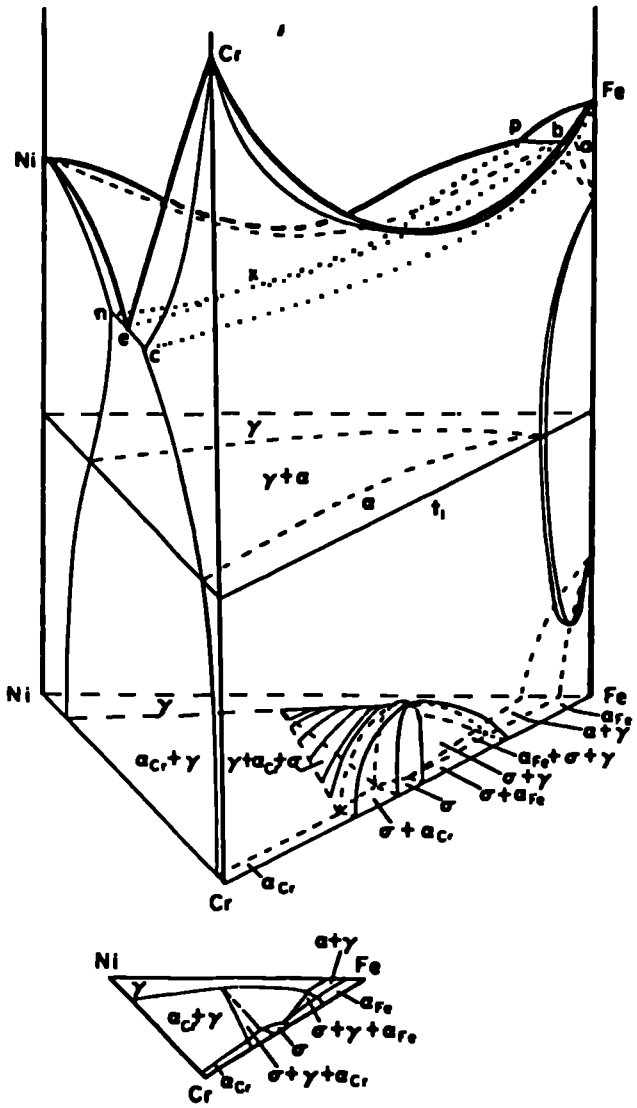

FIG. 2.8 The ternary system Fe–Ni–Cr (schematic).[5]

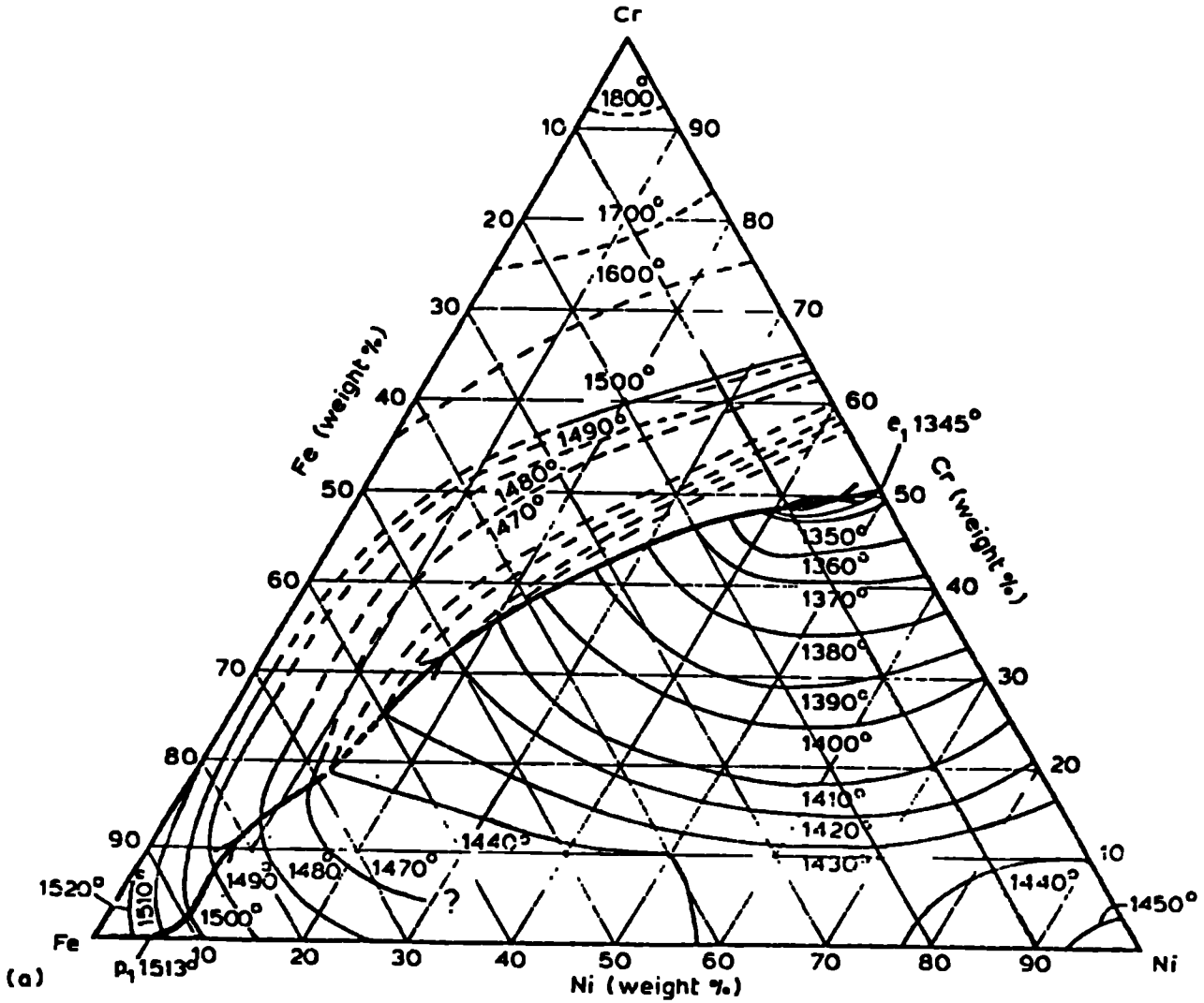

(117) Fig. 2.9 Cr–Fe–Ni system

(*a*) Liquidus projection

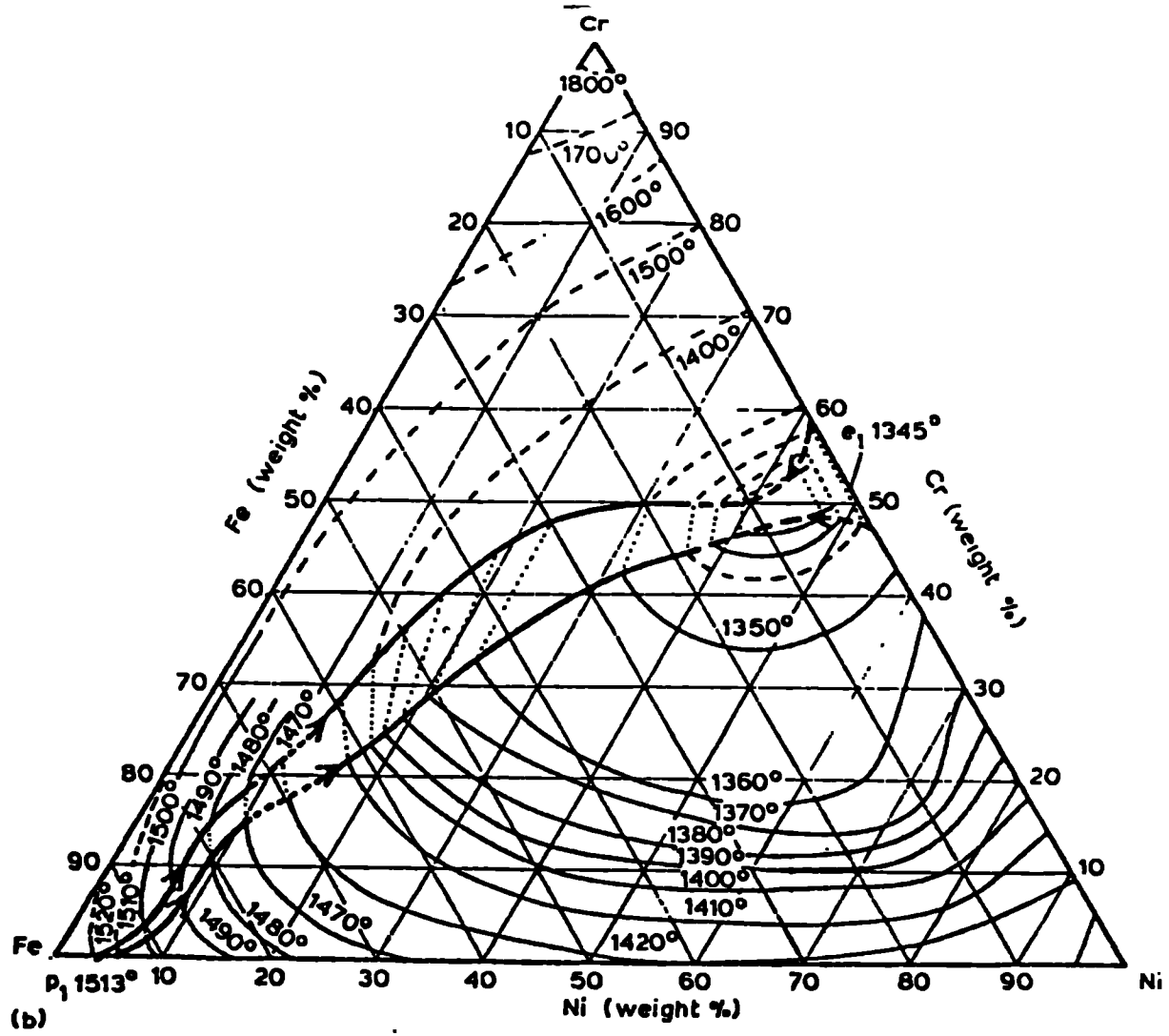

Fig.2.9 (*cont.*)

(*b*) Solidus projection [117]

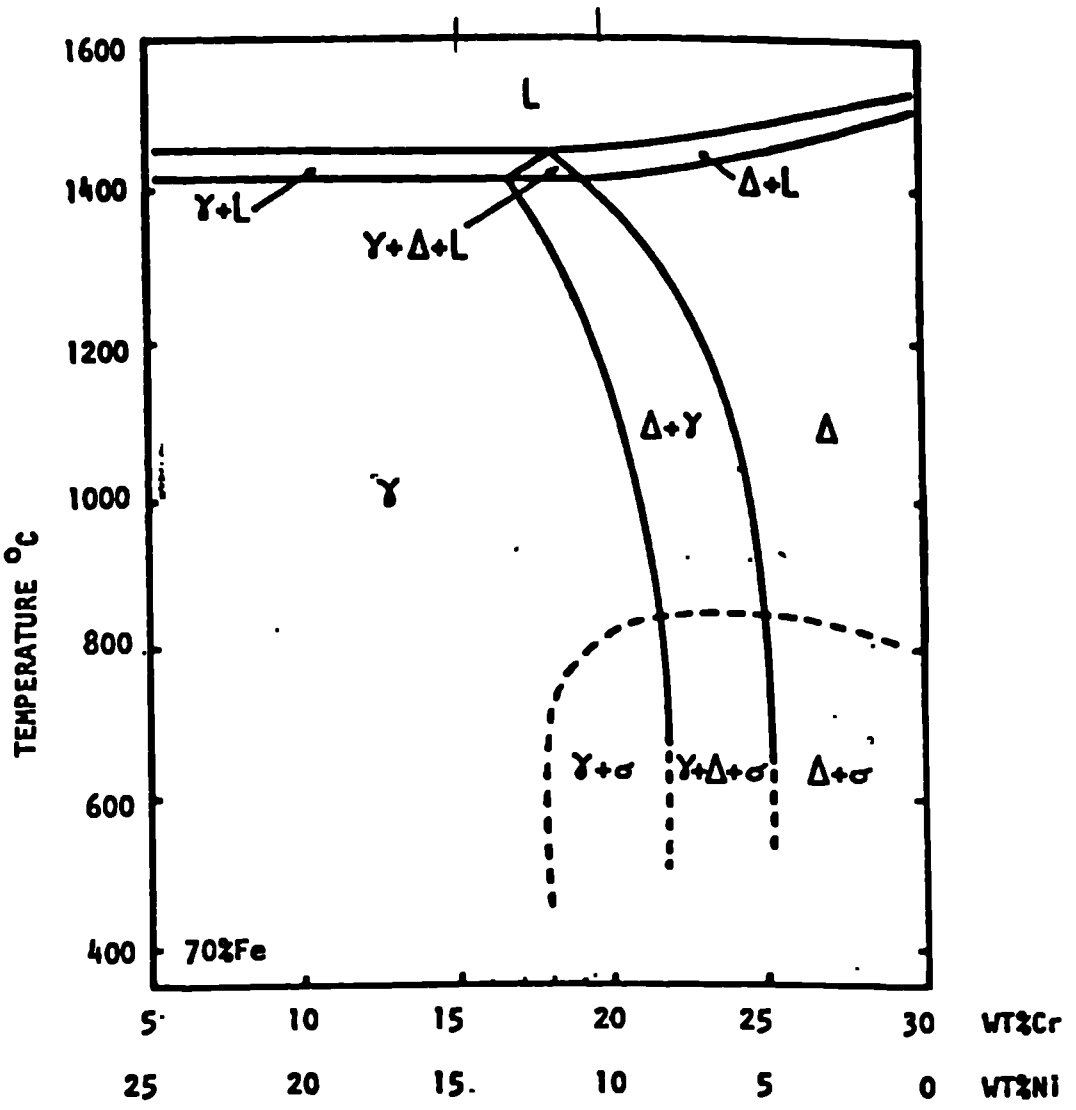

Fig.2.10 (a) pseudobinary section through the Fe-Cr-Ni ternary equilibrium diagram at 70 wt% Fe showing the effect of composition on the freezing mode. (41,86,90)

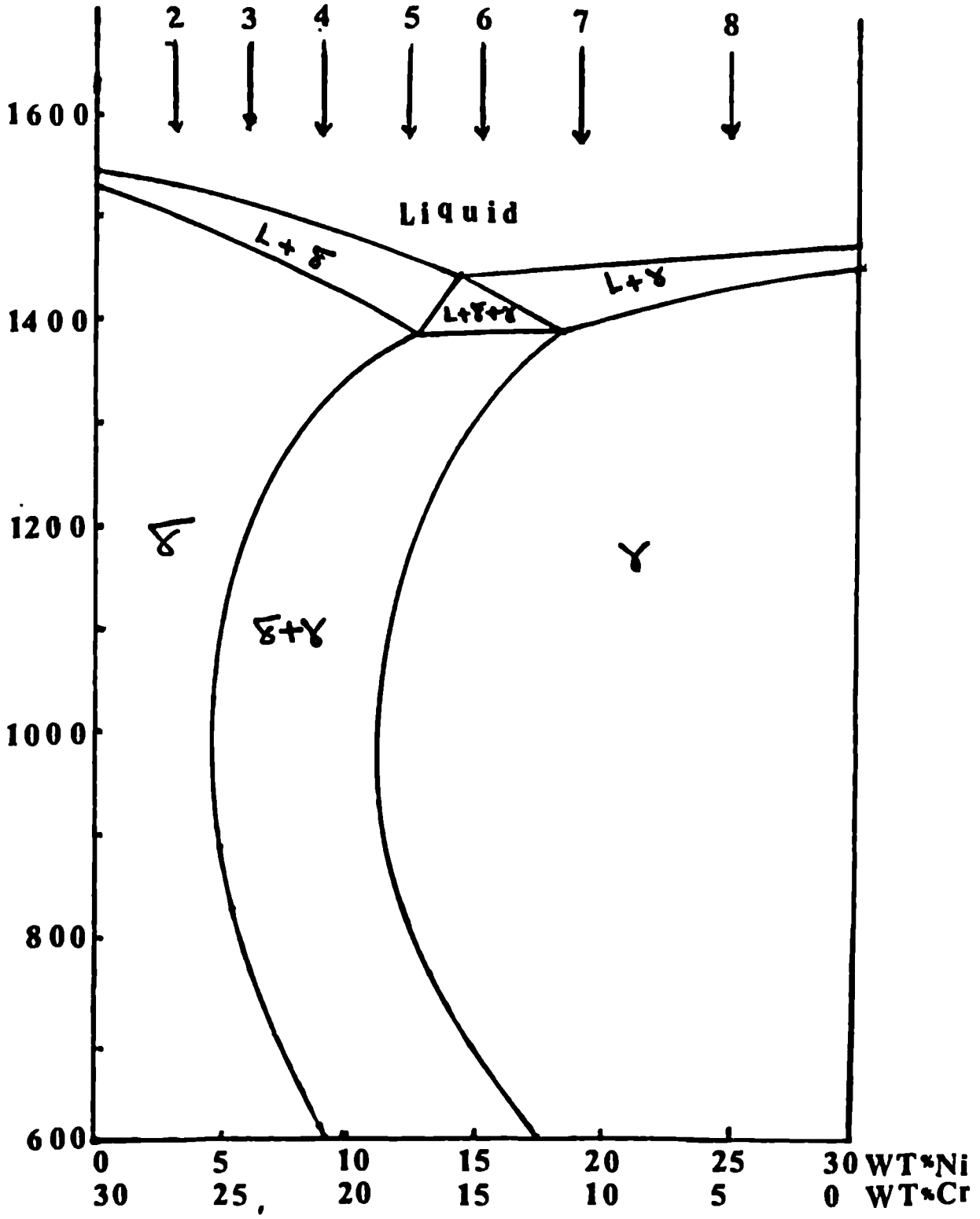

Fig.2.10 (b) Pseudo binary section through the Fe-Cr-Ni ternary equilibrium diagram at 70 wt% Fe showing the effect of composition on the freezing mode. (90)

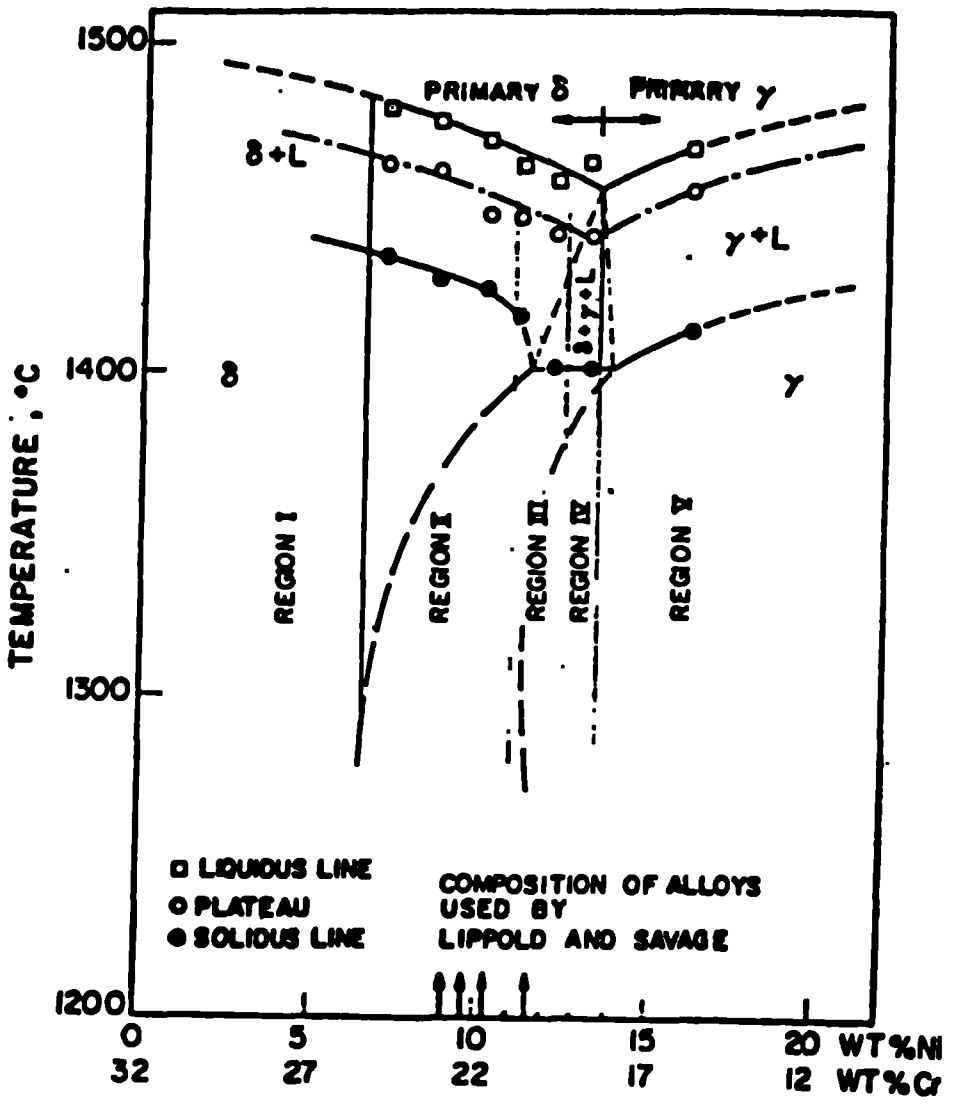

Fig.2.10 (c) Pseudobinary section through the Fe-Cr-Ni tenary equilibrium diagram at 68 wt% Fe showing the effect of composition on the freezing mode. (90)

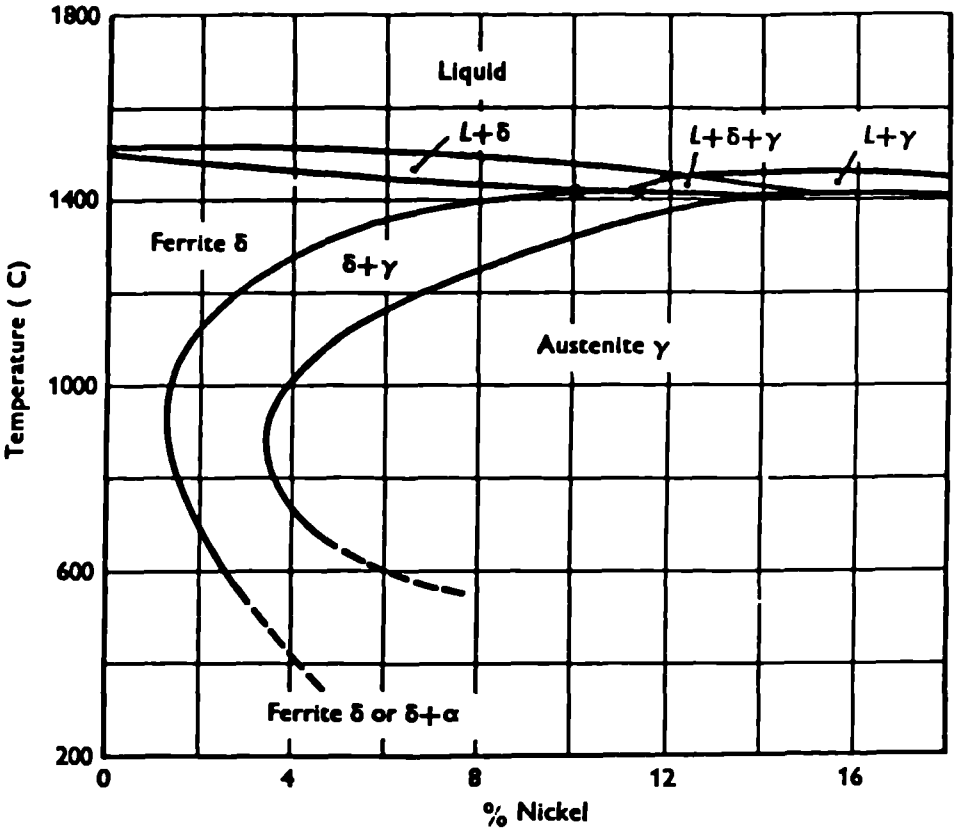

Fig.2.11 Vertical section of very low carbon Fe, Cr-Ni alloys at 18% chromium.(8)

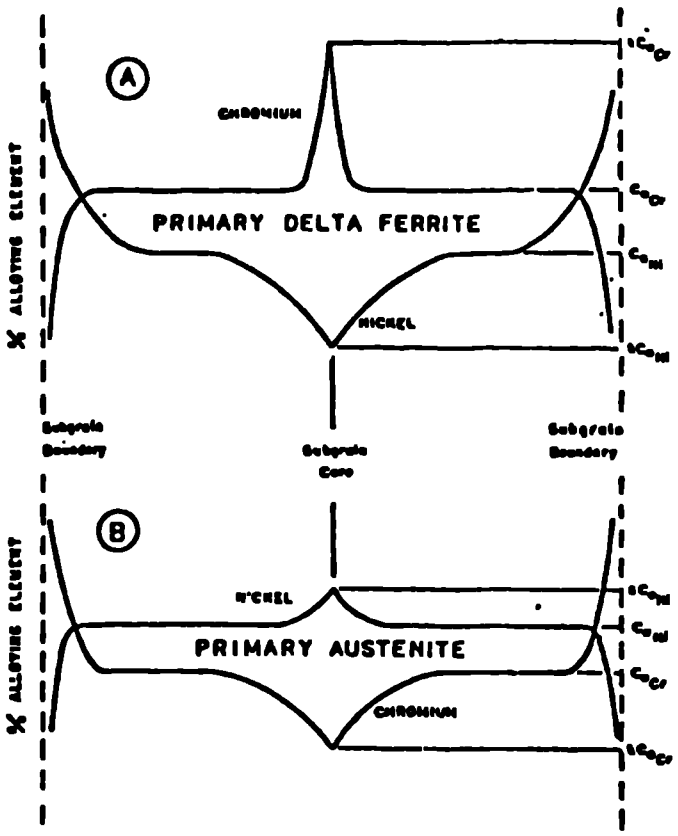

Fig.2.12 Schematic illustration of chromium and nickel distribution across a subgrain following solidification as (A) primary delta ferrite, (B) primary austenite (41,103)

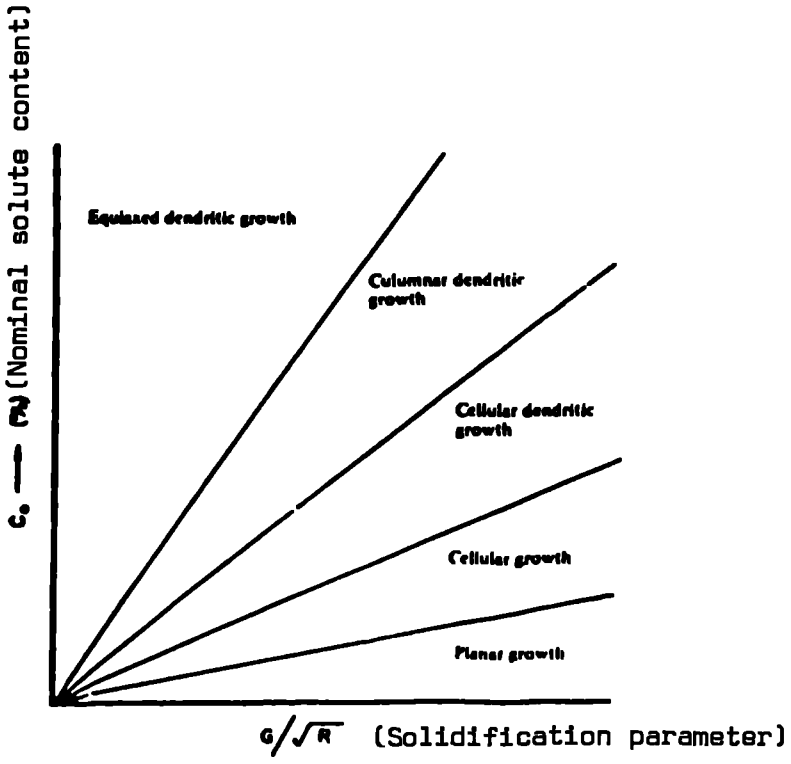

Fig.2.13 . Schematic summary of factors controlling growth mode during solidification. (110,112)

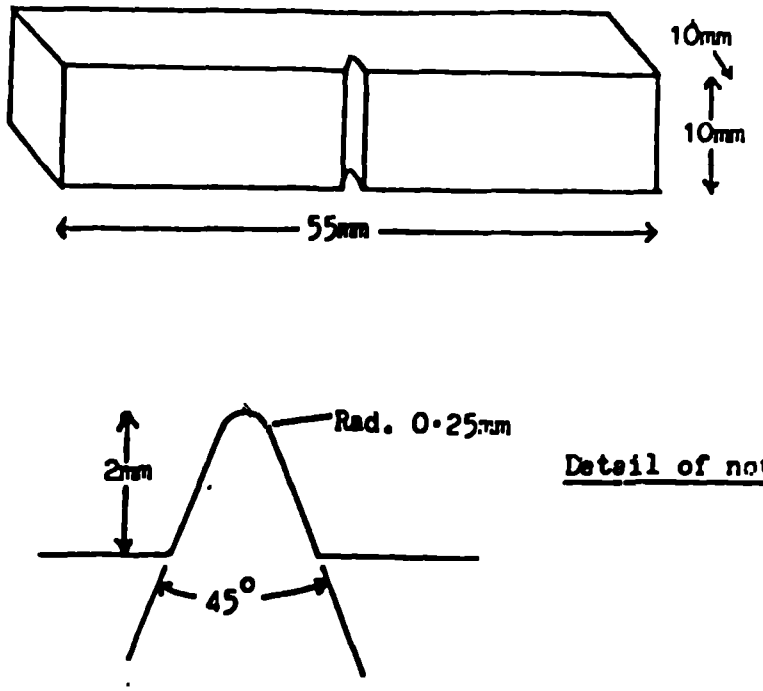

Fig.3.1 **Charpy V-notch specimen.**

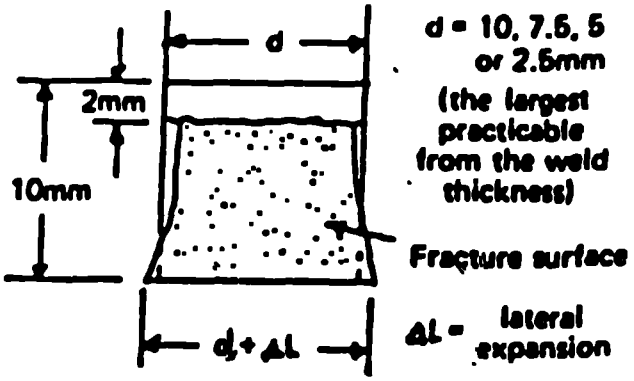

Fig.3.2 Lateral expansion in charpy V specimen.

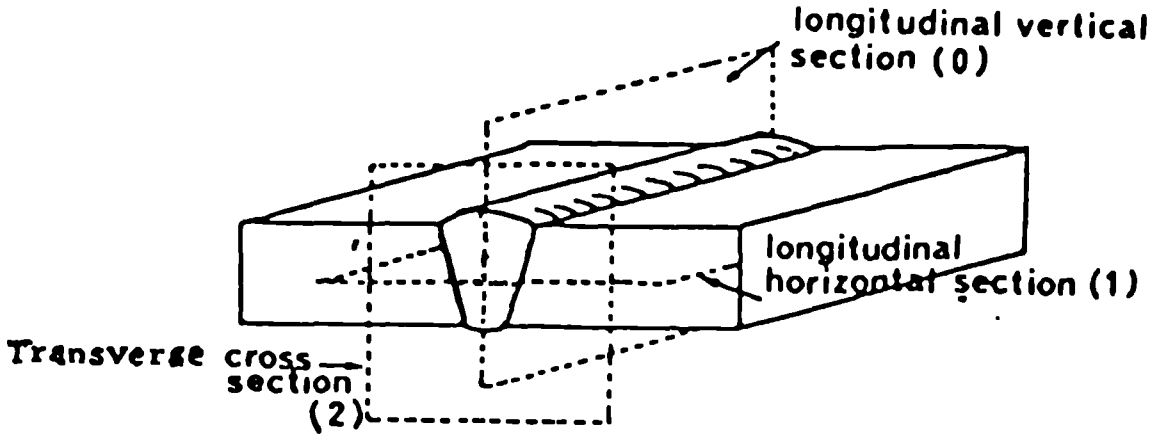

Fig.3.3 The arrangement for metallographic specimen preparation.

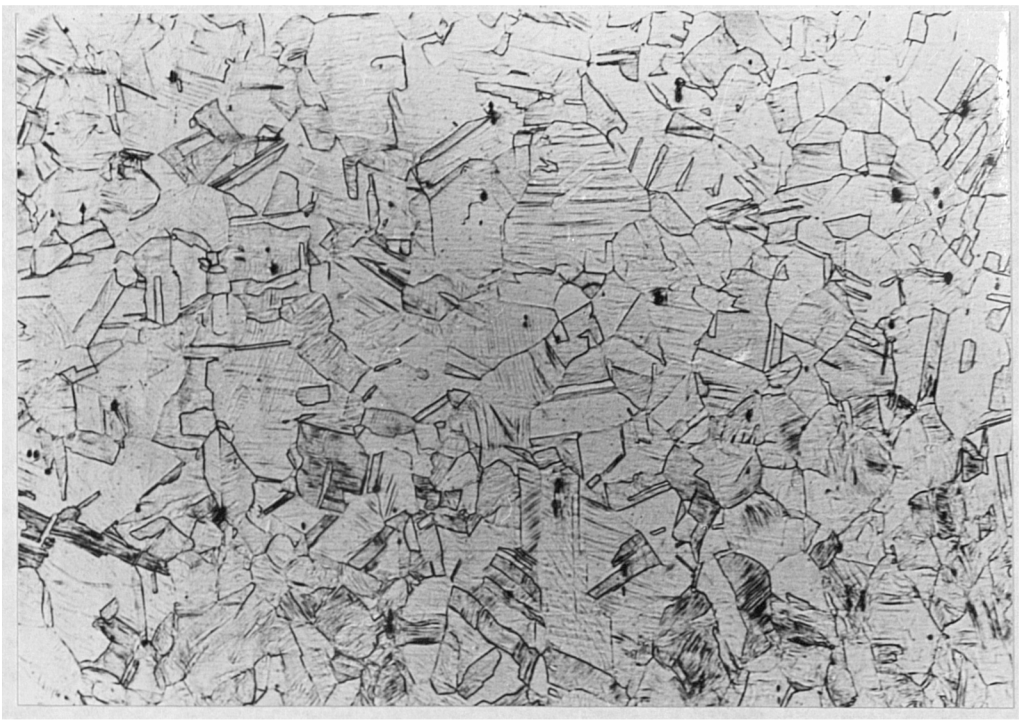

200µm

Fig.4.1 Optical micrograph of austenitic stainless steel AISI 316L parent plate prior to welding.

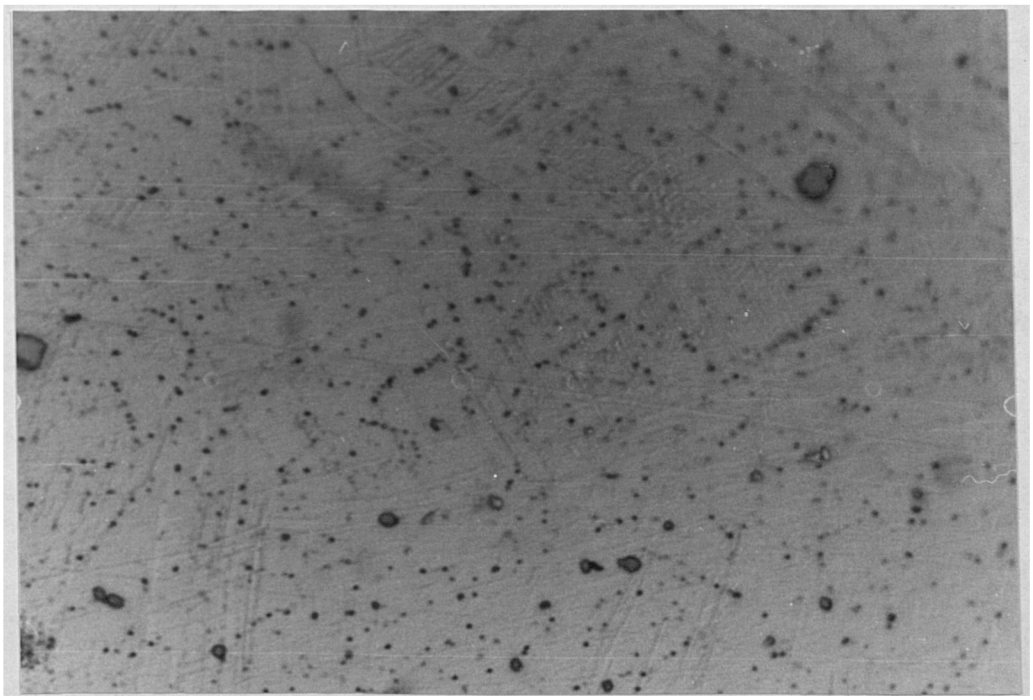

200µm

Fig.4.2 Optical micrograph of austenitic stainless steel AISI 321 Note the presence of Ti, C. and N particles in slightly etched parent plate specimen prior to welding.

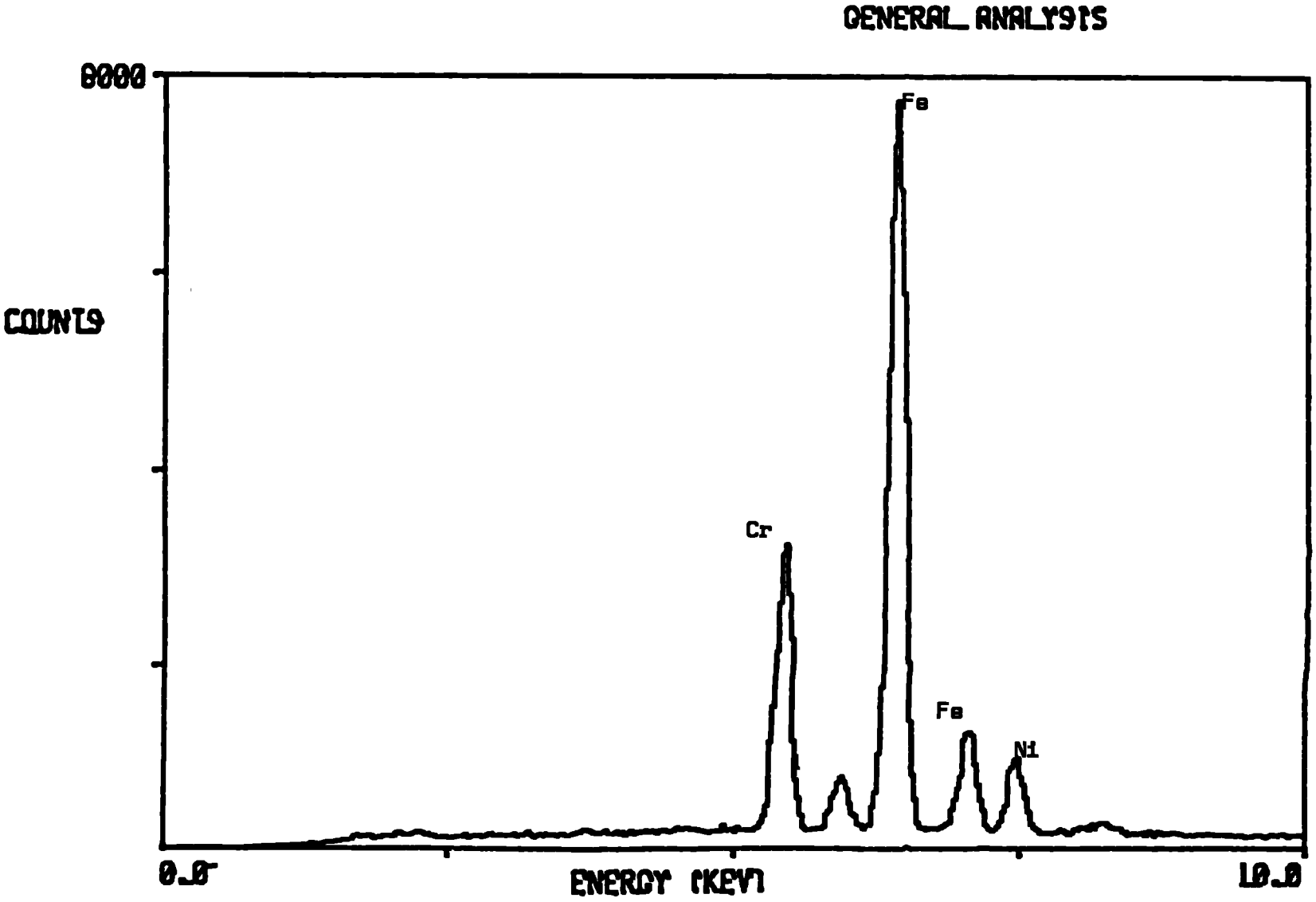

Fig.4.3 Energy dispersive x-ray for matrix general analysis of AISI 321 parent plate specimen.

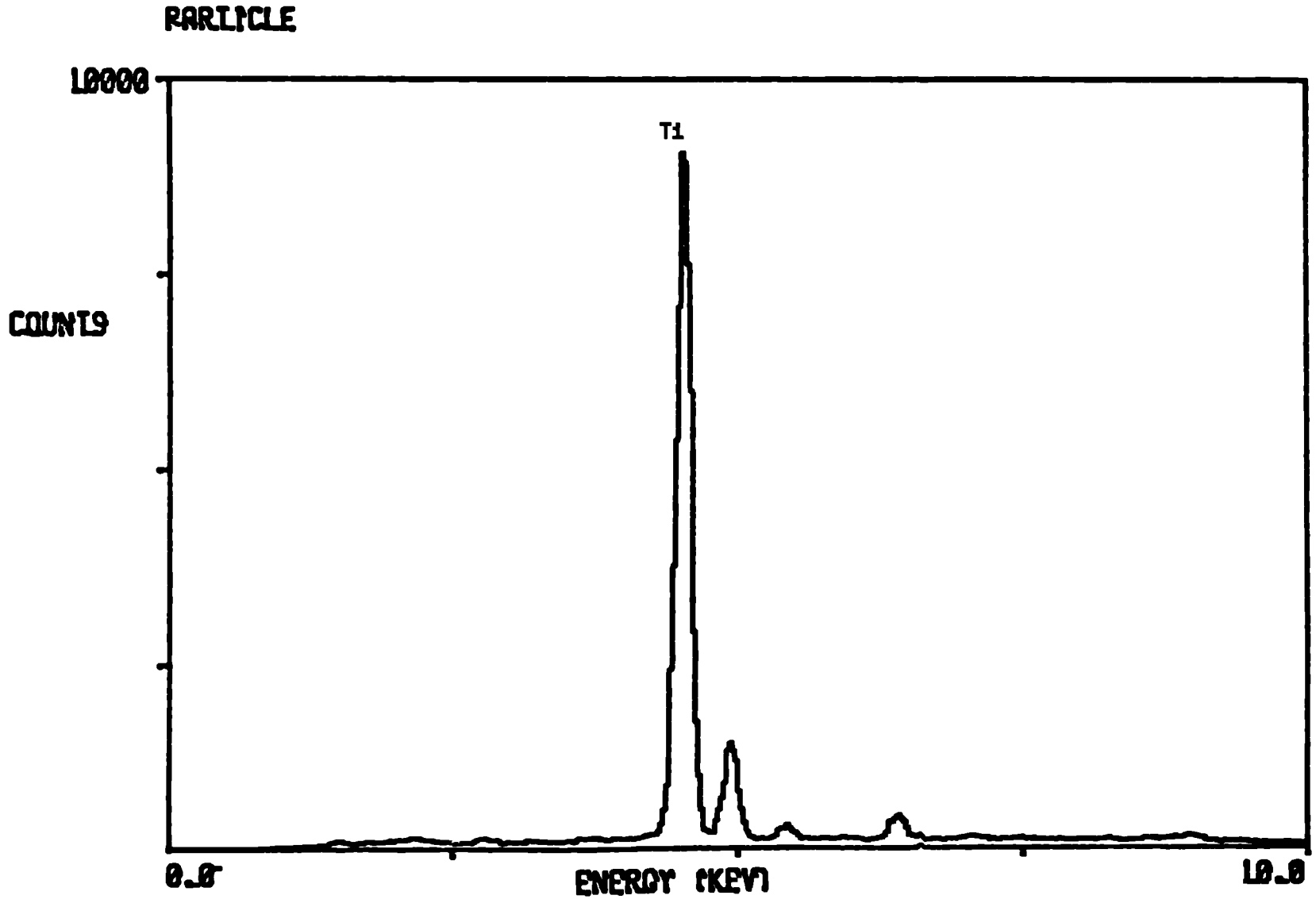

Fig.4.4 Energy dispersive x-ray analysis of selected second phase particles in AISI 321 parent plate specimen.

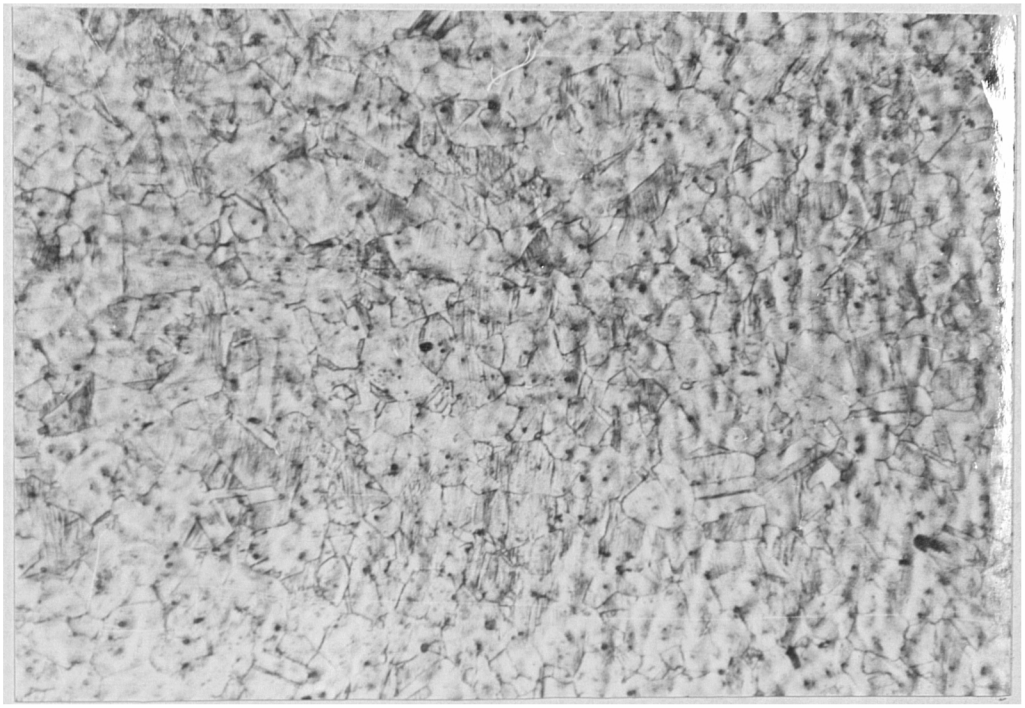

133µm

Fig.4.5 Optical micrograph of austenitic stainless steel AISI 316L parent plate etched in mixed acid with a high degree of etching.

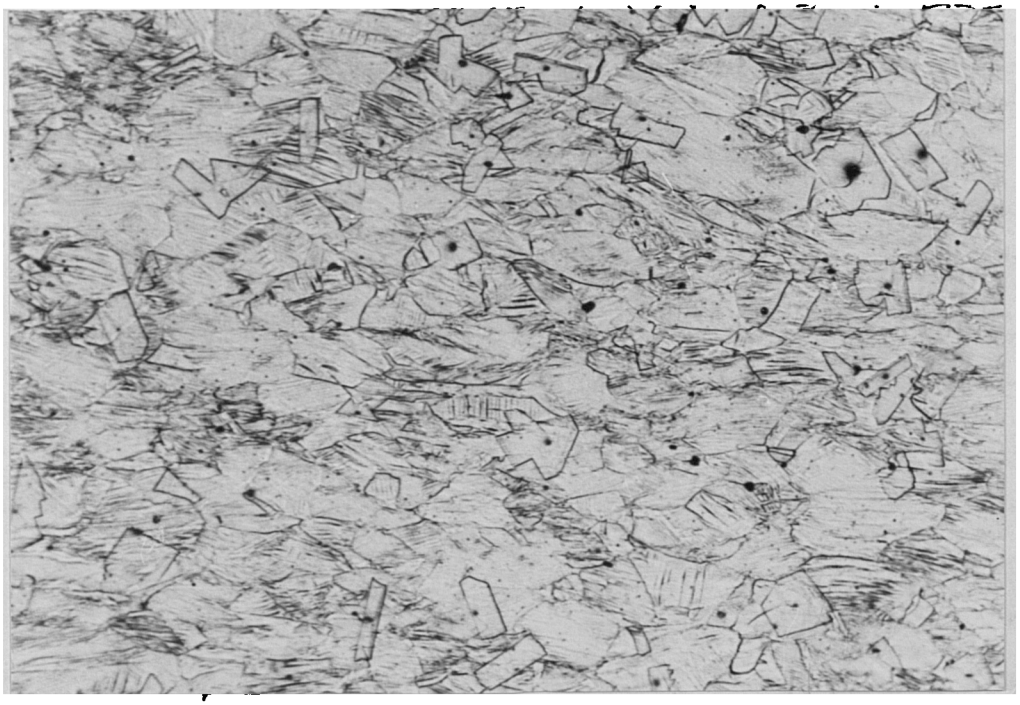

100µm

Fig.4.6 Optical micrograph of cold rolled austenitic stainless steel AISI 316L parent plate.

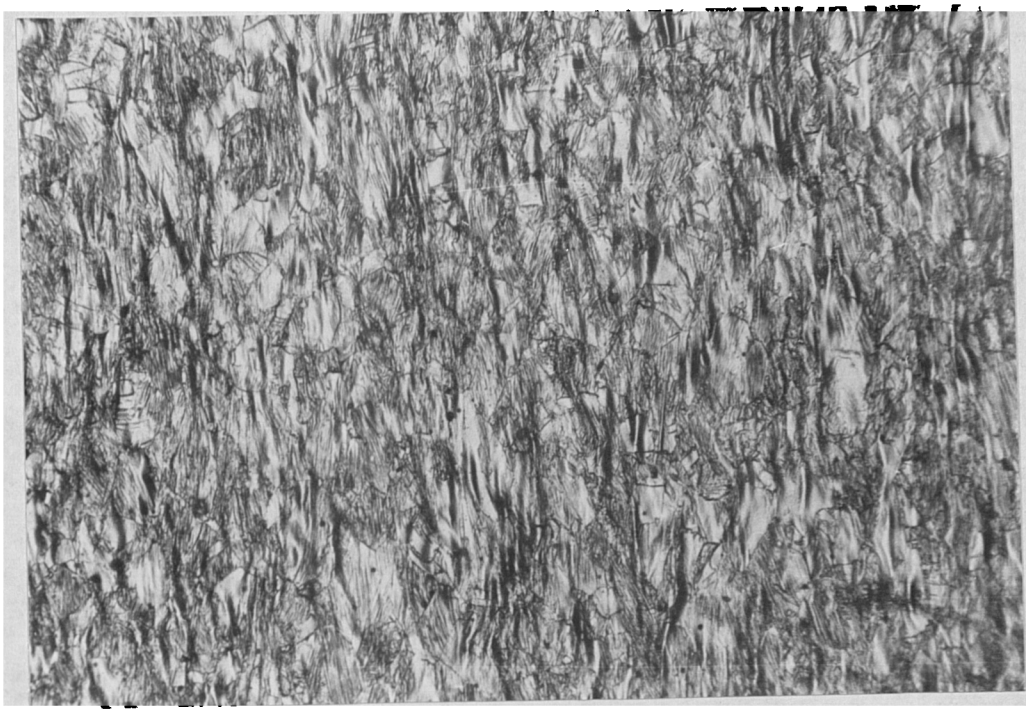

Fig.4.7 Optical micrograph of cold rolled austenitic stainless steel AISI 316L parent plate etched with mixed acid.

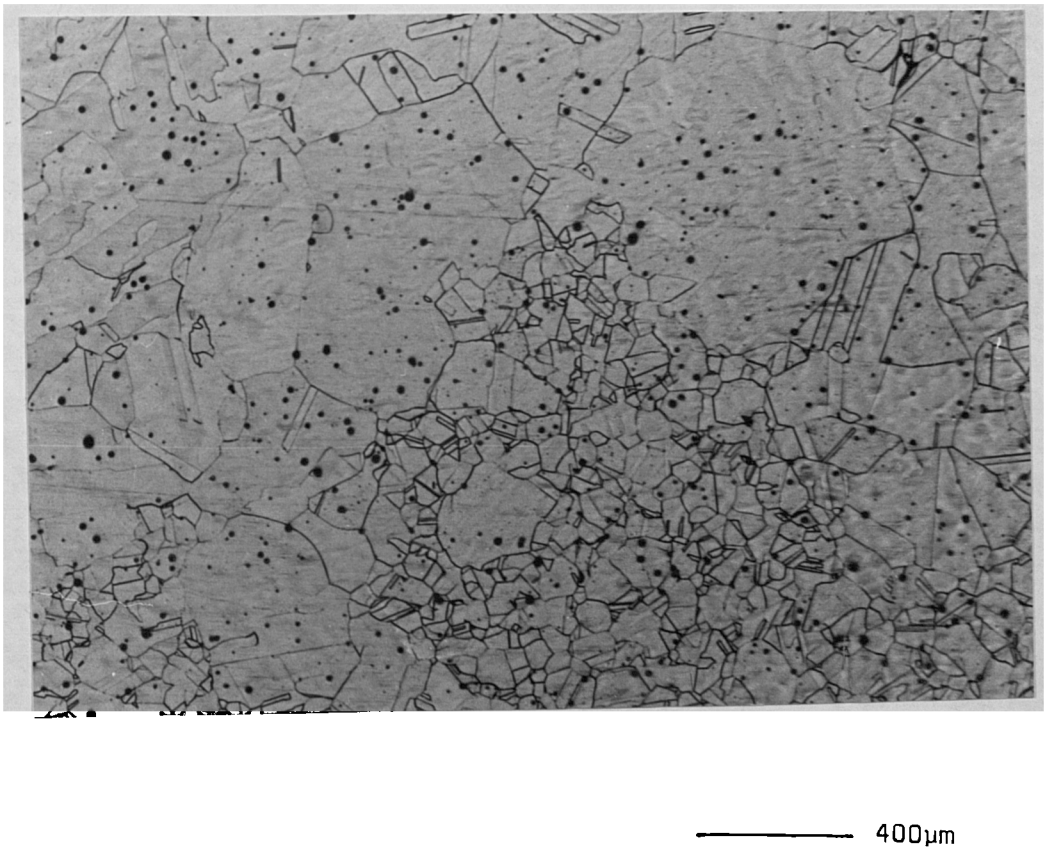

Fig.4.8 Optical micrograph of hot rolled AISI 316L parent plate showing partial recrystallization of austenitic grains.

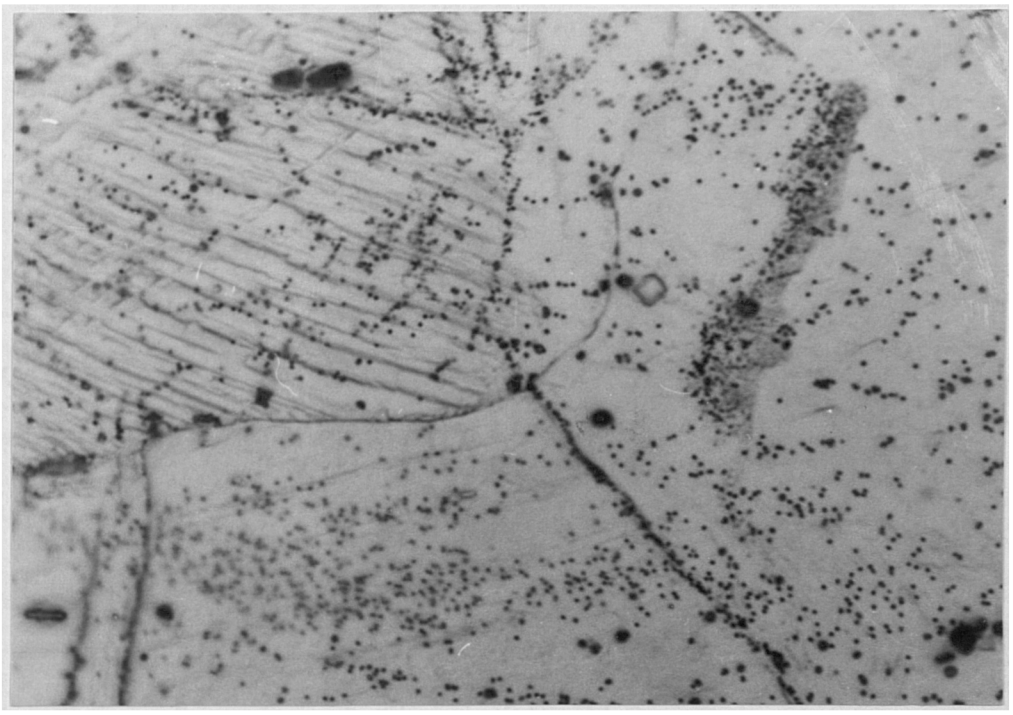

Fig.4.9 Optical micrograph of hot rolled austenitic stainless steel AISI 316L parent plate showing precipitated particles within austenite and at the grain boundaries.

(a)

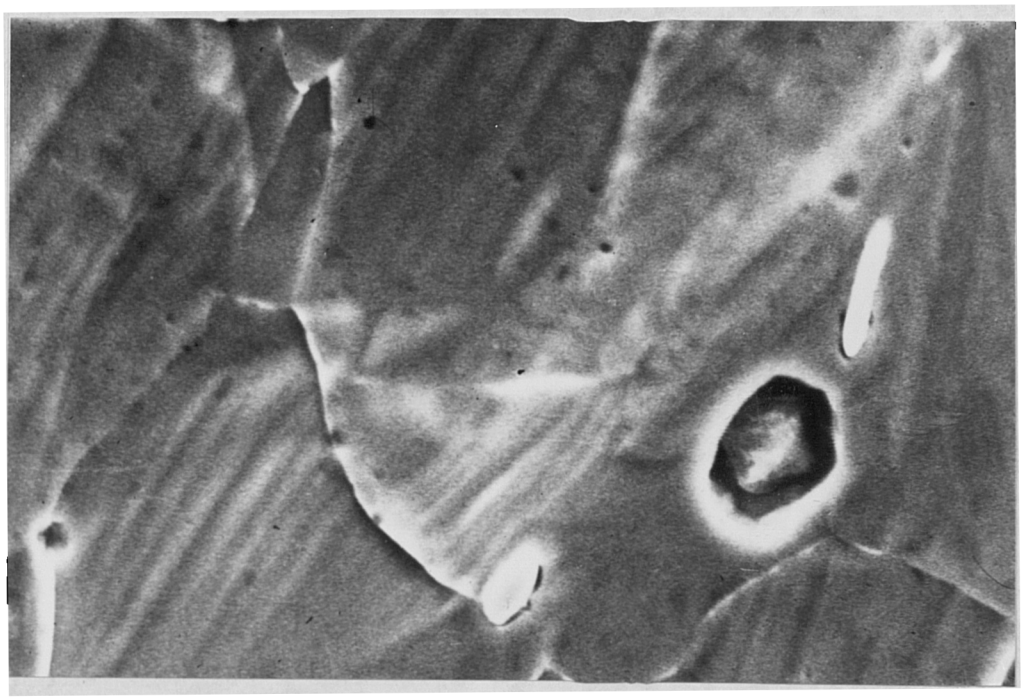

7 µm

(b)

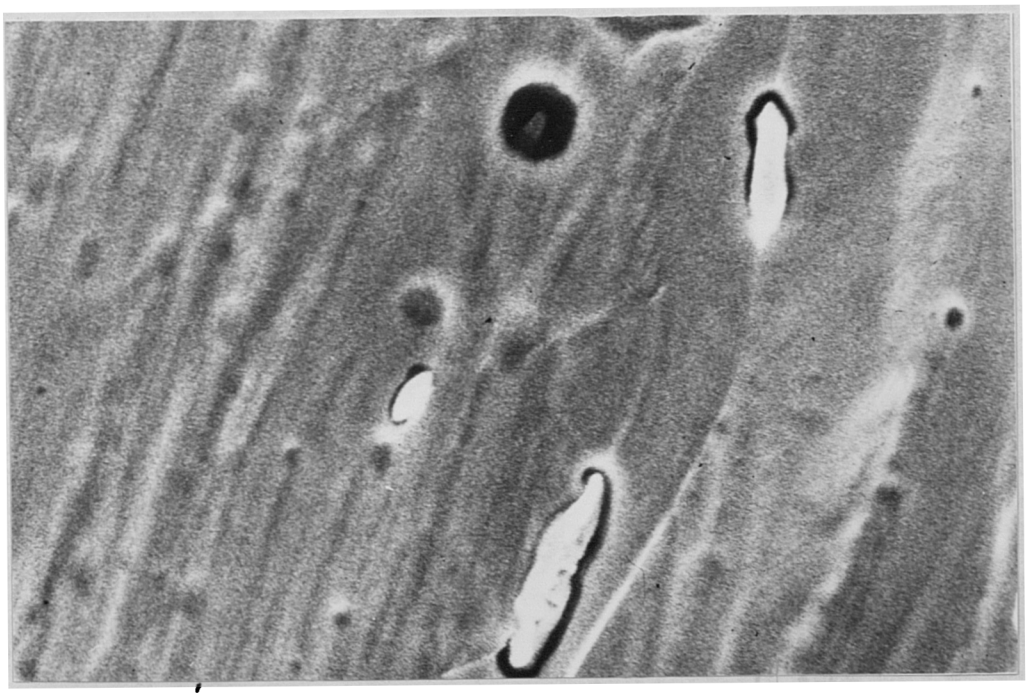

7 µm

Fig.4.10 S.E.M. micrograph of AISI 316L parent plate prior to welding showing selected second phase particles.

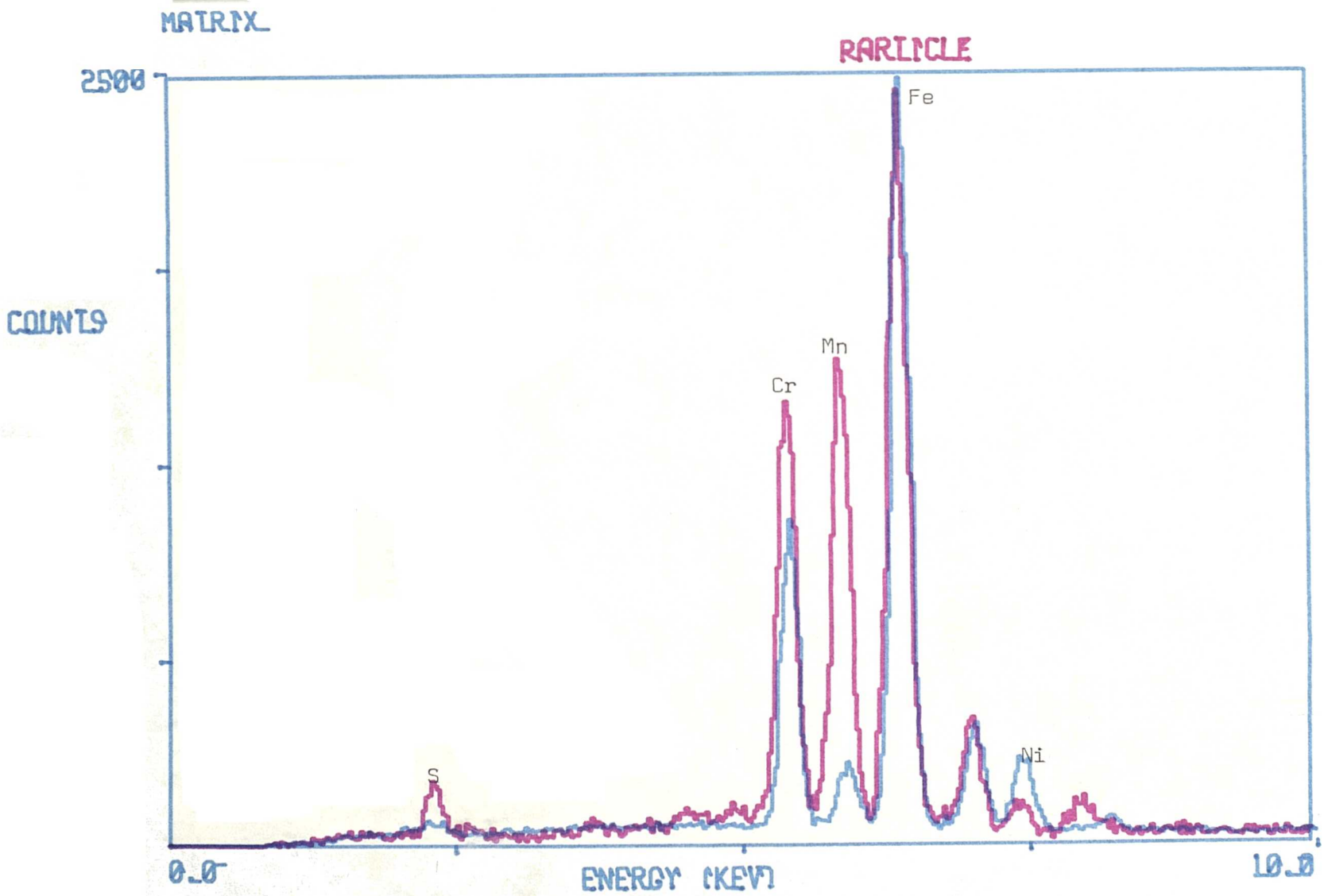

Fig.4.11 Energy dispersive x-ray analysis of matrix and second phase particles in AISI 321 parent plate specimens.

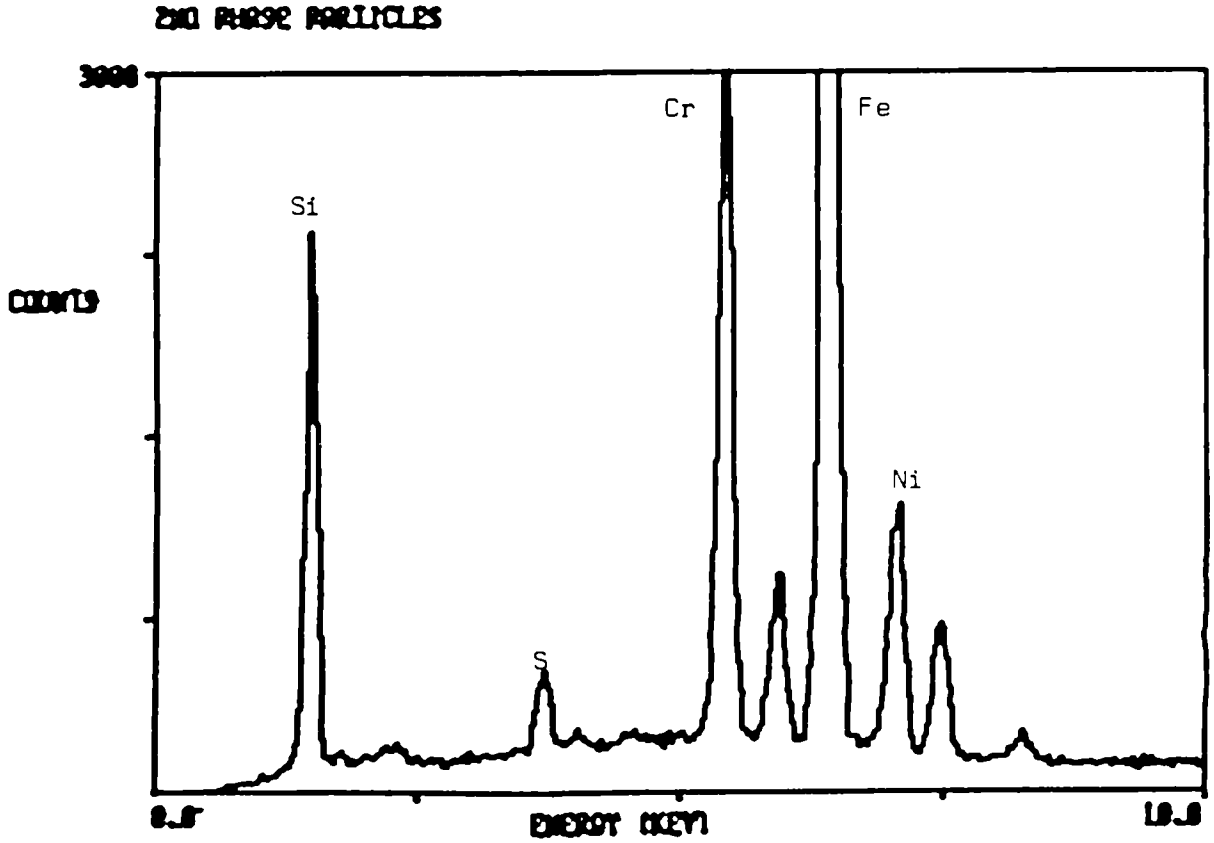

Fig.4.12 Energy dispersive x-ray analysis of selected second phase particles AISI 316L parent plate specimen.

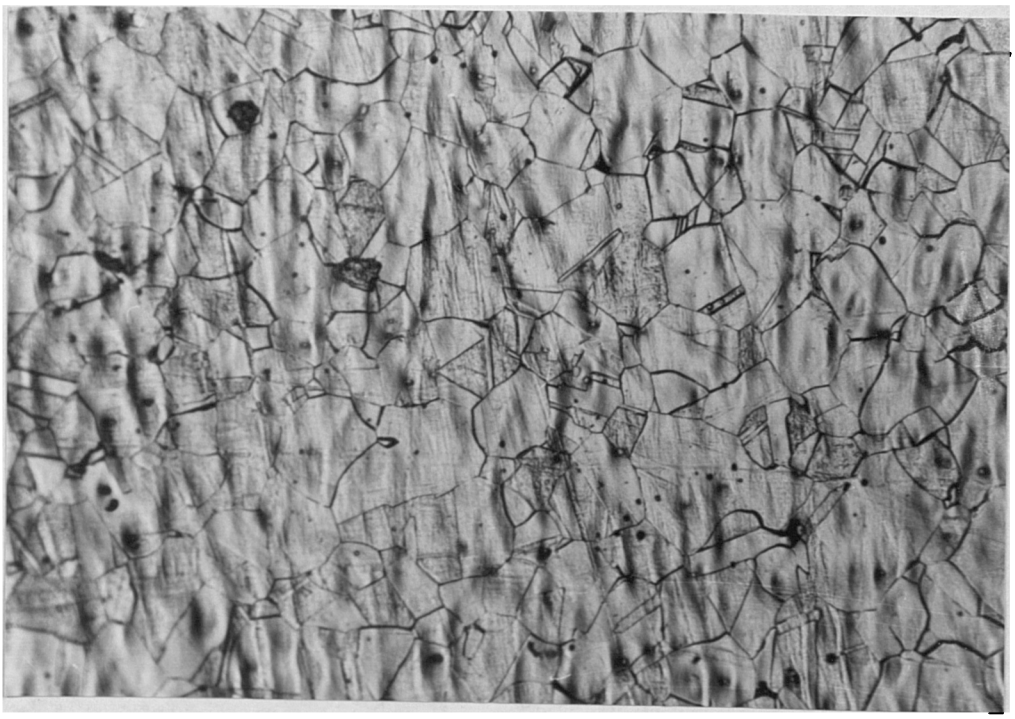

200μm

Fig.4.13 Optical mircograph of hot rolled austenitic stainless steel AISI 316L parent plate showing cored structure within the austenitic grains etched with mixed acid.

(a)

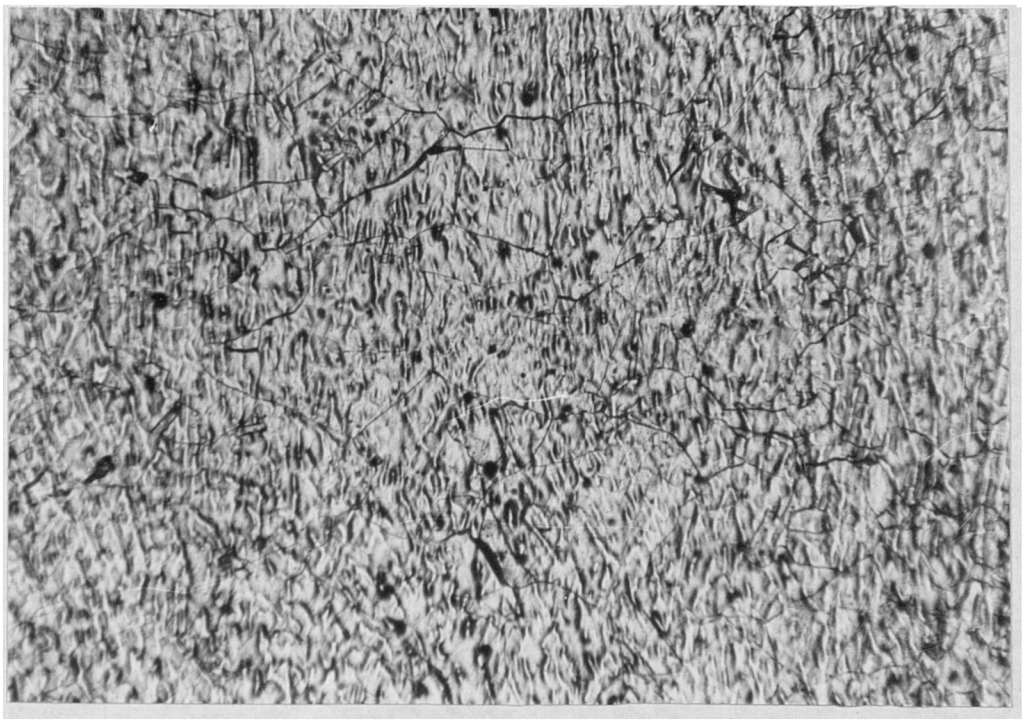

400μm

(b)

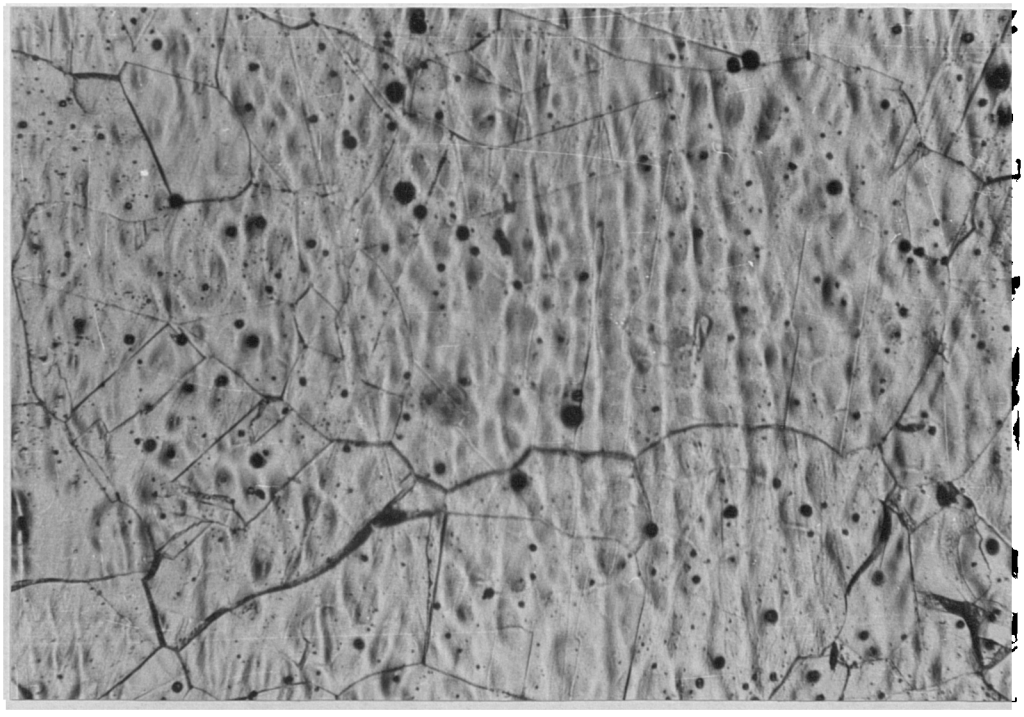

200μm

Fig.4.14 Optical micrograph of hot rolled austenitic stainless steel AISI 316L parent plate showing cored structure of austenite grains.

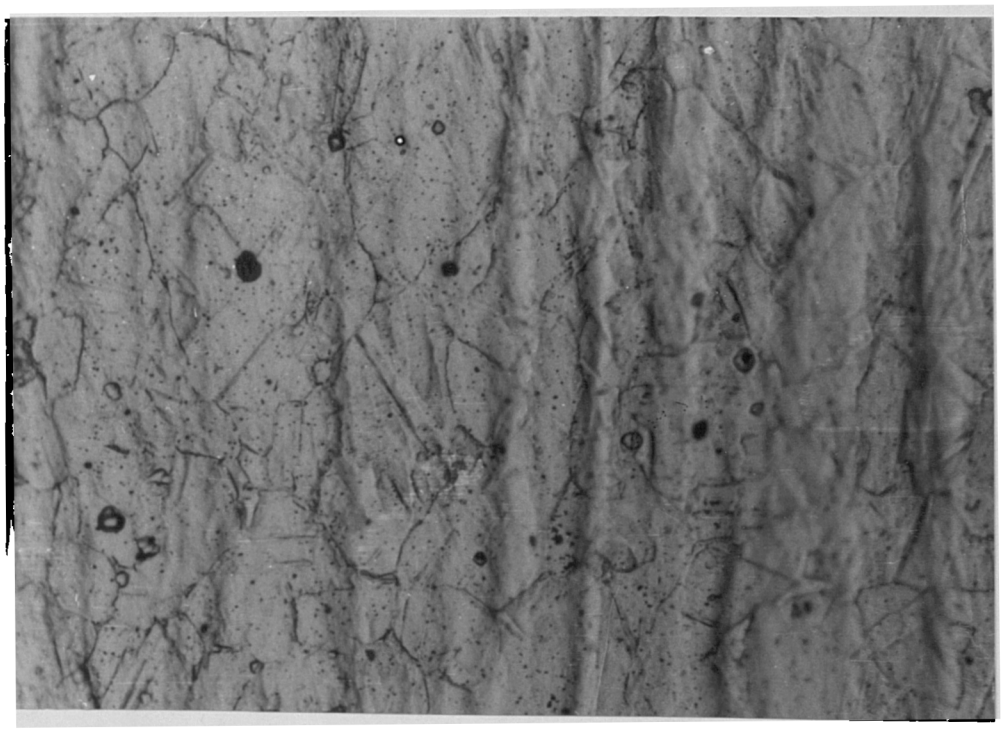

Fig.4.15 Optical micrograph of hot rolled austenitic stainless steel AISI 321 parent plate showing second phase particles, cored structure and strain pattern within the austenite grains.

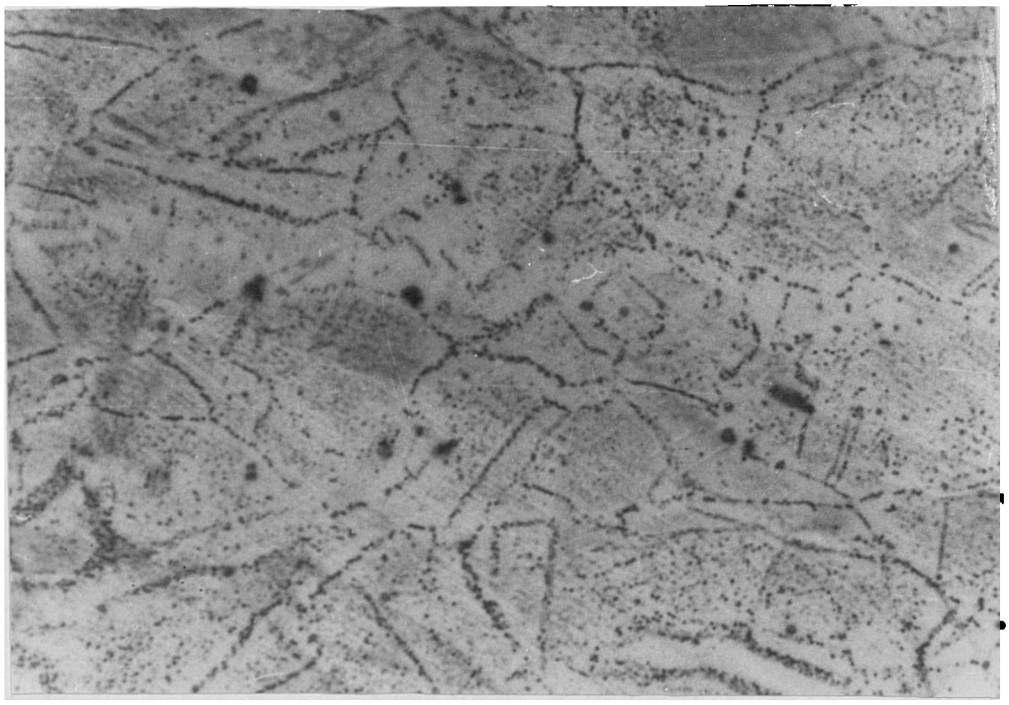

Fig.4.16 Optical micrograph of hot rolled - furnace cooled austenitic nitic stainless steel AISI 316L parent plate P.

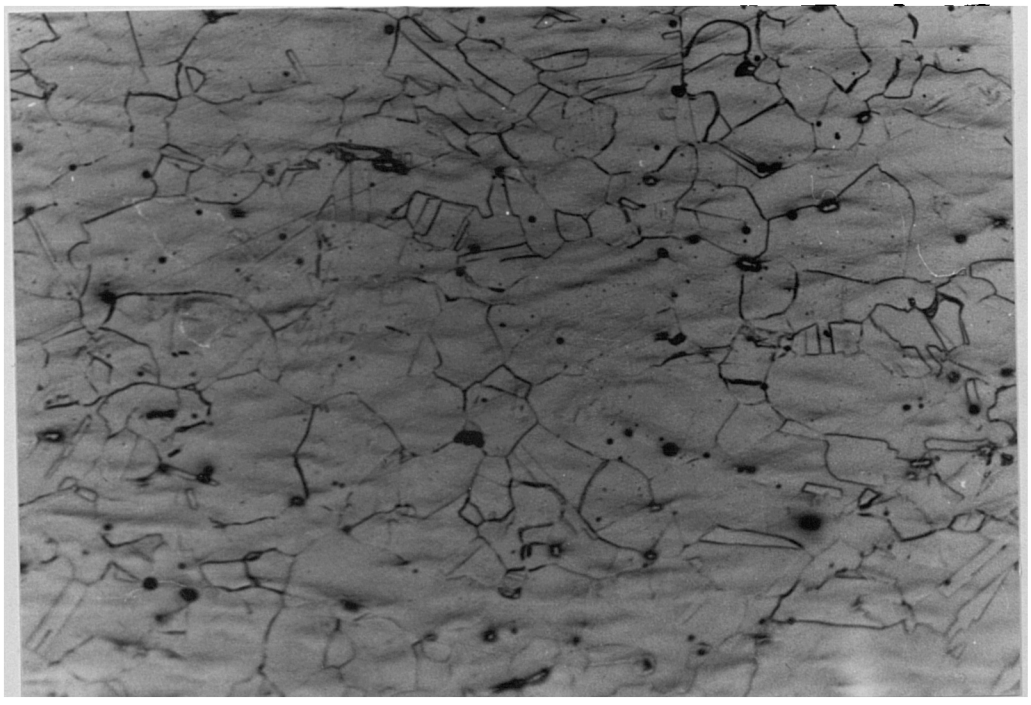

Fig.4.17 Optical micrograph of hot rolled - water quenched austenitic stainless steel AISI 316L parent plate S.

27μm

Fig.4.18 Thin foil micrograph of austenitic stainless steel AISI 316L parent plate at low magnification revealed by T.E.M.

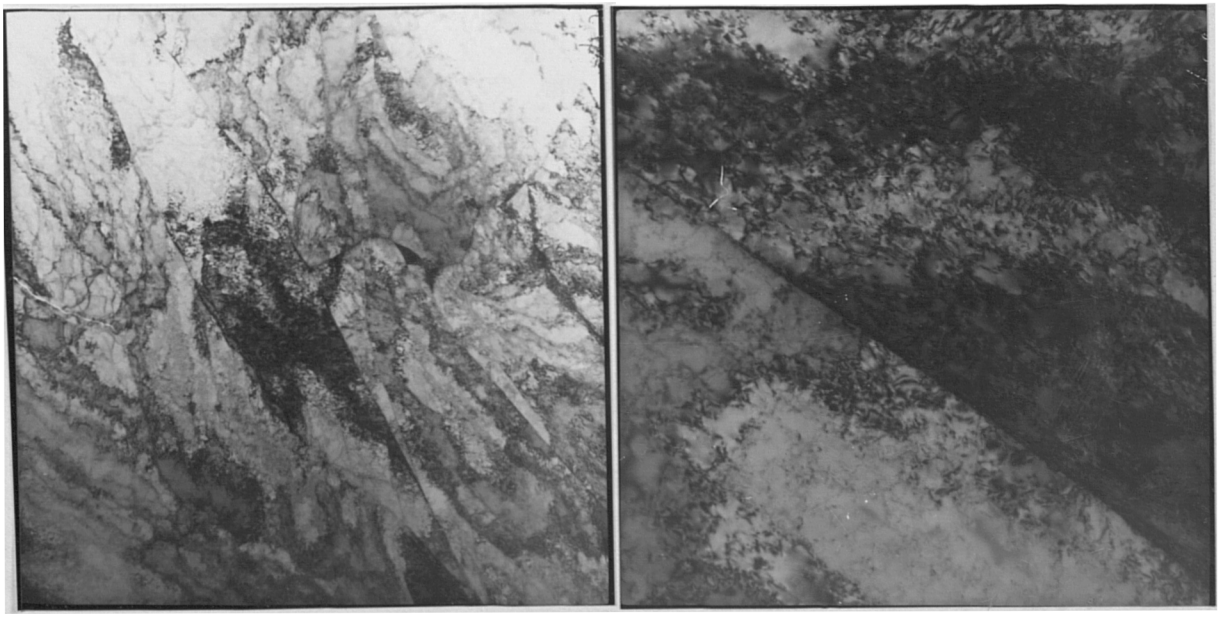

2μm (a)

0.4μm (b)

Fig.4.19 T.E.M. micrograph of austenitic stainless steel AISI 316L parent plate. (a) at low magnification, (b) at high magnification.

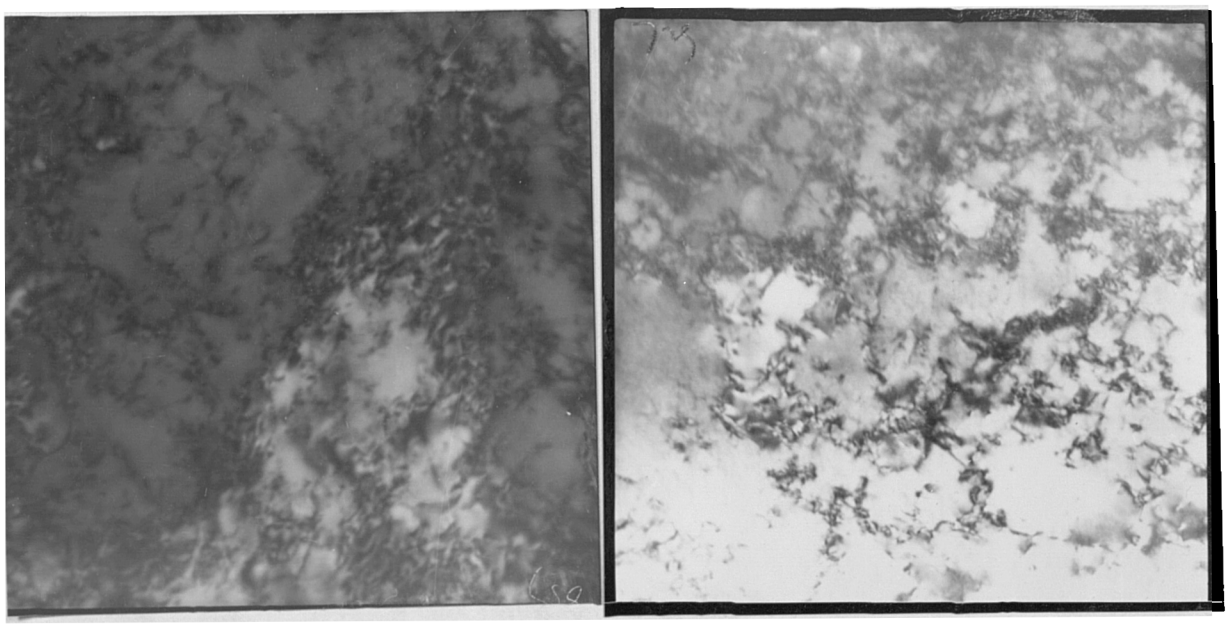

0.2μm

(a)

0.4μm

(b)

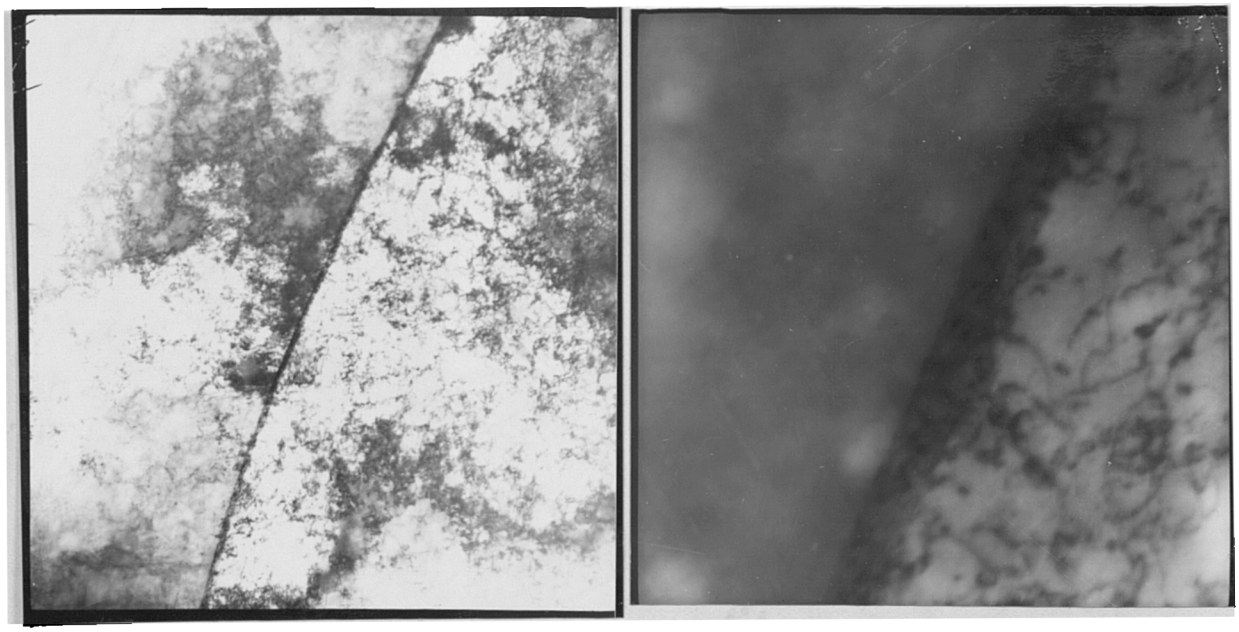

1.25μm

(c)

0.2μm

(d)

Fig.4.20 T.E.M. micrograph of austenitic stainless steel AISI 316L parent plate.

(a) and (b) showing dislocation cell structure within the austenite grains.

(c) and (d) showing dislocation pile up at austenite grain boundaries.

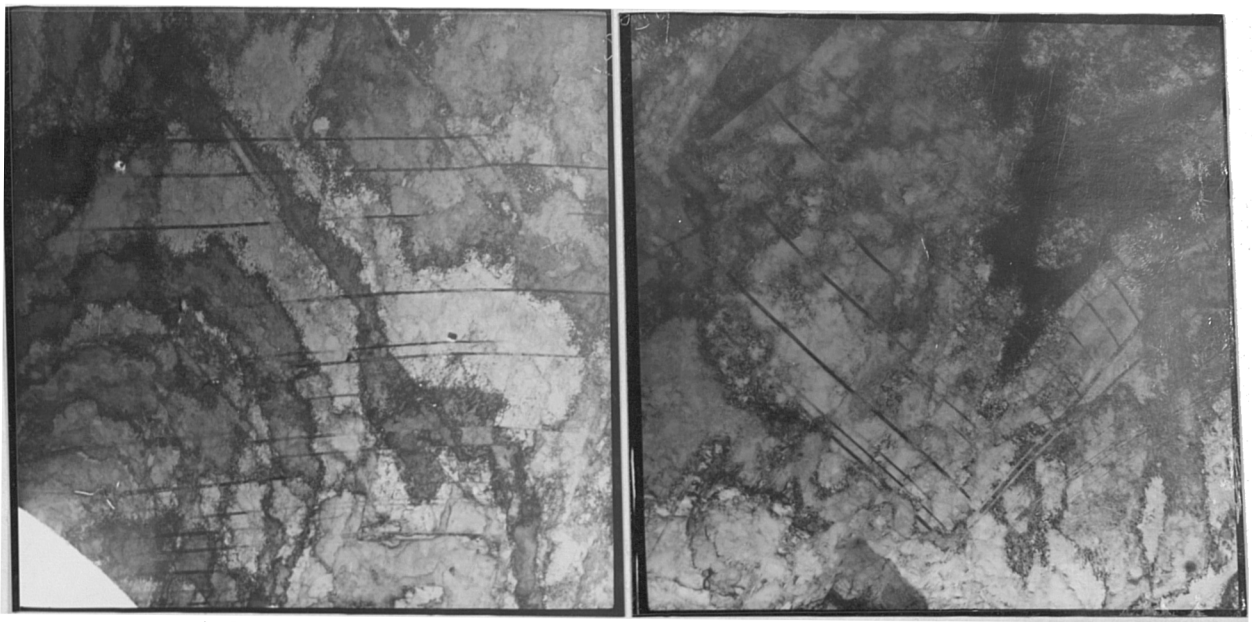

Fig.4.21 T.E.M. micrographs of austenitic stainless steel AISI 316L rolled at 400°C - furnace cooled.

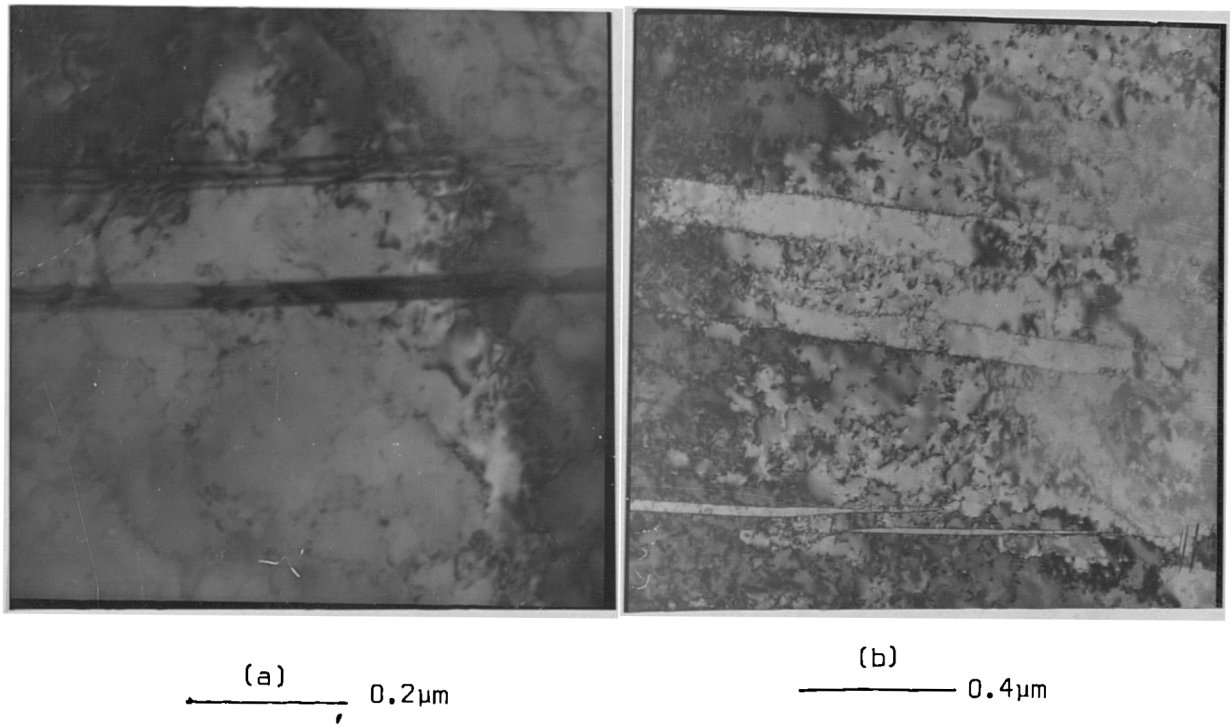

Fig.4.22 T.E.M. micrographs austenitic stainless steel AISI 316L parent plate rolled at 400°C - furnace cooled.

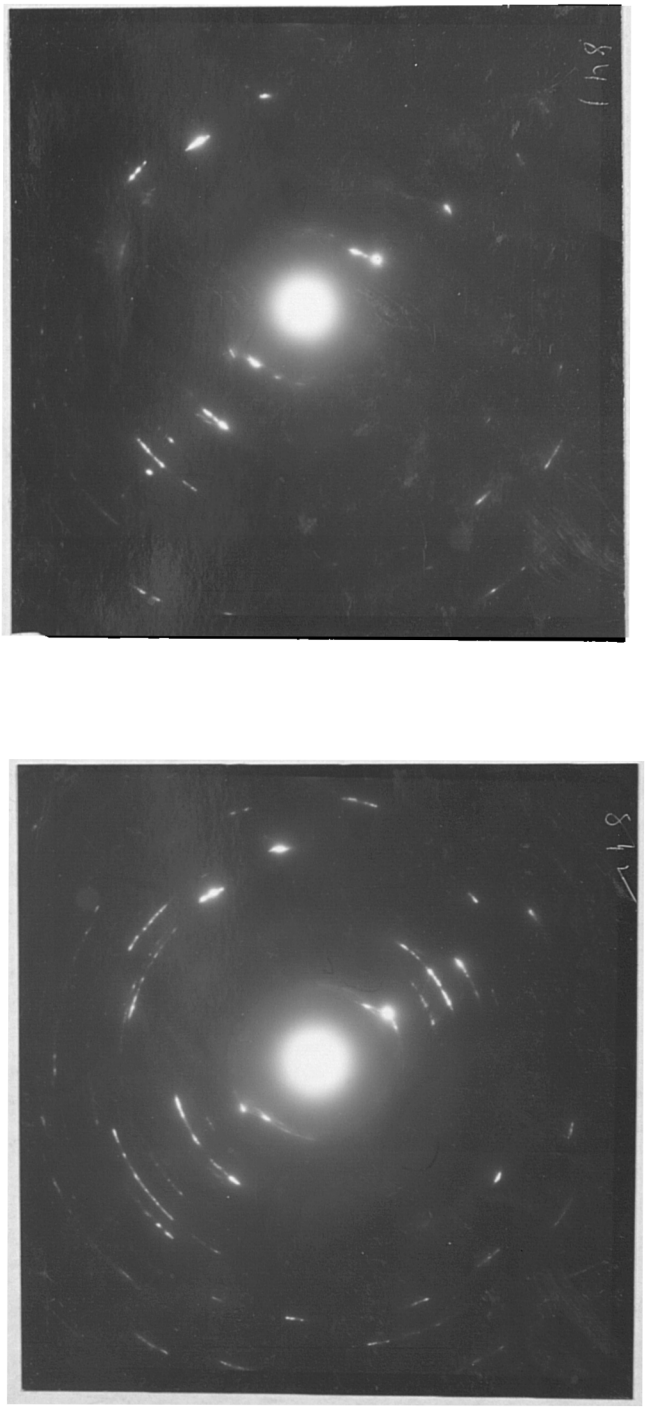

Fig.4.23 Electron diffraction pattern of austenitic stainless steel AISI 316L parent plate.

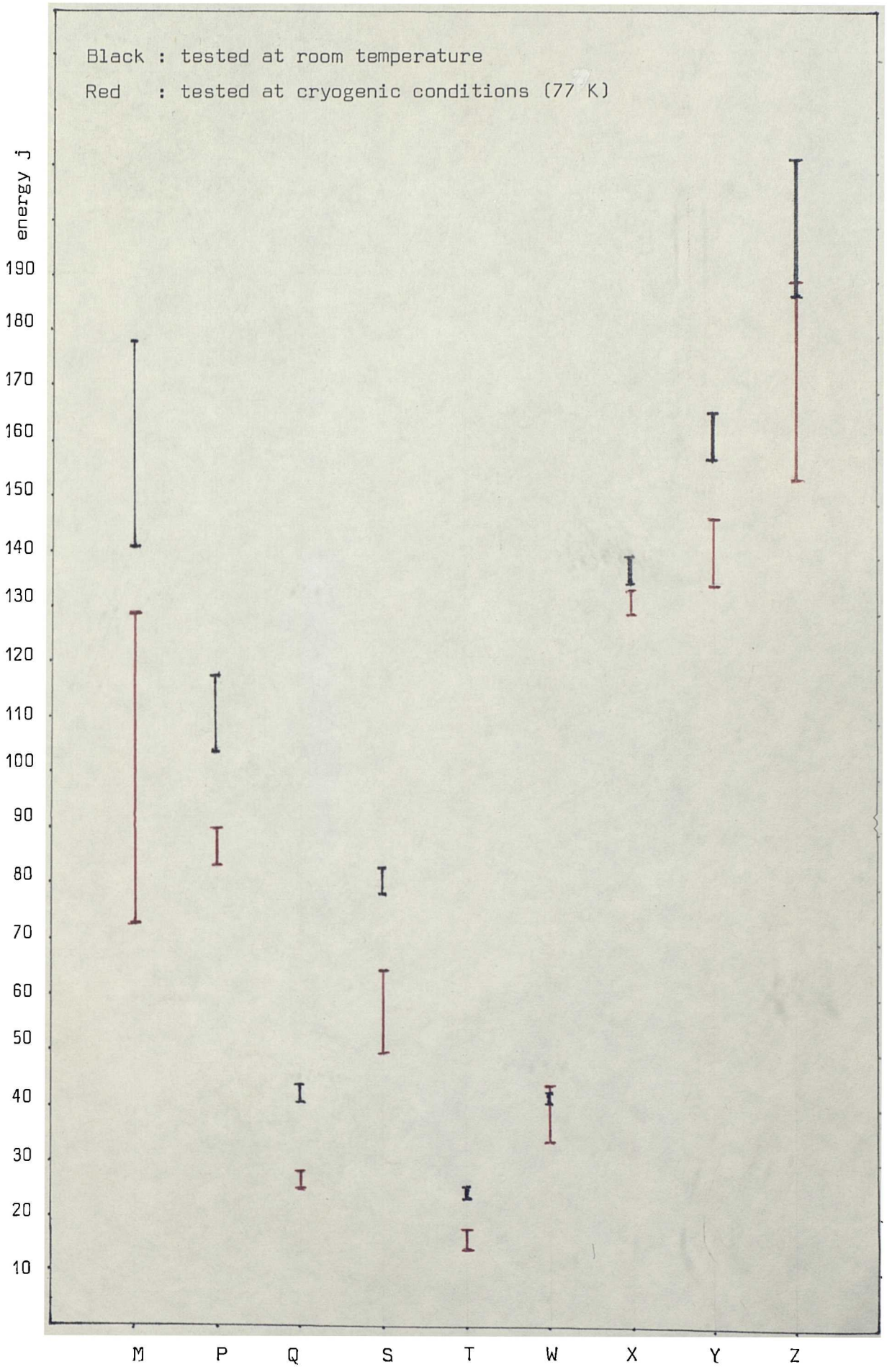

Fig.4.24 Austenitic stainless steel AISI 316L parent plate impact energy

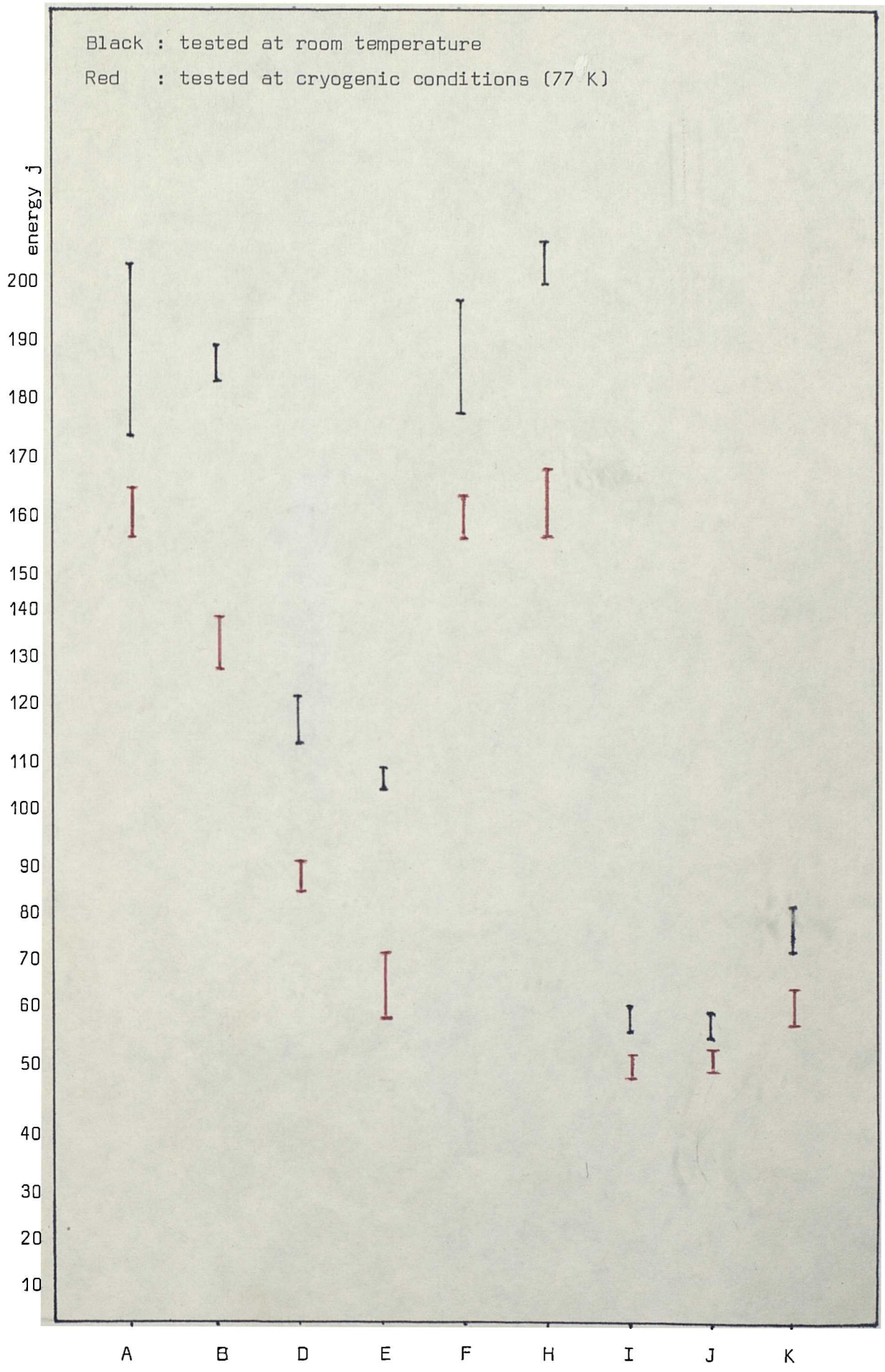

Fig.4.25 - Austenitic stainless steel AISI 321 parent plate impact energy

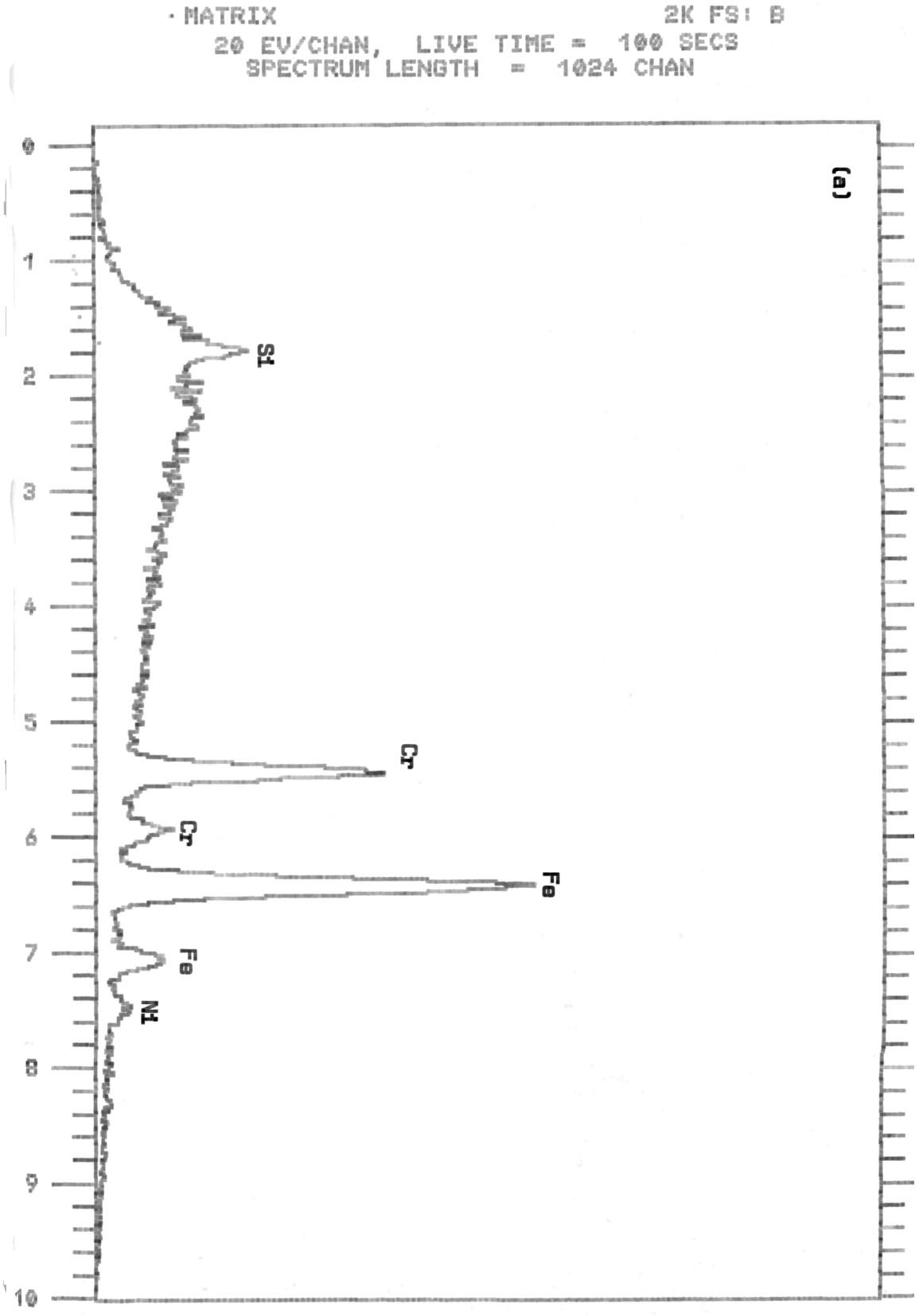

Fig.4.26 Energy dispersive x-ray analysis AISI 316L parent plate specimen hot rolled at 950°C.

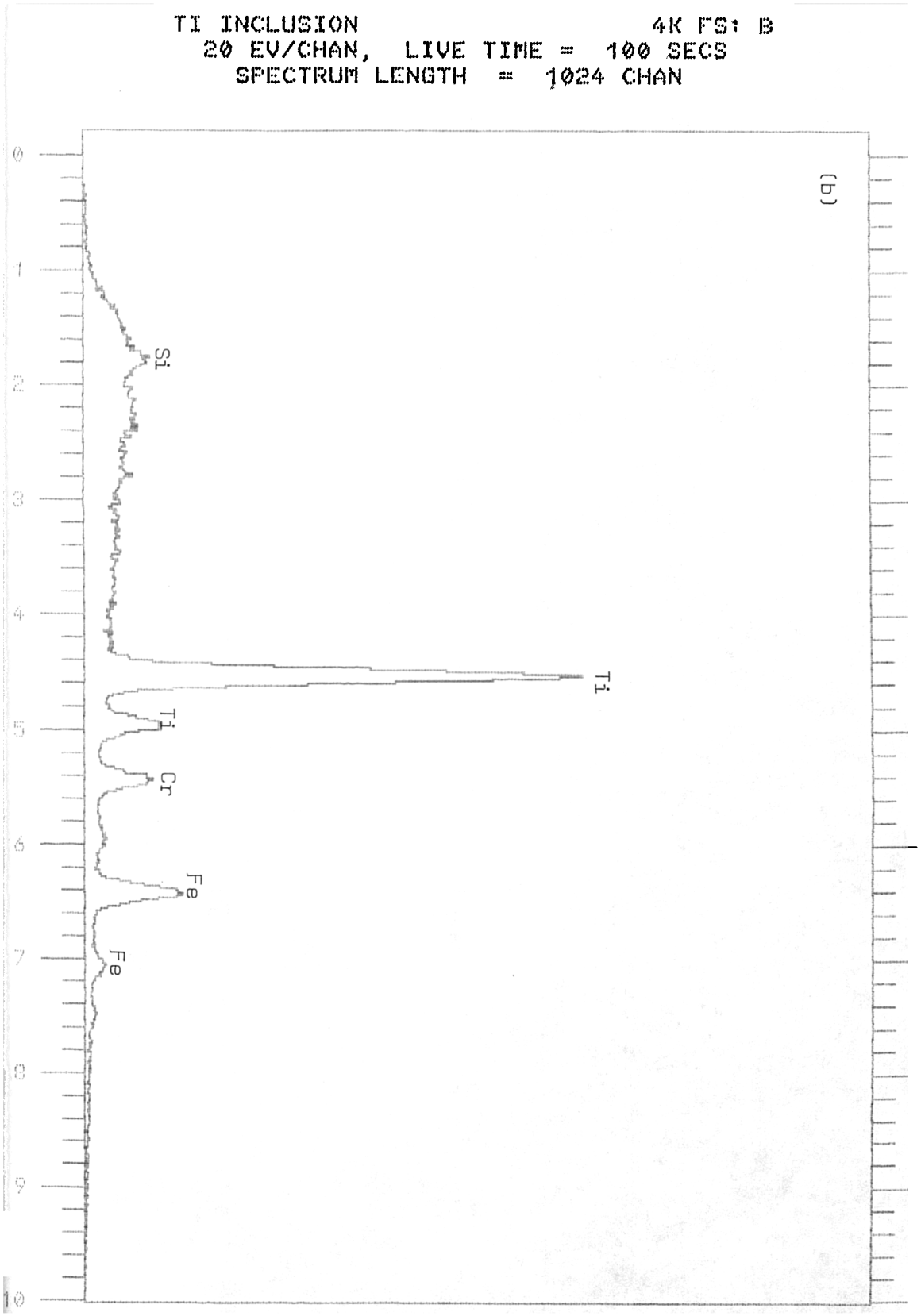

Fig.4.26 (contd)

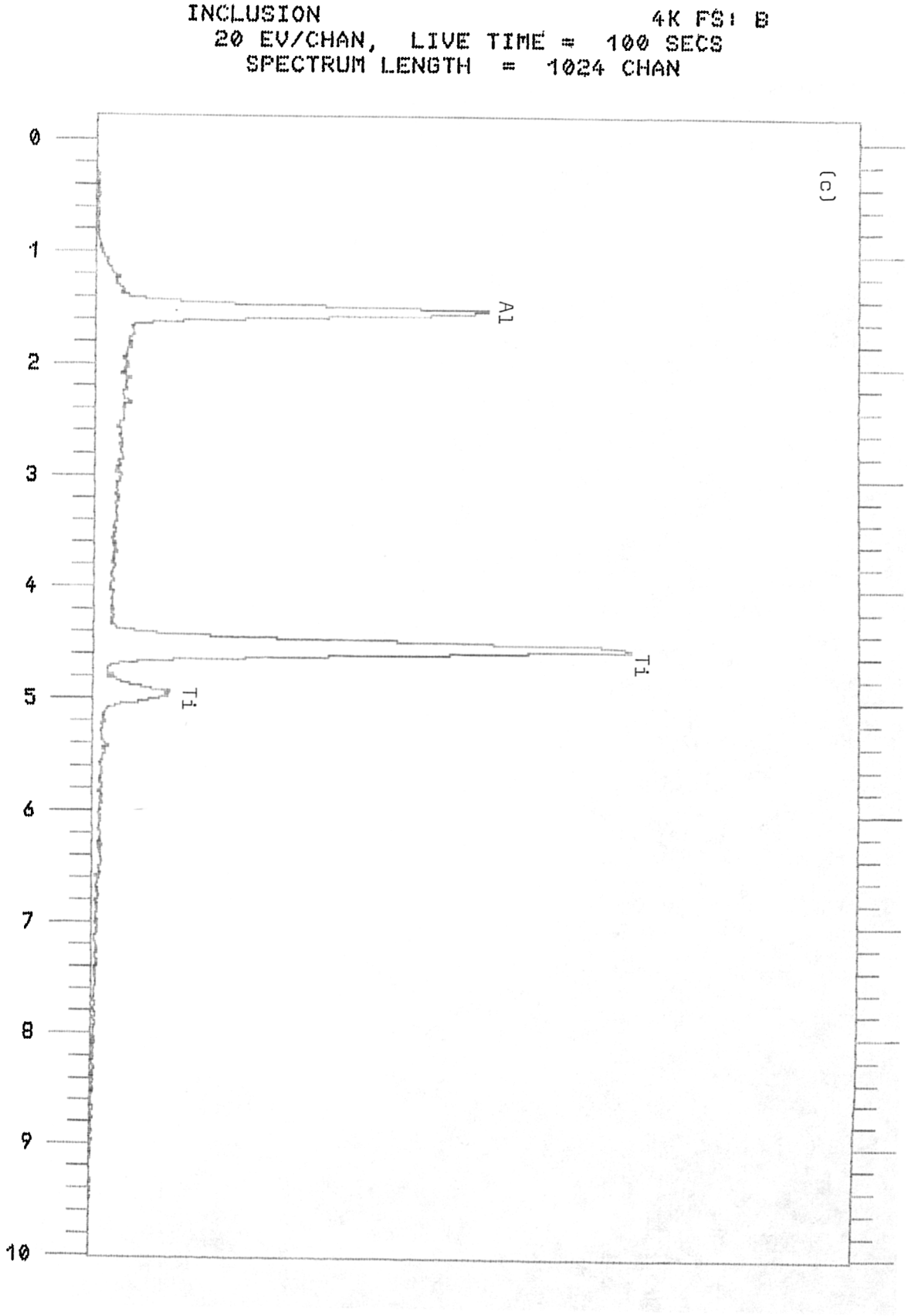

Fig.4.26 (contd

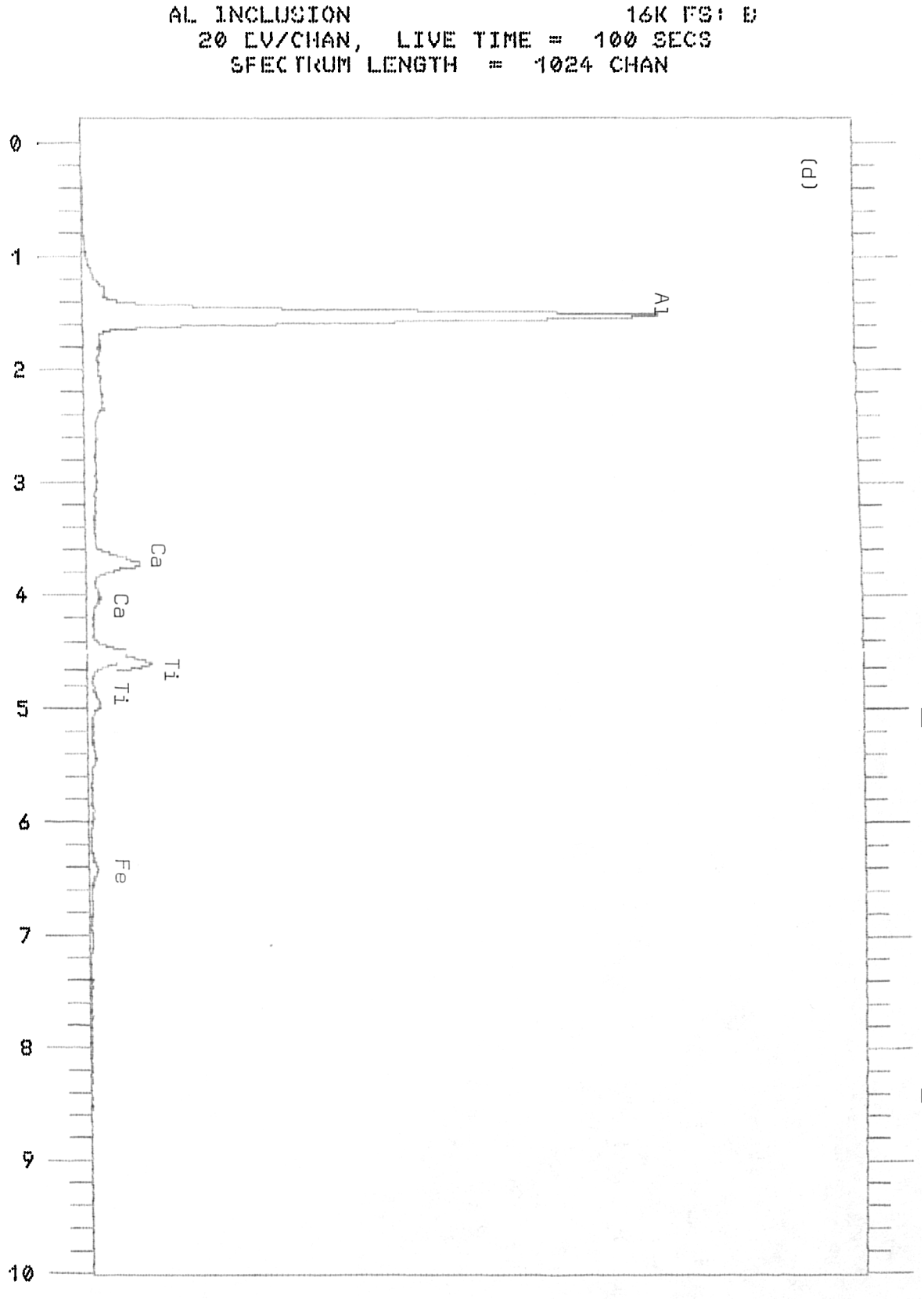

Fig.4.26 (contd)

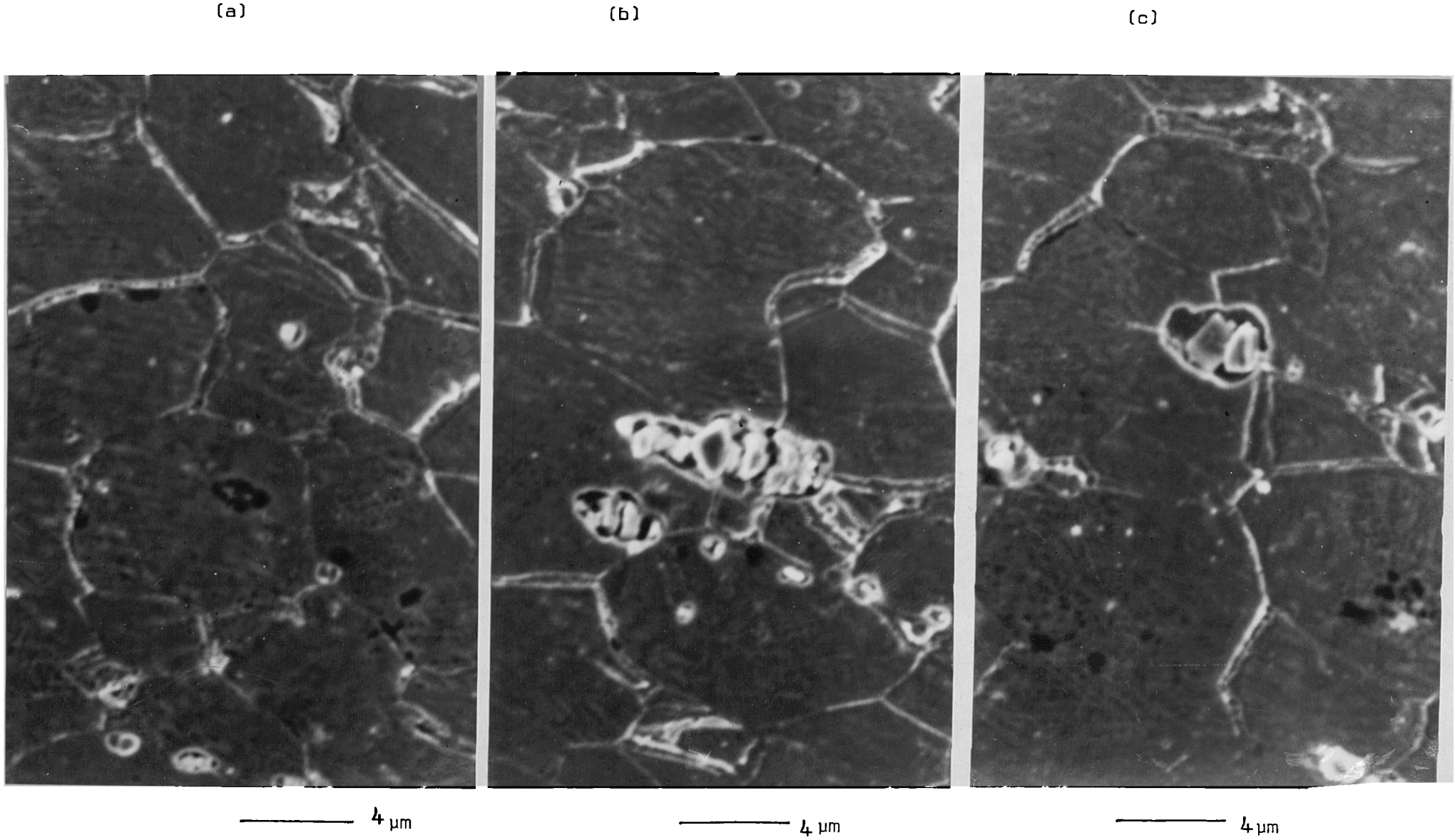

Fig.4.27 S.E.M. micrographs of austenitic stainless steel AISI 321 tensile test specimens.

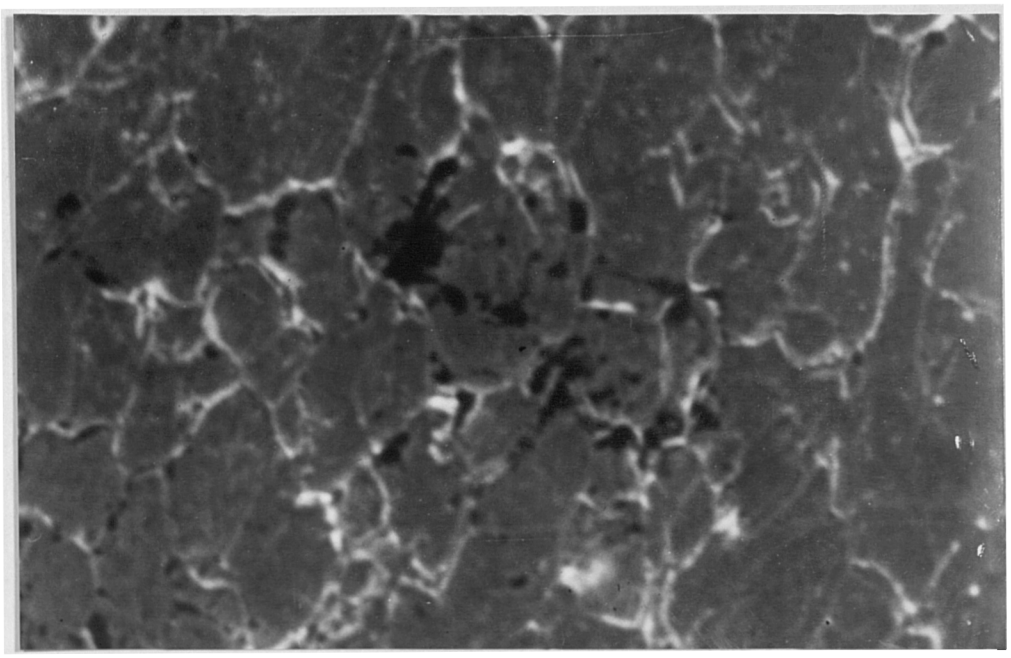

(a)

4 µm

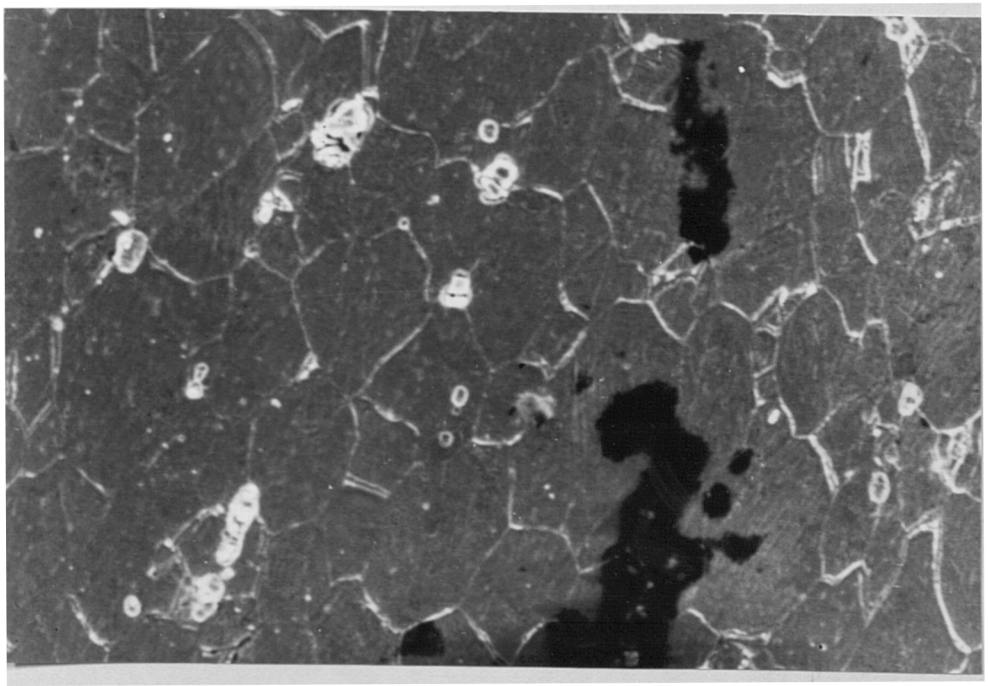

(b)

10 µm

Fig.4.28 S.E.M. micrograph of austenitic stainless steel AISI 321 showing crack propagation and final linkage of crack in tensile test specimen prior to fracture.

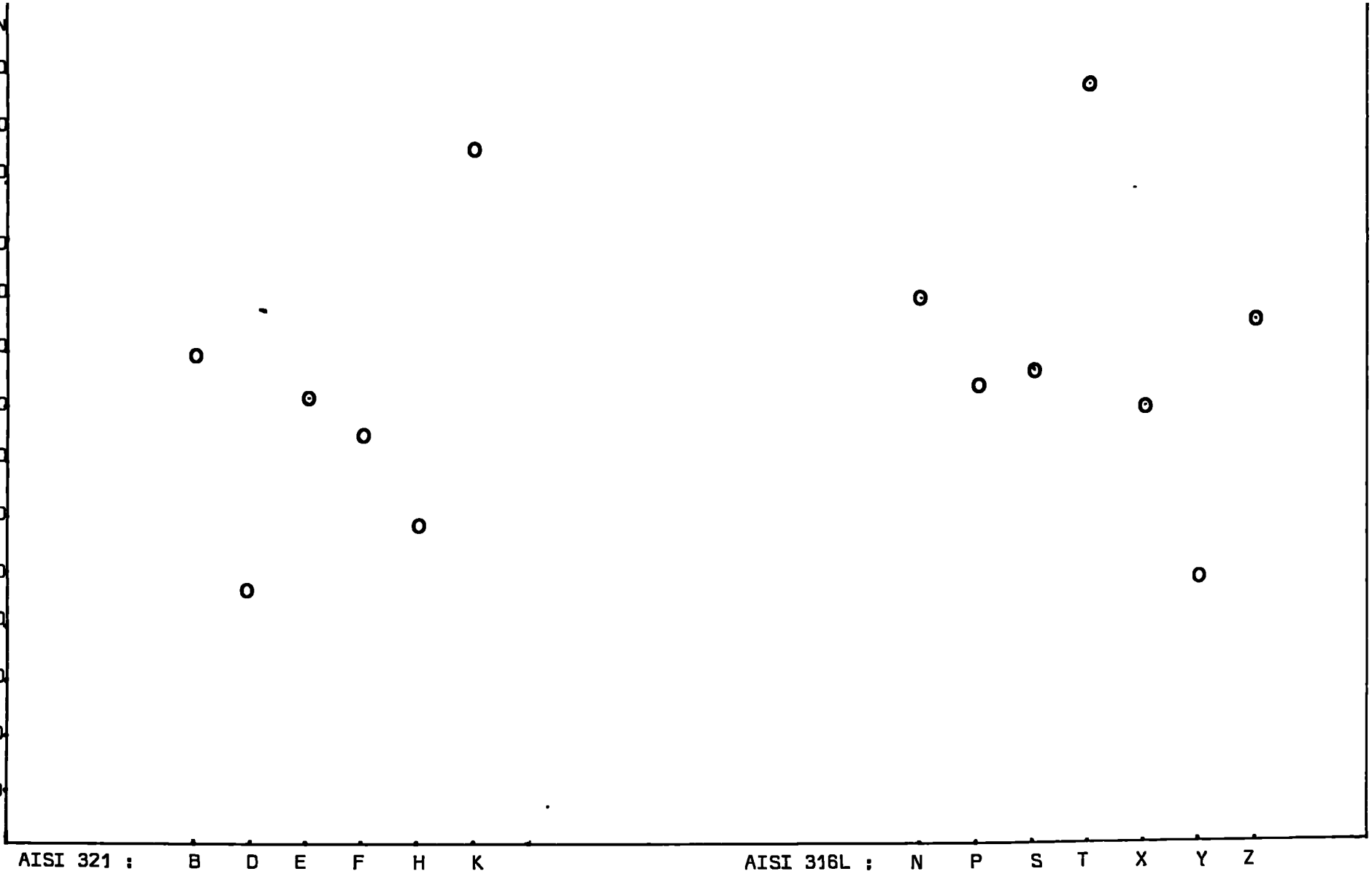

Fig.4.29 Parent plate hardness value (VPN)

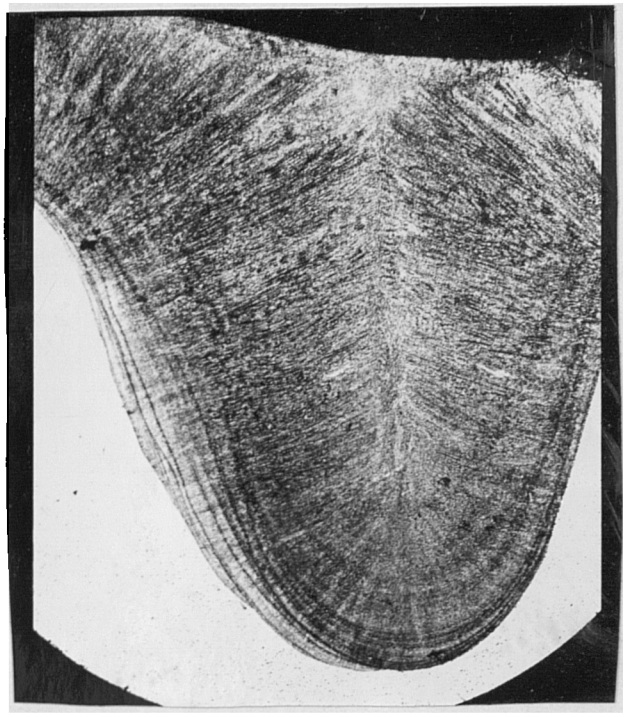

(a)

2000µm

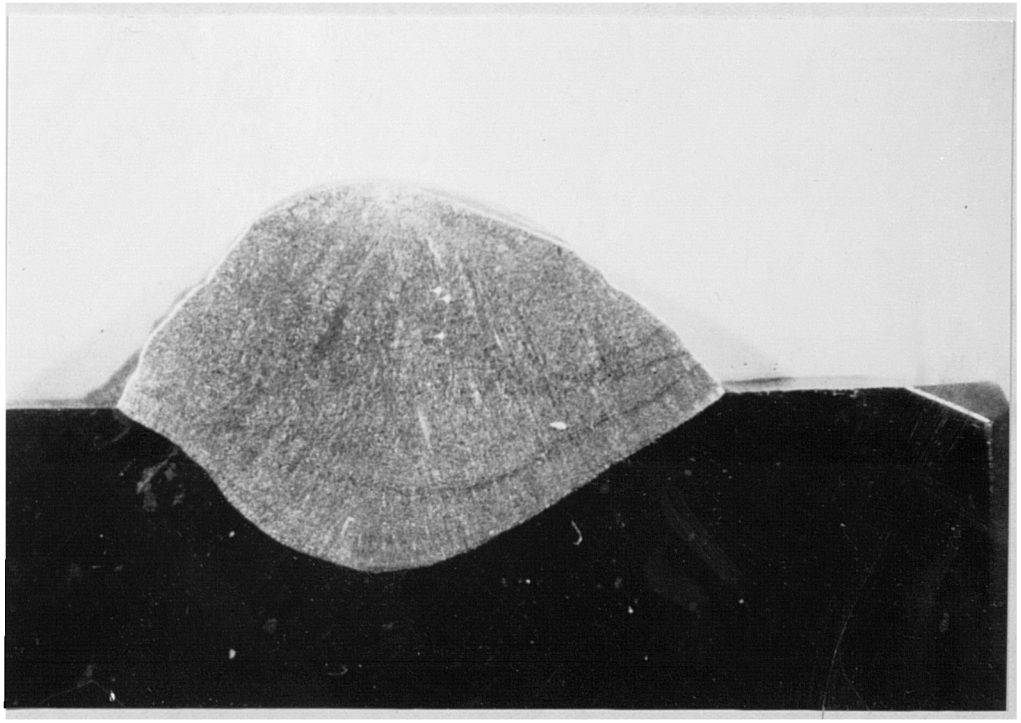

(b)

5000µm

Fig.4.30 Optical micrographs of (a) high heat input and (b) low heat input Bead-on-Plate weld metal produced by Submerged Arc welding.

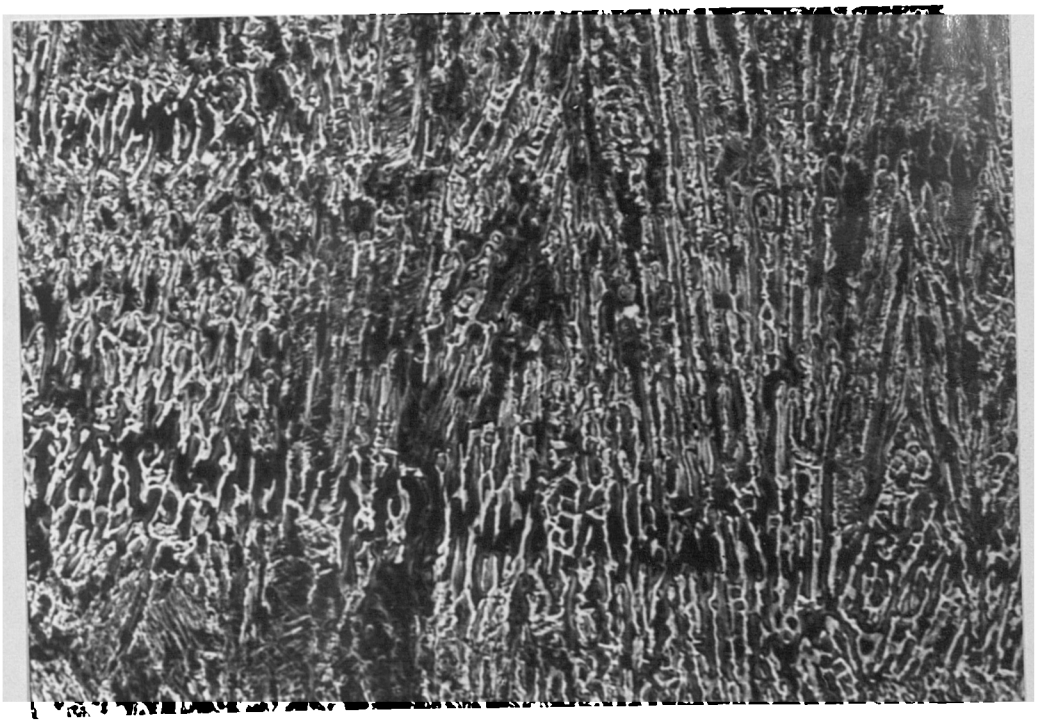

27 μm

Fig.4.31 S.E.M. micrograph of austenitic stainless steel AISI 316L weld metal showing ripple bands at region near to fusion boundary.

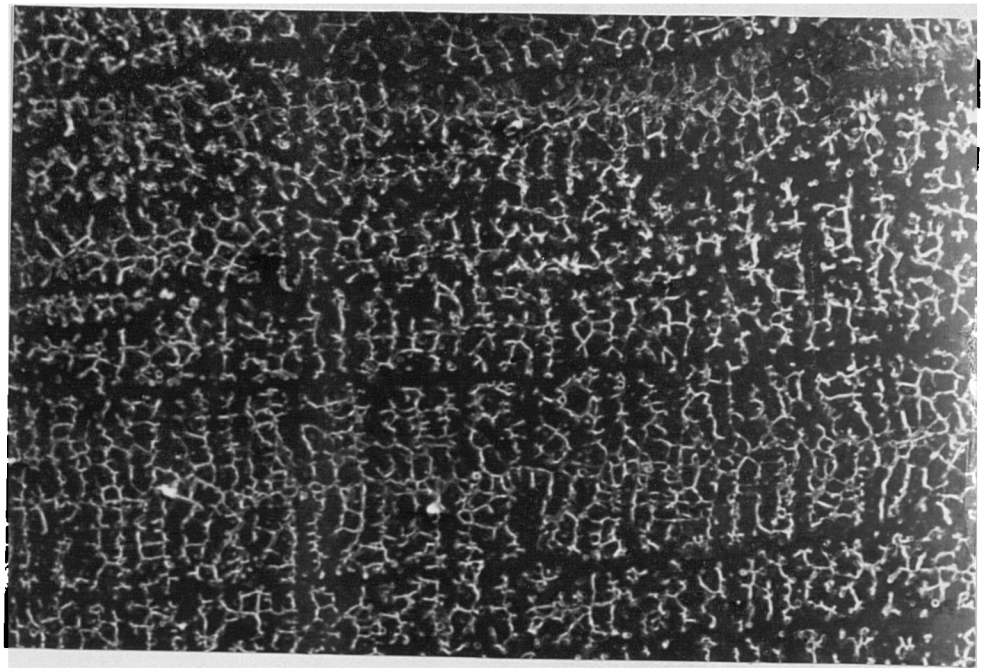

(a)

Fig.4.32 (a) S.E.M. micrograph of high heat input austenitic stainless steel AISI 316L weld metal showing well developed ferrite dendrites (ferrite appears white- austenite black).

(b)

Fig.4.32 (b) Optical micrograph of high heat input austenitic stainless steel AISI 316L weld metal from fusion boundary region (ferrite appears black - austenite white).

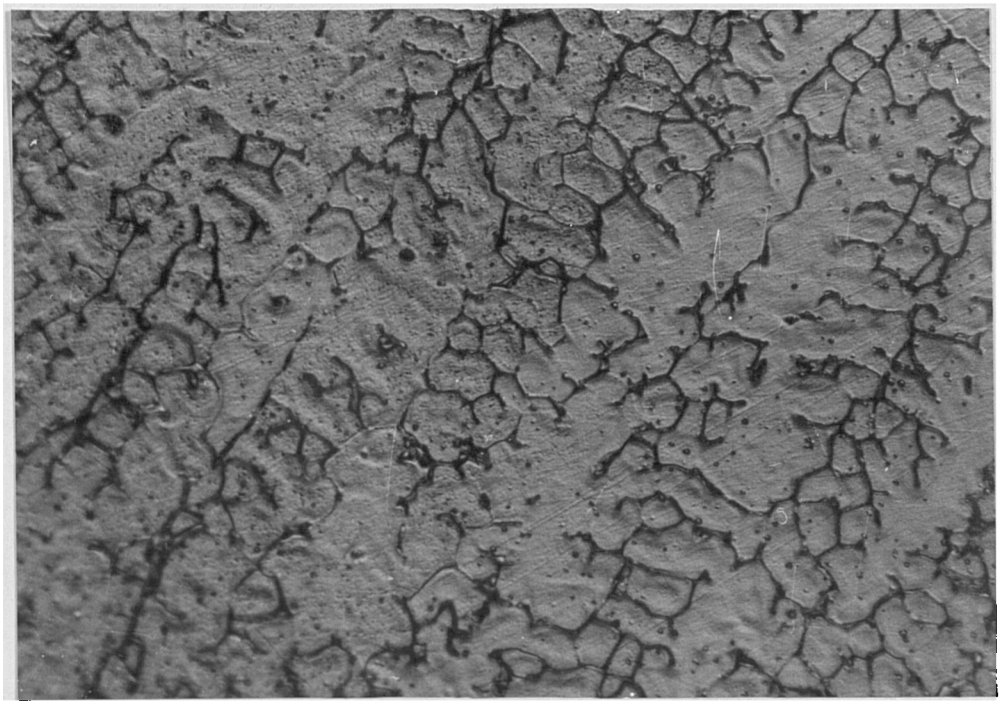

(a)

50µm

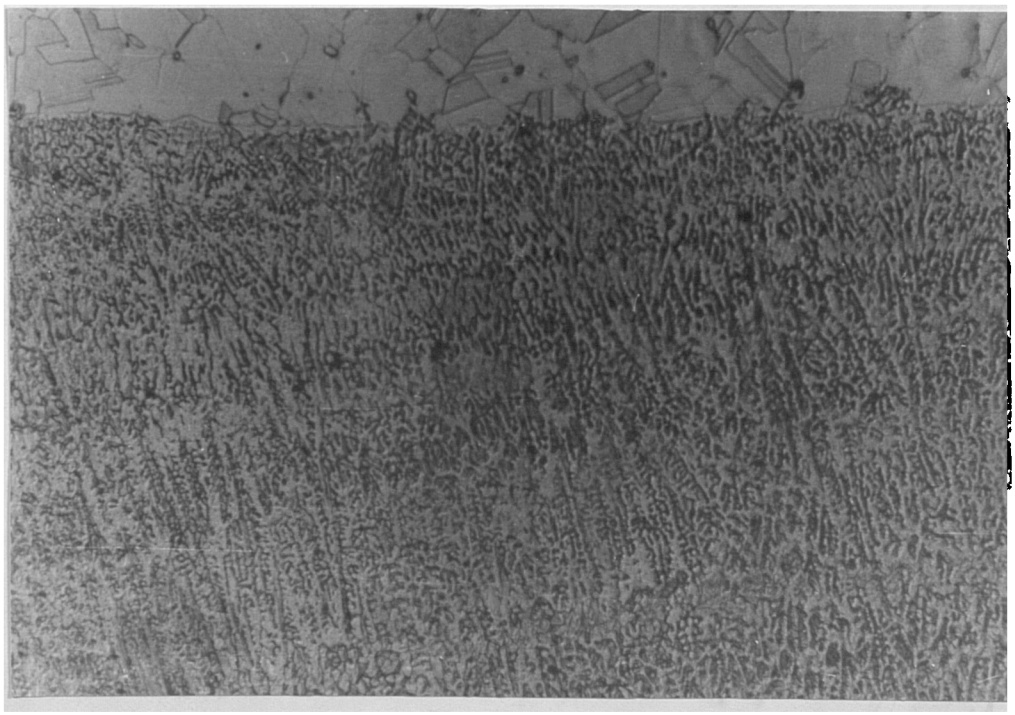

(b)

200µm

Fig.4.33 Optical micrograph of austenitic stainless steel AISI 316L Bead-on-Plate weld metal produced with low heat input (ferrite appears black - austenite white).

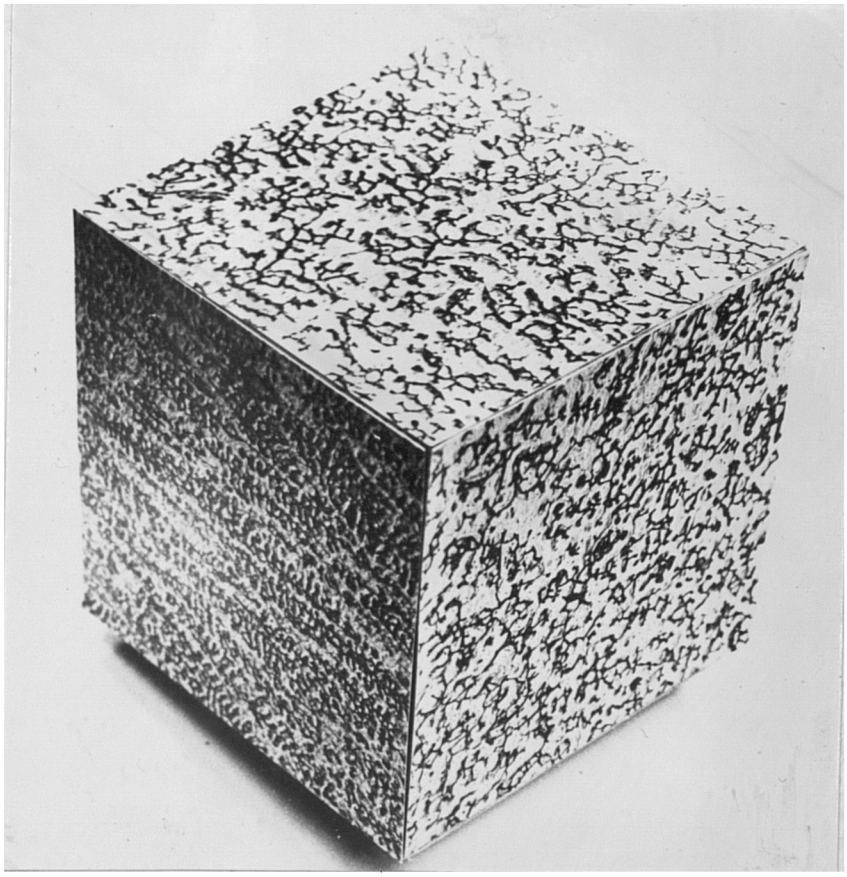

40μm

Fig.4.34 Optical micrograph of a three dimensional microstructures of austenitic stainless steel of AISI 316L Bead-on-Plate weld of high heat input.
(Original magnification x500 reduced in reproduction)

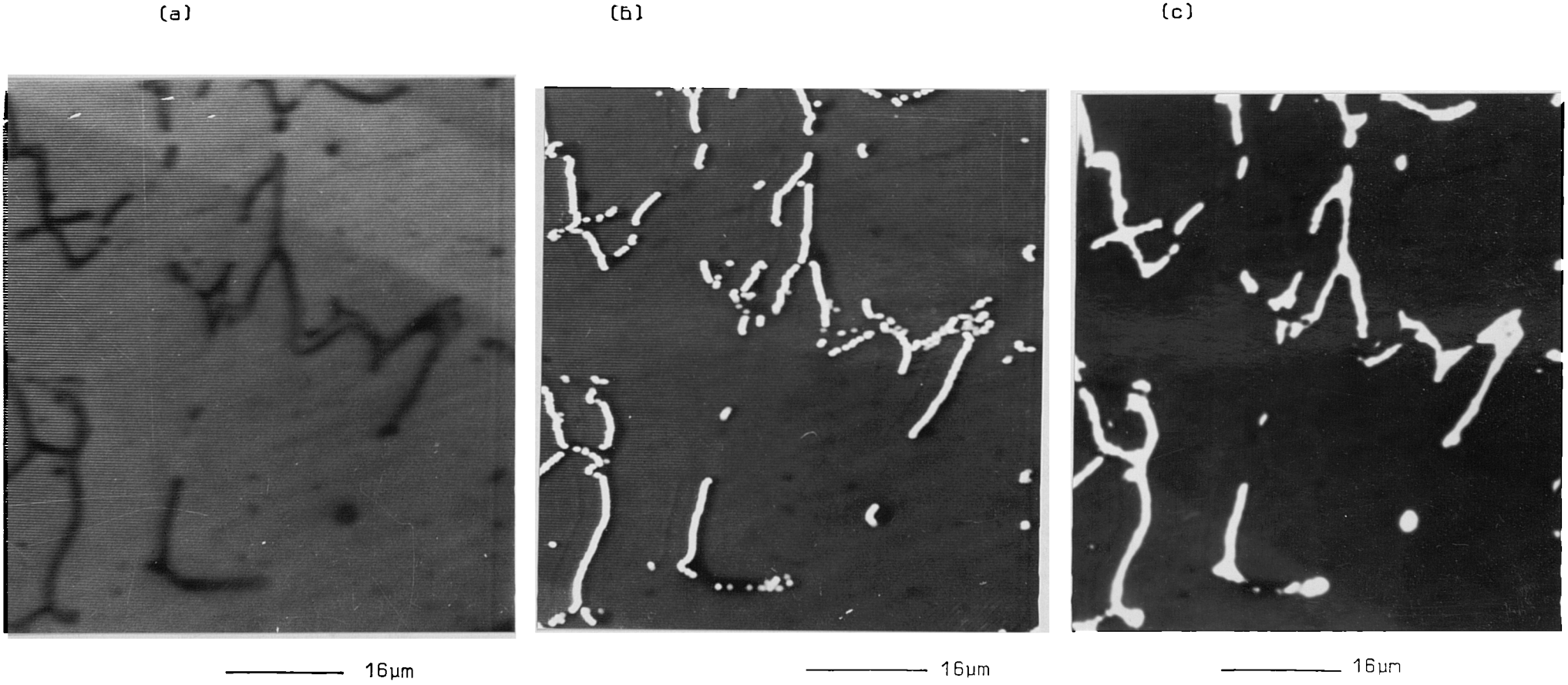

Fig.4.35 Typical weld metal ferrite appearance by Q.M.T. for quantitative metallography

(a) optical micrograph

(b) under field (fine appearance)

(c) over field (coarse appearance)

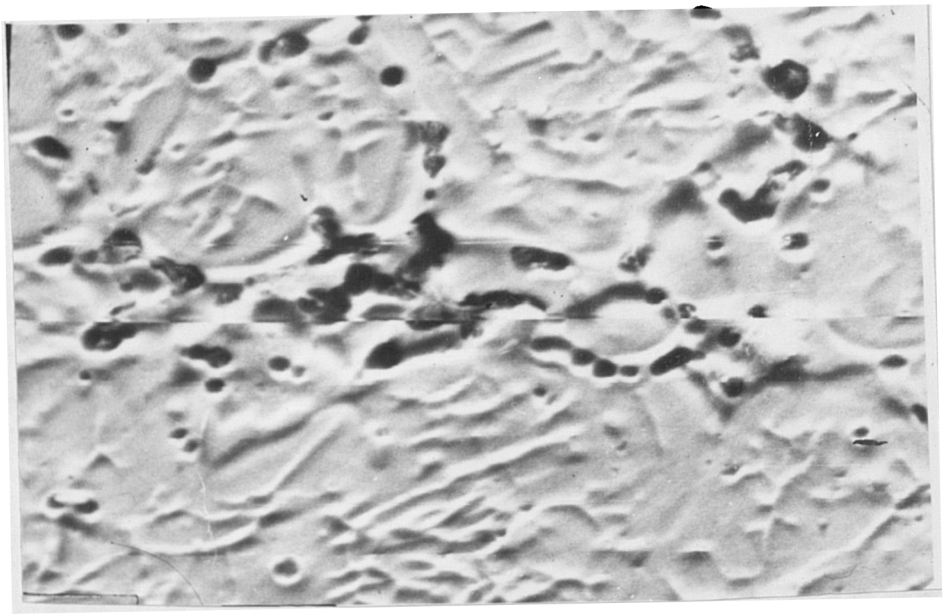

(a)

13 µm

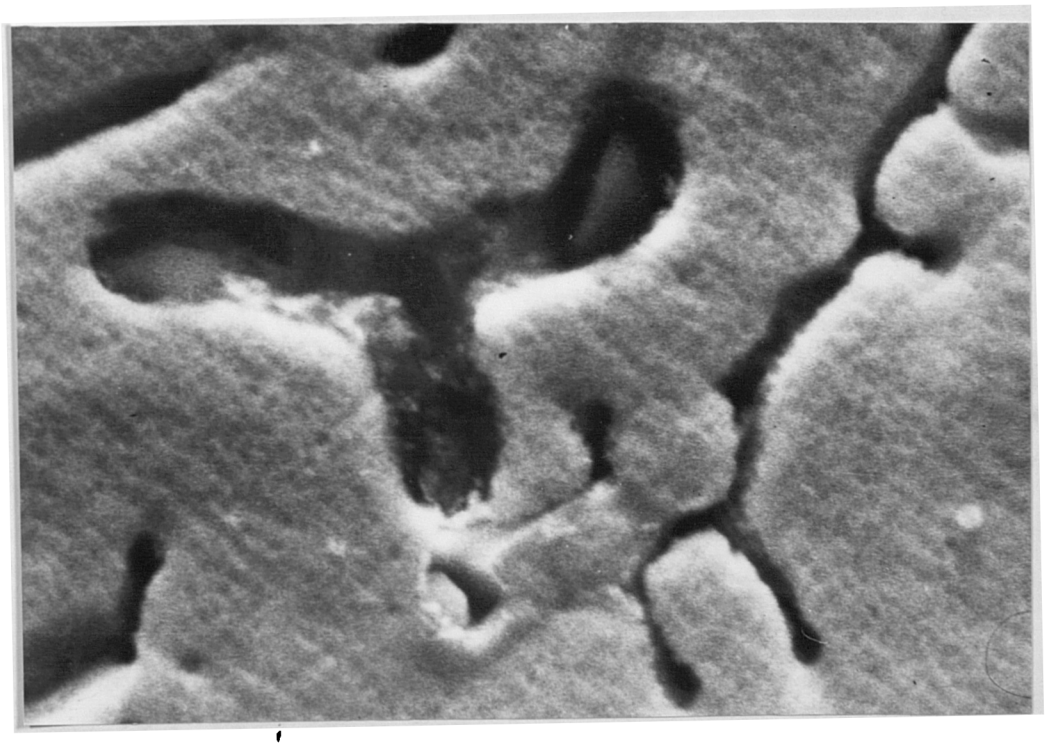

(b)

6 µm

Fig.4.36 Typical S.E.M. micrographs of austenitic stainless steel weld showing second phase particle, internal fissure in conjunction with delta ferrite phase.

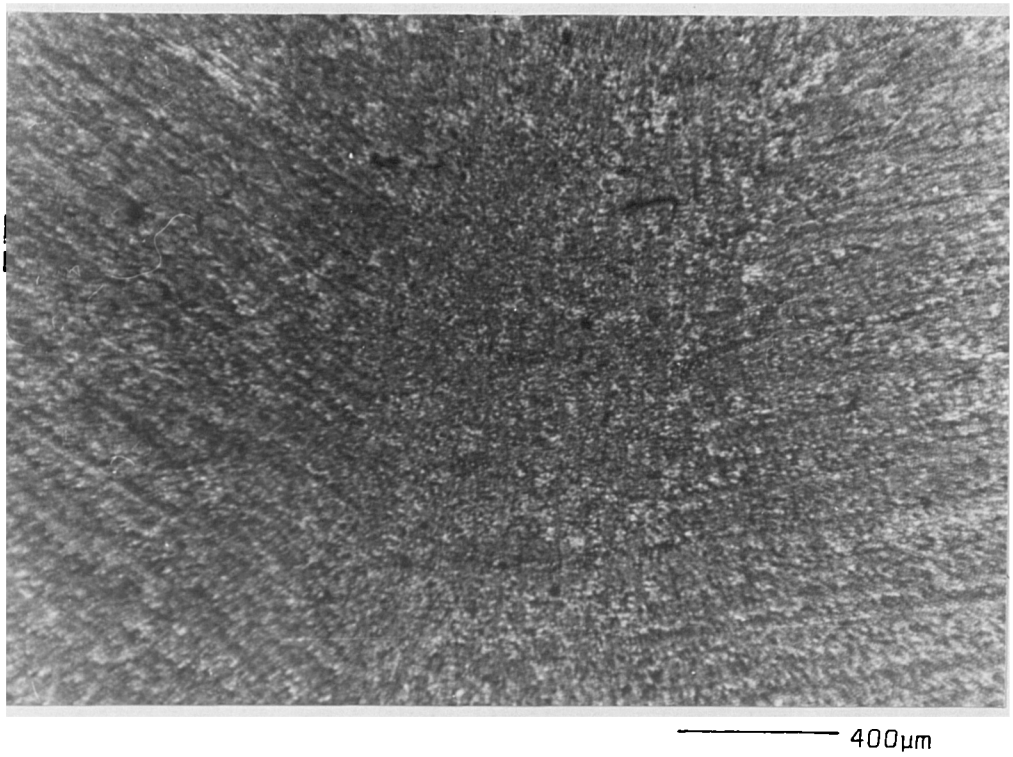

Fig.4.37 (a) optical micrograph of austenitic stainless steel AISI 316L Bead-on-Plate weld metal produced in restrain parent plate, showing axial or raft structure in central region.

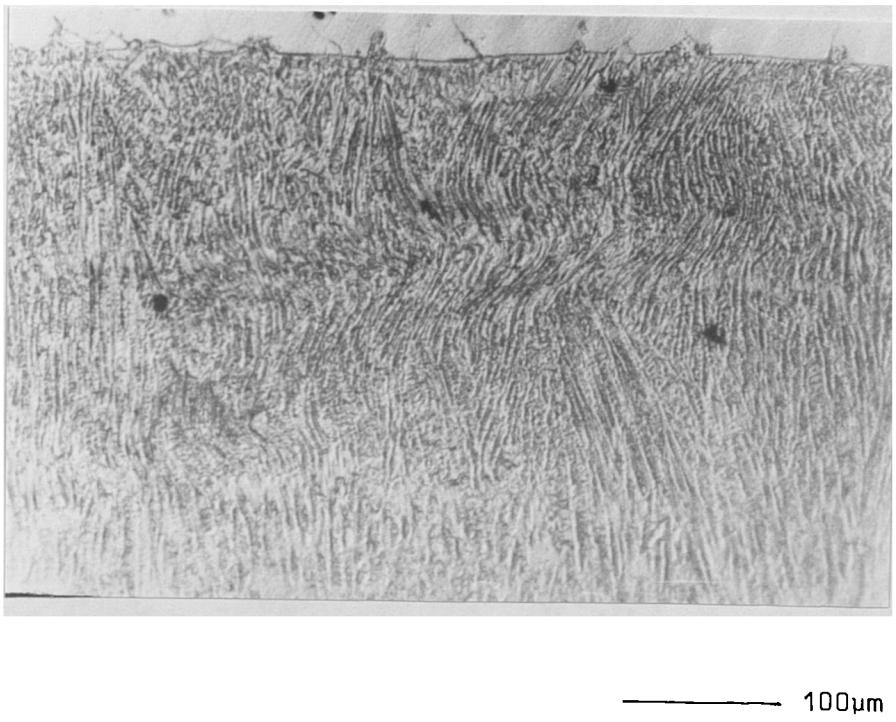

Fig.4.37 (b) Optical micrograph of austenitic stainless steel AISI 316L Bead-on-plate weld metal produced in restrained condition with high heat input showing undulating pattern near the fusion boundary.

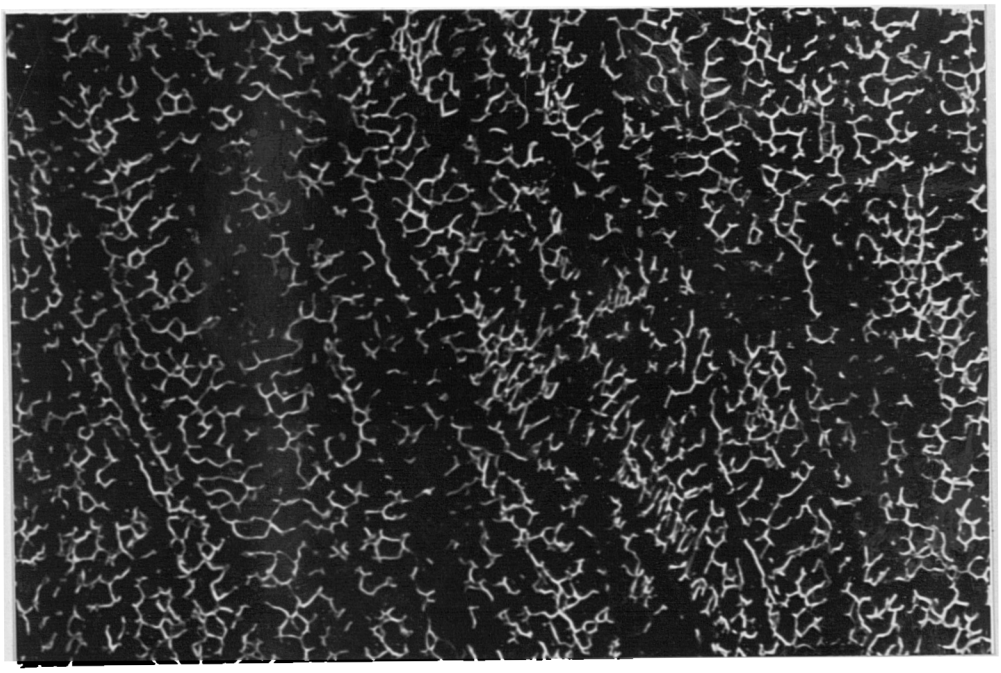

Fig.4.38 SEM micrograph of austenitic stainless steel AISI 316L weld metal produced in restraining parent plate with high heat input condition.

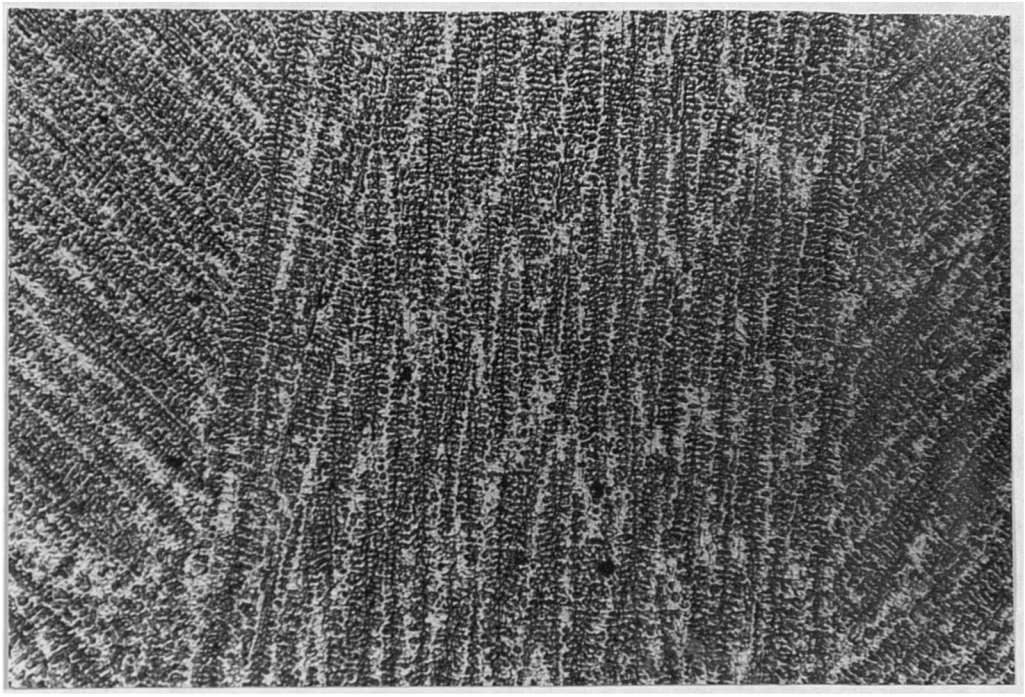

Fig.4.39 Optical micrograph of rapidly cooled Bead-on-Plate AISI 316L weld showing oriented dendritic type ferrite along the weld axes at centre line region.

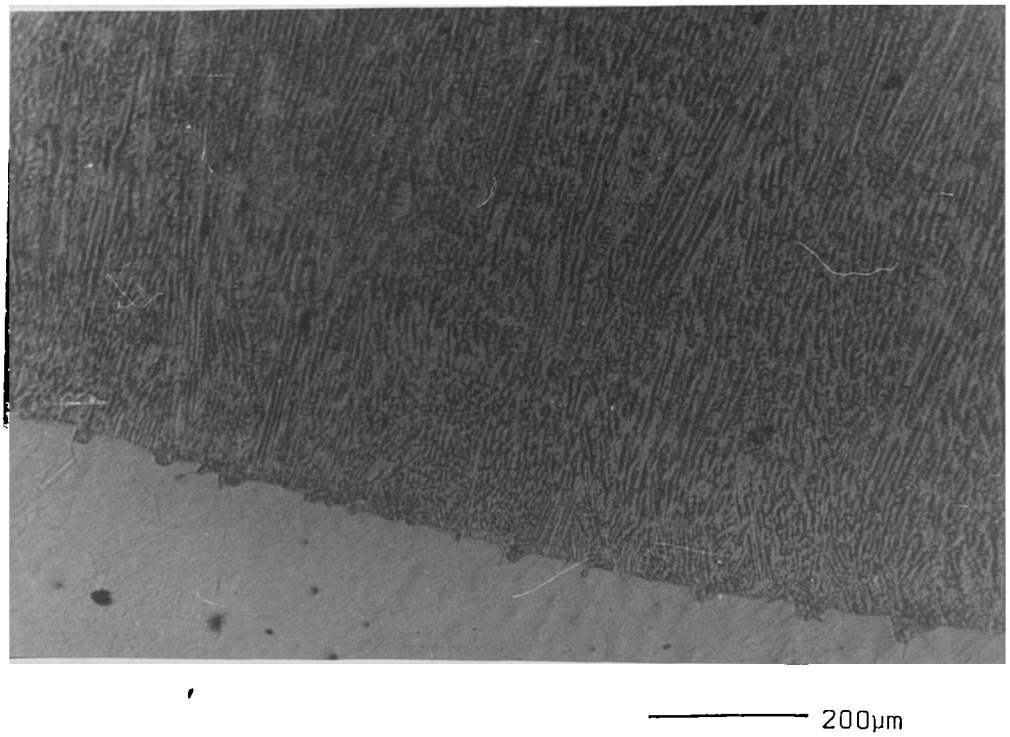

Fig.4.40 Optical micrograph of rapidly cooled Bead-on-Plate AISI 316L weld from the fusion boundary region.

100μm

Fig.4.41 Optical micrograph of AISI 316L Bead-on-Plate Submerged Arc weld near the fusion boundary region.

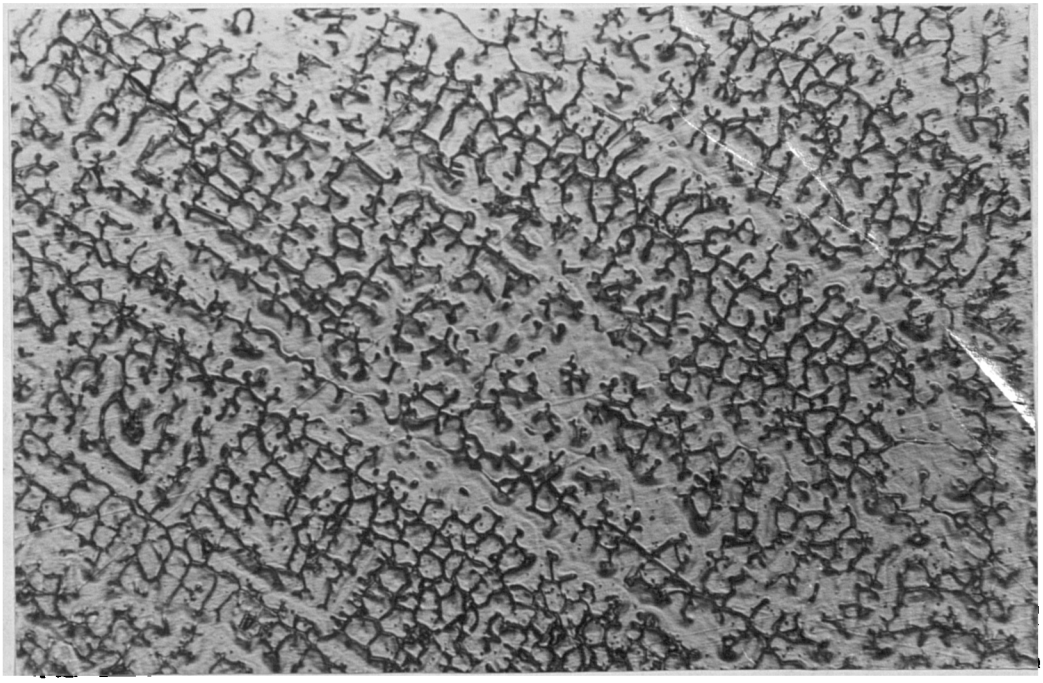

100μm

Fig.4.42 Optical micrograph of AISI 316L Bead-on-Plate Submerged Arc welds from the central region.

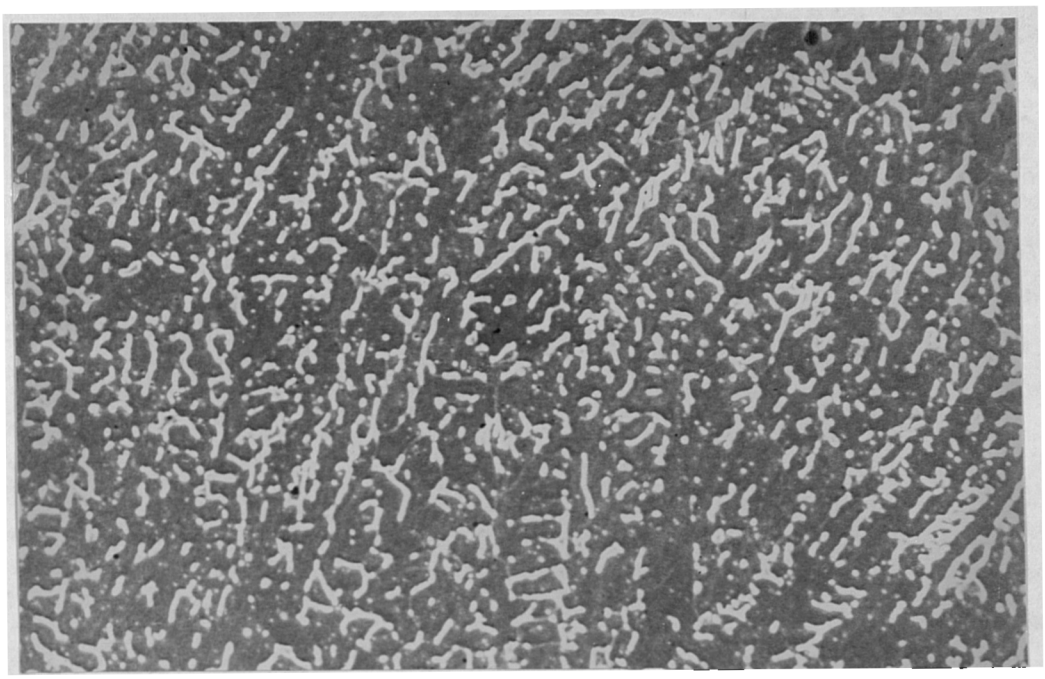

Fig.4.43 SEM micrograph of rapidly cooled Bead-on-plate AISI 316L weld metal.

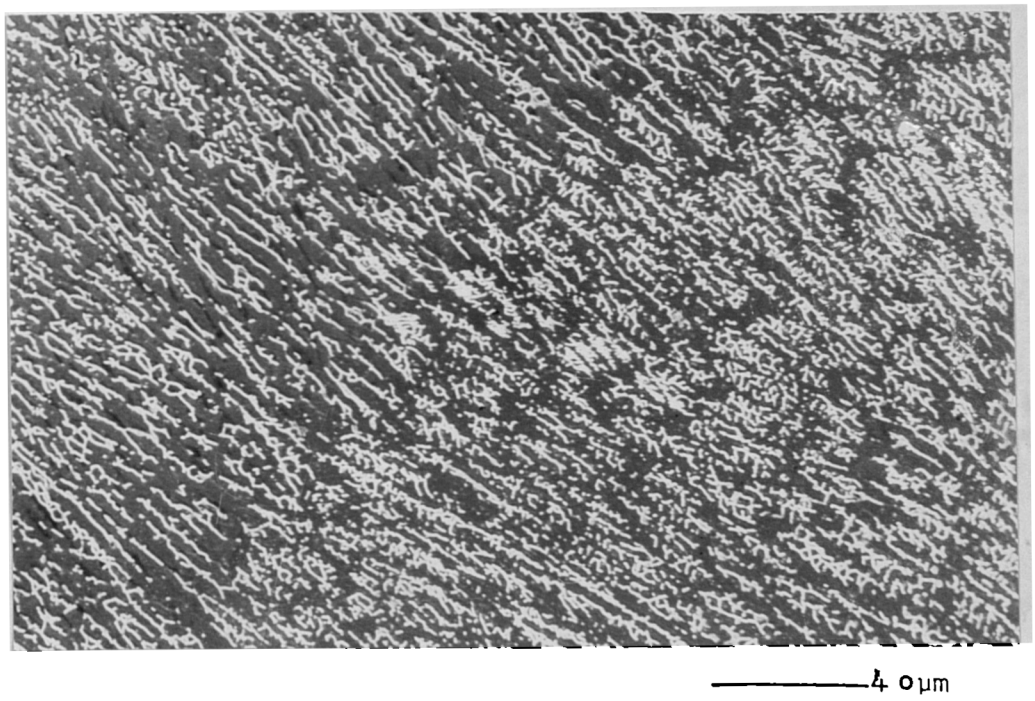

Fig.4.44 SEM micrograph of rapidly cooled Bead-on-Plate AISI 316L weld.

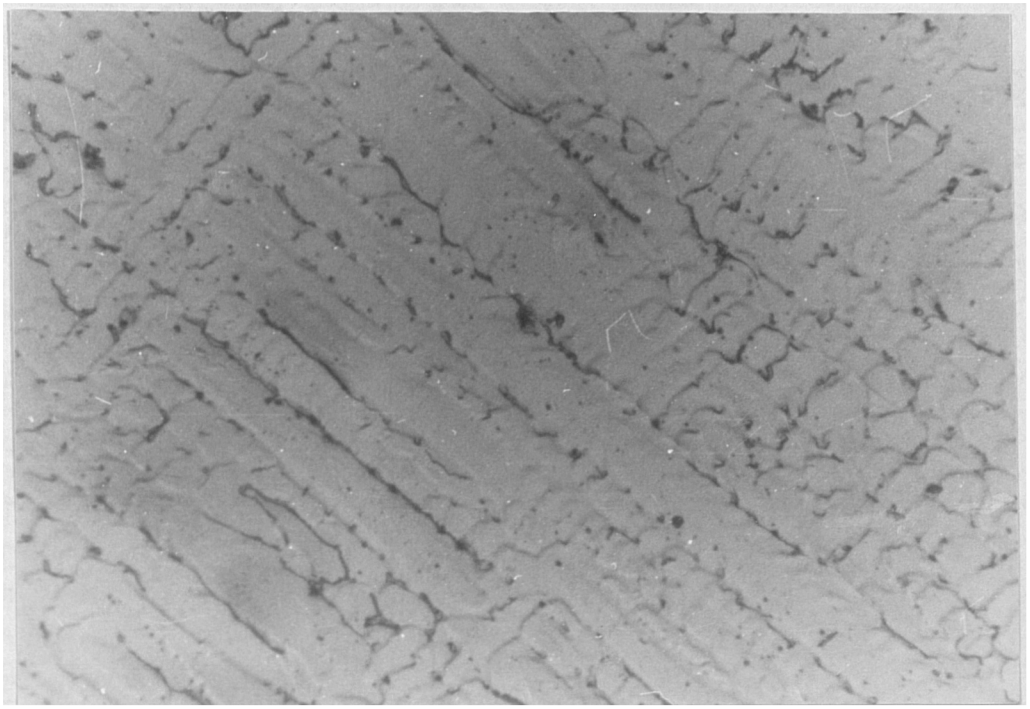

(a)

100µm

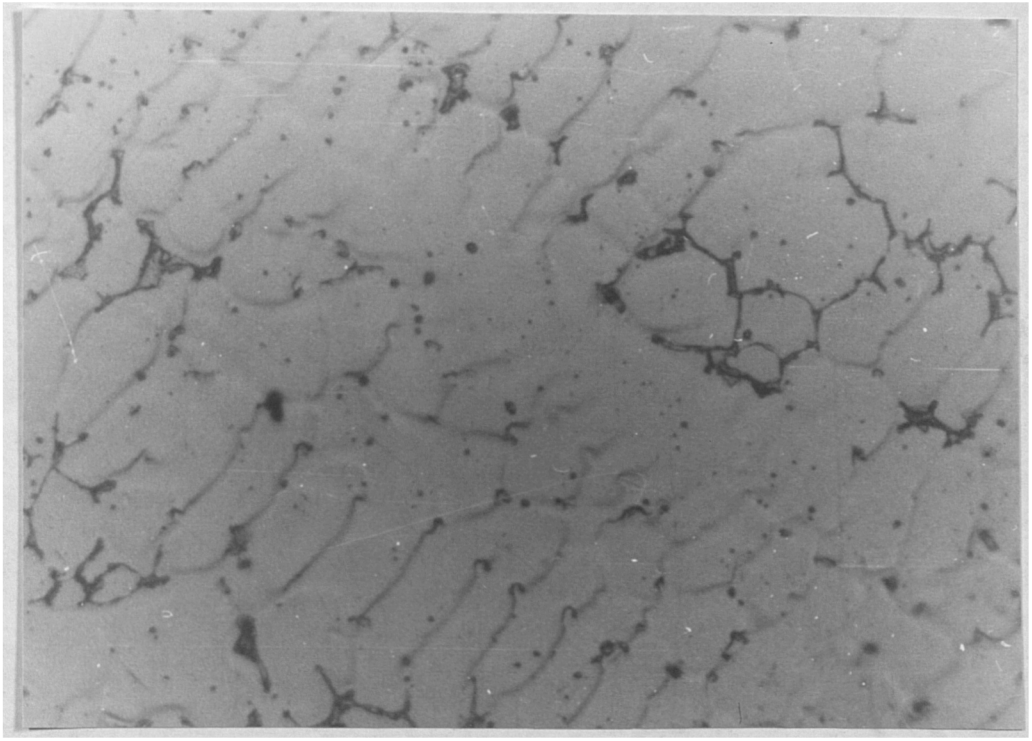

(b)

50µm

Fig.4.45 Optical micrograph of ultra rapidly cooled AISI 316L Submerged Arc Bead-on-Plate weld (Sample 15RN).

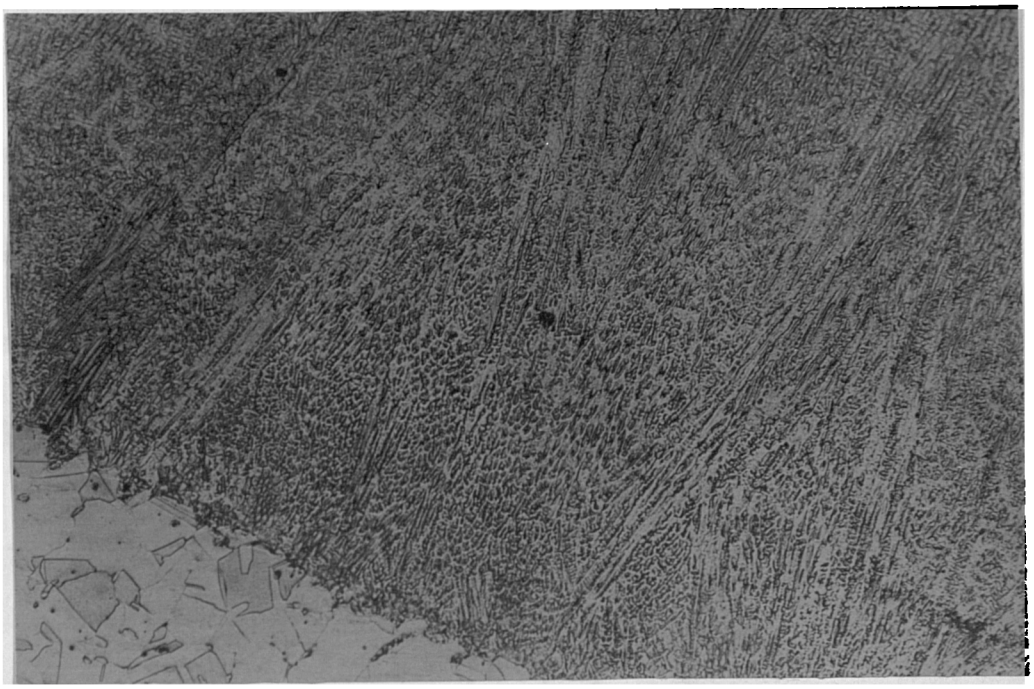

Fig.4.46 Optical micrograph of ultra rapidly cooled Submerged Arc Bead-on-Plate weld 18FN (fusion boundary region).

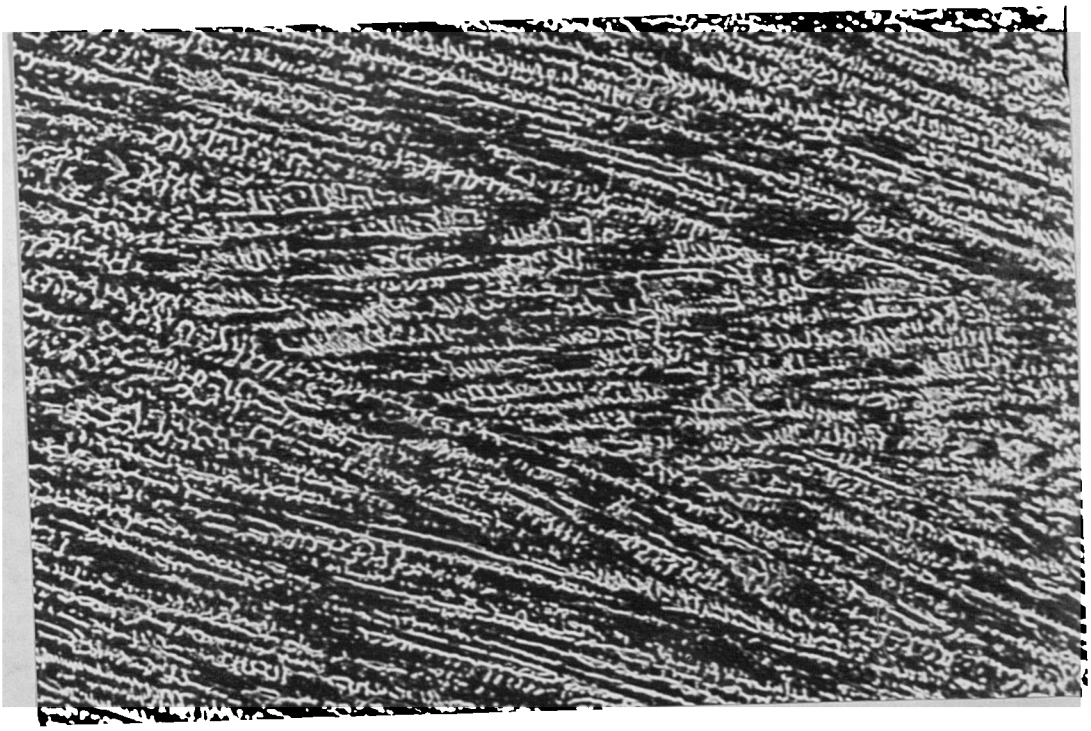

Fig.4.47 SEM micrograph of ultra rapidly cooled Submerged Arc Bead-on-Plate weld 18FN.

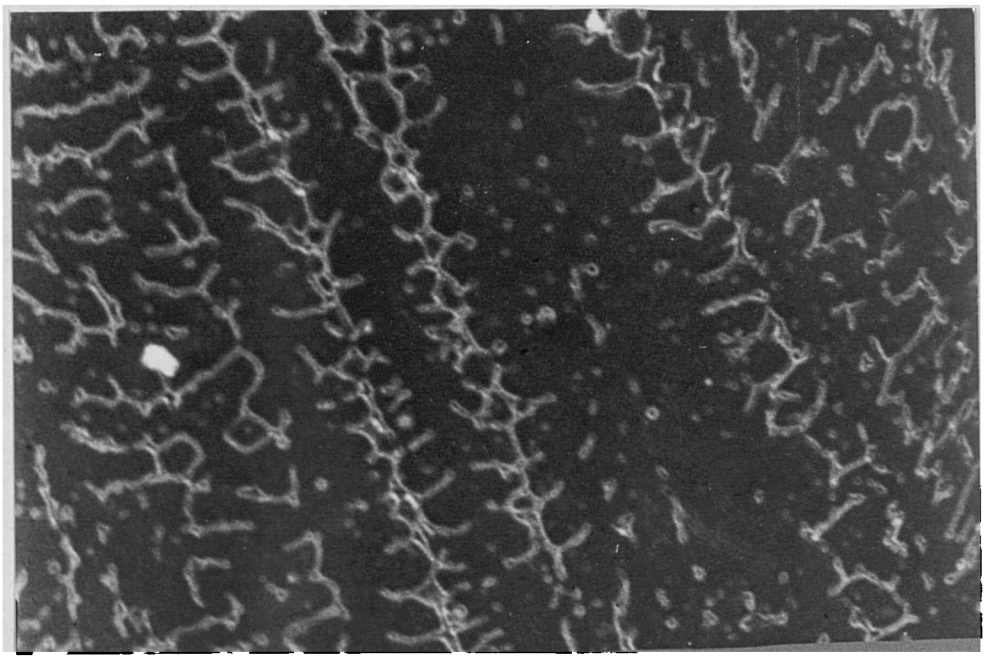

Fig.4.48 SEM micrograph of ultra rapidly cooled Submerged Arc Bead-on-Plate weld 18FN.

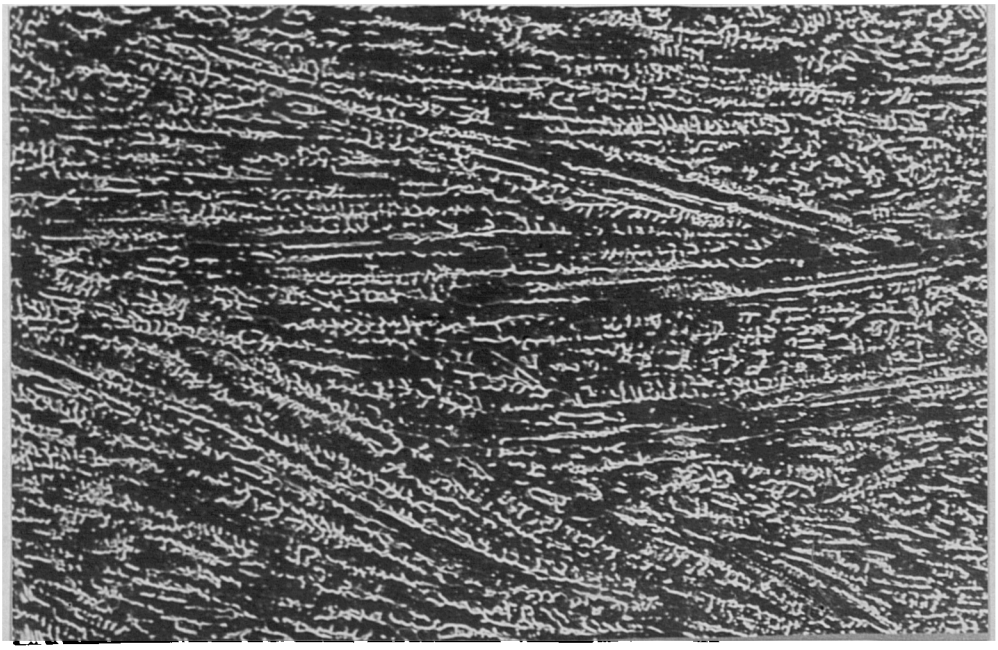

Fig.4.49 SEM micrograph of restrained Submerged Arc Bead-on-Plate weld R16 from the region near the fusion boundary.

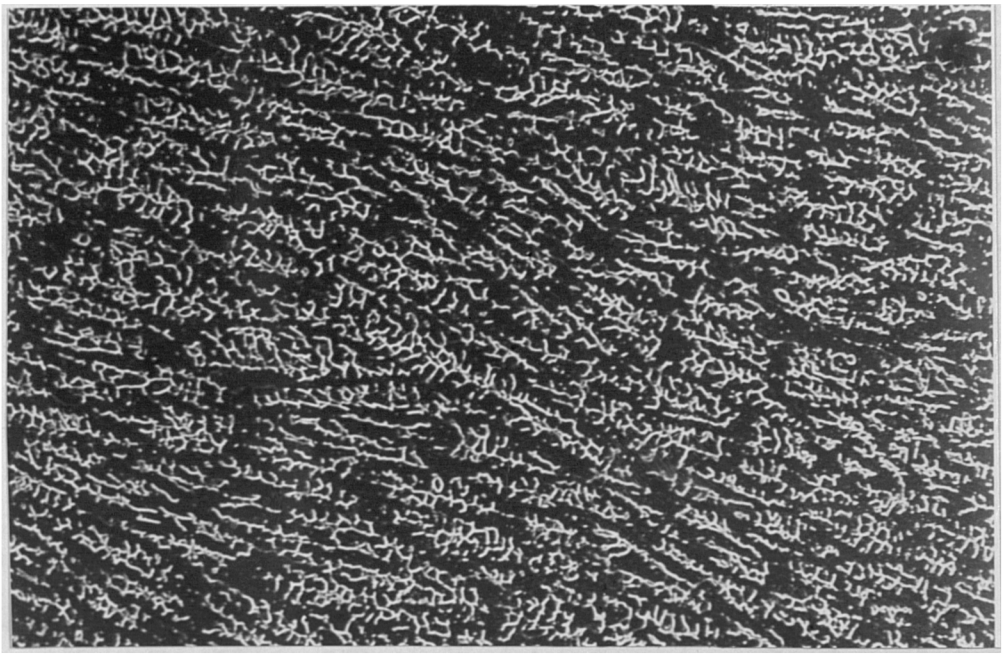

Fig.4.50 SEM micrograph of austenitic stainless steel AISI 316L Bead-on-Plate welds (Sample R16).

Fig.4.51 SEM micrograph of austenitic stainless steels AISI 316L Bead-on-Plate welds (Sample R16).

a

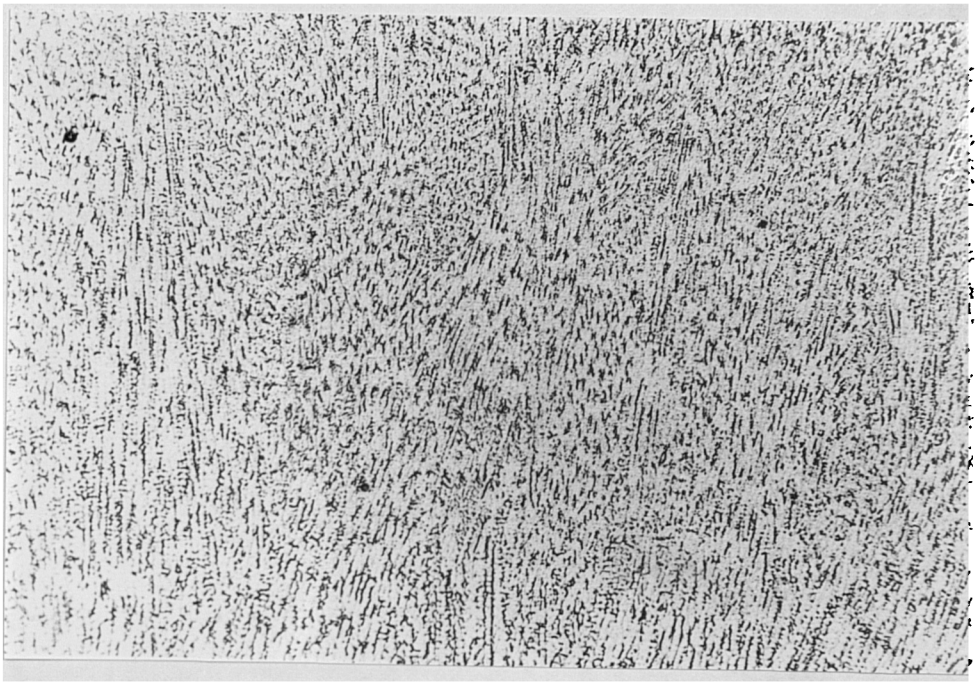

200µm

b

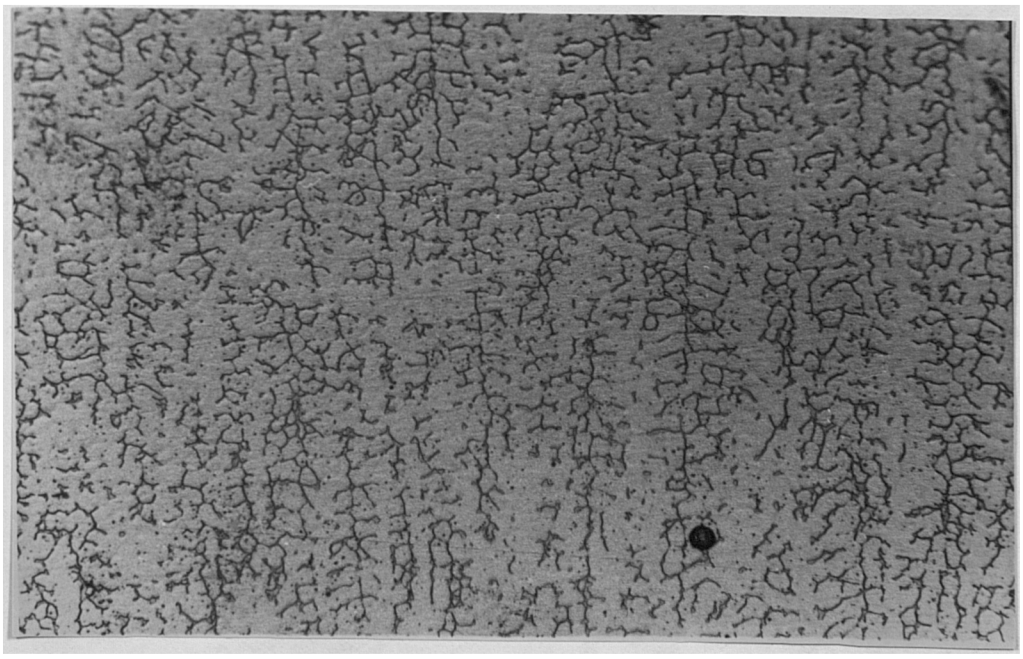

100µm

Fig.4.52 Optical micrograph of austenitic stainless steel AISI 316L Bead-on-plate Submerge Arc weld metal (Sample 250RH)

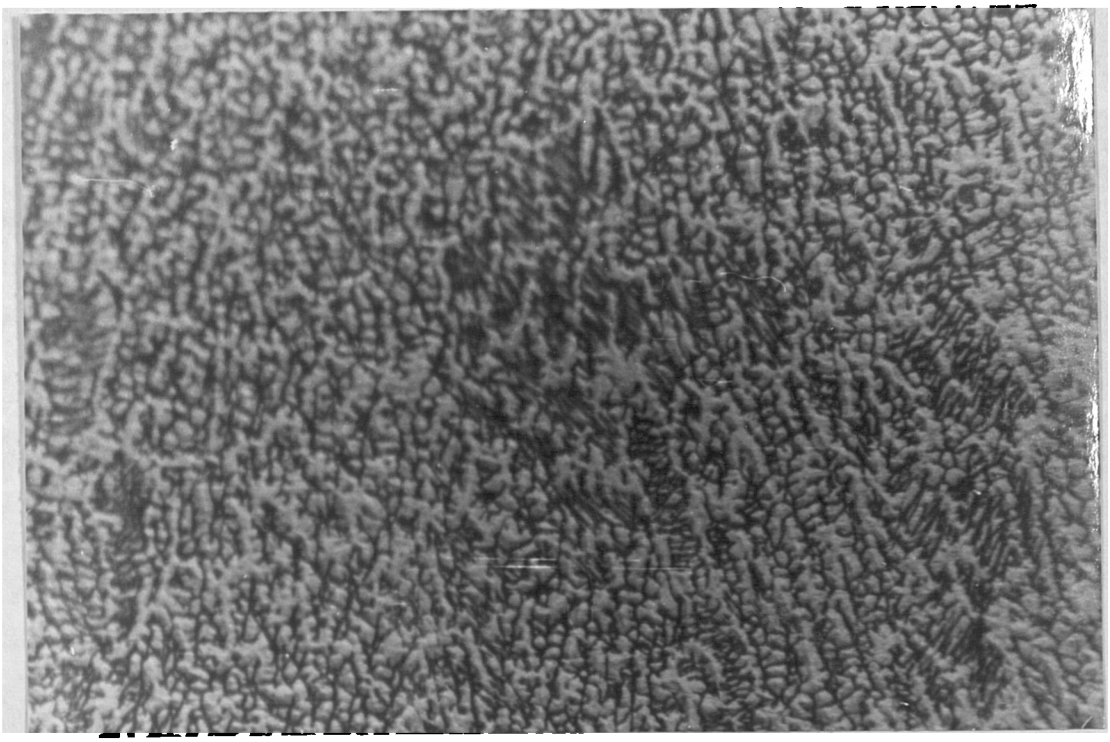

Fig.4.53 Optical micrograph of austenitic stainless steel AISI 316L Bead-on-Plate MIG welds (Sample M).

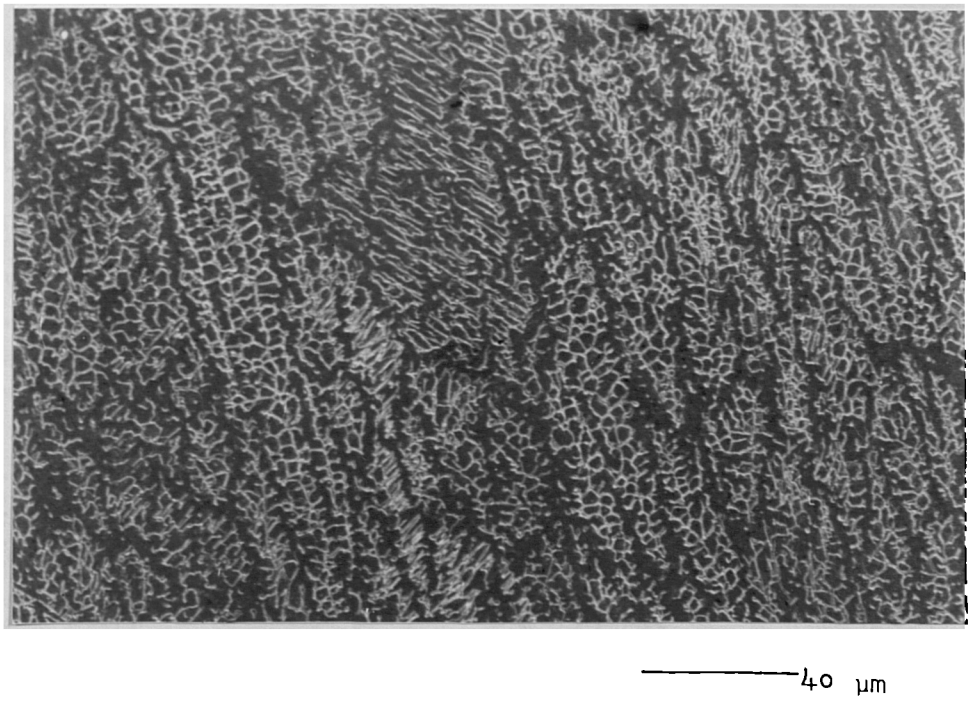

Fig.4.54 SEM micrograph of austenitic stainless steel AISI 316L Bead-on-Plate MIG welds (Sample T_3)

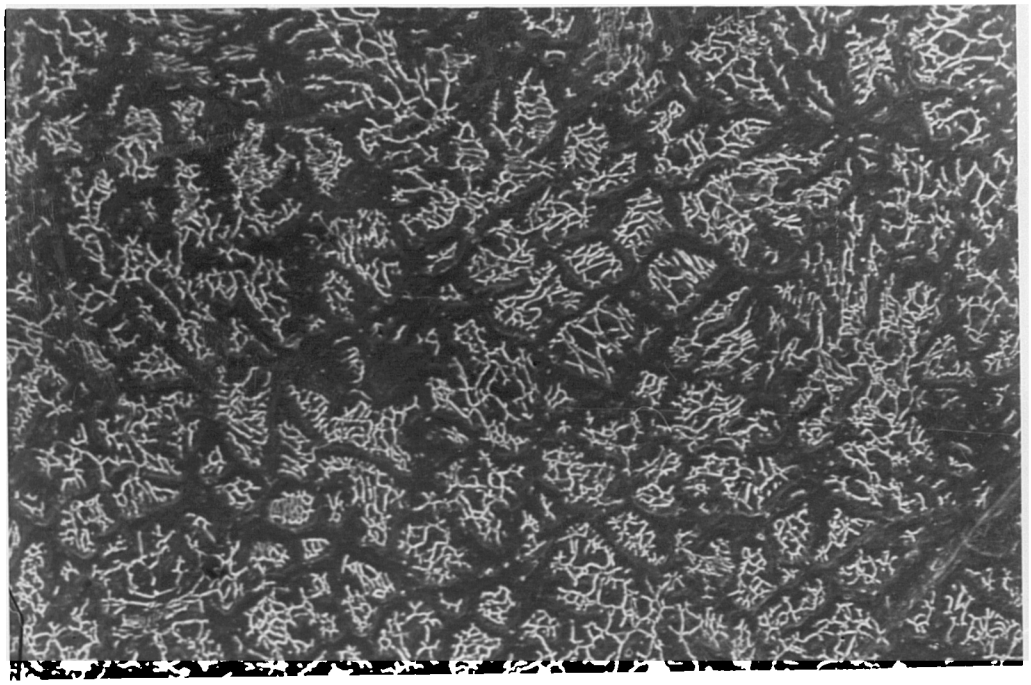

(a)

40 µm

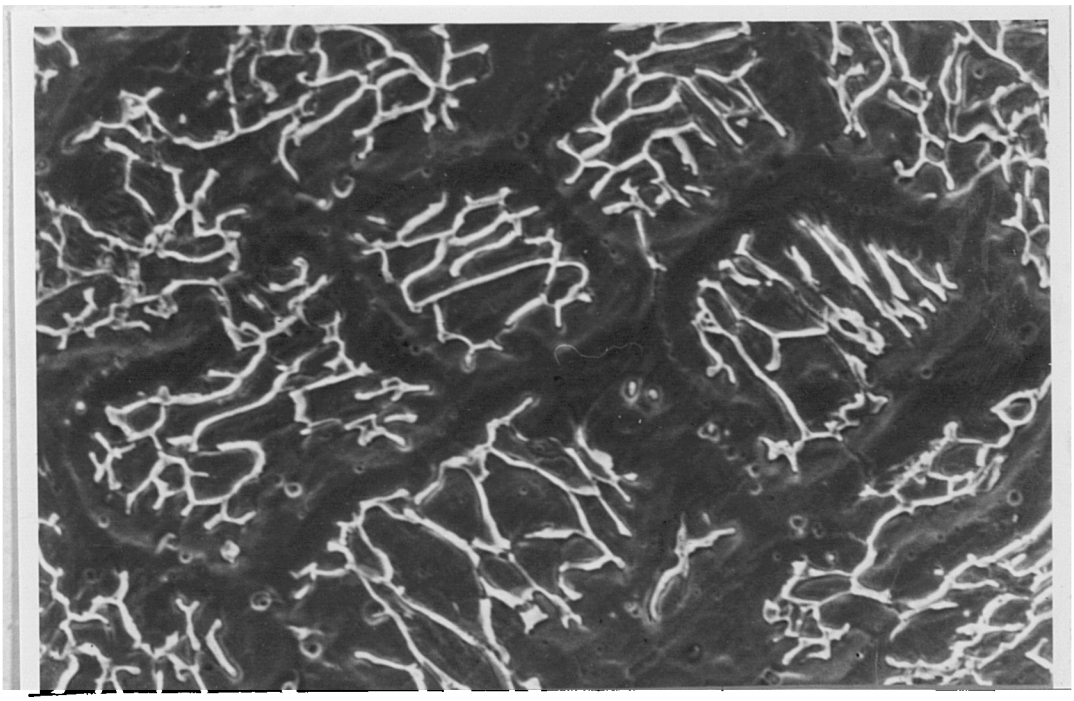

(b)

10 µm

Fig. 4.55 SEM micrograph of austenitic stainless steel AISI 316L Bead-on-Plate MIG weld (Sample T_3).

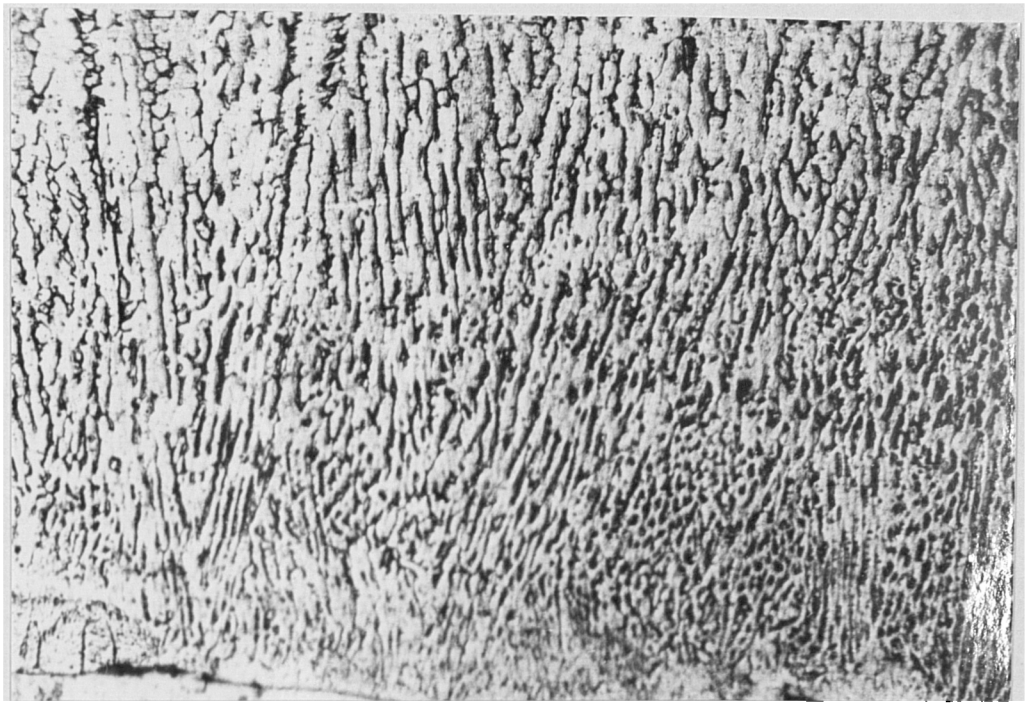

Fig.4.56 Optical micrograph of austenitic stainless steel AISI 316L. Bead-on-Plate MIG weld. Sample Z_3 - near fusion boundary.

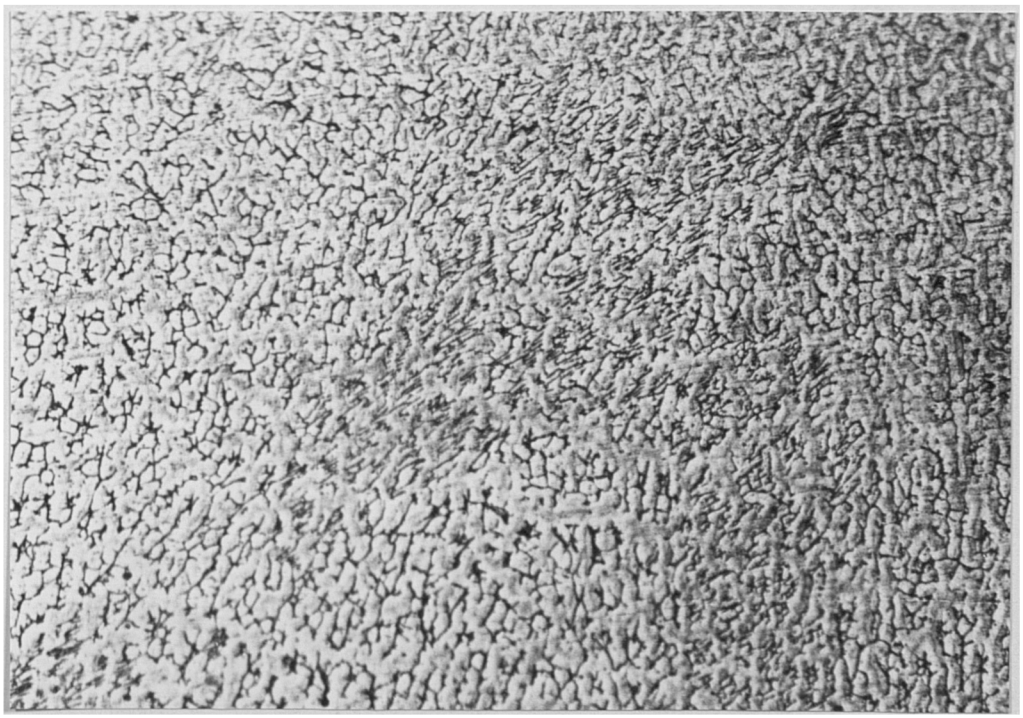

Fig.4.57 Optical micrograph of austenitic stainless steel AISI 316L Bead-on-Plate MIG weld sample Z_3 (towards the centre of weld).

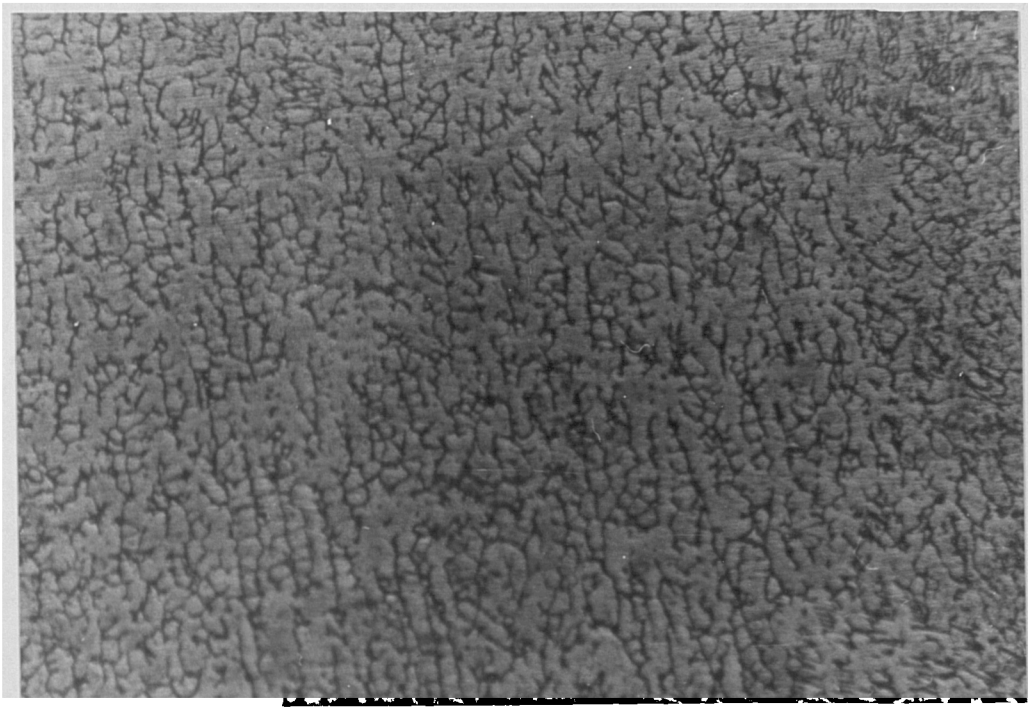

100μm

Fig.4.58 Optical micrograph of austenitic stainless steel AISI 316L Bead-on-Plate MIG weld. (Sample Z_3).

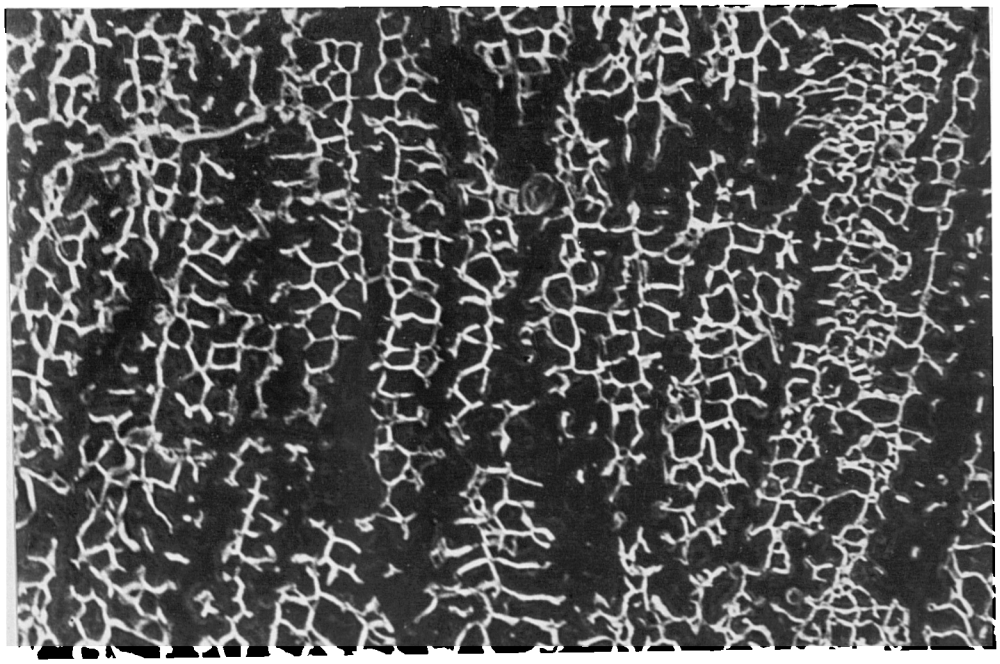

(a)

22µm

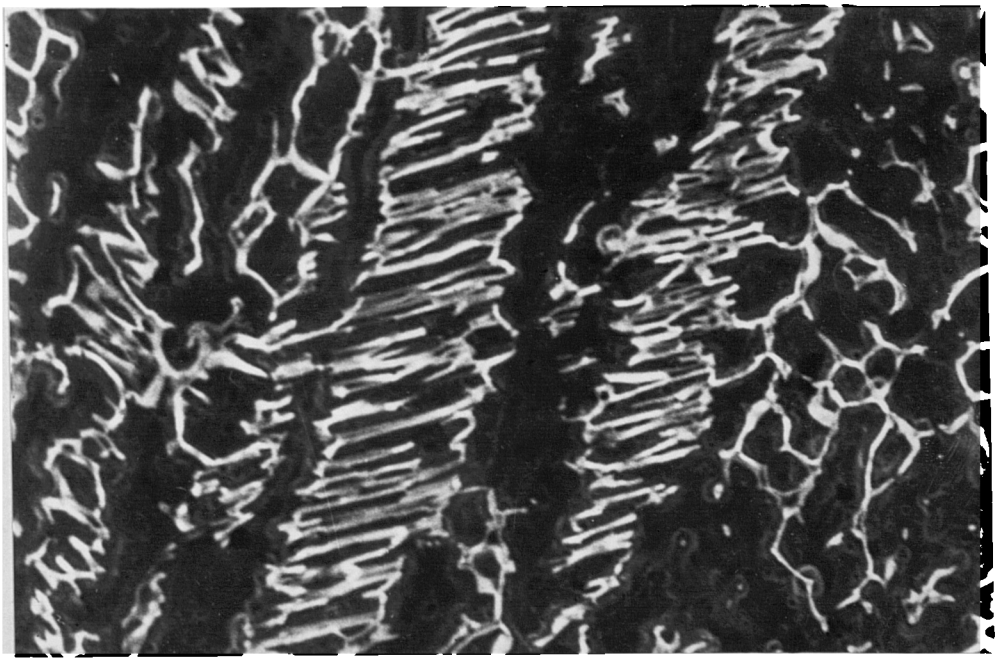

(b)

11µm

Fig.4.59 SEM micrograph of austenitic stainless steel AISI 316L Bead-on-Plate MIG weld (Sample X_2).

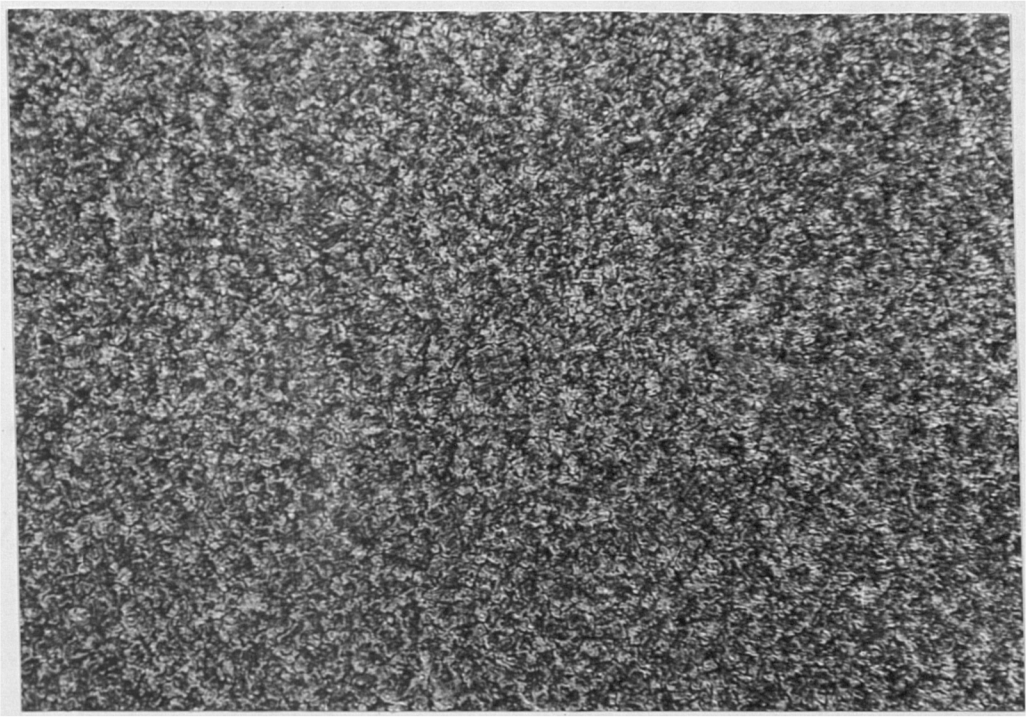

1000µm

Fig.4.60 Low magnification optical micrograph of austenitic stainless steel AISI 321 Bead-on-Plate MIG weld. (Sample K) . Original magnification X20, enlarged in reproduction.

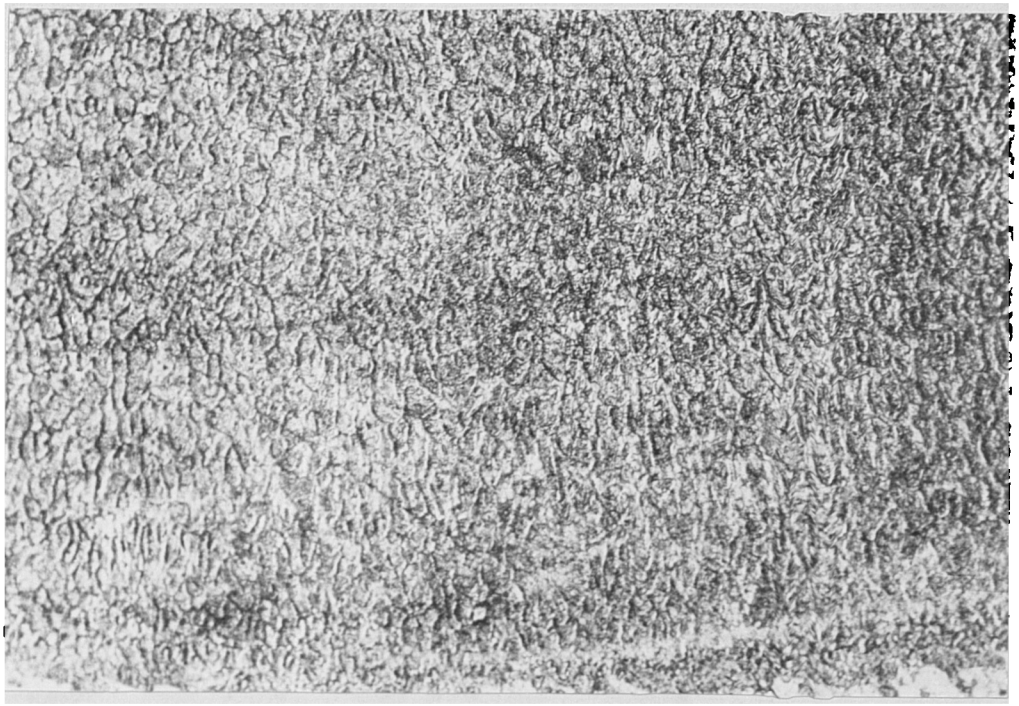

(a)

200µm

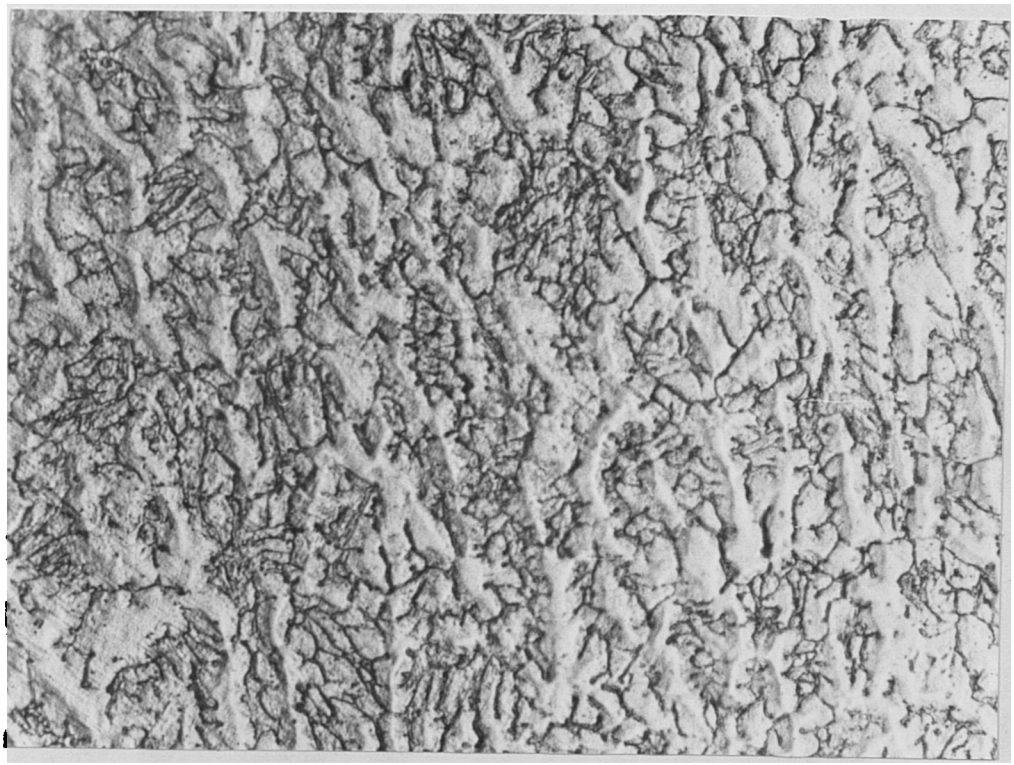

(b)

50µm

Fig.4.61 Optical micrographs of austenitic stainless steel AISI 321 Bead-on-Plate MIG weld. Sample K

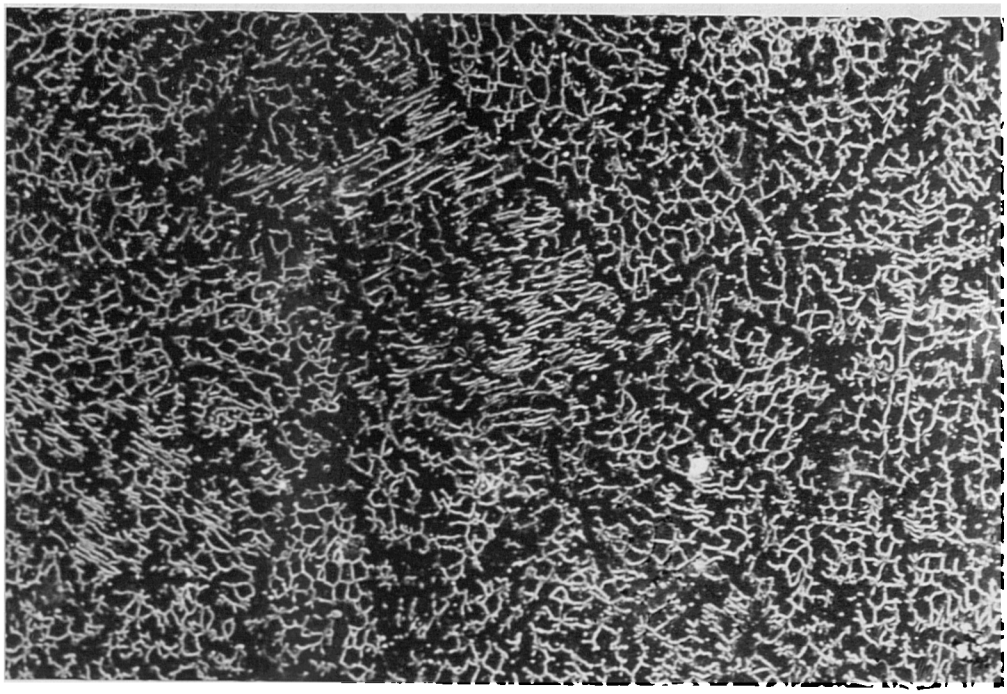

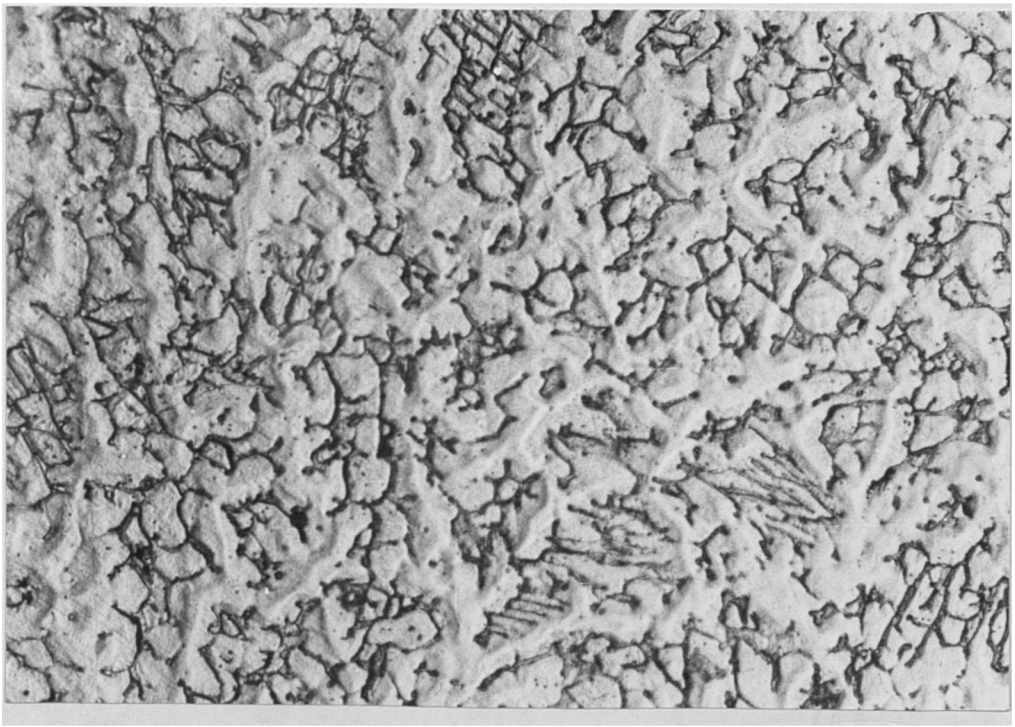

Fig.4.62 (a) SEM micrograph of austenitic stainless steel AISI 321 Bead-on-Plate weld. Sample K (Note: ferrite appears as white phase - austenite black).
(b) Optical micrograph of sample K. (ferrite appears black, austenite white)

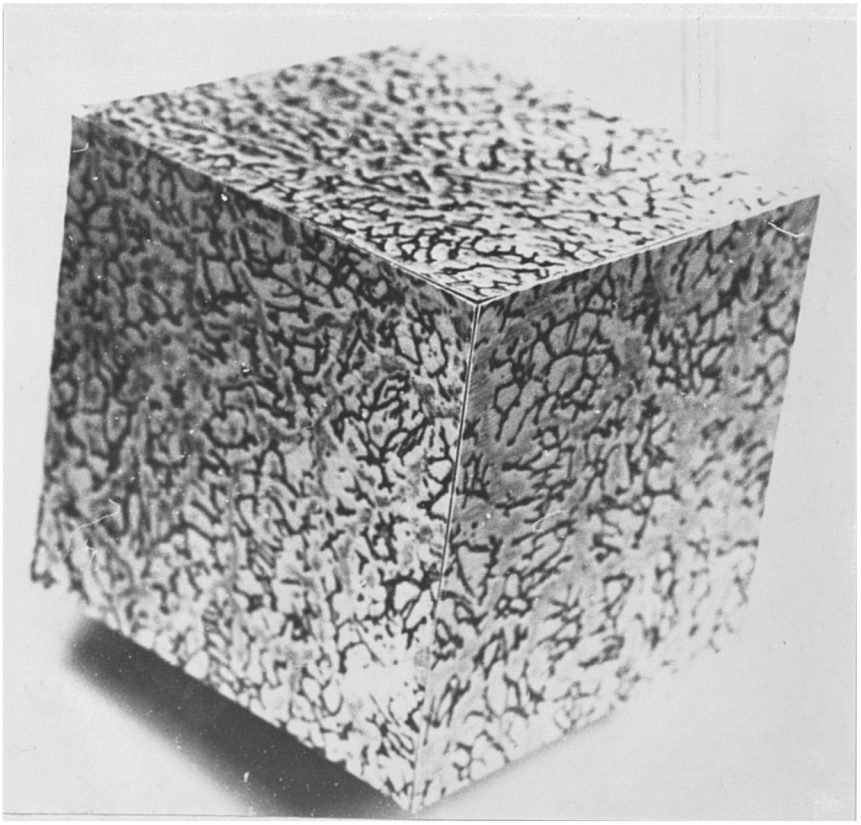

40μm

Fig.4.63 A three dimensional micrograph of austenitic stainless steel AISI 321 Bead-on-Plate MIG weld. (Sample K_3) Original magnification X500, reduced in reproduction.

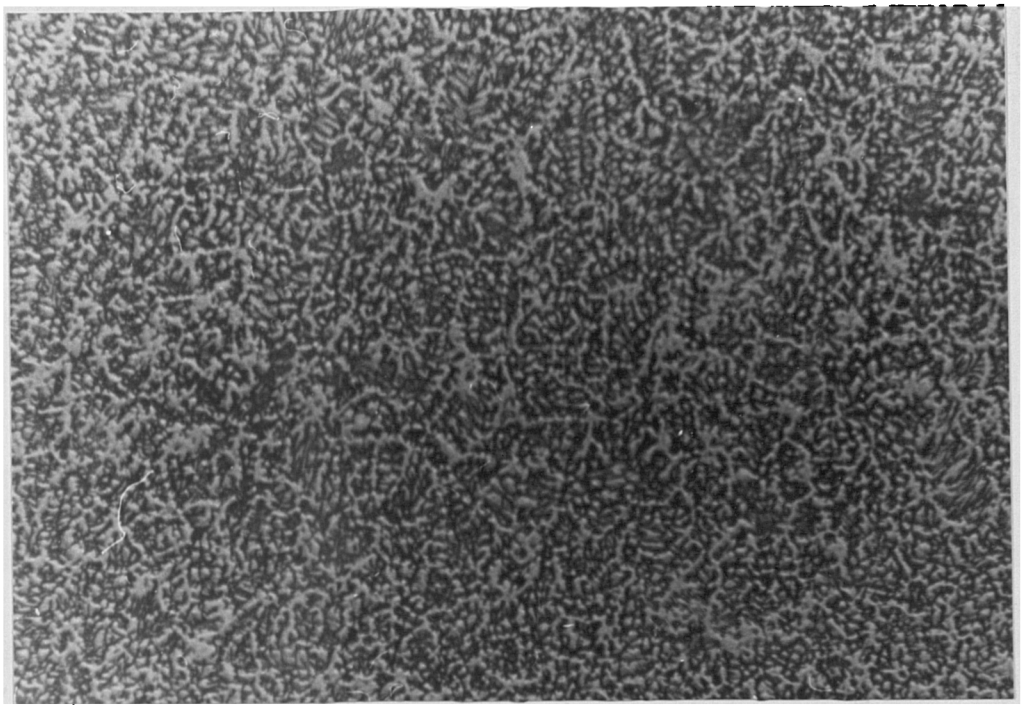

200µm

Fig.4.64 Optical micrograph of austenitic stainless steel AISI 321 Bead-on-Plate MIG weld. Sample 3F.

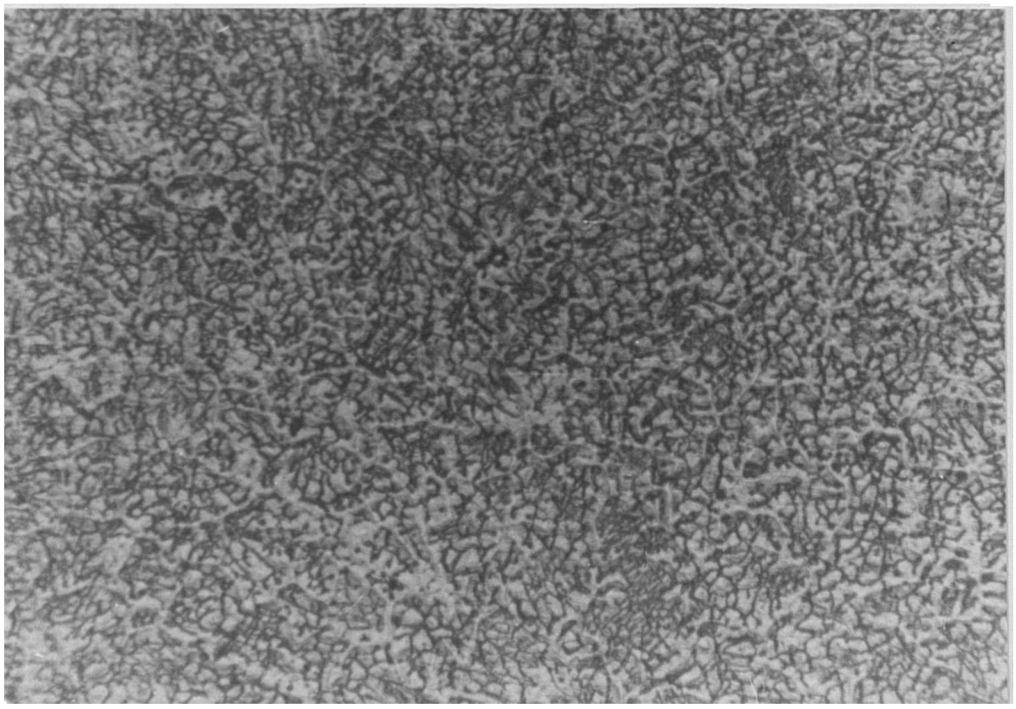

200µm

Fig.4.65 Optical micrograph of austenitic stainless steel AISI 321 Bead-on-Plate MIG weld. Sample 3E.

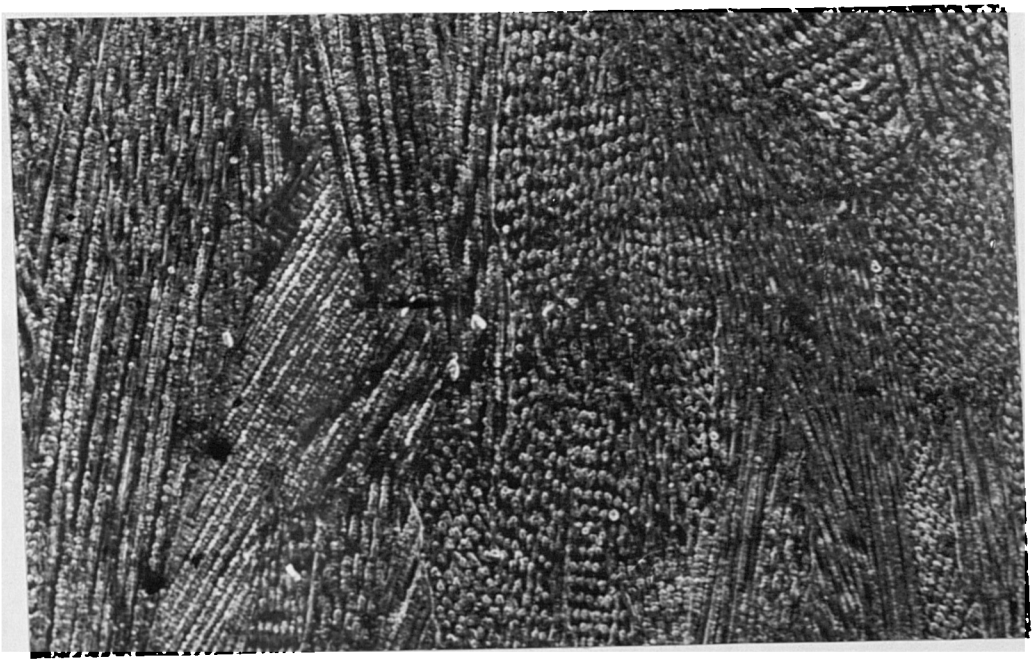

Fig.4.66 SEM micrograph of austenitic stainless steel AISI 304 Bead-on-Plate MIG weld with austenitic type structure.

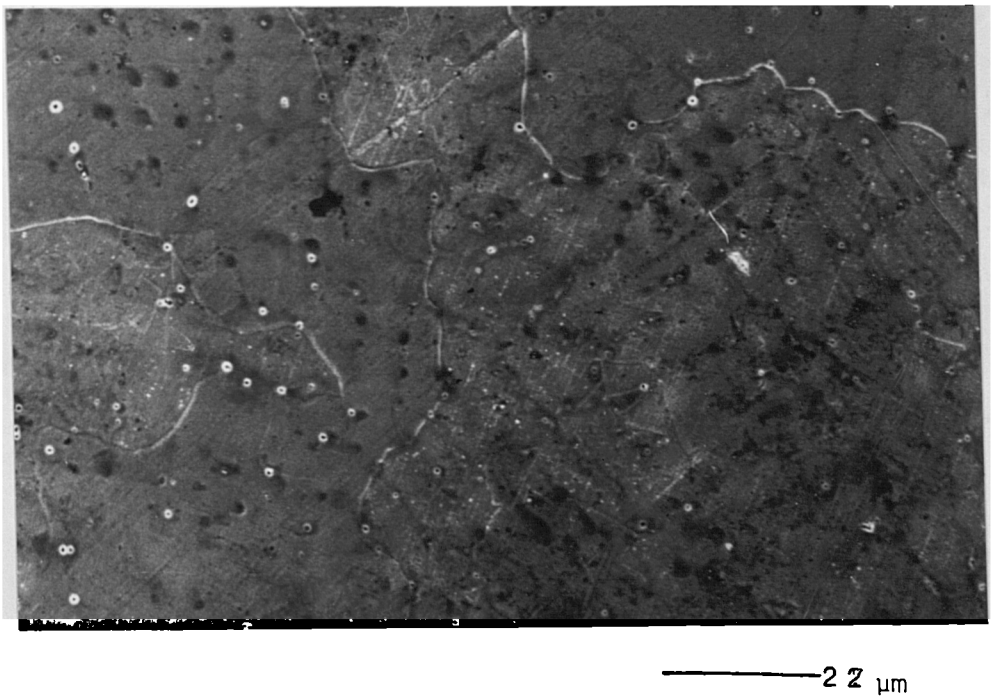

Fig.4.67 SEM micrograph of austenitic stainless steel AISI 304 Bead-on-Plate MIG weld with austenitic type structure.

Fig.4.67 cont. Optical micrograph of austenitic stainless steel AISI 304 Bead-on-plate MIG weld with austenitic type structure.

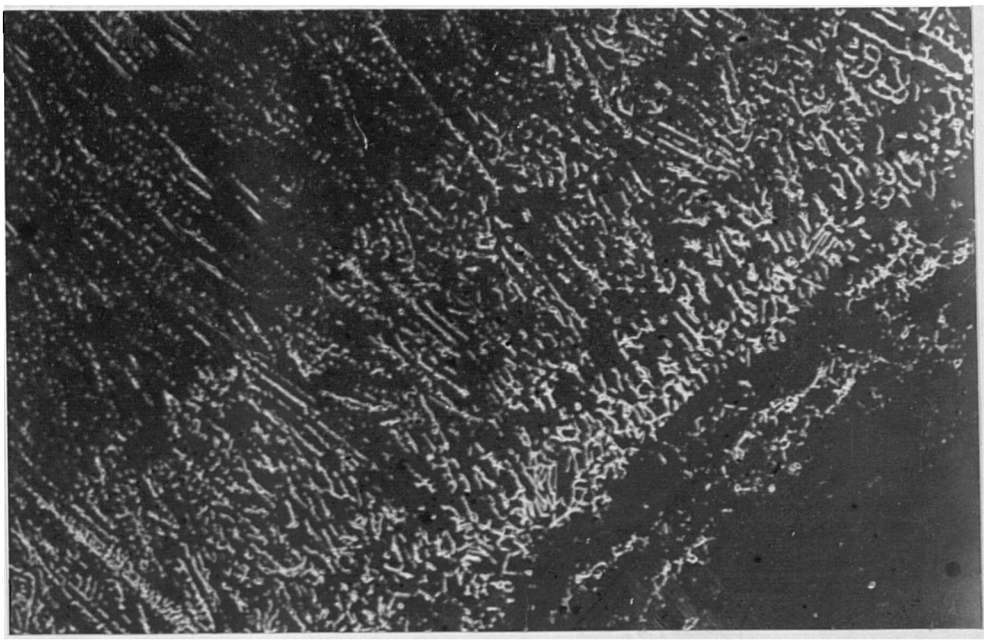

Fig.4.68 SEM micrograph of austenitic stainless steel AISI 321 Bead-on-Plate MIG weld with austenitic type structure (near fusion boundary). Sample L10.

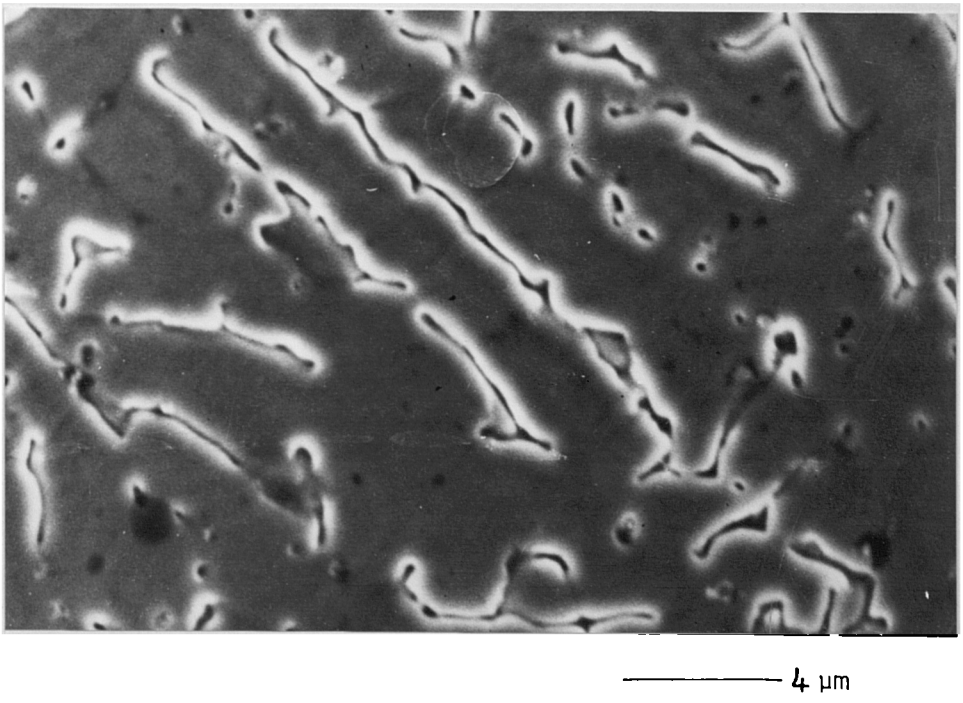

Fig.4.69 (a) SEM micrograph of austenitic stainless steel AISI 321 Bead-on-Plate MIG weld with austenitic type structure. Sample L10.

(b) 4μm

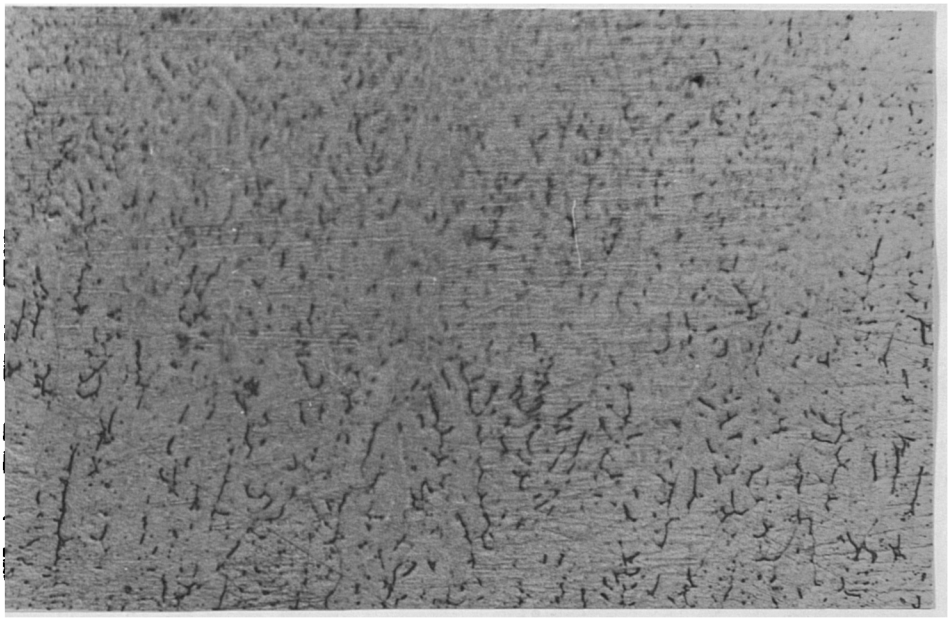

(c) 100μm

Fig.4.69 cont. Microstructure of austenitic stainless steel AISI 321 Bead-on-plate MIG weld with austenitic type structure.

Sample L10

(b) SEM micrograph (c) Optical micrograph

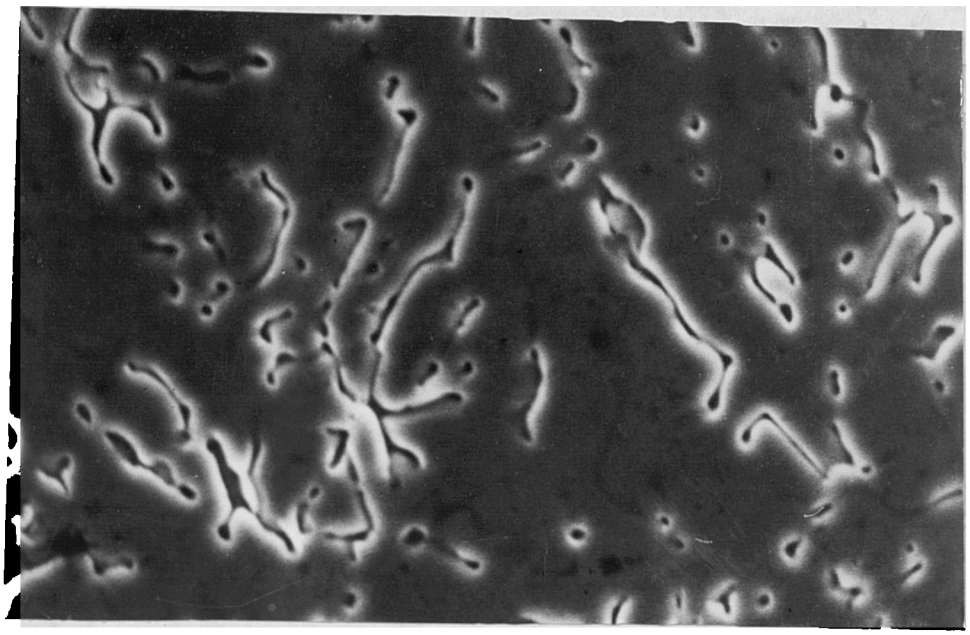

(a)

4µm

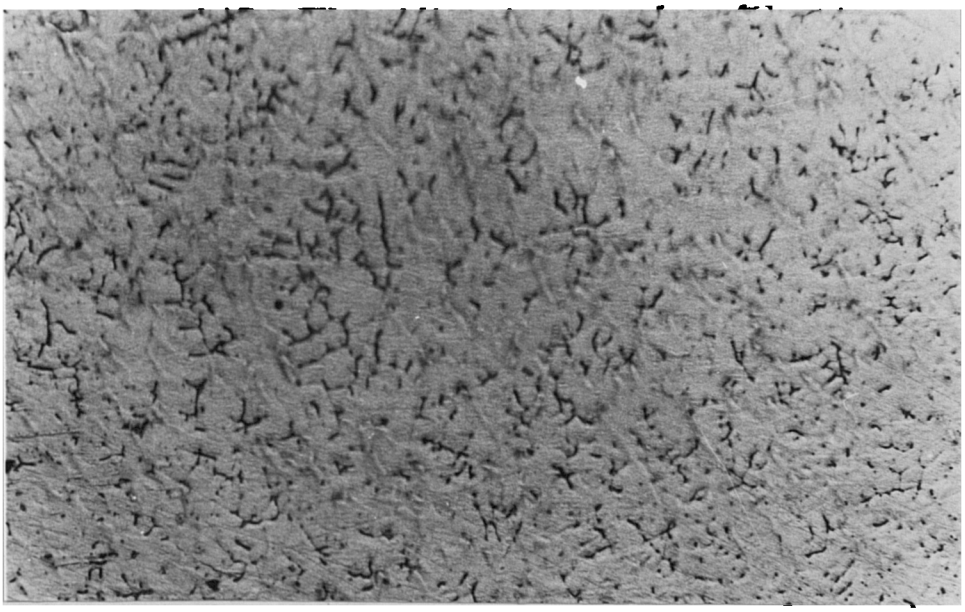

(b)

100µm

Fig.4.70. Microstructure of austenitic stainless steel AISI 321
Bead-on-plate MIG weld with austenitic structure.

(a) SEM micrograph (b) Optical micrograph

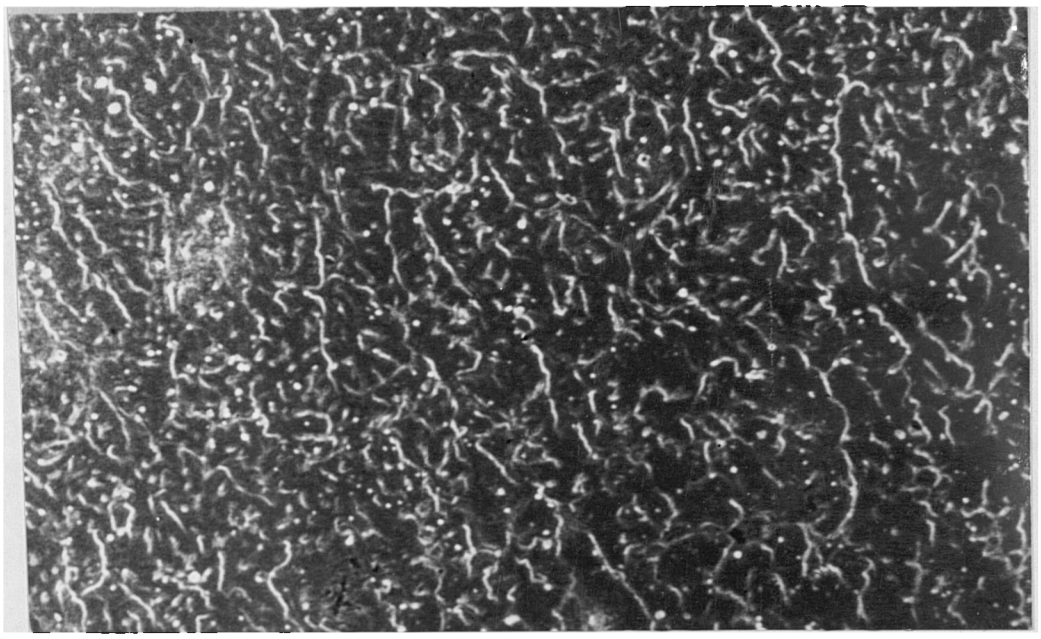

(a) 20µm

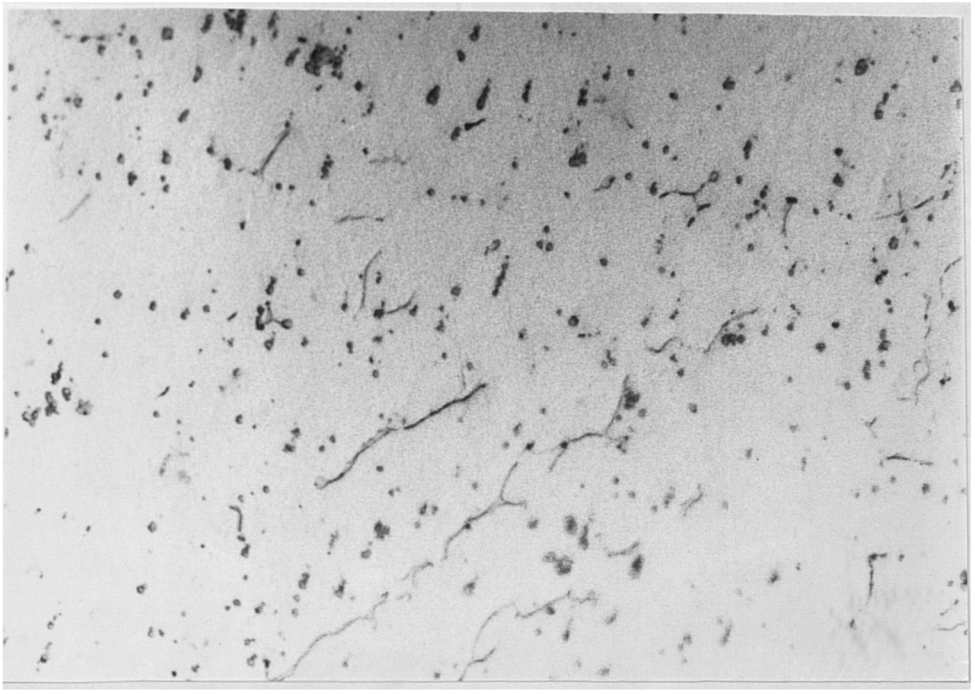

(b) 3.7µm

Fig. 4.71. Microstructure of austenitic stainless steel AISI 316L
Bead-on-plate MIG weld with austenitic type structure
(a) SEM micrograph (b) optical micrograph

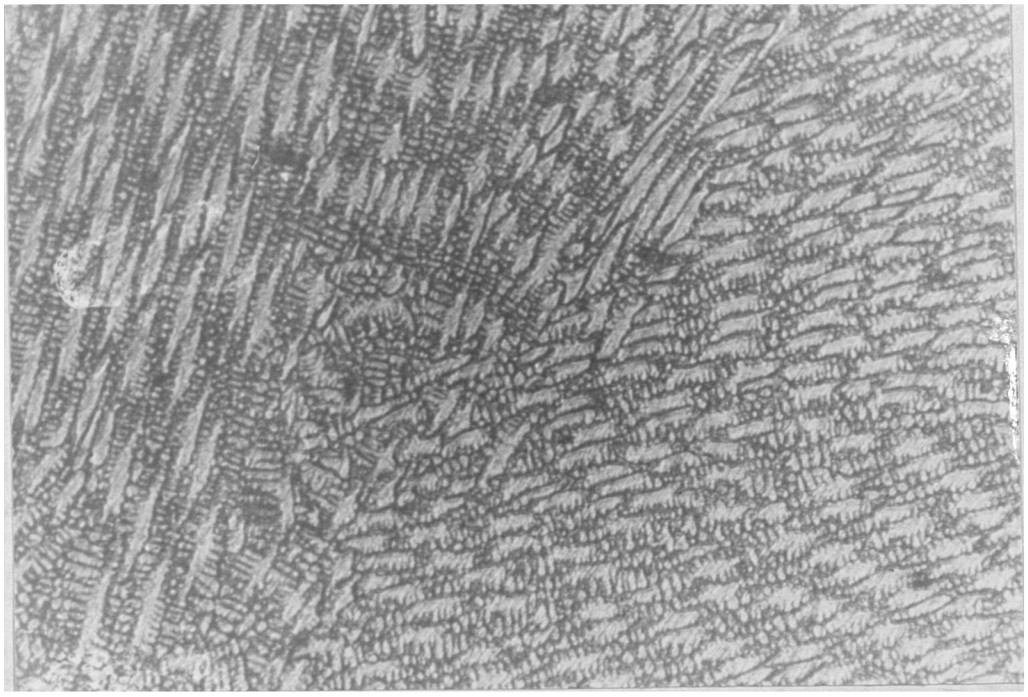

200µm

Fig.4.72. Optical micrograph of submerged Arc Butt weld prepared on austenitic stainless steel AISI 316 parent plates.

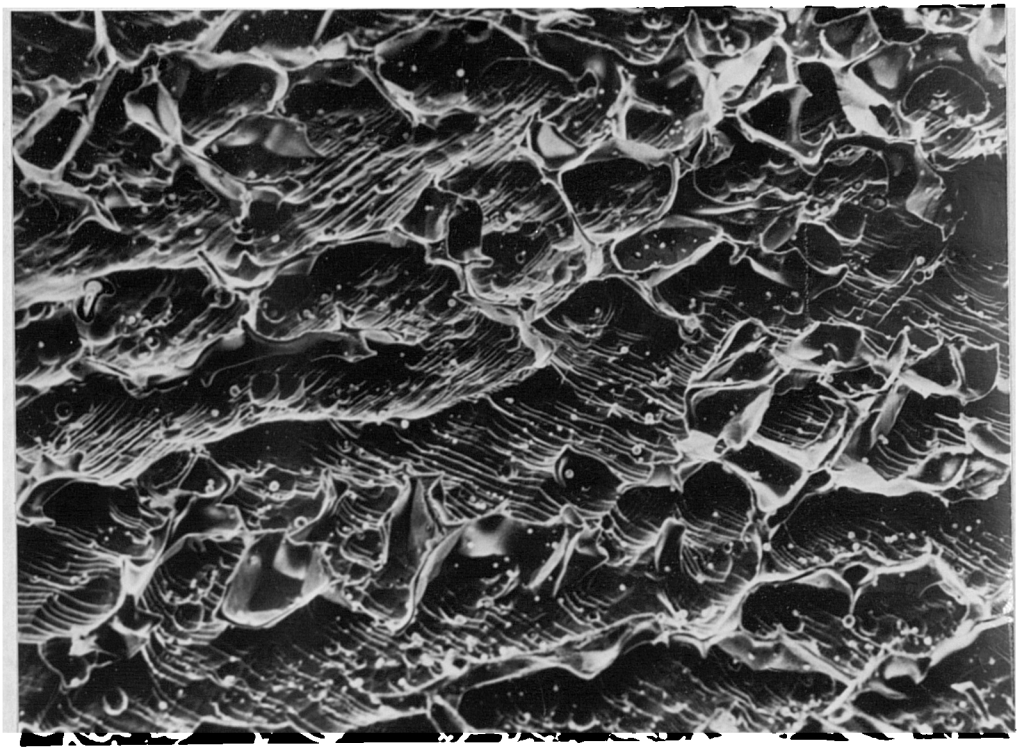

20µm

Fig.4.73 SEM micrograph austenitic stainless steel AISI 316L Submerged Arc Butt weld. Sample T13.

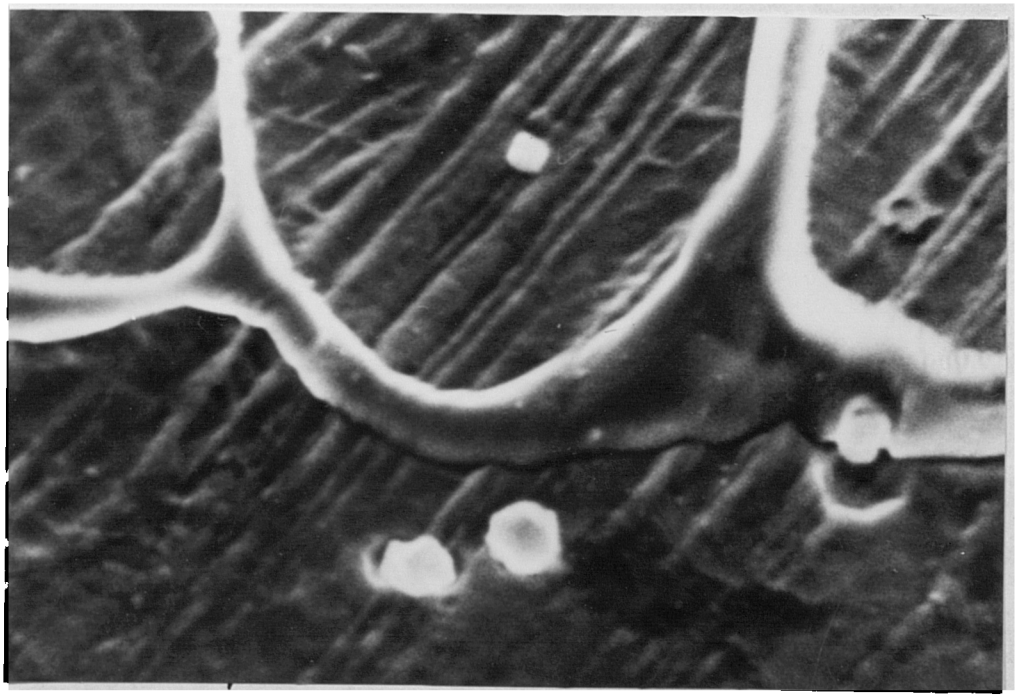

1.6µm

Fig.4.74 SEM micrograph austenitic stainless steel AISI 321 Submerged Arc Butt weld. Sample F2.

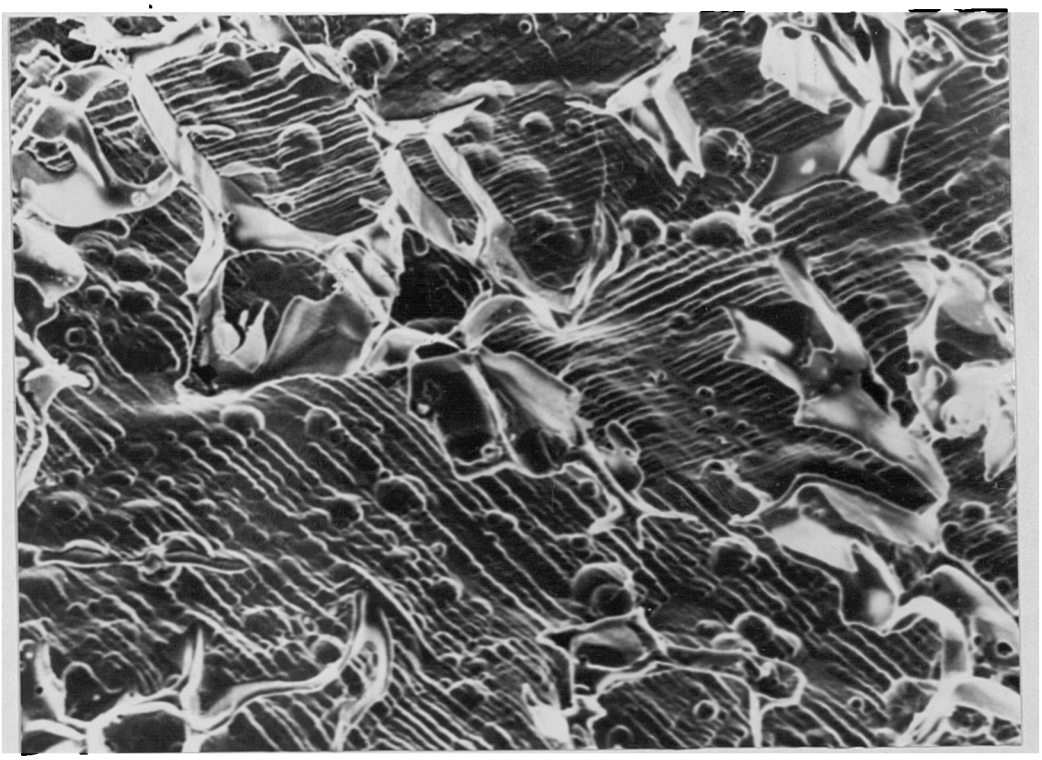

11.5µm

Fig.4.75 SEM micrograph of austenitic stainless steel AISI 316L Submerged Arc Butt weld. Sample U2.

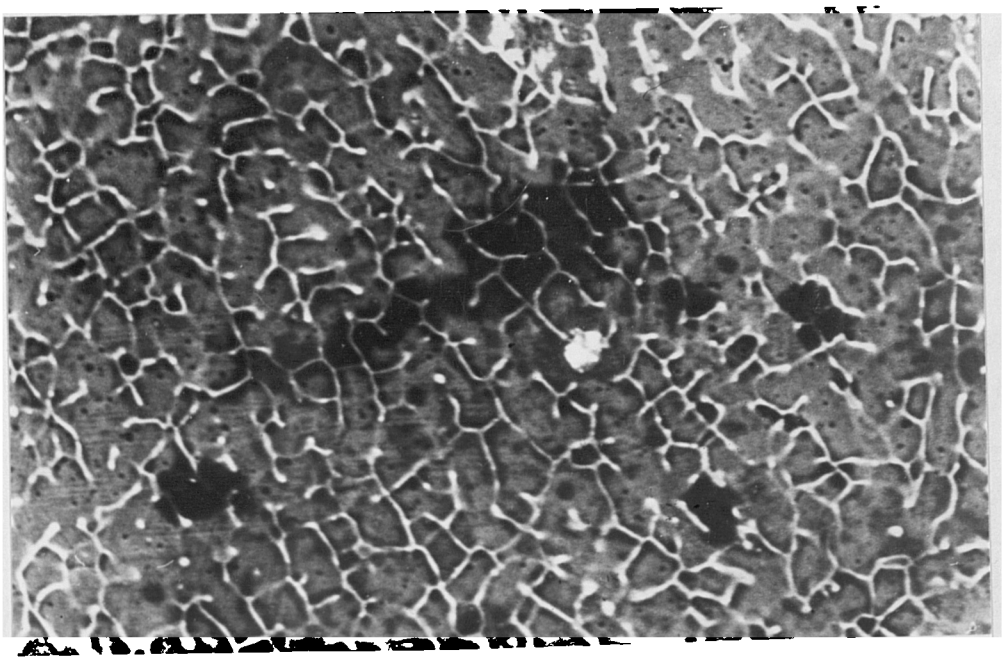

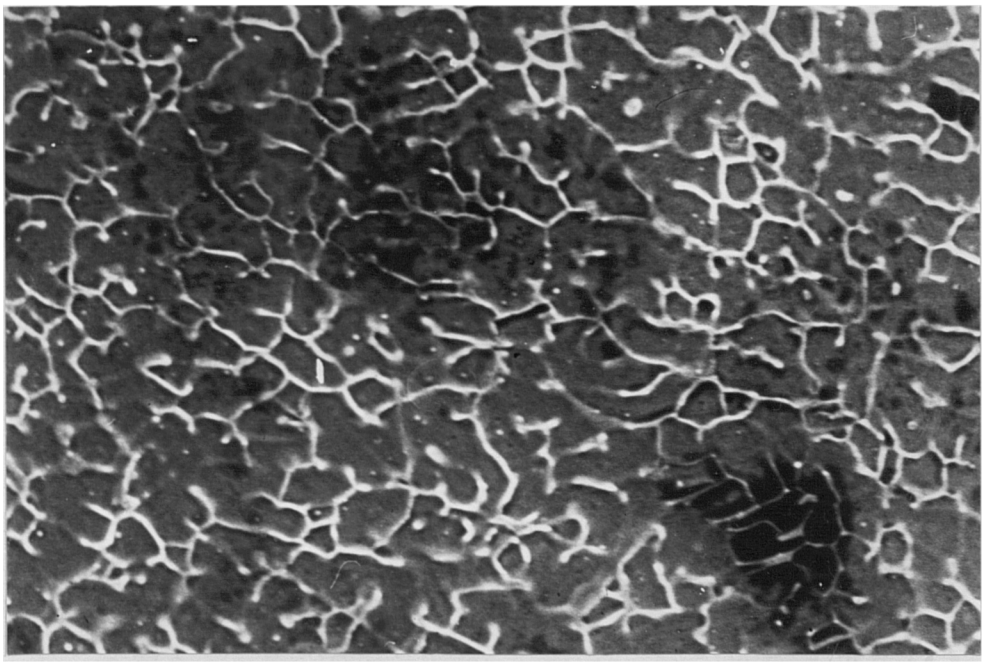

Fig.4.76 SEM micrograph of austenitic stainless steel AISI 316L Submerged Arc Butt weld. Sample V_3

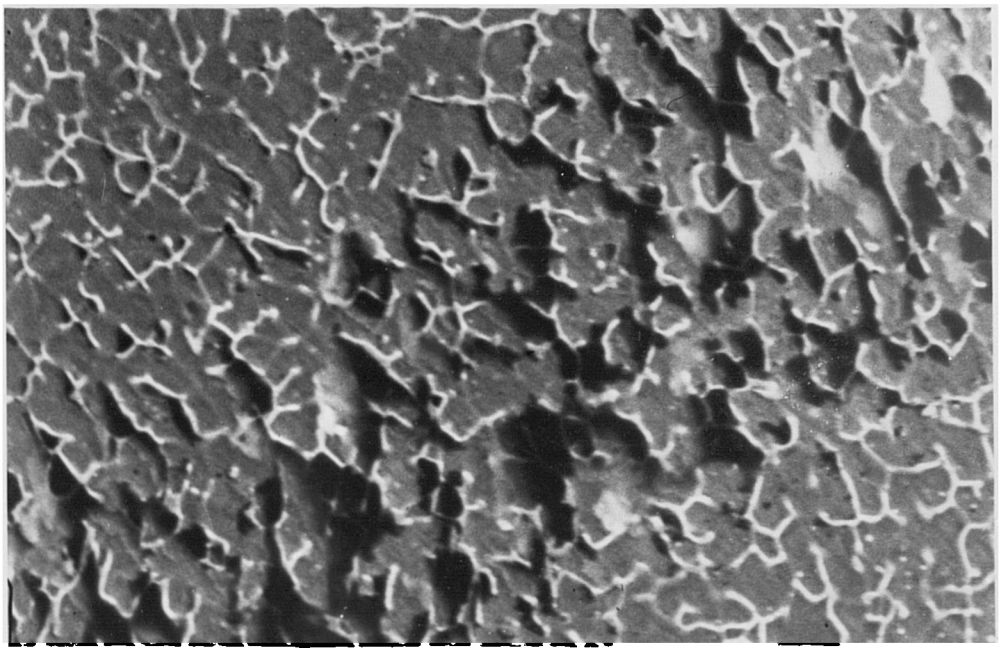

Fig.4.77 SEM micrograph austenitic stainless steel AISI 316L Submerged Arc Butt weld. Sample T_{13}

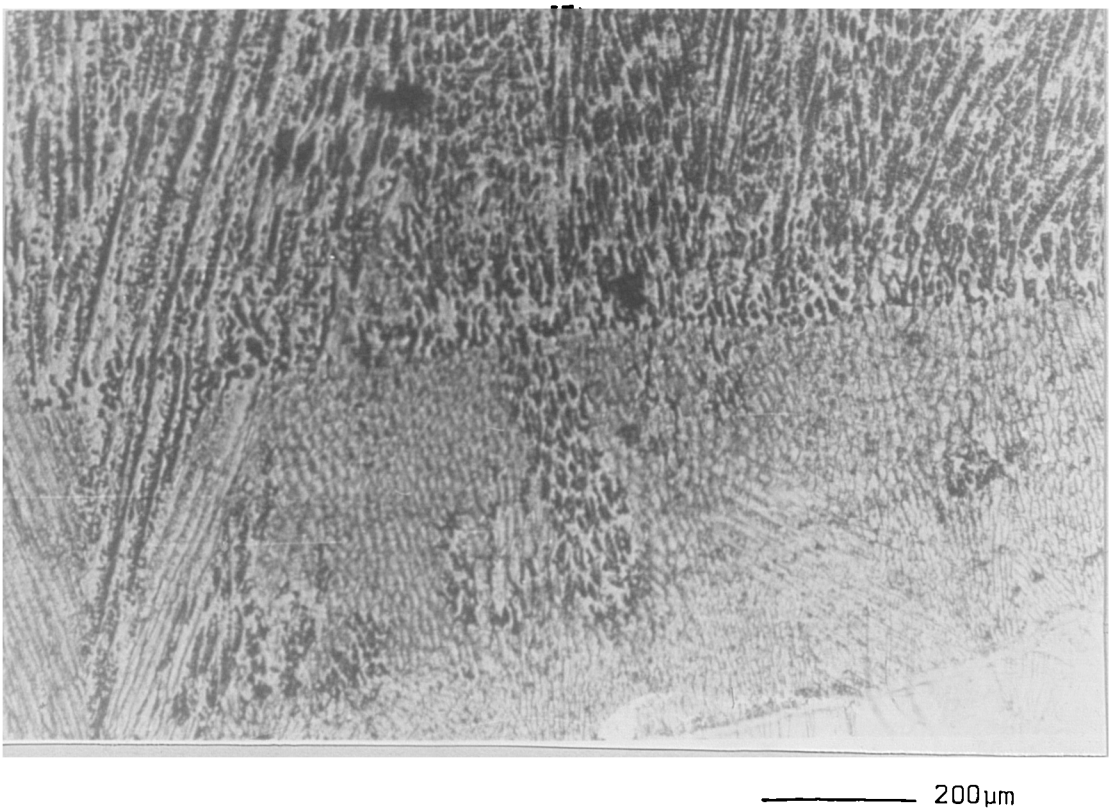

Fig.4.78 Optical micrograph of austenitic stainless steel AISI 316L Submerged Arc Butt weld from the fusion boundary region.

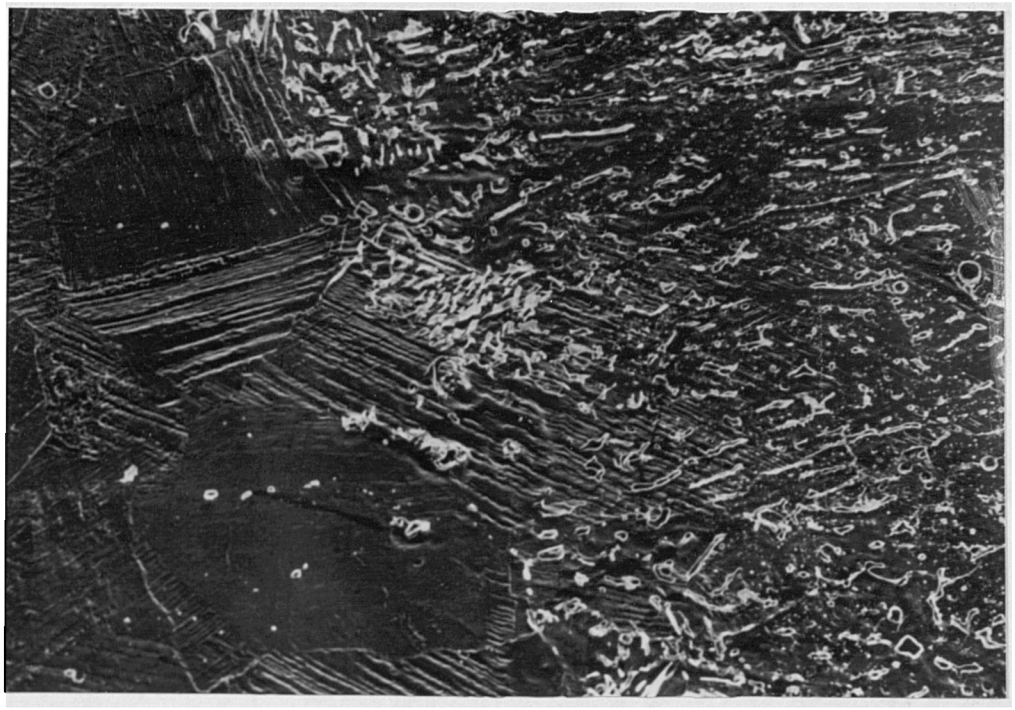

(a) ——— 27μm

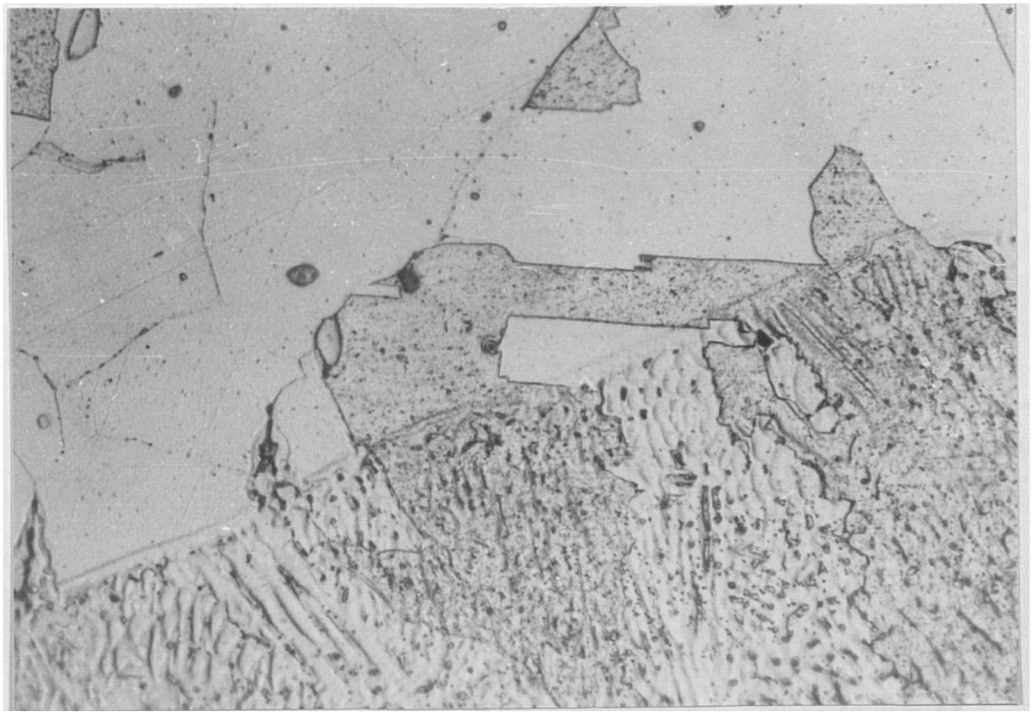

(b) ——— 50μm

Fig.4.79 Microstructure of fusion boundary region of Submerged Arc weld metal of different welds.

(a) SEM micrograph (b) Optical micrograph

(a)

100μm

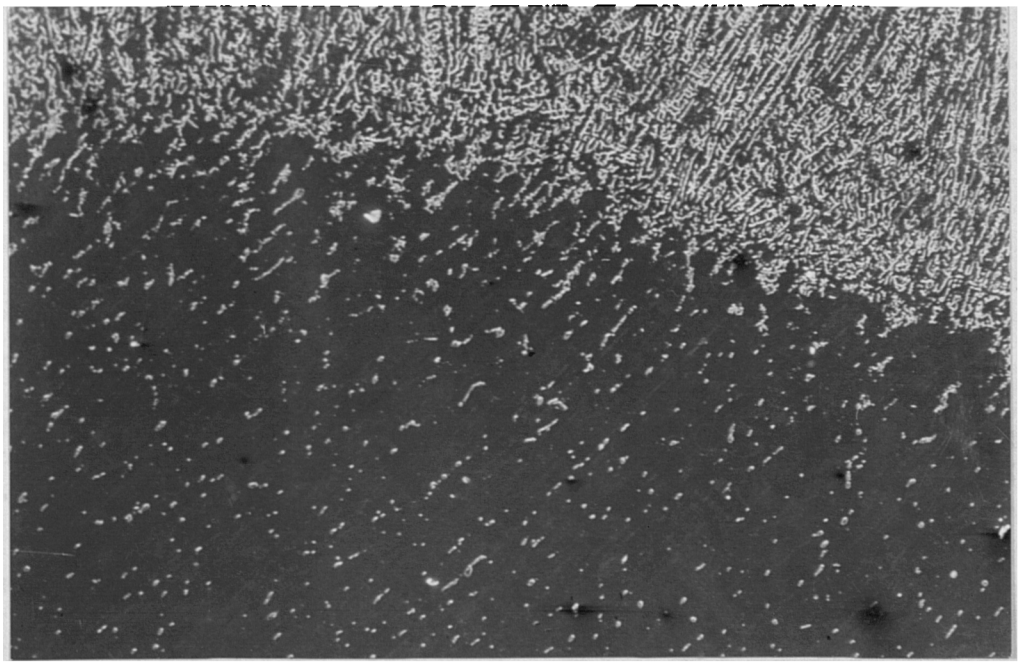

(b)

25 μm

Fig.4.80 Microstructure of fusion boundary region of different austenitic stainless steel weld metal.
(a) 321 austenitic stainless steel weld
(b) 316L austenitic stainless steel weld

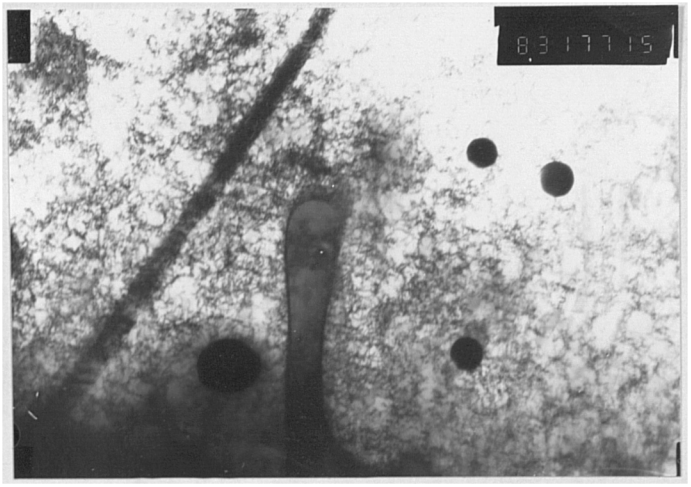

(a)

2.4µm

(b)

1.5µm

Fig.4.81 STEM micrograph of austenitic stainless steel AISI 316L Submerged Arc bead-on-plate weld. Sample 250

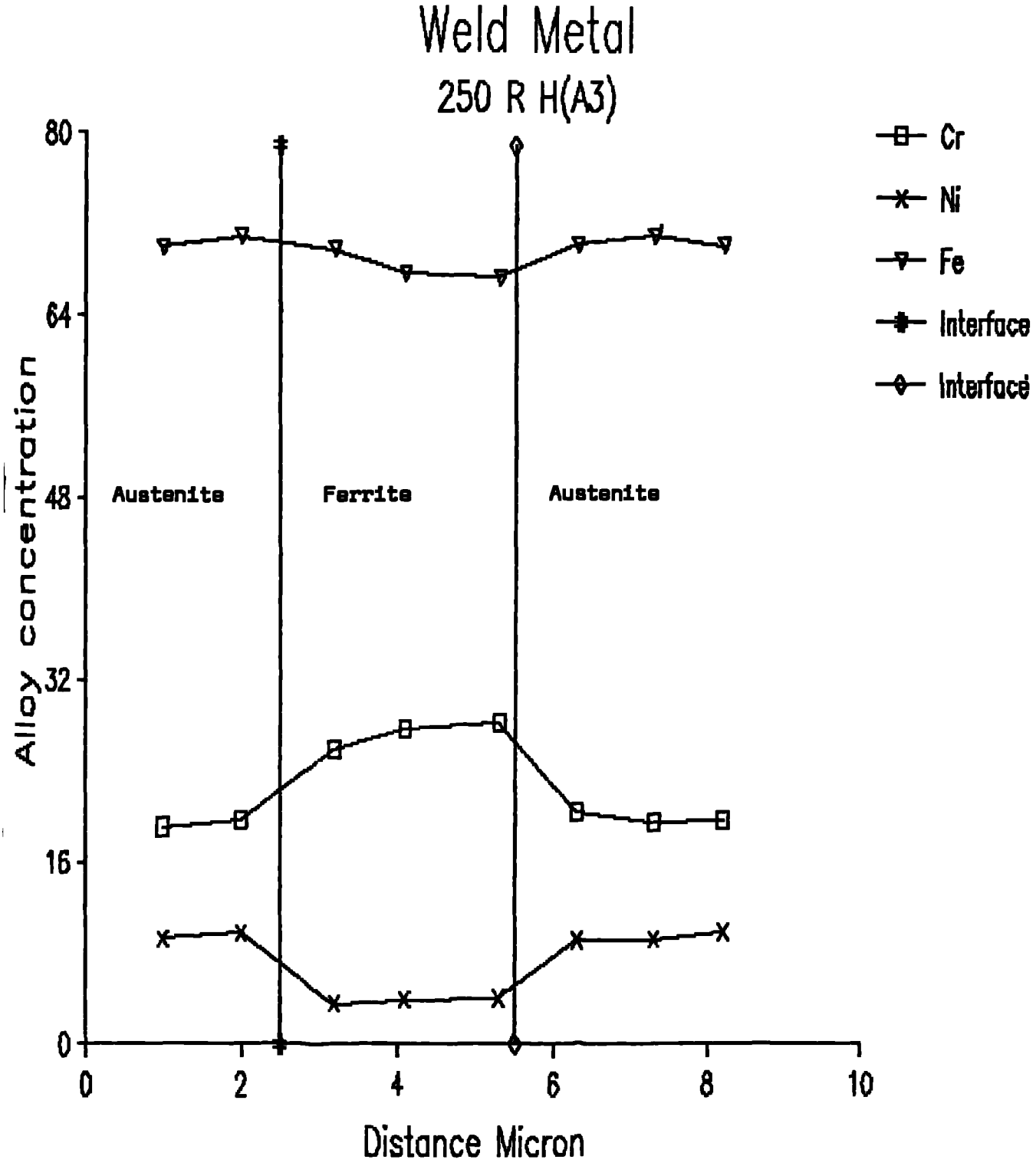

Fig.4.82(a) STEM spot analyses of Chromium Nickel and Iron traversing ferrite/austenite region.

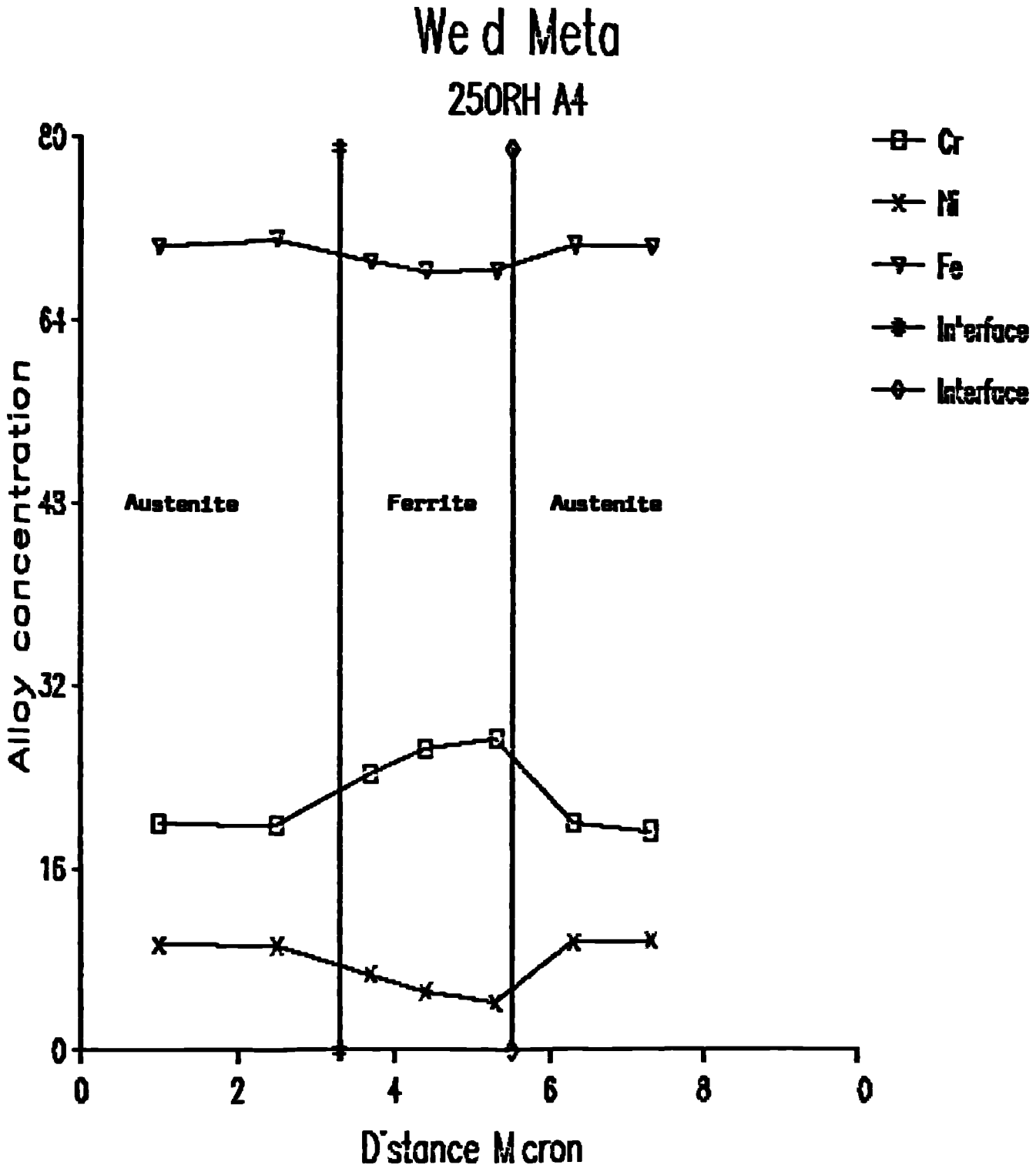

Fig.4.82(b) STEM spot analyses of Chromium Nickel and Iron traversing ferrite/austenite region.

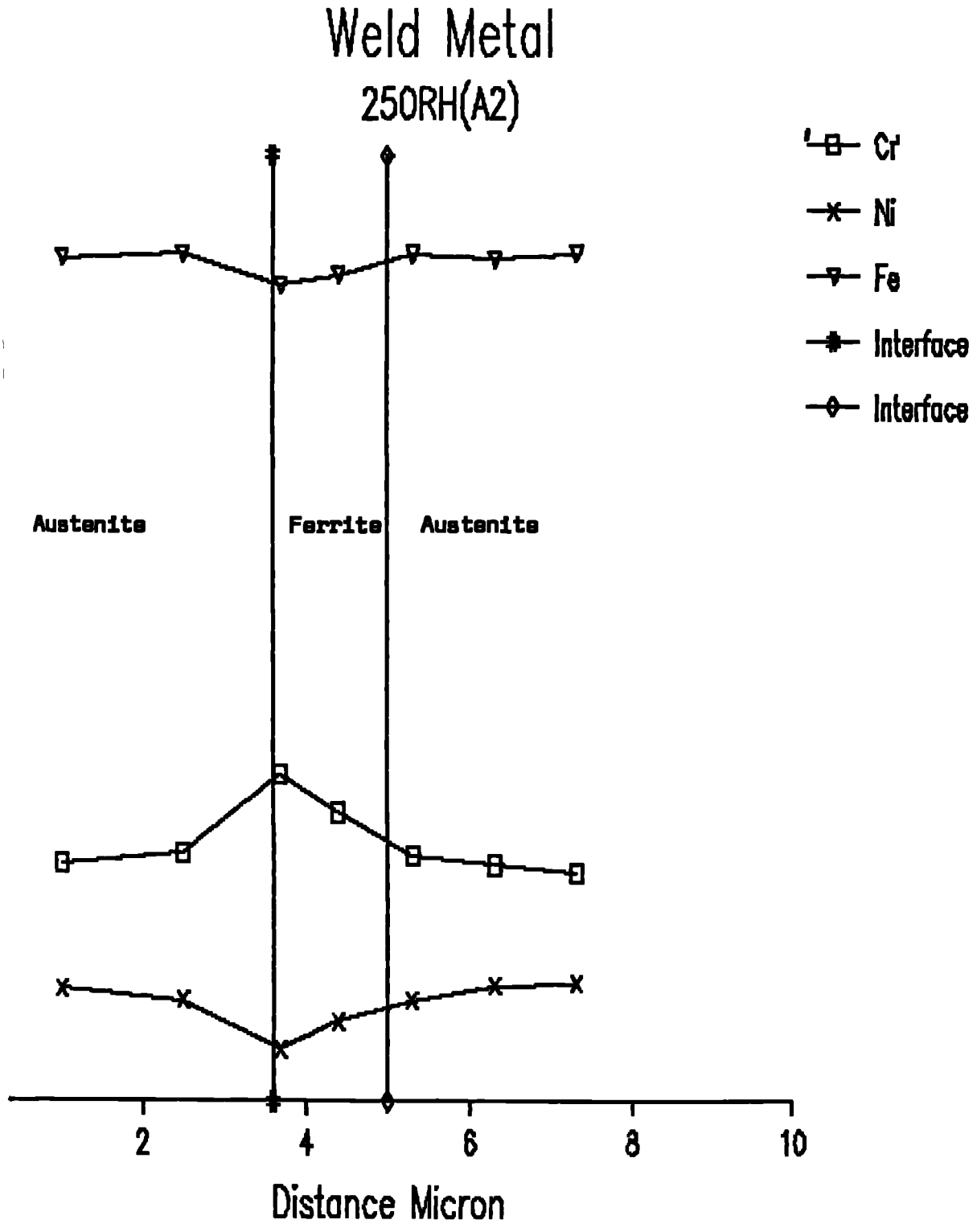

Fig.4.82(c) STEM spot analyses of Chromium Nickel and Iron traversing ferrite/austenite region.

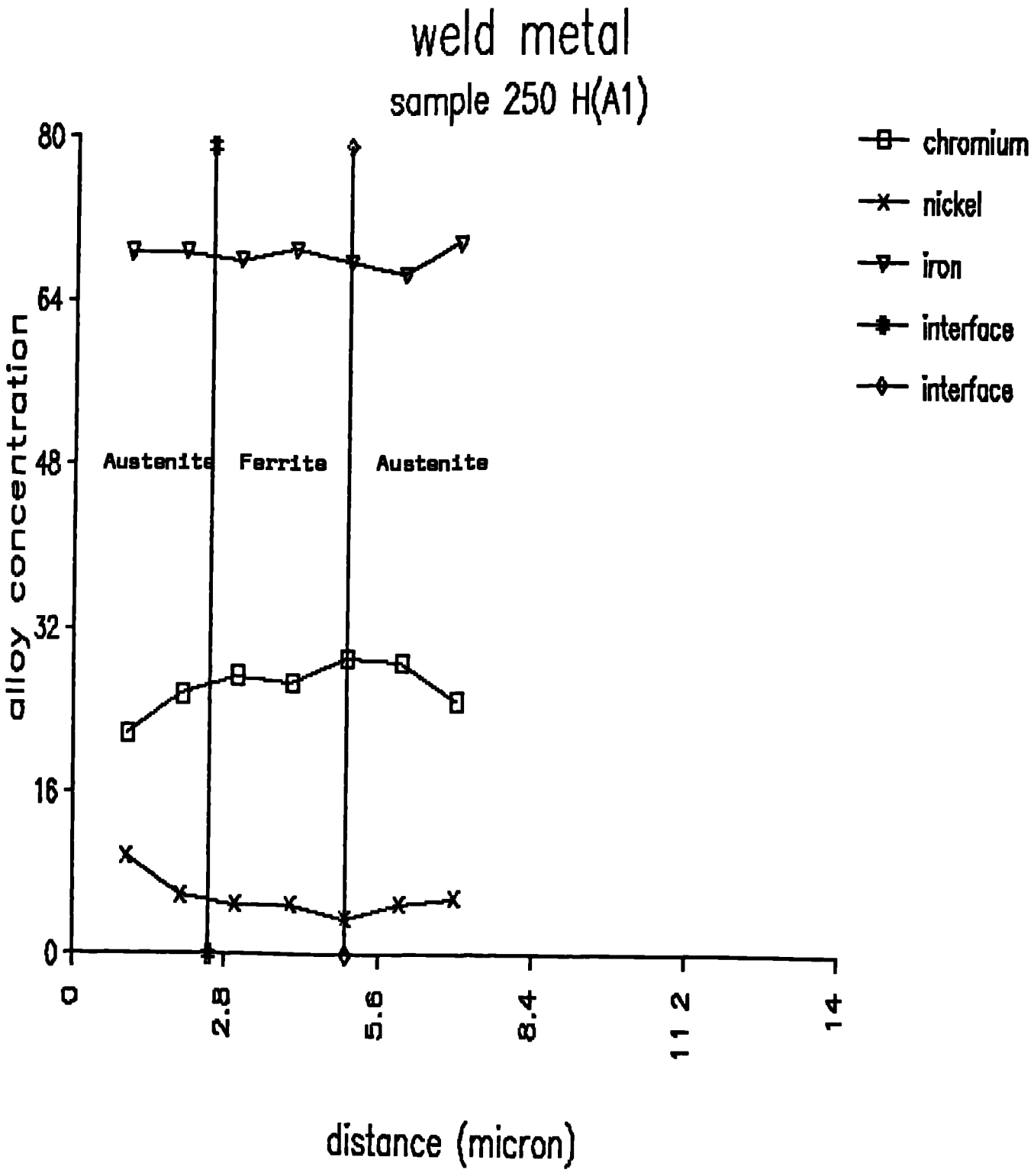

Fig.4.82(d) STEM spot analyses of Chromium Nickel and Iron traversing ferrite/austenite region.

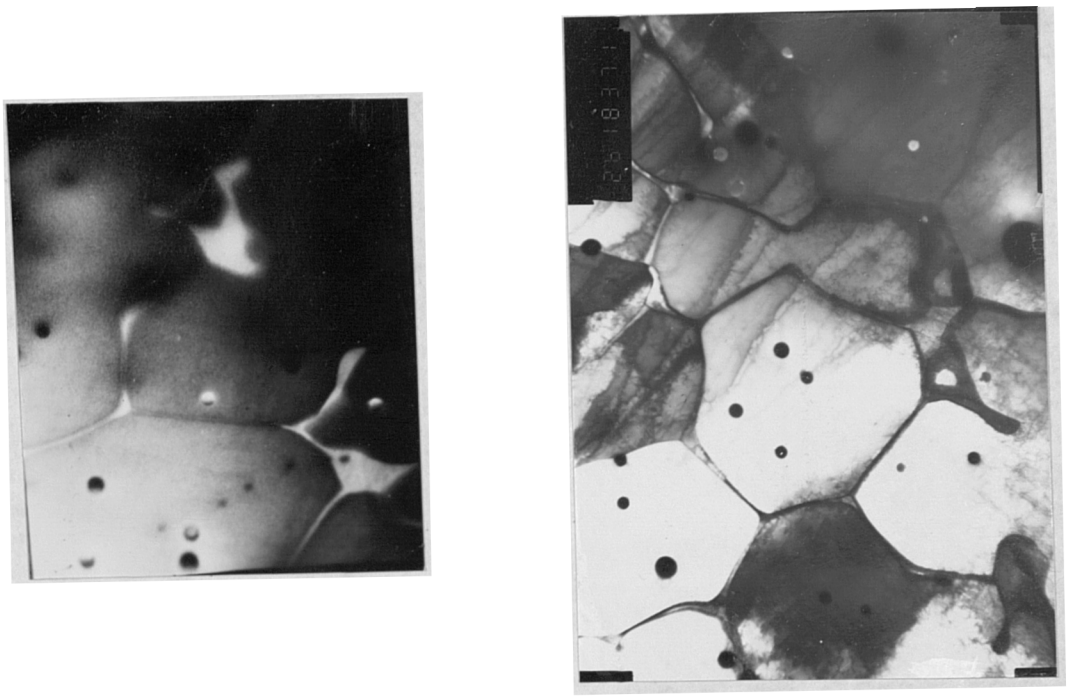

(a) 3.3µm (b) 7.7µm

Fig.4.83 STEM micrograph of austenitic stainless steel AISI 316L Submerged Arc Bead-on-plate weld (Sample 18FN)

(a) 2.7µm (b) 2.4µm

Fig.4.84 STEM micrograph of austenitic stainless steel AISI 316 Submerged Arc Bead-on-plate weld (Sample 18FN)

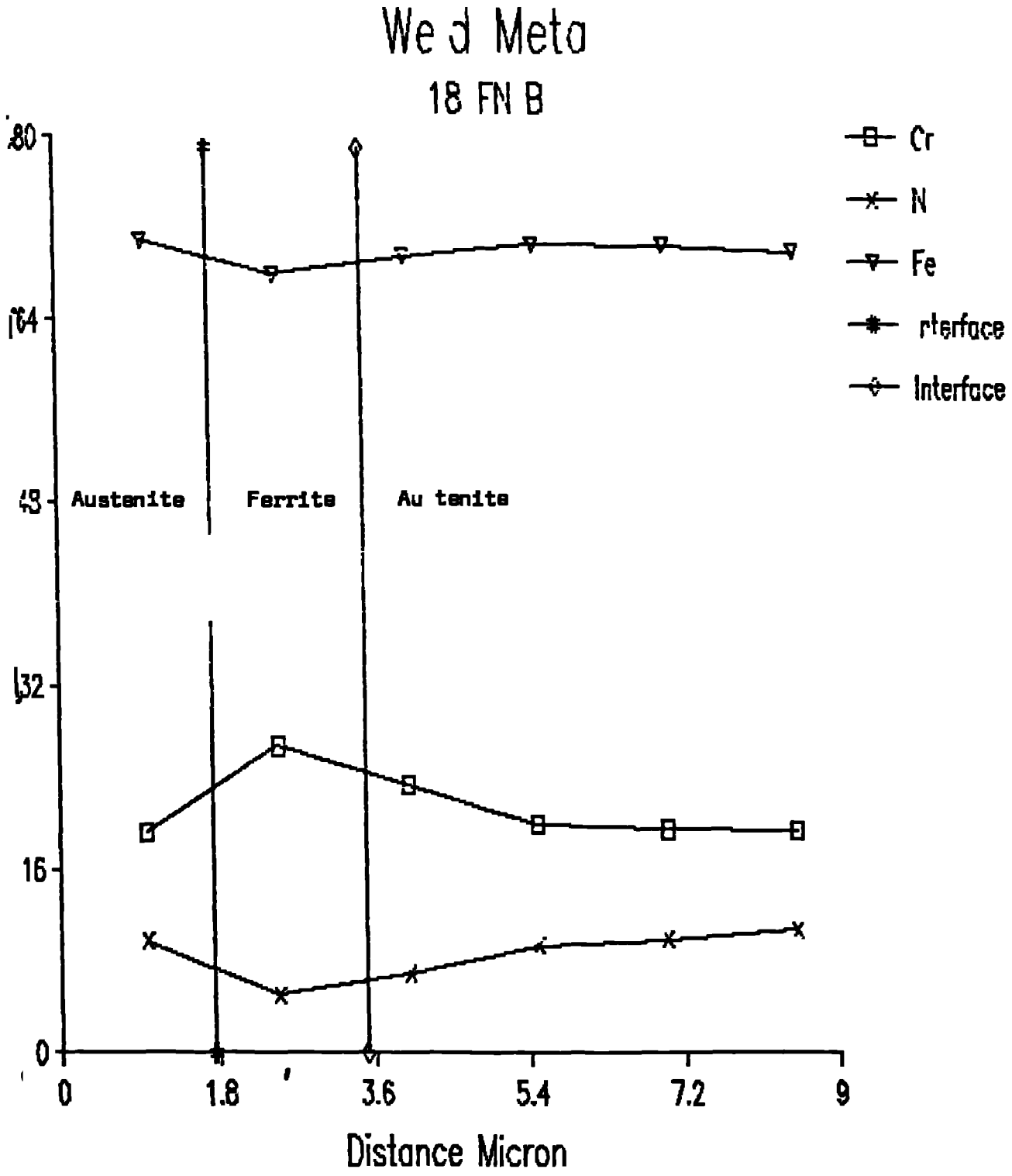

Fig.4.85(a) STEM spot analyses of Chromium Nickel and Iron traversing ferrite/austenite region.

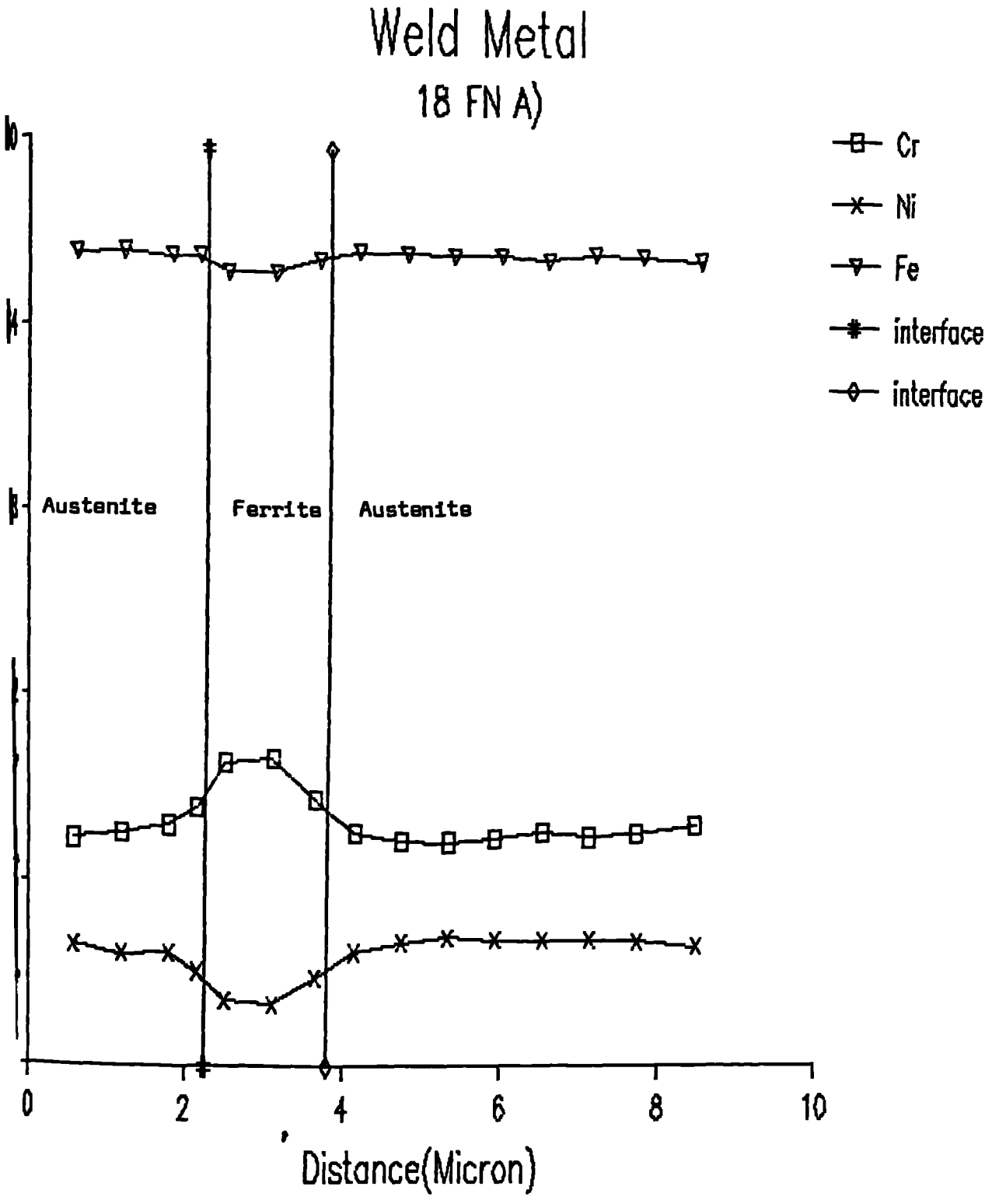

Fig.85(b) STEM spot analyses of Chromium Nickel and Iron traversing ferrite/austenite region.

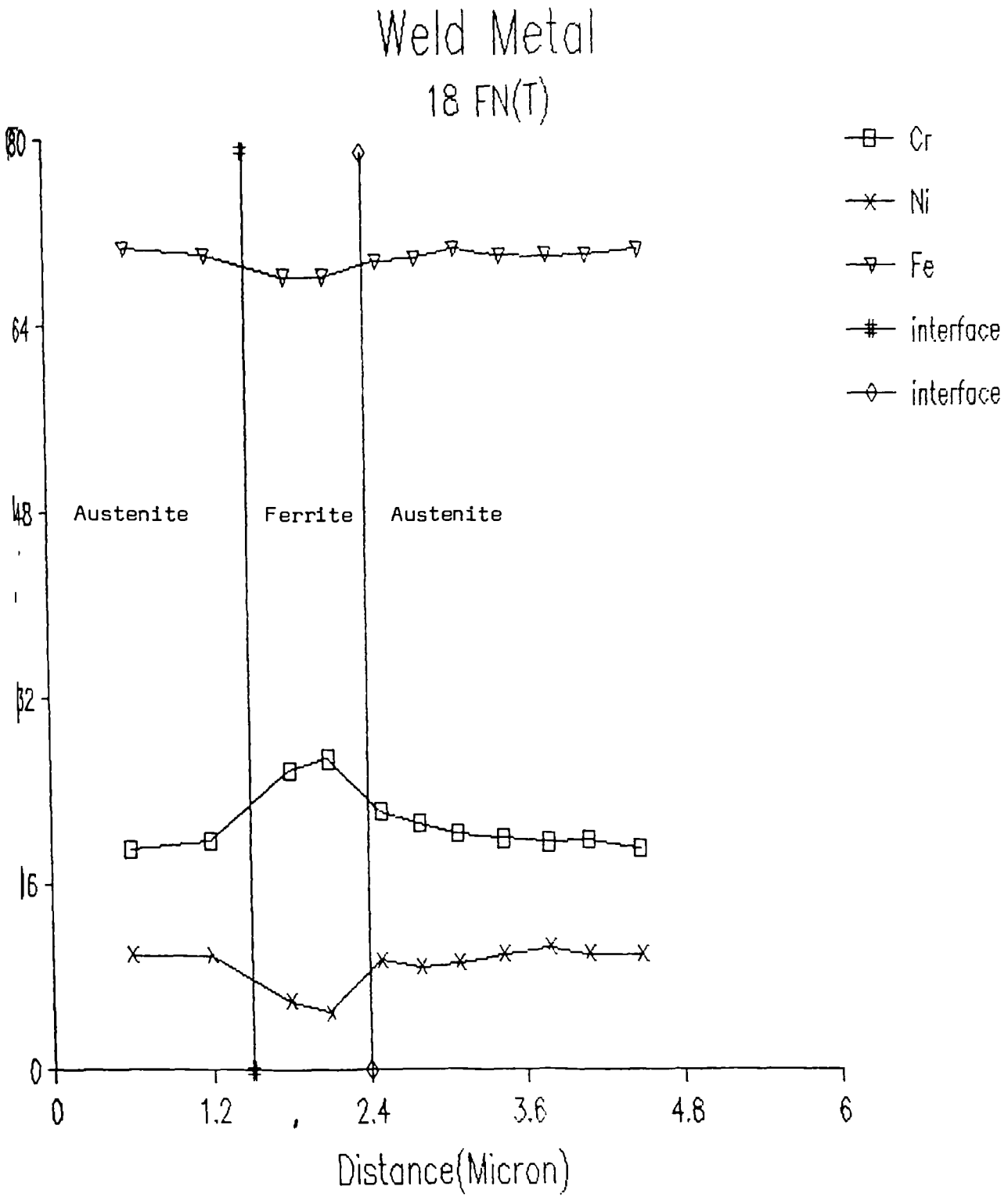

Fig.4.85(c) STEM spot analyses of Chromium Nickel and Iron traversing ferrite/austenite region.

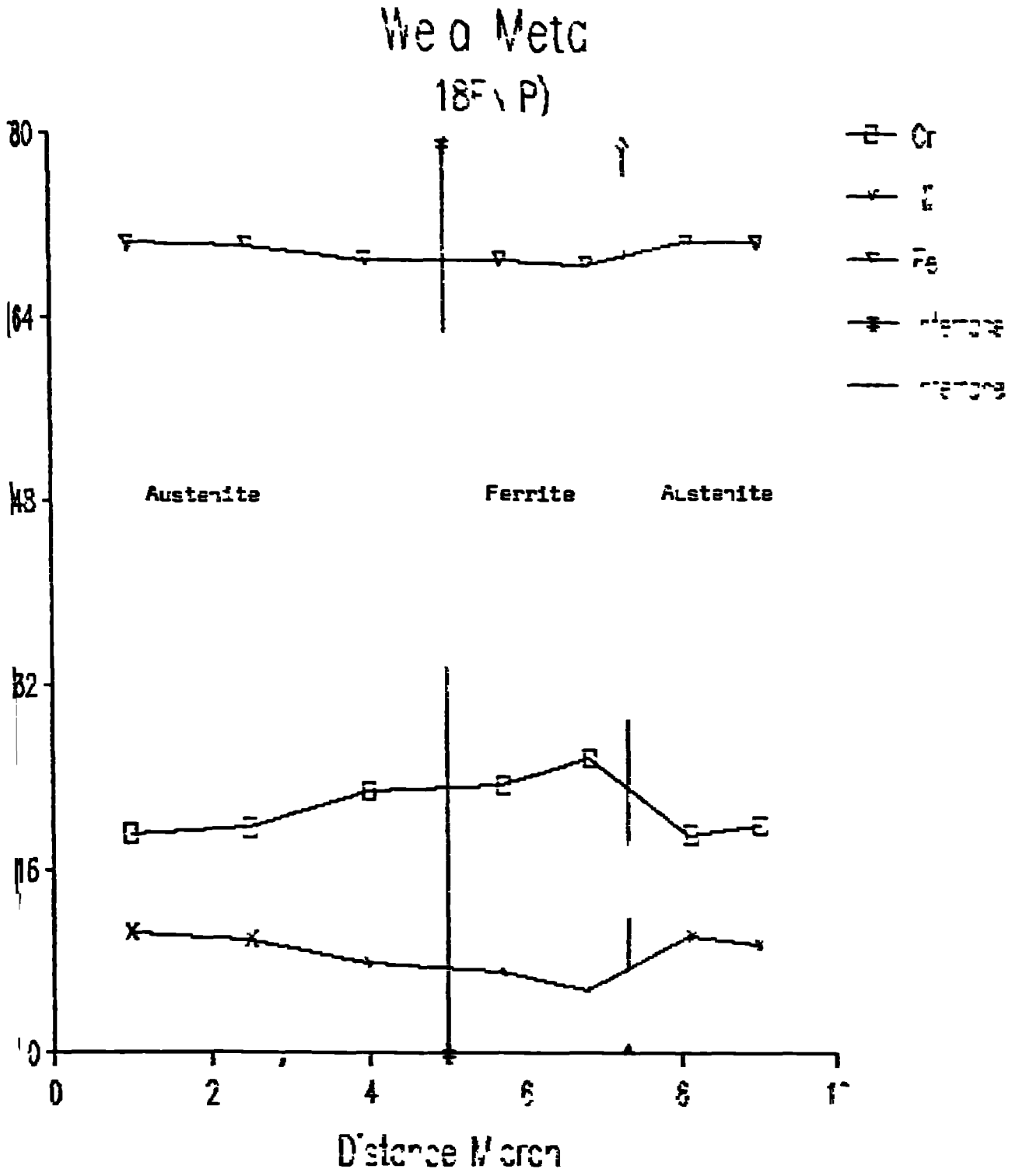

Fig.4.85(d) STEM spot analyses of Chromium Nickel and Iron traversing ferrite/austenite region.

0.6 µm

Fig.4.86 STEM micrograph of Submerged Arc weld metal (Sample K)

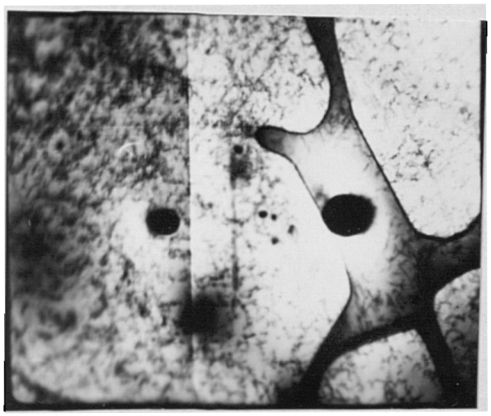

2 µm

Fig.4.87 STEM micrograph of Submerged Arc weld metal (Sample U)

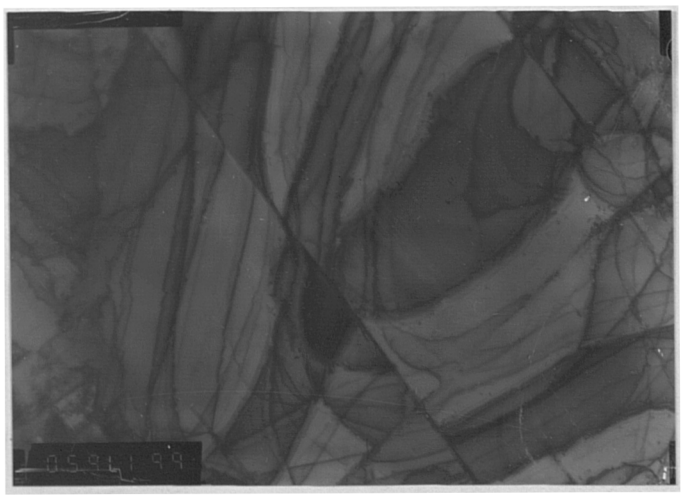

3µm

Fig.4.88 STEM micrograph of Submerged Arc weld metal (Sample K)

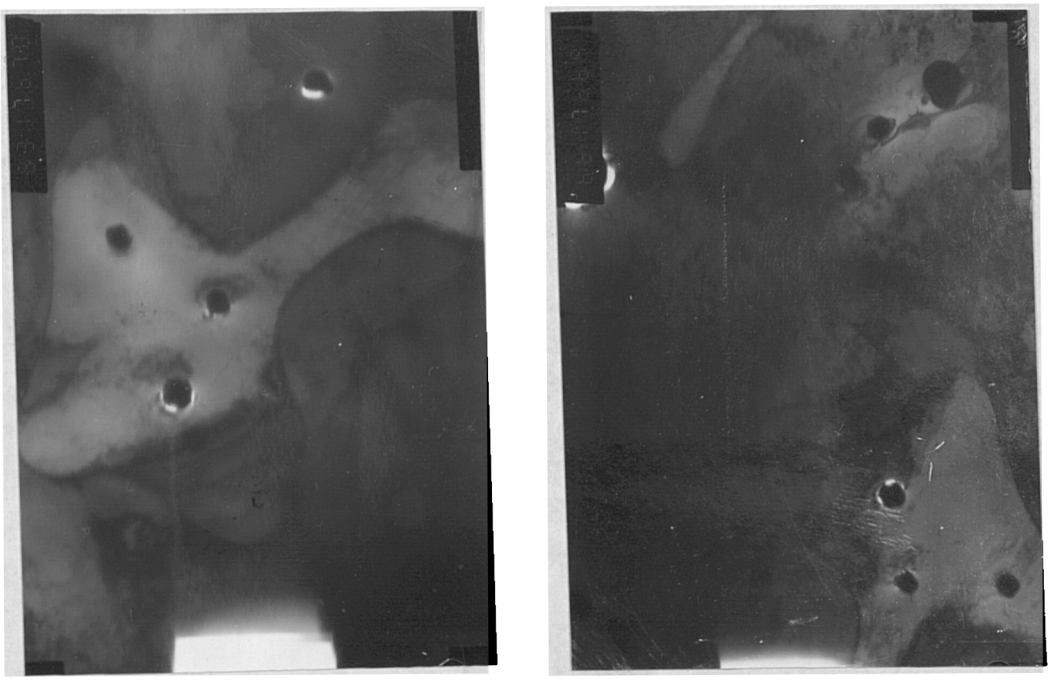

Fig.4.89 STEM micrograph austenitic stainless steel AISI 316L Submerged Arc Butt weld. Sample U.

Fig.4.90 STEM micrograph of austenitic stainless steel AISI 321 Submerged Arc Butt weld with duplex structure. Sample K.

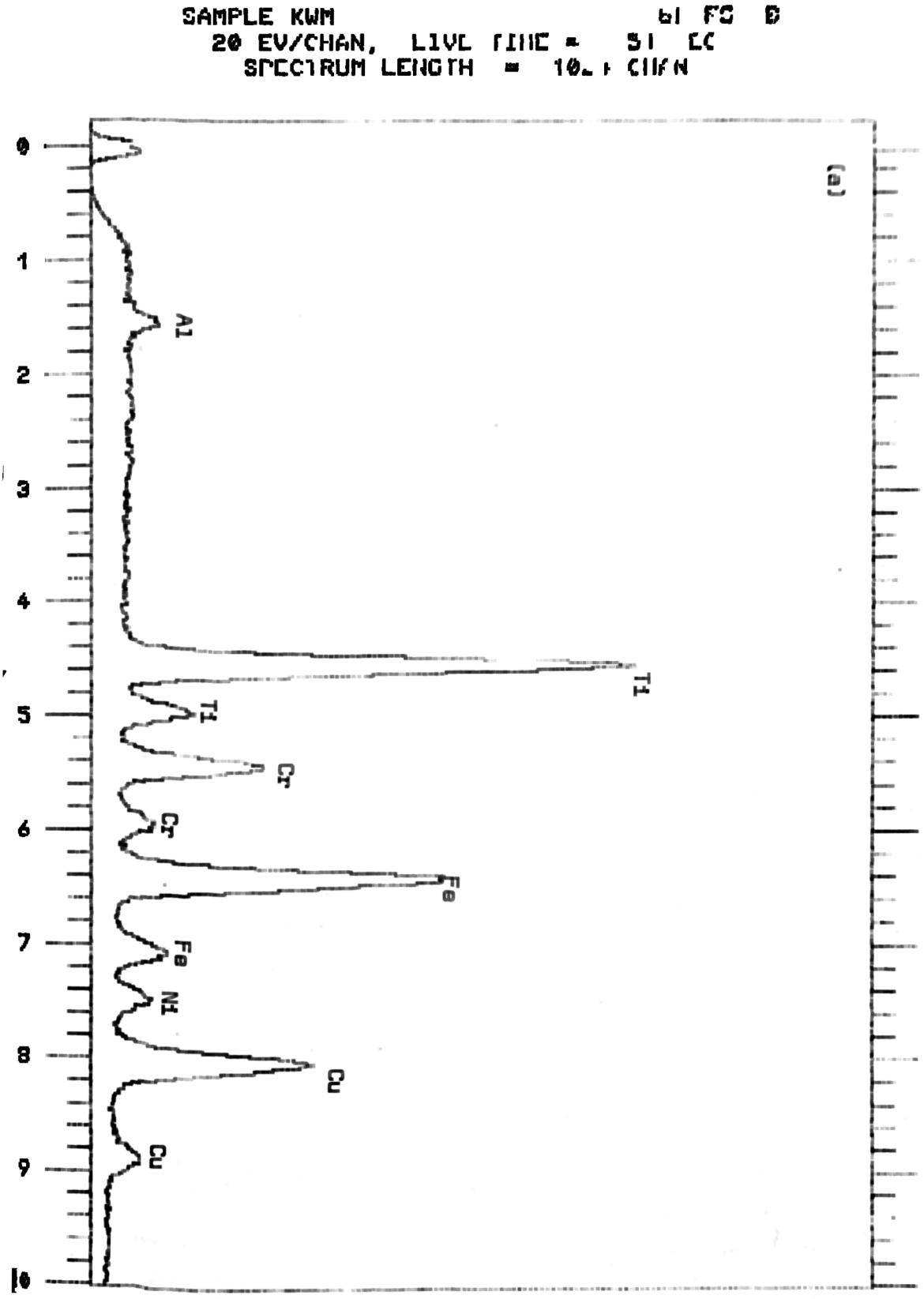

Fig.4.91 Energy dispersive x-ray analysis AISI 316L weld metal (sample K).

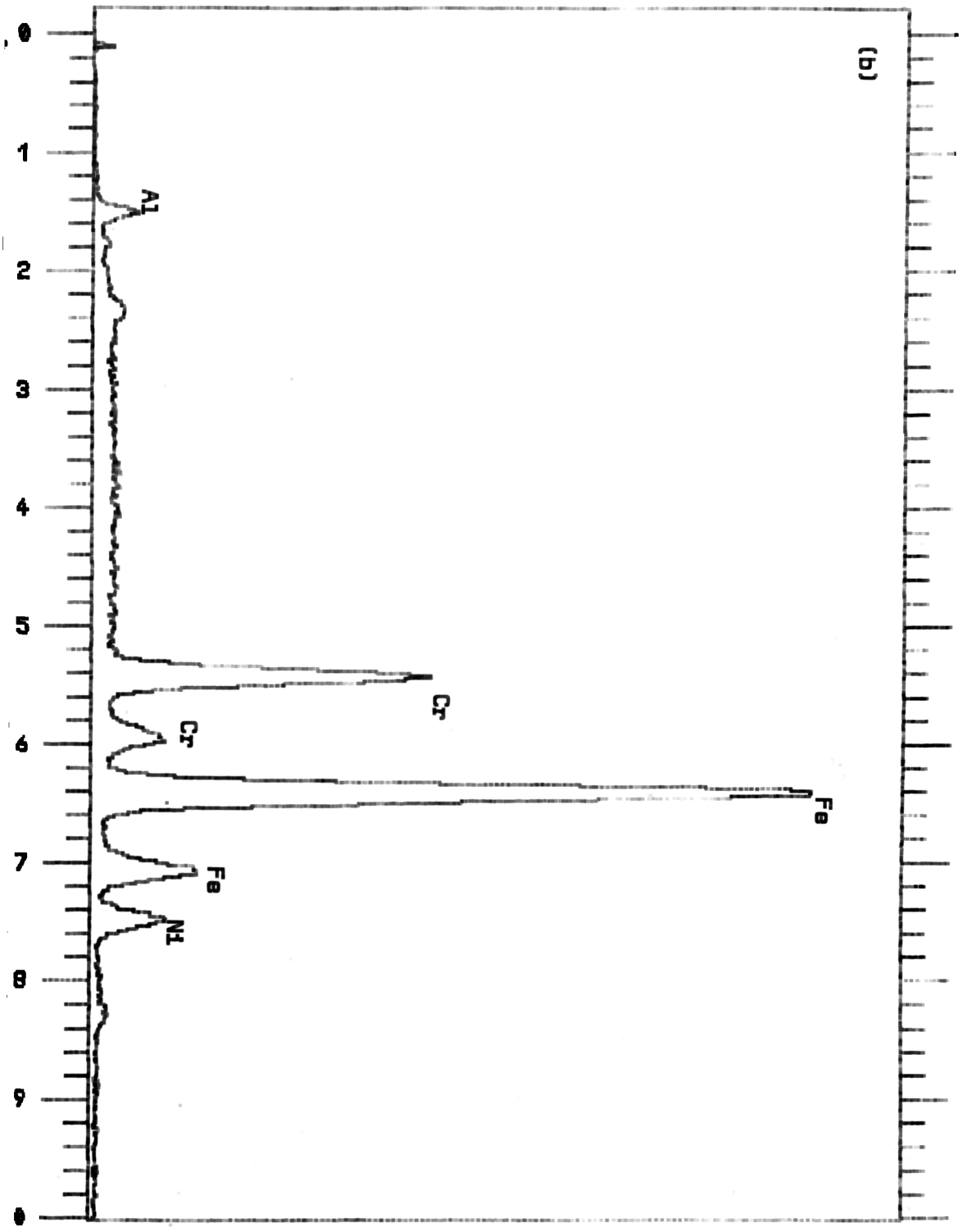

Fig.4.81 (contd)

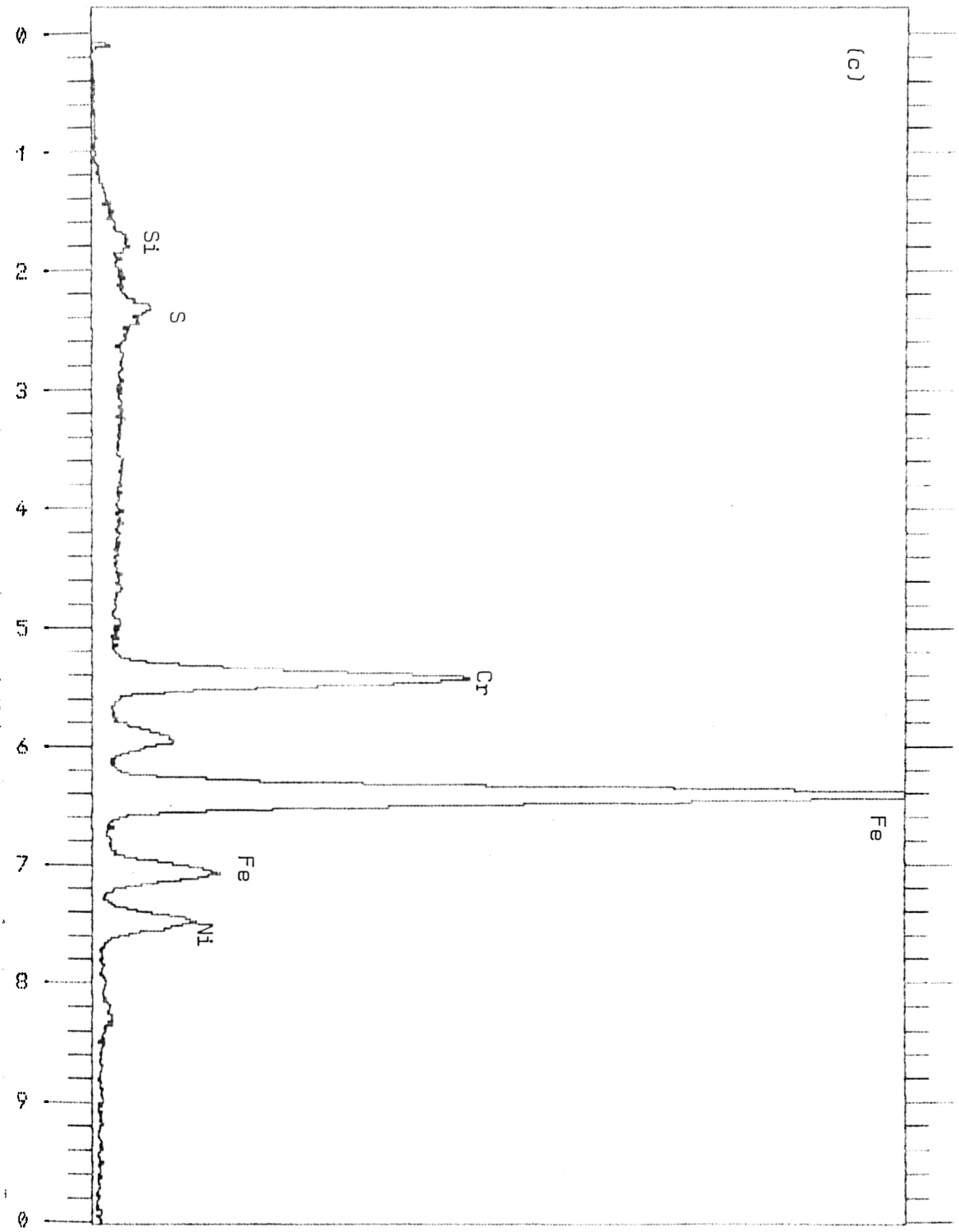

Fig.4.91 (contd)

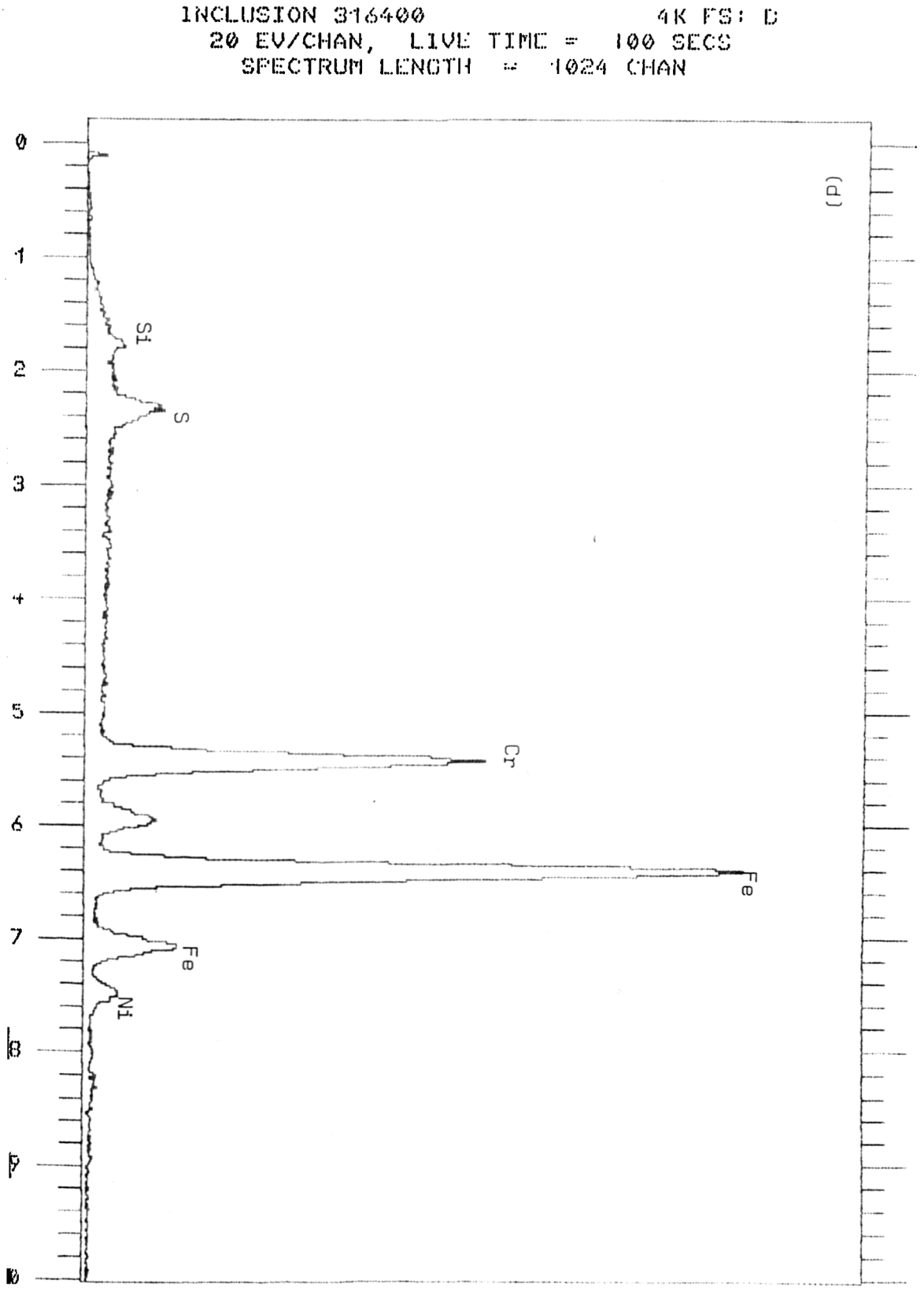

Fig.4.91 (contd)

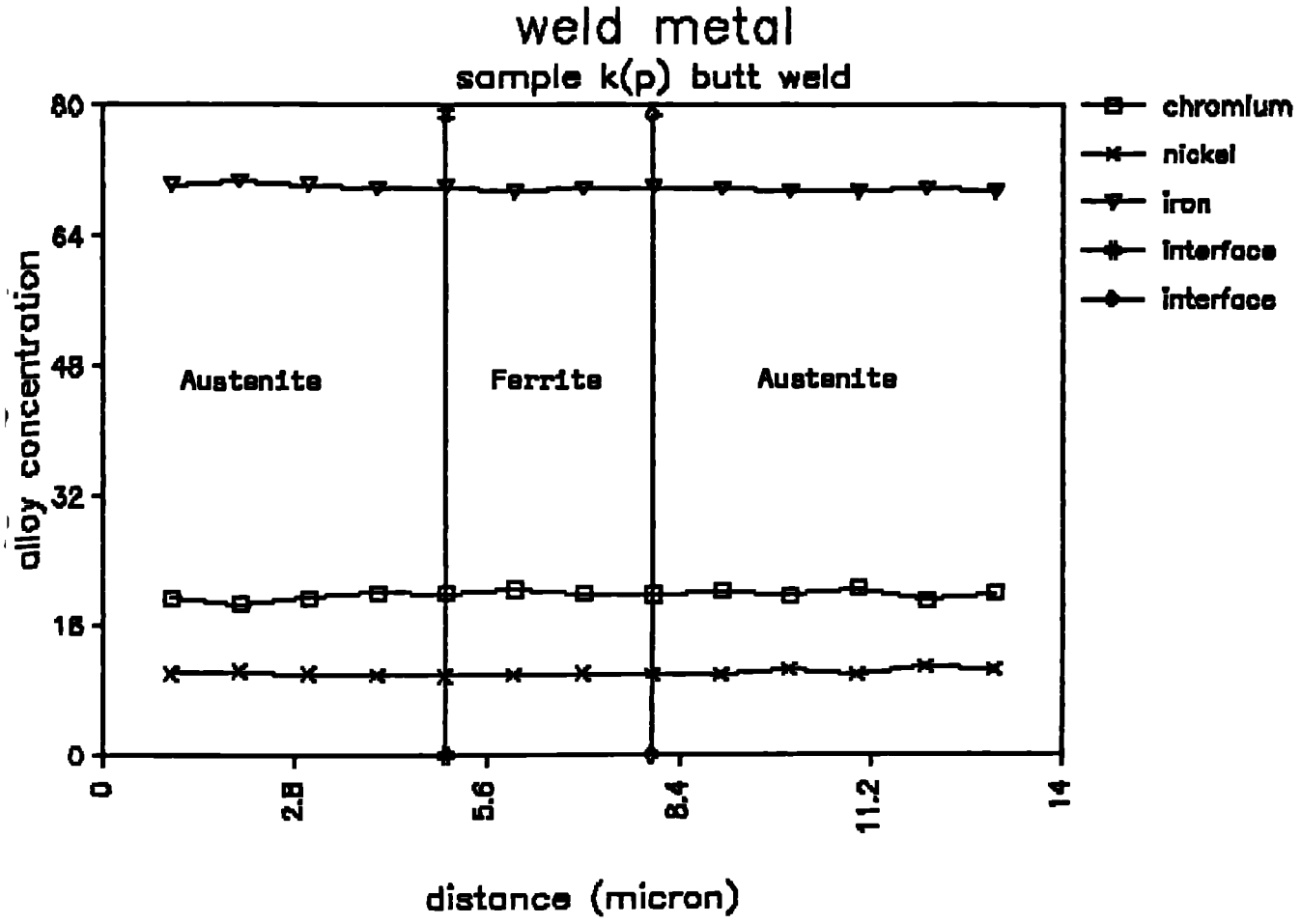

Fig.4.92(a) STEM spot analyses of Chromium Nickel and Iron traversing ferrite/austenite region.

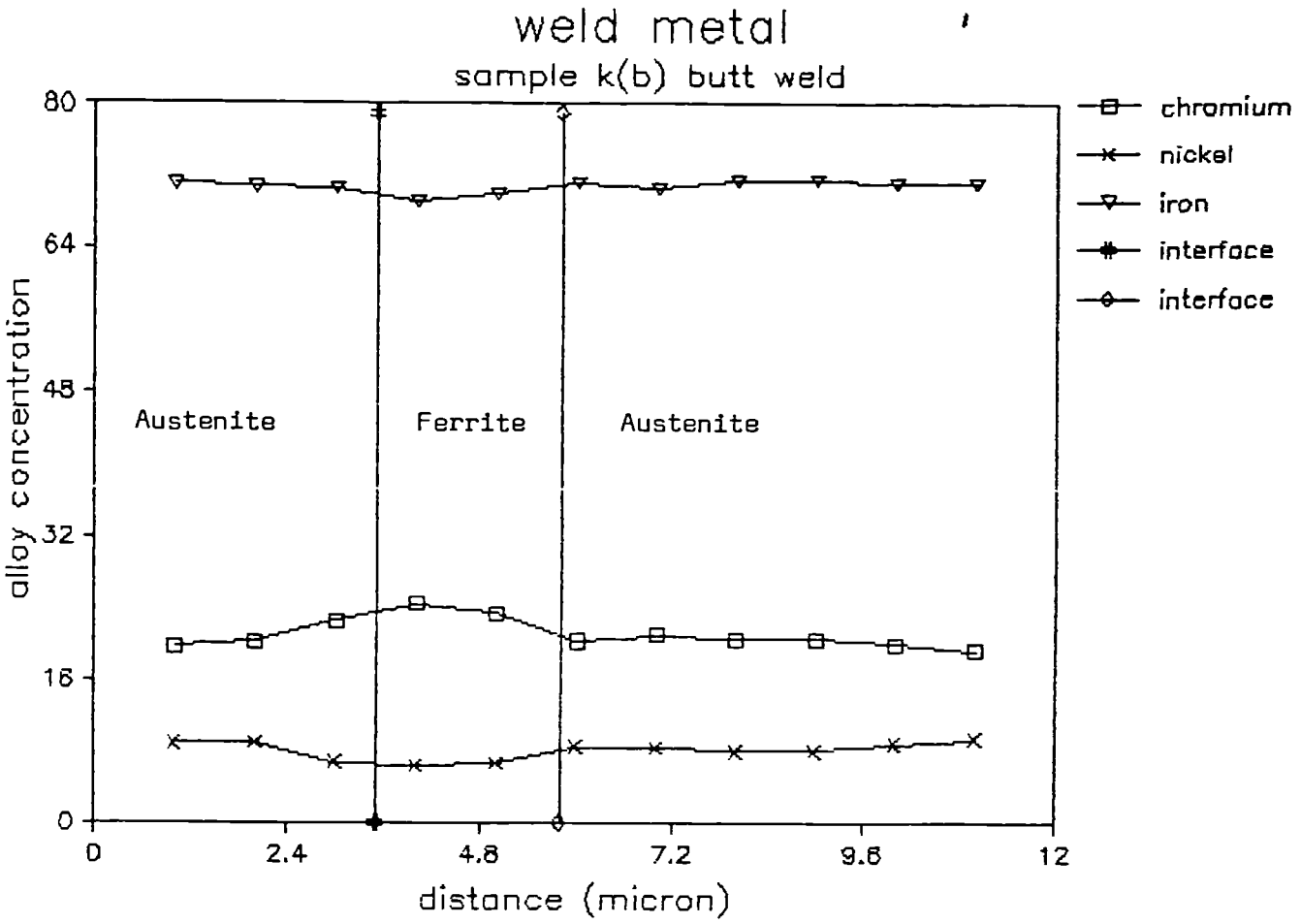

Fig.4.92(b) STEM spot analyses of Chromium Nickel and Iron traversing ferrite/austenite region.

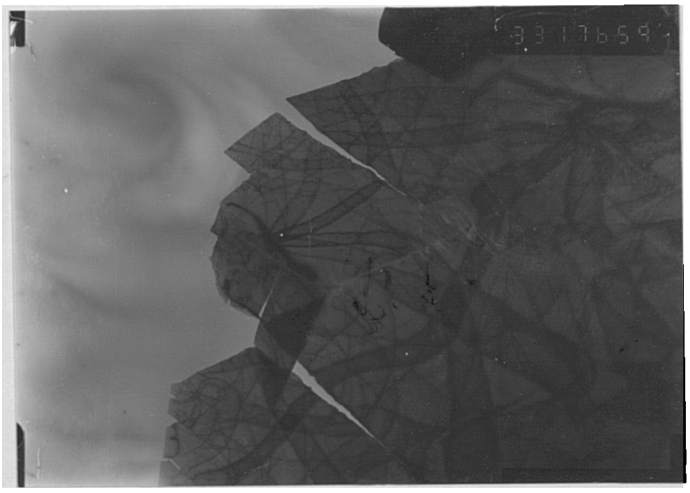

6µm

Fig.4.93 STEM micrograph of austenitic stainless steel AISI 321. Submerged Arc Butt weld. Sample K.

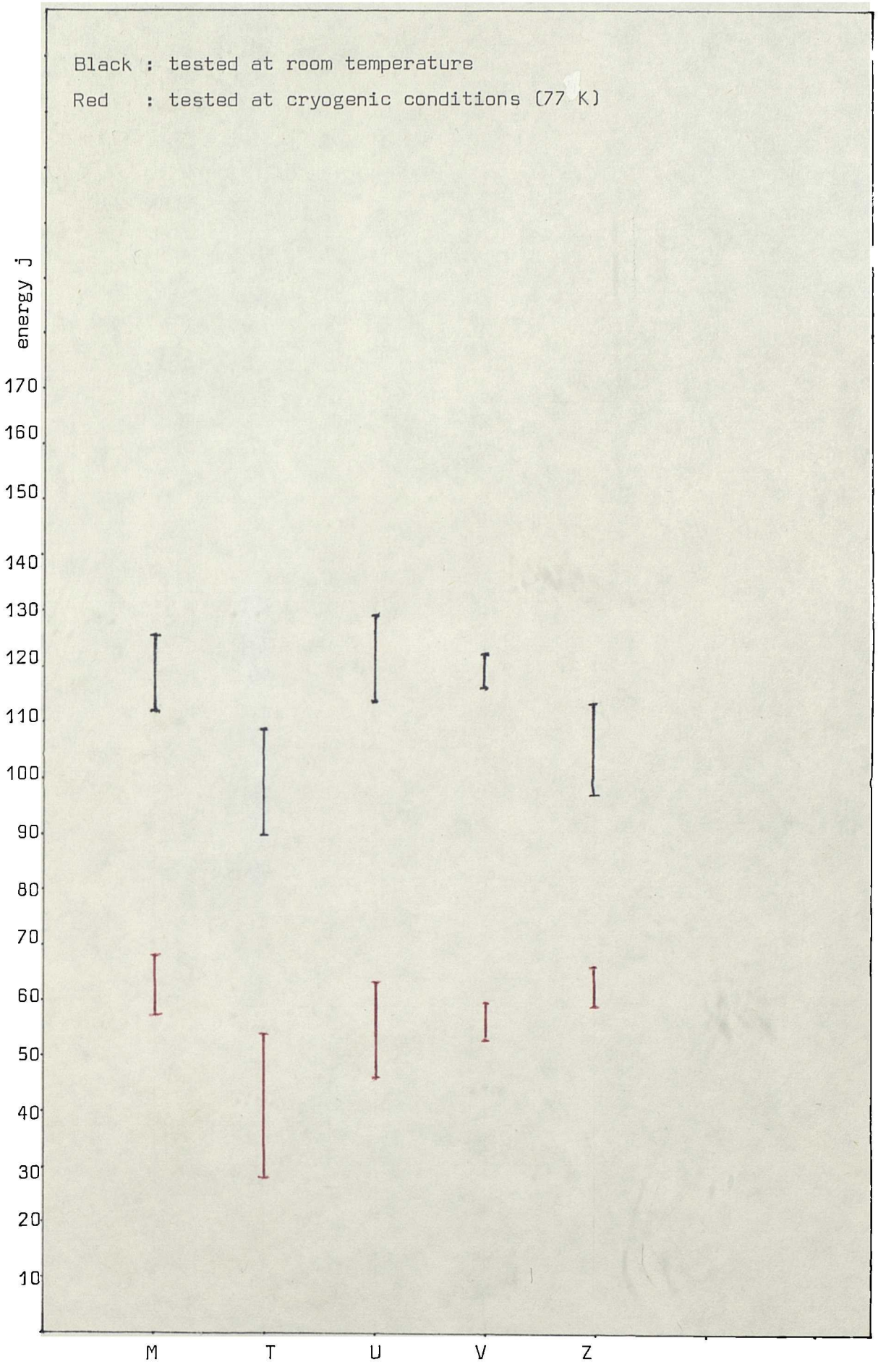

Fig.4.94 Austenitic stainless steel AISI 316L weld metal impact energy

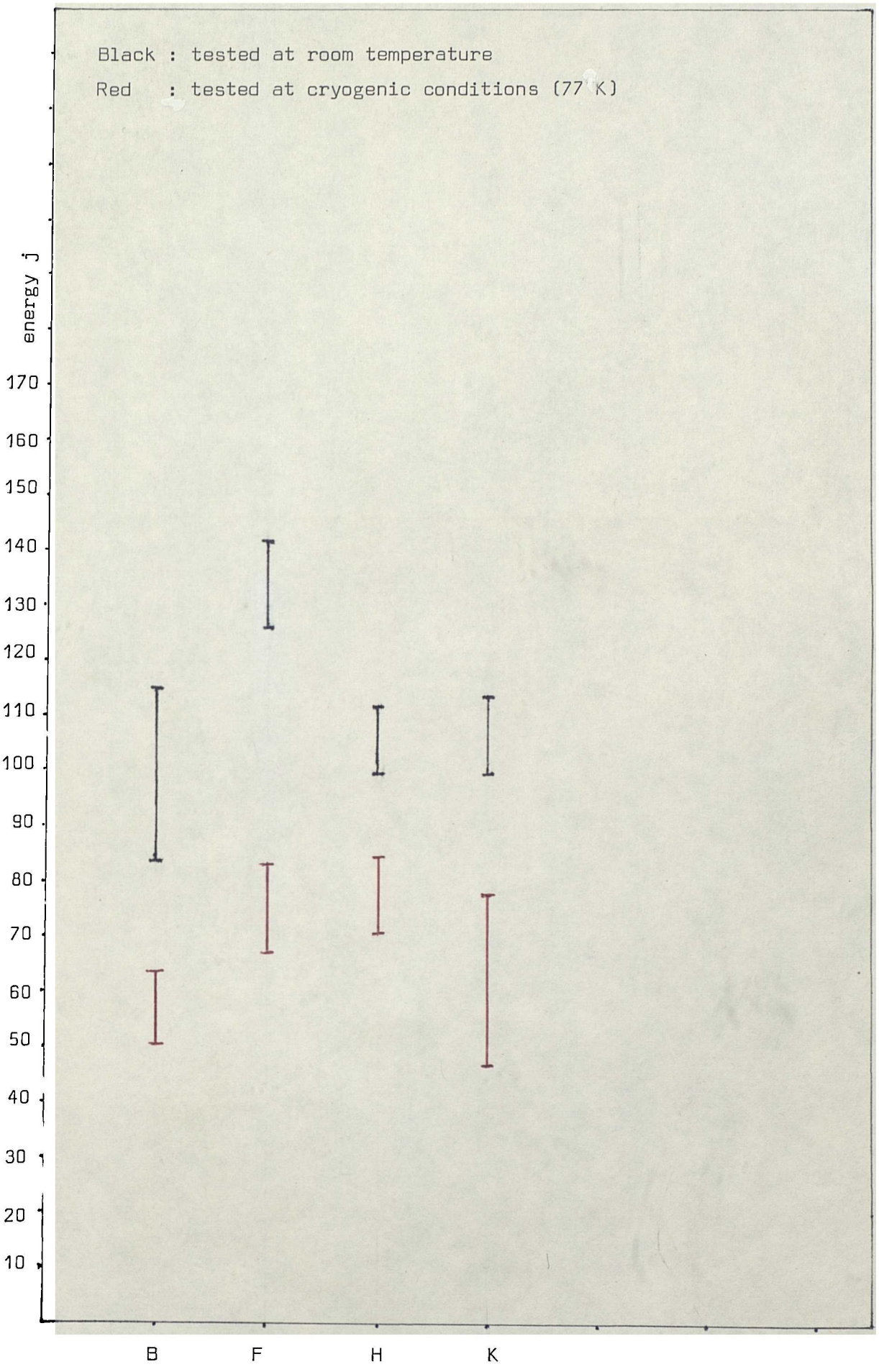

Fig.4.95 - Austenitic stainless steel AISI 321 weld metal impact energy

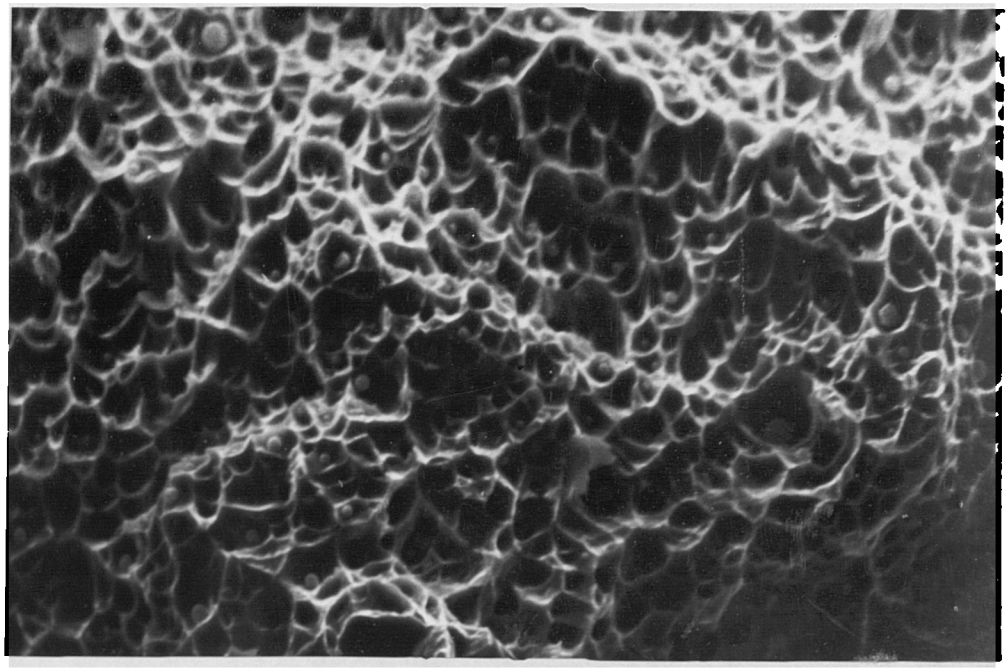

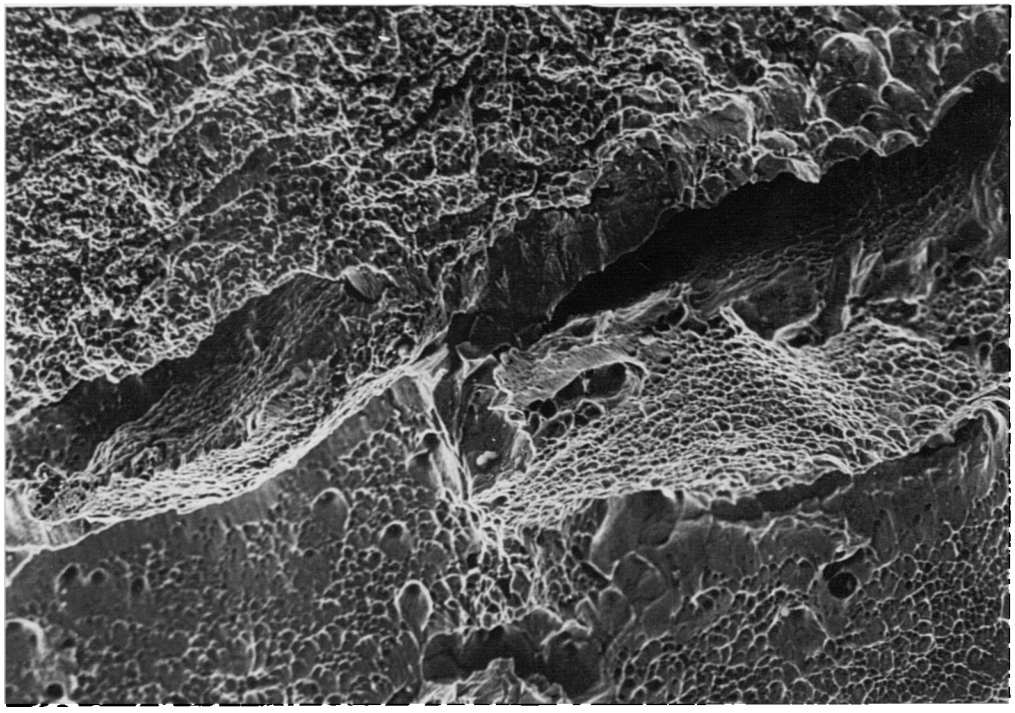

Fig.4.96 SEM micrograph of fracture surface resulting from impact test specimen of weld metal (Butt weld Y)

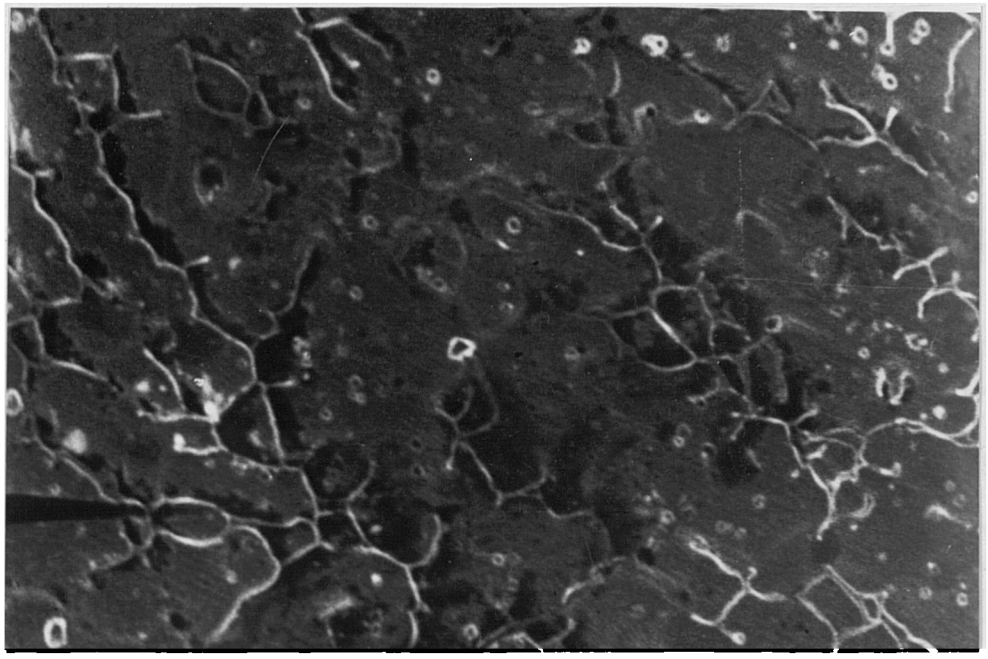

10 µm

(a) AISI 316L Butt weld N.

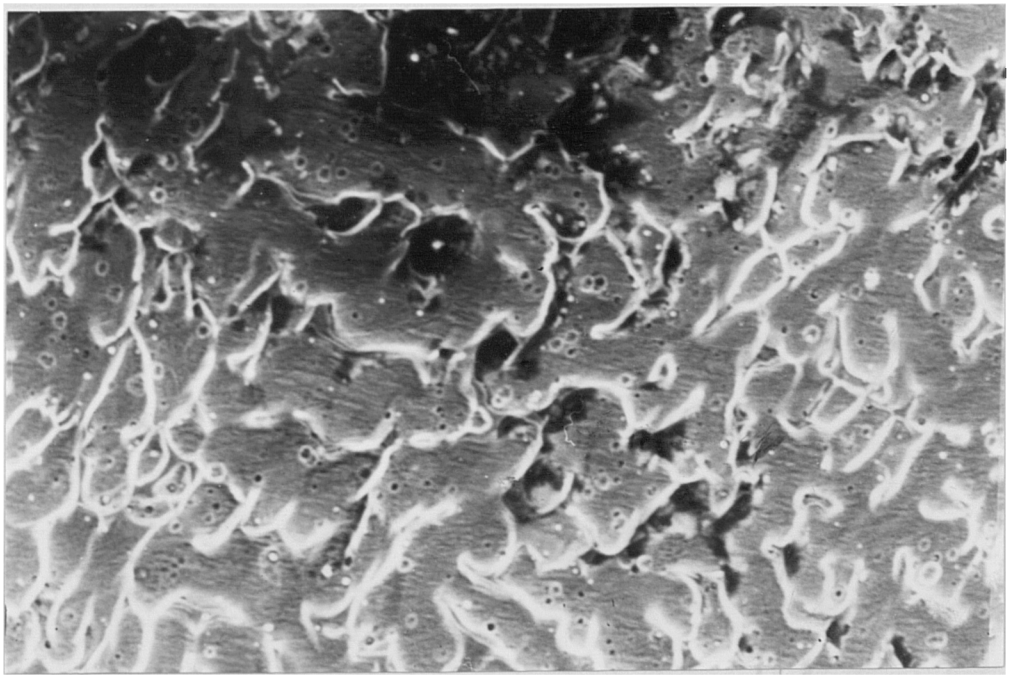

(b) AISI 321 Butt weld L75. 10 µm

Fig.4.97 SEM micrograph of austenitic stainless steel different welds.

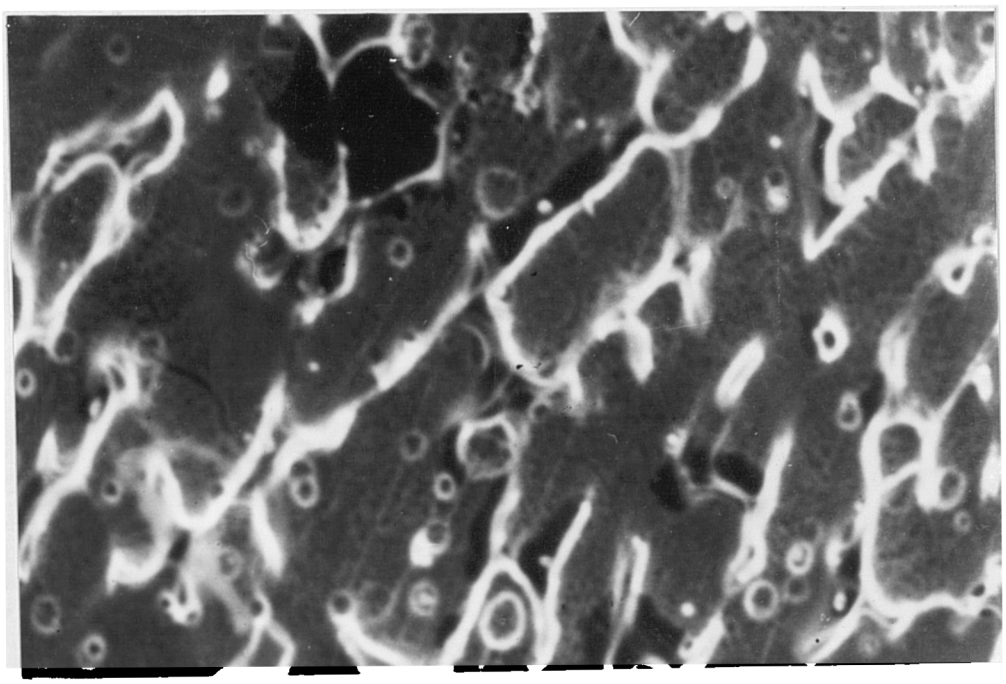

(c) AISI 321 Butt weld K. ——— 4 µm

Fig.4.97 (continued)

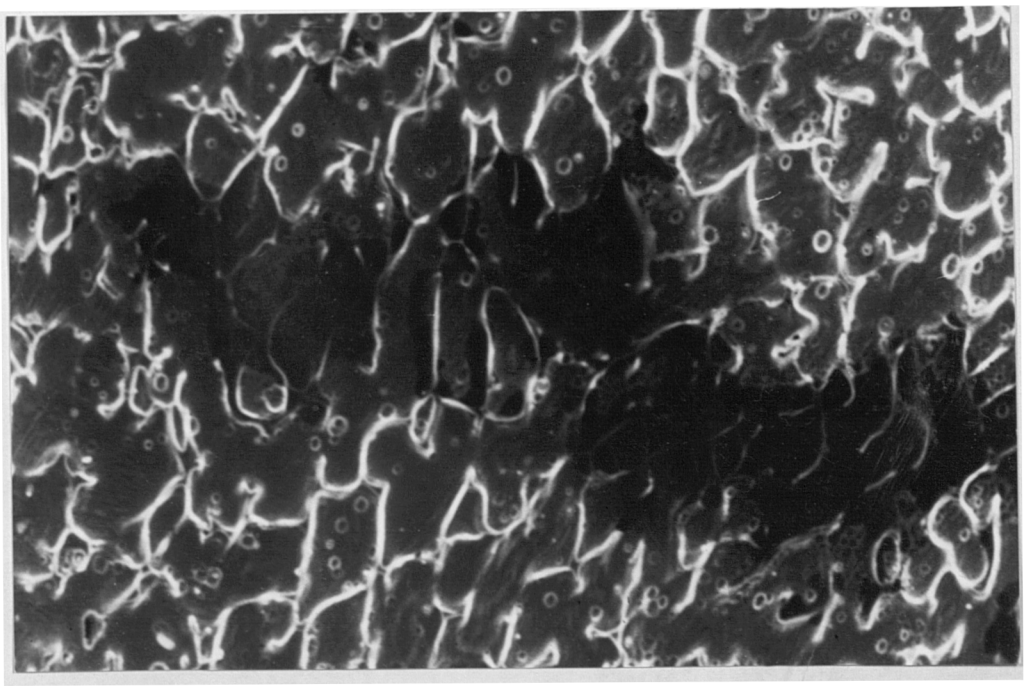

——— 1 10µm

Fig.4.98 SEM micrograph austenitic stainless steel AISI 316L Submerged Arc Butt weld (Sample V3)